An investigation into Nano-particulates reinforced SAC305-based composite solders under Electro- and Thermo-migration conditions

by

Guang Chen

A Doctoral Thesis

Submitted in partial fulfilment of the requirements

for the award of

Doctor of Philosophy of Loughborough University

December 2017

Abstract

With the rapid development in electronic packaging due to product miniaturisation, the size of solder joints is decreasing considerably, thus the failure of solder interconnects induced by electro-migration (EM) and thermo-migration (TM) became a reliability concern. The incorporation of foreign reinforcement can effectively improve properties of the solder alloys. However, this presents an imperative need for a further investigation to elaborate the underlying fundamentals associated with the reliability of reinforced solders.

In this study, the Sn-Ag-Cu (SAC) based solder alloy powders as matrix were incorporated with Fullerene (FNS), TiC and Ni-coated graphene (NG) reinforcements to form composite solders through powder metallurgical method. These composite solders were then characterised in terms of their microstructure, physical property, solderability, followed by a systematic investigation of their performance under isothermal ageing, current stressing and large thermal gradient, respectively.

The results showed that three types of reinforcements were successfully incorporated into the solder matrix; with all reinforcements added being embedded in the solder matrix or around the intermetallic compounds (IMC). The average loss of FNS and TiC particles in the solders was approximately 80% after the initial reflow, while this was only 40% for NG particles. It has been observed that β-Sn and Ag_3Sn in the SAC solder alloys can be refined by adding appropriate amount of FNS and TiC, which is beneficial to the wettability with a reduced coefficient of thermal expansion (CTE) with the minimal influence on the melting point and electrical resistivity of solder alloys.

For the SAC alloys without reinforcements, obvious extrusion of interfacial IMC at the anode was present after 360 hours of current (1.5×10^4 A/cm^2) stressing, while the changes of surface profiles of all reinforced solders were unnoticeable.

Under the current stressing regimes, a continuous increase of interfacial IMCs at the anode of the original SAC alloys was observed, but decreased at the cathode with stressing time. For the composite solders, both anode and cathode showed a continuous growth of interfacial IMCs; the growth rates of IMCs at the anode were greater than that at cathode. In addition, NG and TiC were found to be most effective to retard the growth of Cu_3Sn IMC under current stressing. A gradient in hardness across the stressed SAC joints was present, where it was harder at anode. However, no such obvious gradient was found in SAC/FNS and SAC/NG solder joints. FNS and NG were proven to be beneficial to prolong the service life of solder joints up to approximately 7.6% and 10.4% improvements, respectively.

Thermal stressing made the interfacial IMC in the original SAC joints to grow at the cold end considerably; causing serious damage at the hot end after 600 hours under temperature gradient of 1240K/cm stressing; a large number of IMCs, cracks and voids appeared in the SAC solder joints. However, a uniform increase of IMCs at both sides in the composite solders was observed without apparent damages at the interfaces under the same thermal stressing conditions, indicating an effective reduction of the elemental migration in the reinforced solders. Although there were also some voids and IMCs formed in the composite solder joints after a long-term thermal stressing, the integrity of the composite solder joints was enhanced compared with the SAC alloys. During thermal stressing, the dissolution rate of Cu atom into the SAC solder joints was estimated to be 3.1×10^{-6} g/h, while the values for SAC/FNS, SAC/NG and SAC/TiC were only 1.22×10^{-6} g/h, 1.09×10^{-6} g/h and 1.67×10^{-6} g/h, respectively.

Keywords: Composite solders; Isothermal ageing; Electro-migration (EM); Thermo-migration (TM); Microstructural evolution; Mechanical properties

List of Publications

Journal papers

1. **G. Chen**, F.S. Wu, C. Liu, W.S. Xia, H. Liu, Effect of Fullerene reinforcement on the performance of 96.5Sn–3Ag–0.5Cu lead-free solder, *Mater. Sci. Eng., A,* 2015 (636) 484-492.

2. **G. Chen**, F.S. Wu, C. Liu, V.V. Silberschmidt, Y.C. Chan, Microstructures and properties of new Sn-Ag-Cu lead-free solder reinforced with Ni-coated graphene nanosheets, *J Alloy Compd*, 2016 (656) 500-509.

3. **G. Chen**, B.M Huang, H. Liu, Y.C. Chan, Z.R. Tang, F.S. Wu, An investigation of microstructure and properties of Sn3.0Ag0.5Cu -XAl_2O_3 composite solder, *Solder Surf Mt Tech*, 2016(28) 84-92.

4. **G. Chen**, L. Liu, F.S. Wu, C. Liu, V.V. Silberschmidt, Y.C. Chan, Retained ratio of reinforcement in SAC305 composite solder joints: Effect of processing and reflow cycle, *Solder Surf Mt Tech*, 2016(28) 159-166.

5. **G. Chen**, H. Peng, V.V. Silberschmidt, Y.C. Chan, F.S. Wu, C. Liu, Performance of Sn–3.0Ag–0.5Cu composite solder with TiC reinforcement: physical properties, solderability and microstructural evolution under isothermal ageing, *J Alloy Compd*, 2016 (685) 680-689.

6. **G. Chen**, L. Liu, J. Du, V.V. Silberschmidt, Y.C. Chan, F.S. Wu, C. Liu, Thermo-migration behaviour of SAC305 lead free solder reinforced with fullerene nanoparticles, *J Mater Sci*, 2016 (51) 10077–10091.

7. **G. Chen**, L. Liu, V.V. Silberschmidt, F.S. Wu, C. Liu, Y.C. Chan, Microstructural evolution of SAC305 lead free solder reinforced with Ni-coated graphene reinforcement under large temperature gradient, *J Electron Mater,* 2016 (XX) XX-XX (Minor revise).

8. H. Peng, **G. Chen**, L. Mo, Y. C. Chan, F.S. Wu, An investigation on the ZnO retained ratio, microstructural evolution, and mechanical properties of ZnO doped Sn3.0Ag0.5Cu composite solder joints, *J Mater Sci-Mater El,* 2016 (24) 1-11.

9. L. Liu, Z. W. Chen, Z. X. Zhou, **G. Chen**, F.S. Wu, C. Liu, Diffusion barrier property of electroless Ni-W-P coating in high temperature Zn-5Al/Cu solder interconnects, *J Alloy Compd*, 722 (2017) 746-752.

10. **G. Chen**, L. Liu, V.V. Silberschmidt, Y.C. Chan, F.S. Wu, C. Liu, Electro-migration behaviour of SAC305 lead free solder reinforced with foreign reinforcement, *J* Electron *Mater* (in preparation).

Conference papers

1. **G. Chen**, F.S. Wu, C. Liu, H. Liu, H.Y. Wang, Effect of Ni-coated graphene on the microstructure and properties of SAC305 solder, ICEPT, Chengdu (2014) 209 - 213.

2. **G. Chen**, F.S. Wu, C. Liu, Y.C. Chan, Effect of fullerene-C60&C70 on the microstructure and properties of 96.5Sn-3Ag-0.5Cu solder, ECTC (2015) 1262-1267.

3. P. Hao, B.M. Huang, **G. Chen**, F.S. Wu, H. Liu, Y.C. Chan, Effect of 0.8 wt% Al_2O_3 nanoparticles addition on the microstructures and electromigration behavior of Sn-Ag-Cu solder joint, ICEPT (2016) 1014-1017.

4. W. Shen, X.H. Cai, **G. Chen**, F.S. Wu, W.S. Xia, W.B. Zhu, R. Liu, Y. Zhang, The study of novel Metal/Composite thermal interface materials for chip testing, ICEPT, Chengdu (2014) 352-355.

5. Y. Xu, L. Huang, **G. Chen**, F.S. Wu, W.S. Xia, H. Liu, Electromigration induced failure mechanism and lifetime prediction in Ni/Cu thin film, ICEPT, Chengdu (2014) 1071-1075.

6. B.M. Huang, **G. Chen**, F.S. Wu, W.S. Xia, L. Mo, H. Liu, Preparation, microstructure and properties of Sn-Ag-Cu solder reinforced with Al_2O_3 nanoparticles, ICEPT, Chengdu (2014) 243-246.

7. K.S. Xu, **G. Chen**, F.S. Wu, W.S. Xia, H. Liu, Effect of SiC whiskers addition on microstructure, micro-hardness and wettablility of Sn-Ag-Cu solder, ICEPT, Chengdu (2014) 310-312.

Acknowledgement

This research is funded by the joint PhD programme between Loughborough University (LU, UK) and Huazhong University of Science and Technology (HUST, China) based on Marie Curie International Research Staff Exchange Scheme Project within the 7th European Community Framework Programme (Grant No. PIRSES-GA-2010-269113), entitled "Micro-Multi-Material Manufacture to Enable Multifunctional Miniaturised Devices (M6)". The research was also supported by the National Nature Science Foundation of China (NSFC) and The Research Grants Council (RGC) Joint Research project (Grant NO. 61261160498 and NO.CityU101/12).

I would like to take this opportunity to express my sincere gratitude and deep appreciation to my supervisors, Prof. Chanqing Liu, Prof. Vadim V. Silberschmidt in LU and Prof. Fengshun Wu in HUST, for their valuable guidance, continuous support and constructive suggestions throughout all my PhD study period. I am grateful to my independent assessor, Prof. Liguo Zhao, for his advice and discussions for the project. Heartfelt thanks are given to Mr. Simon Neal and Mr. JaGPal Singh, for their help in preparing and characterising samples. Deep gratitude is also expressed to Dr. Keith Yendall, Dr. Sabrina Yan and Mr. Shaun Fowler in Department of Materials and LMCC, Loughborough University, for providing training and assistance on material characterizations using scanning electron microscopy and focused ion beam.

Thanks are also extended to my colleagues in both China and UK, for their help and knowledge. In particular, I would like to acknowledge the help with sample characterization and analysis from Ms. Li Liu in LU and Mr Ming Xiao in University of Waterloo. Besides, special thanks for the financial support of Loughborough University studentship for my PhD study. Finally, I would like to express my deepest gratitude to my family for their great love, deep understanding, endless patience and encouragement during all the years of this education.

Table of Contents

List of Figures

List of Tables

List of Abbreviations

AC	Alternating current
at.%	Atomic Percentage
BGA	Ball Grid Array
CTE	Coefficient of Thermal Expansion
C-S Analyser	Carbon and sulphur analyser
DSC	Differential scanning calorimeter
EDX	Energy Dispersive X-ray Spectrometer
EM	Electro-migration
FC	Flip Chip
FEM	Finite Element Model
FIB	Focused Ion Beam
FNS	Fullerenes
GNS	Graphene
IC	Integrated Circuit
ICP-OES	Inductively Coupled Plasma Optical Emission Spectrometry
IMC	Intermetallic Compound
MA	Mechanical alloying
MWCNT	Multi-wall carbon nano-tube
OSP	Organic solder-ability preservative
RROR	Retained ratio of reinforcement
SEM	Scanning Electron Microscopy
SWCNT	Single-wall carbon nano-tube
TM	Thermo-migration
TMF	Thermo-mechanical fatigue
TEM	Transmission Electron Microscopy
UTS	Ultimate tensile strength

UBM	Under bump metallization
vol.%	Volume Percentage
wt.%	Weight Percentage
XRD	X-ray diffraction
YS	Yield strength

Chapter 1 Introduction

1.1 Context of the Research

The present states of development of new interconnect materials and their understanding on a decreasing length scale is at the root of progress in modern microelectronic devices [1]. The trend to smaller structures, that is miniaturization, is well known in the manufacturing and microelectronics industries as evidence by the rapid increase in the power of device through reduction on chips of the area and volume per transistor. To fulfil the service performance that are measured as thermo-mechanical fatigue (TMF), dimensional stability, and mechanical reliability of electronic interconnects, there have been several attempts to incorporate foreign reinforcements in lead-free solder matrices to form the composite solders/interconnects.

Most of the previous and recent investigations are preliminary studies to identify mechanical properties and interfacial microstructures of composite interconnects with alloying elements under condition of thermal ageing or current stressing [2]. However, the failures of solder joints induced by electro-migration (EM) and thermo-migration (TM) under high current density and large temperature gradient become a major barrier in the pursuit of further miniaturized electronic devices. The main failure phenomena -void nucleation- due to EM and TM has a direct relationship with stress, plastic strain and thermal gradient of the specimen [3-4]. The determination of stress, strain and thermal gradient during EM and TM is crucial for failure prediction of newly developed composite interconnects under service conditions. The different electrical resistivity and thermal capacity of individual parts in the package level interconnection structure as well as generated Joule heat under high current density will lead to large thermal gradient across the interconnection. The thermal gradient provides a driving force for atomic diffusion to trigger TM [5]. This driving force of thermal

gradient influences the atoms migration from the higher temperature side to lower one, and thus a reversed flux vacancies mechanisms. Consequently, the interface at the higher temperature side will become more mechanically degraded.

Up to now, although many effects were made to understand the intrinsic mechanisms of EM and TM in plain lead-free interconnects, however, the composite interconnects reinforced with micro- or nano-sized foreign reinforcement that improve the mechanical reliability have not yet been investigated under the EM or TM stressing.

1.2 Research Aims and Objectives

The present thesis is focused on preparation and characterization of the 96.5Sn-3Ag-0.5Cu (SAC305) composite solders containing foreign reinforcement, as well as investigating the microstructural and mechanical evolution of solder joints under the conditions of isothermal ageing, EM and TM stressing. The main objectives and tasks are therefore identified as follows:

1) **Preparation and Characterisation of composite solders**:

   Three composite solders reinforced with FNS, TiC and NG (lab-made) will be prepared using powder metallurgical route. After sintering and rolling, the composite solder alloys will be formed into solder foils with certain thickness. For the convenience of test, these solder foils will be further formed into solder balls using a reflow oven. After that, to fully investigate the basic microstructural and physical characteristics, the initial microstructure of various composite solders will be studied. Further, the melting point, wettability, electrical resistance and CTE of these as-prepared solders will also be comparatively studied. In addition, to understand the actual content of reinforcement in a reflowed solder joint, the retained ratio of different reinforcement will be tested.

2) **Microstructural and mechanical evolution of solder alloys under isothermal ageing**:

Considering the fact that the microstructural and mechanical evolution of a solder joint under thermal ageing condition is an important approach to evaluate the service reliability of a solder alloy, isothermal ageing test will thus be implemented. After different ageing times, the microstructure (including interfacial and matrix) and mechanical properties (including hardness and shear strength) of different composite solder joints will be comparatively analysed.

3) Investigation of EM behaviour of composite solders

In order to understand the effect of three different reinforcements -FNS, TiC and NG- on electro-migration in solder joints, the reliability of newly prepared composite solder alloys will be evaluated under EM stressing. Microstructural evolution and mechanical properties of different solder systems exposed to different times of EM stressing will be studied. Surface conditions as well as the service life of different solder joints will also be assessed and comparatively analysed. The failure mechanism of different composite solder joints under EM stressing will be discussed as well.

4) Investigation of TM behaviour of composite solders

TM of the metal atoms in a joint is also likely to cause elemental segregation, an excessive growth of interface IMC and dissolution of an under bump metallurgy (UBM) layer, which may ultimately and seriously affect in service reliability of the solder joint. Microstructural evolution, change in mechanical properties, atomic migration rate and failure mode of solder joints under TM stressing are problems should be solved. In this study, a TM set-up will be designed, prepared and evaluated. After that, evolution of microstructure and mechanical properties of the composite solders under TM stressing will be investigated systematically. In addition, the variation of inner structure and elemental migration rate in different solder joints after different stressing time will also be discussed.

1.3 Main contributions of this work

The thesis focused on the preparation and characterisation of composite solder alloys reinforced with foreign reinforcement; the microstructural and mechanical evolution of these newly prepared composite solder joints under thermal ageing, EM and TM stressing were also systematically studied. It can contribute to the contemporary knowledge on reliability of composite solder joints from following aspects:

1) The Ni particles decorated on graphenes (GNS) nano-sheets were expected to act as a "bridge" that link the GNS nano-sheets and the solder matrix, and it was proven effective to significantly improve the retained ratio of GNS in solder joints. These findings can facilitate the current understanding on preparation of composite solder as well as the interfacial reaction between solder matrix and reinforcement.
2) The quantitative analysis of retained ratio of different reinforcements in solder joints after different reflow cycles can help to understand the exclusion behaviours of reinforcement during reflow process as well as the real content and distribution of reinforcement added in the final solder joint.
3) The experimental results on the microstructural and mechanical evolution of composite solder alloys under thermal ageing confirmed that the appropriate addition of reinforcement can effective suppress the growth of Cu_3Sn IMC as well as lower the degradation of mechanical strength of solder joints. It provides a potential method of retarding the excessive growth of interfacial IMCs, which could be a vital issue in the electronic packaging.
4) The observation and analysis of surface morphology, microstructural evolution, redistribution of hardness and evaluation of service life of different solder joints under EM stressing can improve the fundamental understanding of the effect of addition of foreign reinforcement on reliability of solder joints under EM stressing.
5) The direct observation of temperature distribution in solder joint during TM

stressing provides an intuitive understanding of temperature gradient in a stressed solder joint. The X-ray computed tomography (X-CT) results facilitate the understanding of formation and growth of IMCs and defects in the inner of a solder joint under TM stressing. In addition, the quantitative analysis of diffusion rate of Cu atoms from Cu substrate to solder joint also provides a fundamental understanding for the future research on elemental migration under large temperature gradient.

1.4 Structure of the Thesis

The structure of the thesis is illustrated in the Figure 1.1. **Chapter 1** briefly describes the research background, objectives and main contributions of this research. **Chapter 2** provides a literature review of preparation and characterization of composite solders; the definition of TM and EM as well as relevant reliability problems is also presented in this chapter. **Chapter 3** introduces the processing process of composite solders with a powder metallurgical route, then investigates the solderability and basic physical properties of prepared composite solders. **Chapter 4** comparatively studies the microstructural and mechanical evolution of plain and composite solder joints under isothermal ageing. **Chapter 5** and **Chapter 6** present and discuss the EM and TM behaviours of composite solder joints under EM and TM stressing. Finally, the thesis ends with conclusions and further works presented in **Chapter 7**.

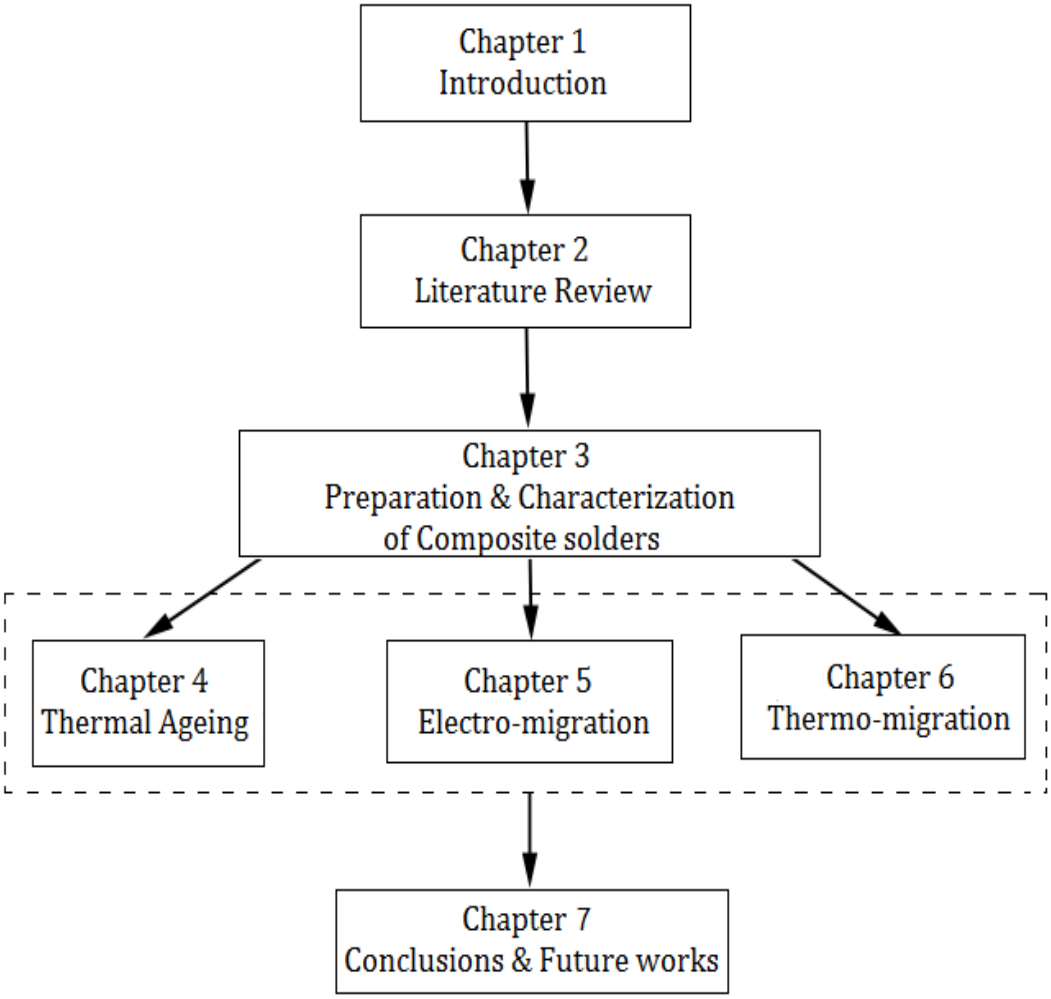

Figure 1.1 Thesis structure

Chapter 2 Literature review

This chapter serves as an overview of existing literature on the fabrication, achievements and problems of composite solders enhanced with foreign reinforcement. Additionally, as the main research focuses, the fundamentals, effects and failure mechanism of EM and TM were also involved in this part.

2.1 Definition of composite solder containing foreign particles

As mentioned in Chapter 1, To improve dimensional stability and mechanical reliability of electronic interconnections, there were several attempts to incorporate suitable reinforcement (including metal, ceramic, IMCs, and carbon nano-materials etc.) into lead-tin or lead-free solder matrices to prepare the composite interconnects.

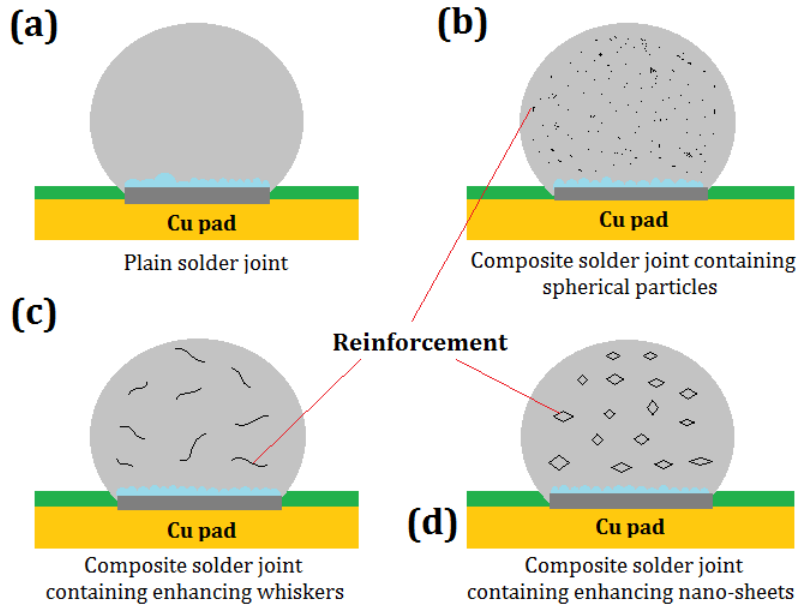

Figure 2.1 Schematic of typical composite solder joints enhanced with different foreign reinforcement

In general, the solders that enhanced with foreign reinforcements are known as composite solders. For instance, three typical composite solder joints reinforced with different foreign particles are illustrated in Figure 2.1. Compare to Figure

2.1a (the unreinforced solder joint), Figures 2.1a, b and c are composite solder joints enhanced with spherical particles (e.g. Al_2O_3), whiskers (e.g. carbon nanotubes) and nano-sheets (e.g. graphene). The existence of different reinforcement added could alter the morphology of interfacial IMCs between solder joints and soldering pads; it might also help to improve the creep resistance and mechanical properties of composite solder joints under harsh service conditions (including high temperature, large temperature gradient and high current density) when compared with the plain solder joints[6-29].

2.2 Type of reinforcement

Based on the reactive conditions between reinforcement and molten solder, foreign reinforcement usually used can be mainly divided into three types: non-reactive reinforcement, reactive reinforcement and composite reinforcement. The specific classification, pros and cons of the reinforcement mentioned in present literatures are listed in Table 2.1.

Specifically, the non-reactive reinforcement usually including metallic oxide, carbide, carbon-based nano-materials and non-metallic elementary substance, which will not react with solder matrix during reflow and ageing process; they will also not coarsening during service period. However, since this kind of particles added cannot be wetted by the molten solder, they are usually found to be expelled from the molten solder during reflow process, leading to a result in a great discrepancy between the actual retained ratio of reinforcements in the final solder joints and their designed weight fraction[116]. The reactive reinforcement, which is widely used in present research, is mainly including metal (or alloy) materials and IMCs. This kind of reinforcement is easily to react with molten solder during reflow process and finally retained in solder joint in the form of IMCs. Nevertheless, the reactive reinforcement is prone to coarsening during service period, giving rise to a decreasing strengthening effect. Recently, researchers also produced some novel reinforcement, such as polyhedral

oligomeric silsesquioxanes polyhedral oligomeric silsesquioxane (POSS) [26] and composite reinforcement with core-shell structure; these reinforcements were reported with good stability and high retained ratio in a solder joint. However, the relatively poor thermal and electrical conductivity of this kind of reinforcement might affect the electrical performance of a solder joint. Further, the problems of complexity, high energy consumption and high cost also restricted the practical progress of this kind of reinforcement.

Table 2.1 Typical reinforcement type in composite solder research

Type	Typical materials	Examples	Pros	Cons
Non-reactive	Oxide	Al_2O_3, TiO_2, Fe_2O_3, ZnO et al[6-9]	Stable physical and chemical properties during reflow process	Low retained ratio in solder joint
	Carbide	TiC、SiC et al[10-11]		
	Carbon-based nano-materials	CNT, GNS et al[12-14]		
	Elementary substance	Diamond et al[15-16]		
Reactive	Metals	Ag, Cu, Fe, Ni, Al, Cr、Mn, Co, et al [17-24]	Higher retained ratio in solder joint	Coarsening during reflow and ageing
	IMCs	Cu_6Sn_5 et al[25]		
	Polymer	POSS[26]	Good dispersibility and high retained ratio in solder joint	Potential risk on reliability; high cost
Composite	Metal/X	Ni-coated CNT[27-28] Ag-coated GNS[29]		

According to previous literatures, in contrast to carbon nanotubes and graphene, buckyball-structural fullerenes (FNSs, of which C60 is the most common), as the first discovered carbon-based Nano material, appear to be somewhat neglected by researchers active in the composite solder research area. C60, the most typical FNS, is a stable molecule composed entirely of carbon atoms in a spherical form; its steady molecular structures result from powerful sp^2C–C bonds, which also give rise to a good electron mobility of approximately

$11cm^2/Vs$, young moduli of 400GPa and compressive strength of 100GPa [30-34]. Owing to these desirable electronic and mechanical properties, C60 has come to be regarded as a powerful reinforcement for synthesizing composite materials (especially in structural metal materials and polymer materials) during the last few decades. Using the powder metallurgy route, Watanabe et al. [35] fabricated a C60 doped Mg-Al-Zn alloy composite, exhibiting a super plasticity with 256% elongation at 548K. Chernogorova et al. [36] produced an aluminium/C60-FNSs composite by rolling the ball-milled powders. This composite revealed an extremely stable nano-structure resulting in a significant improvement in yield strength and hardness. To date, however, there have been no reports on the effects of C60 on the performance of lead-free solder alloys. Unlike CNTs (one-dimensional material) and graphene (two-dimensional material), as the zero-dimensional material, the smaller geometric size, comparable electrical and mechanical properties make C60 a potential reinforcement in the field of composite solders.

In addition, in comparison to other ceramic reinforcing particles, TiC is also a typical ceramic material with excellent chemical stability and high melting temperature (3067 ℃); it also exhibits good mechanical properties, with an elastic modulus of approximately 400 GPa and a shear modulus of 188 GPa [37-39]. Additionally, relatively high electrical and thermal conductivity also make TiC a potential reinforcement for composite solders without affecting significantly their performance.

As mentioned above, since some non-reactive reinforcements added are often found to be expelled from a molten solder during a reflow process, some researchers attempted to form a “bridge” between the reinforcement and solder matrix [40]. Some metal nanoparticles (such as Au and Ni) are regarded as ideal “bridge materials” since they are apt to react with Sn-based solder alloys to form IMCs during a soldering process. Silica nanoparticles with an Au layer were synthesized by Mokhtari et al. [41]; they reported that this core-shell structural reinforcement could be wetted by molten solder. Yang et al. [42-43] studied the

effect of carbon nanotubes with Ni coating (Ni-CNTs) on mechanical properties and microstructures of solder alloys. Their experimental results indicated that addition of Ni-CNTs contributed to improvement of performance of solder alloys. To date, however, there were few reports on the effect of Ni-modified graphene on performance of lead-free solder alloys. In this study, in view of exceptional physical and chemical characteristics of graphene, multi-layer graphene nano-sheets were thus chosen as the basic reinforcement that also served as a carrier for Ni plating. Ni was chosen as the "bridge material" since it could form IMCs by reacting with molten Sn-based solders during soldering process.

In consideration of the favourable physical and mechanical properties of FNS and TiC, as well as the unique structure and properties of NG, these three reinforcements have a great potential of application in preparing a composite solder alloy. Therefore, in this thesis, these three materials were chosen as foreign reinforcement to produce composite solders, so as to understand the effect of addition of these reinforcements on microstructures, mechanical properties and service reliabilities of SAC305-based composite solders.

2.3 Fabrication of composite solders

According to the previous literatures [44-60], methods to fabricate composite solders containing foreign reinforcement can be roughly classified as two: 1) the mechanical mixing; 2) the *in-situ* method. Specifically, foreign particles, fibres and whiskers which have been physically added to solder matrices to strengthen solder alloys are known as the mechanical method. By contrast, in the in-situ approach, precipitation hardening is the main strengthening mechanism to improve the electro-thermo-mechanical fatigue resistance of these composite solders.

2.3.1 The mechanical mixing method

The mechanical mixing method involves adding foreign particles as

reinforcements into solder powder, solder paste or molten solder alloys to fabricate composite solders. Several commonly used processing routes of this method can be summarized as follows.

- **Mixing solder pastes with reinforcement**

The most simple and direct approach to prepare composite solders is mechanically adding micro or nano-sized foreign particles into solder pastes. Liu et al. [44] mechanically mixed SiC particles (the diameter of SiC was approximately 20 nm) with a Sn–3.8Ag–0.7Cu solder paste to prepare a composite solder paste. Nai et al. produced a composite solder paste by mechanically mixing oxide-free Ag nano-particles (10–100 nm) with Sn–0.7Cu solder paste for at least 15 min to ensure the a uniform distribution of the reinforcement particles. Nano-sized TiO_2 and Cu powders were added into conventional Sn–Pb solder by Lin et al. [45-47] to obtain nano-composite lead-tin solder pastes. They weighed different percentages of TiO_2 and Cu nano-powders and a quantity of Sn–Pb solder alloy powder and then blended them physically before adding water-soluble flux to the powder mixtures. Then, the paste-like mixture was stirred for about 30 min so as to ensure a homogeneous distribution of the nano-powders in the composite matrix. After that, the composite mixture was melt in a heating system under the protection of argon gas and then the molten solder was cooled down to room temperature to obtain a solidified composite sample.

- **Mixing solder alloy powders with reinforcement particles**

Another most common method is mixing solder alloy powders with reinforcement particles directly. In such case, the composite solders are usually prepared through the powder metallurgical route. Specifically, the initial solder powder is first homogeneously mixed with foreign reinforcement using a V-blender or ball mill. After that, the ball-milled mixture is mechanically compacted into solder billets for the following sintering process. Then, the sintered solder billets are rolled or extruded into solder foils or rods before further processing. Nai et al. [48-50] prepared a multi-wall carbon nano-tube (MWCNT)

reinforced Sn–Ag–Cu composite solder using the powder metallurgical synthesis approach. They pre-weighted the desired amount of solder alloy powders and MWCNTs and then put them into a V-blender. The blender was set to a rotational motion at 50 rpm for 10 h, after which the mixture was uniaxially compacted into solder billets at 140 bar and sintered at 448 K for 2 h in an inert argon atmosphere. Finally, the composite solder billets were extruded at room temperature into solder rods with diameter of 8 mm, employing an extrusion ratio of 20:1. The same method was also adopted by Kumar et al. [51-52] to prepare single-wall carbon nano-tube (SWCNT) enhanced Sn–Ag–Cu lead-free composite solders. As well as that, by using similar processing route, the nano-Al_2O_3 strengthened Sn–In–Ag–Cu composite solder and the Sn–37Pb/Sn–0.7Cu composite solder were prepared by Nai et al. [53] and Shi et al. [54], respectively.

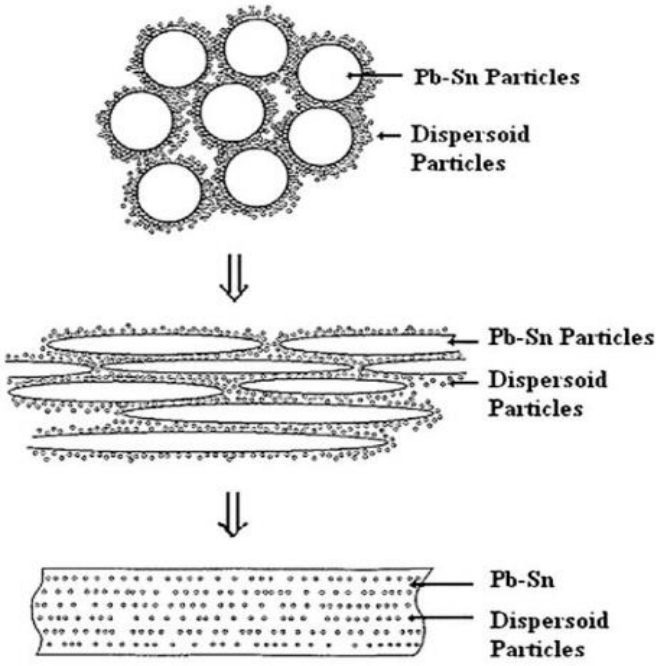

Figure 2.2 Schematic of powder mixing approach for dispersion strengthening of solder

In addition, to homogeneously distribute the foreign particles into solder matrices, Mavoori and Jin [55-56] developed an approach of coating particles and then plastically deforming them to achieve a well distribution of nano-sized particles in a solder matrix. In their researches, eutectic Sn–37Pb solder alloy powders (with diameter of 35μm) and nano-sized TiO_2 (with diameter of 5

nm)/Al_2O_3 (with diameter of 10 nm) powders were thoroughly dispersed in ethanol with vigorous shaking and mixed in the desired proportions (3% by volume of nano-particles). After a constant stirring, the slurry of Sn–Pb particles coated with the finer oxide particles was prepared, as shown schematically in Figure 2.2. The gravity-induced segregation of the oxide particles were minimized by controlling the amount of ethanol and the viscosity of the slurry. After drying, the powder mixture was compacted in a die (at room temperature) at a pressure of 196 MPa to form 50mm×10mm×5mm billets, which was then subjected to repeated compressive mechanical deformation (with a mean-compressive stress of 915 MPa) at 393 K in an inert argon atmosphere. Each compressive step resulted in a reduction of thickness, after which the flattened piece was cut into six pieces, the pieces stacked, and pressed again to get a six-fold reduction in thickness. For maximum strengthening, it is desirable to have the inter-dispersed spacing reduced as much as possible. While the inter-dispersed spacing obtained is larger than the calculated 0.8 nm spacing due to the plastic flow of the matrix alloy and the limited number of added foreign particles, a nano-scale, relatively random dispersion with a particle size distribution of 5–50 nm was observed.

- **Mixing solder component powders with reinforcements particles**

This method is essentially a mechanical alloying process to produce composite solders. Kao et al. [57] and Lee et al. [58] adopted a mechanical alloying (MA) process to prepare Sn–Ag–Cu and Sn–Ag–Ni composite solders by adding nano-sized Cu_6Sn_5/Ni_3Sn_4 IMC particles into pure Sn and pure Ag powders and then mixing them together to form nano-composite solders. An RMA flux was added into the composite powders prepared at room temperature and mixed in a glass container until uniform composite solder pastes were achieved.

2.3.2 The *in-situ* method

The *in-situ* method refers to a technique by which strengthening phases are formed upon processing the bulk solder alloys themselves. Here, the

reinforcement particles embedded in the solder matrix are not come from the introduction of foreign particles. According to present studies, there are two main *in-situ* approaches to fabricate composite solders. One approach for producing composite solders enhanced with nano-sized IMCs particles is by hot-rolling and pressing technology. Lee et al. [59] successfully prepared a Cu_6Sn_5 reinforced composite solder by this process. They added Cu powder (with diameter of 1 μm) coated with RMA type flux into a Sn–3.5Ag eutectic solder and then melted the mixture under an argon atmosphere. The molten solder with the Cu powder was mechanically stirred, while the ambient temperature was set as 573 K in order to promote the reaction between the Sn and Cu powders. After keeping at this temperature for 1 min, the solder was then quenched into alcohol to cause solidification. The solidified ingot was subsequently hot-rolled into thin sheets, which were punched into disks. The disks were re-melted in a column shaped container with silicon oil, which had a temperature gradient with the highest temperature 523 K at the top. During the sedimentation through the container, the molten disks became spherical balls with diameter of 760 μm due to the surface tension of the solder. By this process, a composite solder with uniform distribution of Cu_6Sn_5 phase was achieved.

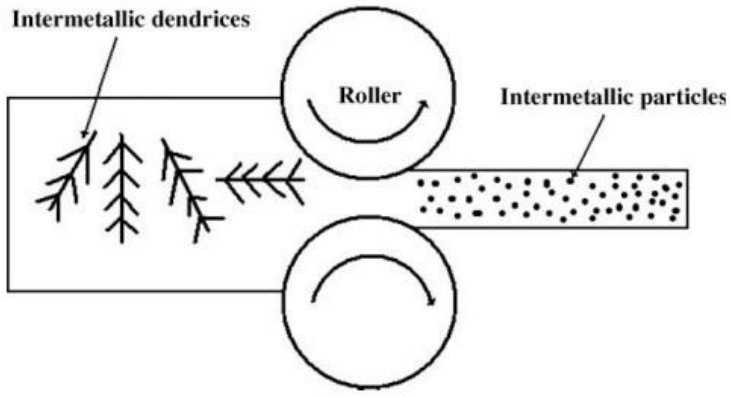

Figure 2.3 The schematic of in-situ method [60]

Another *in-situ* method was developed by Hwang et al. [60] to prepare a composite solder as follows: the pre-weighted pure Sn, Cu and Ag ingots were melted in a porous porcelain crucible under an argon atmosphere, and then the

resultant solder mixtures were cast in a steel die. The solder strips reinforced with IMC particles, were fabricated by rolling the cast ingot as shown in Figure 2.3. Each cast ingot was rolled to strip with thickness of 0.07mm, which were then punched to discs of 1.5 mm diameter. Then the solder ball with diameter of 630 μm was obtained by using a similar spheroidizing process in a hot oil bath. Since the primary IMC dendrites formed in the solder matrix during casting can be crushed into fine particles by means of plastic deforming, the IMC particles were redistributed uniformly throughout the solder matrix.

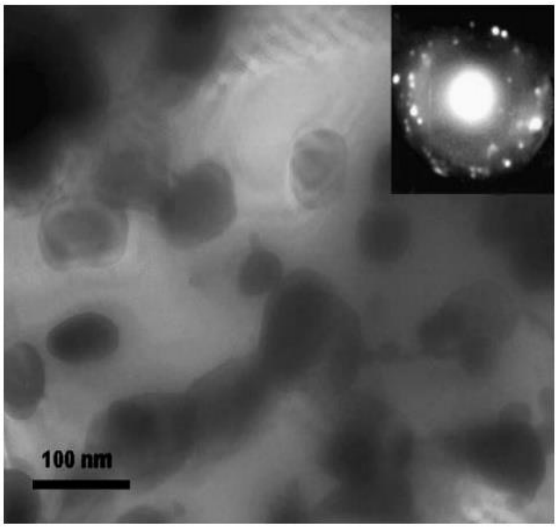

Figure 2.4 TEM images of Ag_3Sn IMC particles [61]

In addition, rapid solidification technology was adopted by Shen et al. [61] to prepare a nano-composite solder. In their research, a Sn–3.5Ag solder was produced from bulk rods of pure Sn and Ag. The melting process was carried out in a vacuum furnace under argon atmosphere to prepare button-like samples with a diameter of approximately 35 mm. In order to get a homogeneous composition within the ingot, the solder alloy was re-melted for four times. Then the molten alloy was cast into a water-cooled copper die, in which the cooling rate can reach 10^4 K min^{-1}, to obtain a rod with a diameter of 5 mm. The rapid cooling process can promote the nucleation of Ag_3Sn IMC particles and leads to rapid heat dissipation during solidification, making the long-range diffusion of Sn and Ag atoms impossible. While the nucleation of Ag_3Sn particles was greatly prompted, their growth in the alloy matrix was suppressed, thus yielding a large number of

uniformly distributed nano-sized Ag_3Sn IMCs in the solidified matrix (as shown in Figure 2.4).

2.4 Achievements with the composite solders developed

The original motivation for preparing particles doped composite solders was to improve the creep and thermo-mechanical fatigue resistance of the solder alloys, so as to utilize them under harsh service conditions. However, with the development of relevant researches in composite solders, more improvements were achieved in other aspects.

2.4.1 Micro-structural modification

As reported in recent researches, most of foreign particles added could change the microstructure of solder matrices to some extent and these variations were usually proved to be positive and helped to improve the mechanical properties of composite solders [44-47, 51-55, 63]. This phenomenon was mainly because the reinforcement added contributed to decrease the grain size in solder matrices and thus improve the strength of the solder alloys according to the Hall–Petch relationship [62]. Shen et al. [63] reported that the addition of ZrO_2 nano-particles into a Sn–Ag solder reduced the average size of Ag_3Sn phases significantly. Kumar et al. [51] reported the average size of the secondary phases (Cu_6Sn_5 and Ag_3Sn) were about 3.75–4.25 μm in the Sn–Ag–Cu solder without any reinforcement, while the size of counterparts in the 1wt% SWCNT reinforced solders were 0.5–0.8 μm. Similar results can also be found in other studies [45-47, 54-55, 44]. However, the addition of some other reinforcement in lead-free solders resulted in different microstructural evolutions due to the microstructure of lead-free solders is different from that of conventional lead-based solder. For example, the addition of a small amount of TiO_2 nano-particles to the eutectic tin–lead solder was found to give some agglomerates in the solder matrix [47]. However, for lead-free composite Sn–Ag–Cu solders, two types of IMCs (Ag_3Sn

and Cu_6Sn_5) were observed dispersed uniformly in the β-Sn matrix while with SWCNTs their distribution was at the boundaries of the Ag_3Sn grains [51].

2.4.2 Variations in melting point

The melting points of most lead-free solders are higher than those of the conventional lead-tin solders, which may lead to extra expenditure on modified or new plant and thus increases the total cost of the final product. Therefore, a main purpose in the development of novel composite solders to be used in the microelectronic industry is that the reinforcement should not significantly increase the melting point of the solder alloy. Doubtlessly adding reinforcement into solder matrix would change the composition of solder alloys and then vary the fusion and solidification processes of the solder alloy.

Lin et al. [46] reported that the addition of Cu nano-particles influenced the solidification of a Sn–Pb solder. In their research, the cooling curves of the composite solders indicated a decrease of the solidification temperature due to the Cu nano-particles dissolved in the molten solder changed the alloy composition of the solder. However, researches regarding the influence of the addition of inert nano-particles on the melting temperature of solder alloys are controversial. After carrying out differential scanning calorimeter (DSC) tests, Nai et al. [49-50] reported that no significant changes were found in the melting point of composite solders reinforced with MWCNTs. However, Kumar et al. [51-52] found that the melting points of SWCNT-reinforced composite solders were slightly decreased compared with an unreinforced solder alloy. This variation could be ascribed to the high surface free energy and interfacial instability of the SWCNT-reinforced composite solders compared to that of the unreinforced solders. The similar results were obtained by Liu et al. [44], in which a reduction (approximately, 1K) in the melting point was found in a Sn–3.8Ag–0.7Cu composite solder reinforced with SiC nano-particles. They also pointed out that this reduction of melting point was possibly ascribed to an increase in the surface instability caused by the addition of

the SiC nano-particles with a higher surface free energy.

According to Lindemann criterion [64], the melting temperature as an inherent physical property of an alloy mainly is determined by the alloy itself. The criterion point out that a crystal will melt when the root mean-square displacement of the atoms in the crystal exceeds a certain fraction of the inter-atomic distance. Since the surface atoms of a crystal usually have low coordination numbers they thus have different bonding forces to that of atoms in the bulk. As a result, increasing the number of surface atoms will significantly increase the atomic mean-square displacements, and then the melting temperature of the alloy can be decreased slightly. Thus, the melting temperature of an alloy with a nano-size scale is slightly lower than that of the bulk [65-68]. However, the addition of a small amount of inert reinforcements into solder alloys can hardly increase the number of surface atoms of the alloy significantly. In other words, the reinforcement added (especially, those inert particles) will not significantly alter the melting temperature of the alloy.

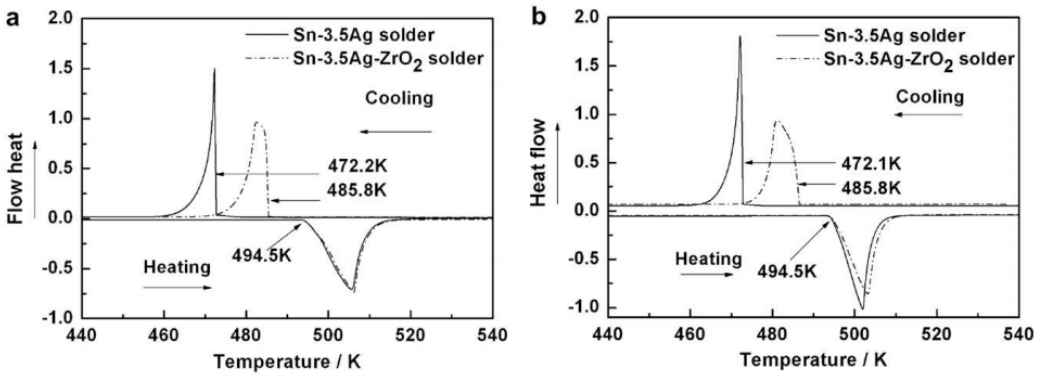

Figure 2.5 DTA curves of the Sn–3.5Ag and the Sn–3.5Ag–ZrO_2 solders in the (a) first and (b) second heat-treatment cycles [63]

In order to verify this point of view, Shen et al. investigated the melting and solidification temperatures of a Sn–3.5Ag–ZrO_2 nano-composite solder with a high precision DSC apparatus [63]. The results indicated that the melting temperature of the Sn–Ag solder was unaffected by the addition of the ZrO_2 nano-particles (as seen in Figure 2.5). However, the addition of ZrO_2 nano-particles increased the solidification temperature of the Sn–3.5Ag solder and

reduced the degree of under-cooling needed for solidification. This result can be explained by classical solidification theory that the ZrO_2 nano-particles acted as nucleation sites, promoting the nucleation in the molten alloy and thus increased the solidification temperature of the solder alloy. The resultant composite solders presented above can be applied by using existing reflow conditions because their melting temperatures were not shown an unacceptable variation.

2.4.3 Variations in wettability

It has been reported by most of researchers that an appropriate amount of foreign reinforcement (especially nano-sized particles) added into solder matrices could improve the wettability of these solders on different substrates. Lee et al. [59] reported that the wettability of a Sn–Ag–Cu solder enhanced with Cu_6Sn_5 IMC particles was improved slightly. A Sn–0.7Cu composite solder reinforced with 0.5% Ag nano-particles presented a better wettability compared to the plain Sn–0.7Cu solder. Also, Ni and Ni_3Sn_4-reinforced composite solder pastes showed a favourable wettability when compared with the unreinforced solder paste [60]. The wettability of Sn–Ag–Cu composite solders was improved by adding an appropriate amount of MWCNTs [49-50]. However, other researchers obtained some different results. Tai et al. [69] found that the contact angle of Sn–0.7Cu composite solder on the Cu substrate was increased after adding the Ag nano-particle. Liu et al. [44] also reported that the maximum contact angle of Sn–Ag–Cu composite solders was achieved when 1.5 vol. % of TiB_2 nano-particles were added. When 5 vol. % of TiB_2 nano-particles were added, the wettability was degraded. This phenomenon was ascribed to the presence of too many nano-particles inhibited the flow of molten solders by increasing its viscosity and further decreases the spread-ability of the solder.

However, up to now, the intrinsic mechanism of minor additives of foreign particles on the variations of wettability between molten solder alloys and substrates is still not clear. Hence, further research should be carried out to clarify

the mechanism for the variation in wetting.

2.4.4 Effect on growth of IMC particles

The effect of foreign particles on the growth of IMC phases in solder matrices and solders/substrates interface has been extensively investigated [6-30, 43-63]. During solidification process, the IMC phases in solder matrices are formed in the boundaries between grains, while the interfacial IMC layers between the solder and substrate, meanwhile, are formed due to an interfacial reaction. According to the present literatures, most of active particles (metal or IMC particles [17-25, 28-29, 45, 57-58]) and inert particles (ceramics and carbon nano-materials [6-15, 27, 30, 44-55]) added were found helpful to suppress the growth of IMCs phases in both solder matrices and interfaces during reflow or thermal ageing.

Amagai [70] studied the influence of Co, P, Cu, In, Sb, Pt, Al, Zn, Ge, Ni, Ag, and Au nano-particles on the growth of IMC layers between Sn–Ag lead-free solder and organic solder-ability preservative (OSP) Cu pads after four reflow cycles, the morphological evolution of interfacial IMC under thermal ageing were also observed. Their results indicated that Ni, Co and Pt nano-particles were very effective in suppressing the growth of IMC layers and improved the drop test performance compared with other particles. The morphological characteristics of the interfacial IMC layers between molten Sn–3.5Ag and Sn–3.5Ag–0.7Cu lead-free solders and pure Cu and Ni substrates were studied by Yu et al. [71]. They found that Ag_3Sn nano-particles were formed on the IMC layer surface during solidification, which would decrease the interfacial energy and supress the excessive growth of the IMC layer. In order to suppress the formation of bulk Ag_3Sn IMC particles during solder alloy solidification, Shen et al. added ZrO_2 nano-particles into a Sn–Ag solder and achieved positive results [63].

A problem should be mentioned is that the inert nano-particles as surface-active materials are more likely to accumulate at the phase boundaries in

solder alloy matrices or in interfacial IMC layers since they do not react with the metallic elements in the solder. Here, surface absorption theory can be used to explain the inner mechanism of the suppression of the growth of IMC in particles-doped composite solders during reflow and ageing. According to the theory of surface adsorption of a surface-active material [72], the surface energy of a whole crystal can be described as:

$$\sum_k \gamma_{(c)}^k A_k = \sum_k \left(\gamma_{(0)}^k - RT \int_0^c \frac{\Gamma^k}{c} dc \right) A_k \qquad (2\text{-}1)$$

Here, $\gamma_{(0)}^k$ is the surface tension of the initial crystal planes k without adsorption, $\gamma_{(c)}^k$ is the surface tension of crystal planes k with adsorption, Γ^k is the adsorption of surface-active material at crystal planes k, A_k is the area of the crystal planes k. c is the concentration of the surface-active material, T is the absolute temperature , R is the theoretical gas constant. Due to the volume of a crystal is constant; the surface energy of the crystal planes can be kept to a minimum in the equilibrium state. As shown in formula (2-2):

$$\sum_k \gamma_{(0)}^k A_k - RT \sum_k A_k \int_0^c \frac{\Gamma^k}{c} dc \rightarrow \min \qquad (2\text{-}2)$$

where $\sum k \ \gamma_{(0)}^k A_k$ is assumed to be constant because of the independence of the concentration of surface-active materials. So, $RT \sum_k A_k \int_0^c \frac{\Gamma^k}{c} dc$ should be maximized, which means the effect of the crystal plane with the maximum amount of adsorption, is most active.

In general, the crystal plane with the maximum surface energy grows rapidly. However, the foreign nano-particles which are regarded as effective surface-active agents can substantially decrease the surface energy of the crystal and therefore decreases the growth velocity of this crystal plane. From this point of view, this nano-sized reinforcement may be adsorbed on the surface of the IMC particles or IMC layers to suppress their excessive growth. However this explanation for the mechanism of the suppression of IMC growth is controversial since the explanation is qualitative. As we know, the growth of IMC during the

solidification process involves several interrelated phenomena, including grain boundary diffusion, volume diffusion, grain coarsening and dissolution into the molten solder [73]. Hence, these interrelated factors need to be deeply analysed to understand how the nano-particles added in solder matrices influence these factors.

2.4.5 Enhancement of mechanical properties

In terms of mechanical properties, the foreign particles enhanced composite solders have been reported exhibiting desirable performance (such as high hardness, high tensile strength and high shear strength) compared with solders without reinforcements added. The reinforcements, including metal, ceramic, IMC nano-particles and carbon nano-materials (such as carton nano-tube and graphene) have been reported to enhance the strength of solder matrices significantly.

Tai et al. [69] reported that the average shear strength of solder joints enhanced with Ag nano-particles was much higher than that of plain Sn–0.7Cu solder joints when the volume fraction of Ag nano-particles was higher than 1%. The creep life of Sn–0.7Cu solder joints was prolonged with the addition of 1wt % Ag nano-particles at all testing temperatures and loads. The addition of ceramic nano-particles, such as ZrO_2 [63], SiC [44], Al_2O_3 [55-56, 74], TiO_2 [47], significantly improved the hardness, tensile strength and creep resistance of nano-composite solders. Mechanical characterization results for CNTs doped composite solders revealed that the addition of MWCNTs and SWCNTs in solder matrices led to an improvement of yield strength (YS) , ultimate tensile strength (UTS) and micro-hardness of solder joints，while the ductility of composite solders decreased significantly [48-51]. In addition, nano-composite solders reinforced with MWCNTs and SWCNTs have been found more dimensionally stable than the initial solders because these nano-materials have lower coefficient of thermal expansion (CTE).

According to the classical theory of dispersing strengthening [75], the improvement of mechanical properties of composite solders could be attributed to

the presence and distribution of fine particles in the solder alloy matrices and at the grain-boundaries of solder matrices. These foreign particles tend to change the deformation characteristics of solder alloys by impeding grain-boundary sliding as well as retarding dislocation movement in solder matrices [75-76]. However, to what extent to the size of particles affect the composite solders' mechanical properties cannot reach an agreement. In order to understand the relation between particles' size and the variations in mechanical properties, Shi et al. [54] investigated the effect of the particle size scale on the mechanical properties of the composite solders. They studied the thermal creep resistance of Sn–Pb and Sn–Cu composite solders enhanced with micro-sized and nano-sized Cu and Ag particles. In their research, they found that although the tensile shear strength of composite solder joints reinforced with nano-sized particles was higher than that of composite solder joints reinforced with micro-sized particles, the composite solders reinforced with micro-sized particles exhibited better creep strength than the nano-particles doped counterparts. The reason given by them was that nano-sized reinforcements refine the alloy grains and the fine grain size causes a decrease of the creep strength, which was more effective than the increase of creep resistance by impeding grain boundaries sliding.

However, in order to obtain composite solders with high comprehensive properties, more deep investigations are needed to understand the optimum size of reinforcement particles for solder alloys with different composition and structure.

2.5 Main problems in the composite solders studied

2.5.1 Distribution of reinforcements in a solder matrix

The foreign reinforcement added is usually found to be enriched at the grain boundaries of composite solder alloys, strengthening the thermo-mechanical properties of solder joints. However, an excessive addition of reinforcement is more likely to gather together to form brittle agglomerations in solder matrices, which will harm mechanical strength of the composite solders. Hence, the

reinforcement should be distributed in a solder matrix during processing process as homogeneous as possible.

However, how to prepare a composite solder joint containing uniformly distributed reinforcements is a practically difficult work. In fact, although the composite mixtures (including solder powder or solder paste and foreign particles) are stirred for a long-term, agglomerates are still formed in composite solder matrices. To solve this problem, Mavoori and Jin [55-56] developed a novel method to prepare a composite solder by integrating mechanically mixing with a repeated pressing process. With this approach, a composite structure with a relatively uniform distribution of reinforcement was obtained, though there were some fractures existed at interfaces between the reinforcement and the matrix caused by repeated plastic deformation. Compared with mechanically mixing particles with solder powders and solder pastes, the approach of mixing particles with molten solders may achieve relatively uniform distribution of particles in solder matrices. By mixing ZrO_2 nano-particles with a molten Sn–3.5Ag solder alloy, Shen et al. [63] successfully fabricated a composite solder with a uniform distribution of the ZrO_2 particles. In their experiments, an inert gas environment was employed to avoid the oxidation of the molten alloy and only high stability nano-particles can be used for this preparation route. Because of the different densities of reinforcement and solder matrix, the reinforcement particles' settling or floating during solidification process will cause a non-uniform distribution. Hence, to obtain a relatively homogeneous distribution within the composite solder, the composite alloy needs to be re-melted for several times.

The *in-situ* method would be a better choice when considering the issue of distributing the reinforcement particles in a composite solder matrix homogeneously since the enhancing particles can be formed by the precipitation of IMC phase particles during alloy processing. These particles would distribute in the solder matrix or grain boundaries homogeneously without forming any agglomerates in composite solders.

2.5.2 Reliable bonding between the solder matrices and the reinforcements

To effectively improve the performance of composite solders, the reinforcement added must be captured by solder alloy matrices during soldering process, which means the reinforcement should be wetted by molten solder or linked with solder matrices by forming reliable bonding. Without reliable bonding between solder matrices and reinforcement particles, gas pores and other impurities will easily be formed at the surface of particles during stirring. Moreover, cracks between the reinforcements and the matrices will usually be caused during mechanical deformations, since the interfacial strength and bonding types between reinforcements and the solder matrices could significantly affect the overall mechanical performance of a composite solder alloy.

In fact, there is no difficulty for some particles, for example, metallic and some IMC particles, to bond well with solder matrix. These kinds of particles are capable of reacting with a solder matrix during preparation to form IMC layers between the particles and the solder matrix, which provide a good bonding between the reinforcement and the solder matrix. However, the bonding between inert particles and solder matrices is a tough problem since these inert particles do not react with solder alloys to produce IMC layers that can provide a reliable bonding. Thus, concerns should be given to the wetting or reaction between inert nano-particles and solder alloy matrices.

It should be emphasized that in the preparation of composite solders, although reinforcements may be successful embedded into the solder matrices, during reflow, these particles, especially inert particles, may be expelled from the solder matrices. To solve this problem, solid state bonding techniques were regarded as effective approaches [77-79]. Solid state bonding techniques, including thermal compression, thermo-sonic processes and ultrasonic bonding, have been developed for low-cost and low-temperature flux-less bonding. Since there is no melting happened during bonding process, the properties of the original prepared composite solder may be thus largely retained. Hence, the segregation of

reinforcement that restricts the industrial applications of composite solders would no longer an issue.

2.5.3 Stability of the reinforcement during reflow and ageing

Another important problem regarding the reinforcement is their stability during reflow and ageing. Foreign particles, especially inert particles added in solder alloys matrices would not coarsen. However, the nano-sized metal or IMC reinforcement introduced by mechanical mixing and *in-situ* process into composite solder matrices are facing the problem of coarsening during reflow and thermal ageing. Since these fine and uniformly distributed particles are formed by metallurgical processing, they are generally prone to coarsen at high temperature. In particular, for those composite solders prepared by the *in-situ* method, they have to experience fusion and solidification processes to form solder joints, which means the microstructure of solder joints after reflow is not the microstructure of the composite solder as-prepared.

Based on the *in-situ* method, Shen et al. prepared a composite Sn–3.5Ag solder [61], which has nano-sized Ag_3Sn IMC particles precipitated from the molten solder and distributed in the solder alloy matrix uniformly to enhance the hardness of this solder. However, the Ag_3Sn IMC particles formed in solder joints will not be in the form of nano-sized particles but in the form of bulk plates after solidification. Due to brittleness of these bulk IMC phase plates, they will affect plastic mechanical properties of the solder joints. Hwang et al. [60] stated that the Cu_6Sn_5 IMC particles were distributed uniformly in the solder matrix and coarsened but not re-melted during reflowing because the melting point of these IMC particles was higher than the reflow temperatures. However, this explanation seems to be unreliable since phase equilibrium theories and thermodynamics suggest that on melting the composite matrix a new equilibrium would need to be established which would cause the IMC particles to dissolve in the molten matrix.

Generally, most nano-sized IMC particles would dissolve into the solder

matrix during reflow or coarsen after ageing. However, if solid state bonding techniques are adopted, these IMC particles may be retained in solder matrix with keeping their initial sizes, and thus play a strengthening role. Hence, further researches regarding the novel solid state bonding techniques are needed to solve this problem.

2.6 Fundamental Concepts of EM and TM

2.6.1 Fundamentals of EM

EM is regarded as a mass transport and diffusion-controlled process due to the momentum transfer between conducting electrons and diffusing metal atoms under an applied electric field. The drifting electrons collide with atoms causing one of the atoms to exchange position with a neighbouring vacancy during current stressing. According to Huntigton and Grone [80], the driving force for EM can be described as:

$$F_{em} = (Z^*_{el} + Z^*_{wd})eE = Z^*eE = Z^*e\rho j \quad (2\text{-}3)$$

Here, Z^*_{el}, Z^*_{wd} and Z* are the effective charges of the wind force, direct force and the net force respectively; e is the electron charge, E is the static electric field, j is the current density and ρ is the resistivity. The flux of metal atoms induced by EM can be expressed using an electrostatic analogue and Einstein's equation for diffusion in a potential field:

$$J_{em} = C\frac{D}{kT}Z^*e\rho j \quad (2\text{-}4)$$

where J_{em} is the atomic flux, C is the atomic concentration, D is the thermally activated diffusivity, k is Boltzmann's constant and T is absolute temperature, and kT means the average thermal energy. Z* is effective charge number.

EM has been known as a reliability problem in electronic since 1960s when thin film Al conductors were found to exhibit EM behaviour [81]. However, in the present, demand with respect to miniaturization, resistance-capacitance delay and cost, the industry has moved to Cu-based metallization for chip level

interconnection. Hence the investigation of EM reliability of such an interconnection system is essential. Recently, with the continuous scaling down of dimensions and increase of current densities of solder joints, EM has been a critical reliability concern in solder joints. According to Huntington diffusion model [80], depending on the T_H (T_H is 373K/TM), EM phenomenon can be classified into three types. Usually, solder typically operates well above $T_H > 0.5$ with diffusion where lattice and grain boundary diffusion coefficients are of the same order.

2.6.2 Fundamentals of TM

TM is also known as mass transport caused by a driving force resulting from a thermal gradient. By now, the physical mechanism of TM is not well established. The most accepted theory is related to EM in that the force acting on the diffusing atoms is the momentum exchange from the collisions of diffusing atoms and conduction electrons. The force in the direction of the thermal gradient results from the fact that the energy, and therefore the momentum of the electrons at higher temperatures are greater than that at low temperature. The gradient in the momentum exchange produces a driving force for the mass transport [82]. The driving force for TM is depicted as:

$$F_{tm} = -\frac{Q^*}{T}\left(\frac{\partial T}{\partial x}\right) \tag{2-5}$$

where F_{tm} is the effective driving force of TM, Q* is the heat of transport, T is the temperature in the solder joint, and $\partial T/\partial X$ is the temperature gradient. Also, the atomic flux due to TM can be expressed as:

$$J_{tm} = C\frac{D}{kT}F_{tm} = C\frac{D}{kT}\frac{Q^*}{T}\left(-\frac{\partial T}{\partial x}\right) \tag{2-6}$$

Here, C is the atomic concentration, D is the diffusivity and k is Boltzmann's constant, Q* is the difference between the heat carried by the moving atom and the heat of the atom at the initial state (the higher temperature end or the lower temperature end).

In most solids, Q* is rather small, and TM has been generally neglected.

However, TM has been found in many solder alloys. The Pb-In alloy system has received some attention with respect to TM [83-84]. Under a thermal gradient of 1200℃/cm, both Pb and In moved towards the lower temperature side. Sn-Pb solder system is a typical binary alloy system, TM can be easily observed if the solder alloy is subjected to a large thermal gradient and many results have been reported of TM in Sn-Pb solder joints. However, TM behaviours in lead-free solders are rarely reported.

2.7 Effects of EM on solder joints

2.7.1 Effects of EM on the micro-structural evolution of solder joints

During the current stressing, phase separation and coarsening are likely to occur in the solder alloys due to the different atomic diffusivities under a range of operation temperatures [85]. The effects of current stressing on the micro-structural evolution of a solder joint have gained more attention because the micro-structural evolution is closely related to the thermal fatigue of a solder joint [86].

Ye et al. [87] investigated the effects of a current on Pb phase coarsening in Sn37Pb solder joints. Figure 2.6 shows micro-structural images of solder joints after current stressing, in which phase coarsening is shown. Their results showed that a higher current density leads to faster grain coarsening. Based on the test results, a grain coarsening equation was proposed:

$$d^{5.5} - d_0^{5.5} = Kj^3t \qquad (2\text{-}7)$$

where d is grain size, d_0 is the initial grain size, K is the grain boundary mobility parameters, j is the current density and t is time. They concluded that electric current has a greater influence on Pb phase growth in the solder joint than TM caused by the thermal gradient due to Joule heating during current stressing.

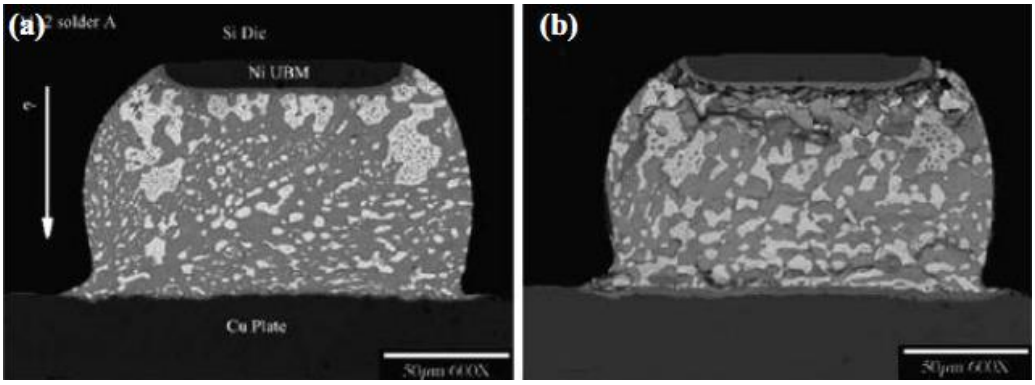

Figure 2.6 SEM images of Sn37Pb solder stressed with current density of 1.13 A/cm^2: (a) before current stressing, and (b) after 36 h [87]

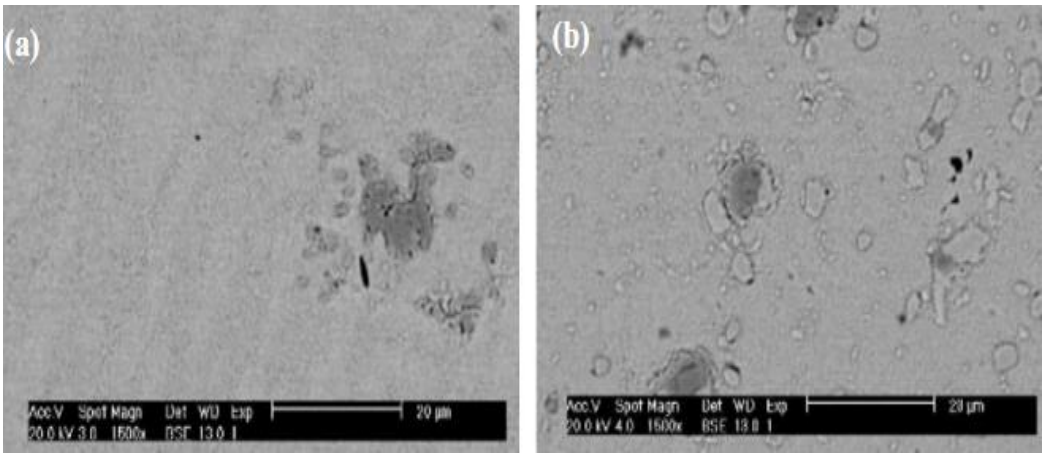

Figure 2.7 Ag-rich particle coarsening in Sn3.5Ag0.5Cu solder joints after current stressing: (a) as-reflowed (0 h), (b) stressed at 125℃ for 600 h [88]

For lead-free solder, Ag-rich phase coarsening was also investigated in Sn3.5Ag0.5Cu solder joints during current stressing [88]. As shown in Figure 2.7, Ag-rich phase growth was observed to be accelerated by current stressing as a result of enhanced diffusion at elevated temperatures and atomic stimulation due to numerous collisions between electrons and atoms.

2.7.2 Effects of EM on the IMC growth of solder joints

The interfacial IMC layer between the solder and the under bump metallization (UBM) is crucial in electronic packaging, which is not stable and grows in reflows and during ageing with service time. However, excessive IMC growth will have an adverse effect on the reliability of the solder joints. Many researchers [89-93] studied the effects of EM on the growth of the IMC layers in

various solder joints and several mechanisms of the effects of electric current on the IMC growth have also been proposed.

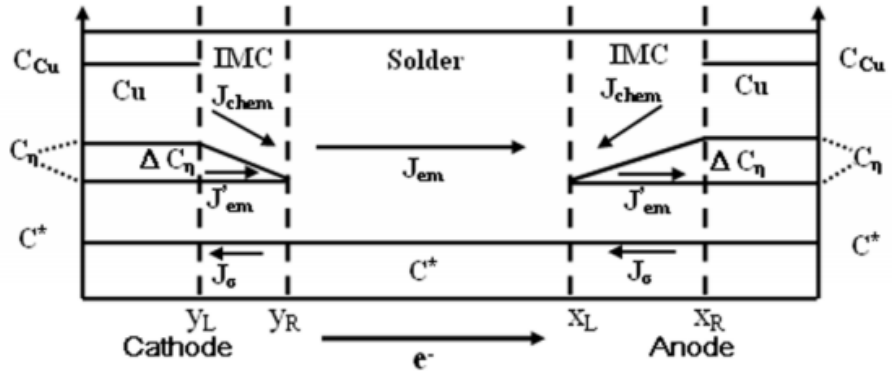

Figure 2.8 Cu atomic flux and concentration profile in a Cu/solder/Cu solder joint undergoing EM [91]

Gan et al. [91] investigated the effects of EM on Cu/Sn3.5Ag0.5Cu/Cu solder joints. Their results showed that the growth of the interfacial IMC layer was accelerated by the electric current at the anode and was retarded at the cathode compared with the no-current case. Furthermore, they found that the growth of the IMC layer at the anode follows a parabolic growth rule. So a kinetic model, based on the Cu mass transport in the sample, was presented to explain the growth rate of the IMC layer at the anode and cathode, as shown in Figure 2.8. In this model, the most important effect is the mass flux (J_σ) induced by the back stress. According to the Nabarro-Herring model [94], with a short interconnect undergoing EM, an electric current pushes atoms towards the anode and builds a compressive stress there, leading to a lower vacancy concentration at the anode side and a higher vacancy concentration at the cathode side. As a result, the vacancy concentration gradient along the sample induces an atomic flux J_σ in the opposite direction to the flux due to EM. J_σ can be described as:

$$J_\sigma = -C\frac{D}{kT}\frac{d\sigma\Omega}{dx} \tag{2-8}$$

By taking the mass flux induced by the back stress into consideration, the atomic flux in a joint can be expressed as:

$$J = J_{chem} + J_{em} + J_\sigma = -D\frac{\partial C}{\partial x} + C\frac{D}{kT}Z^*e\rho j - C\frac{D}{kT}\frac{d\sigma\Omega}{dx} \tag{2-9}$$

where J_{chem} is the diffusion term caused by the chemical potential gradient. This model is in good agreement with the experimental data.

2.7.3 Effects of EM on mechanical degradation of solder joints

The reliability of solder joints often depends directly on the mechanical properties of the solder alloy, so investigating the effects of EM on the mechanical degradation of solder joints is essential. Understanding the mechanism of mechanical degradation of solder joints under EM is an important part to develop a damage model to predict the reliability of solder joints.

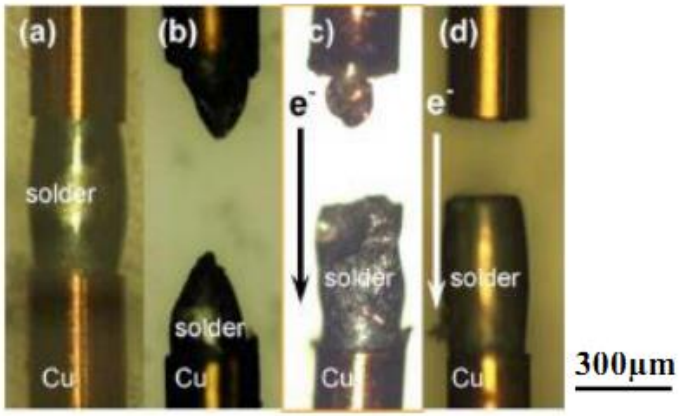

Figure 2.9 Fracture images of tensile tests after EM test: (a) Optical image of original sample, (b) image of fracture without EM, (c) image of fracture after EM, 5×10^3A/cm^2 at 145 ℃ for 96 h, (d) image of fracture after EM, 5×10^3 A/cm^2 at 145 ℃ for 144 h [95]

Ren et al. [95] studied the effects of EM on the ductile-to-brittle transition in one-dimensional bamboo-type solder joints. Their results showed that the ductility of the sample became worse after a long time of EM testing. As shown in Figure 2.9 (c) and (d) that rupture of the solder joints after EM testing was occurred at the cathode interface instead of fracture in the middle of the solder without current stressing (as shown in Figure 2.9b).

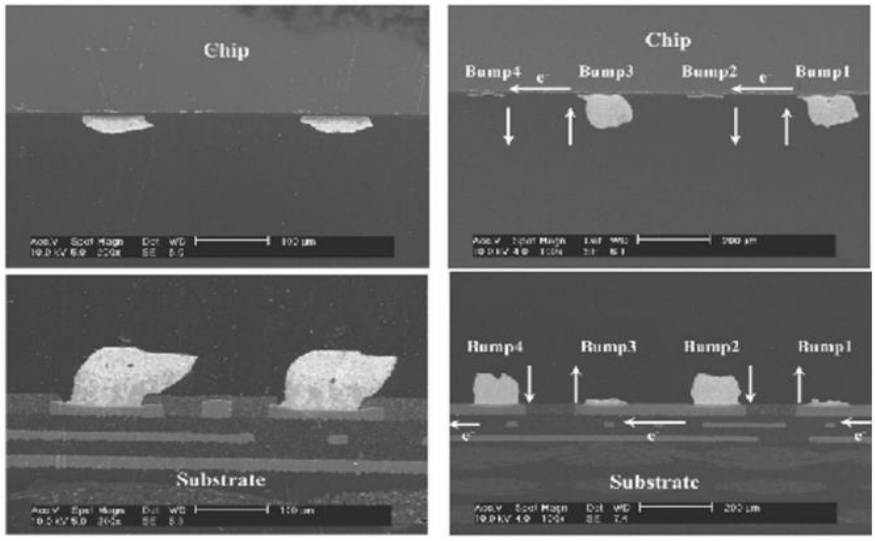

Figure 2.10 SEM images of solder joints after mechanical shear test with or without current stressing [96]

Nah et al. [96] studied the effects of EM on the shear behaviour of solder joints consisting of Sn97Pb and Sn37Pb composite solder joints. They found the failure mode changed after EM test and the mode depends on the direction of electron flow during EM. As shown in Figure 2.10, shear-induced fracture occurred in the solder on the chip side without current stressing, however, after 10 h current stressing at $2.55\times10^4 A/cm^2$ at 140 ℃, it occurred at the cathode interfaces between the solder and IMC.

2.8 Failure modes of EM in solder joints

According to the present literature, the EM failure modes and mechanisms for solder joints could be void formation, hillock extrusion, current crowding, phase coarsening and segregation, dissolution of the UBM and fast development of the IMC layer [98-102]. However, it must be noted that the EM failures in solder joints are usually occur together in solder joints undergoing EM.

2.8.1 Current crowding in solder joints

Figure 2.11 (a) shows FEM simulation of current density distribution,

indicating serious current crowding distribution in solder bumps [98]. A corresponding test vehicle was designed and implemented to verify the simulation results. A cross sectional SEM image of two solder bumps after current stressing with 1.68×10^4A/cm^2 at 125 ℃ for 1431 h is shown in Figure 2.11b.

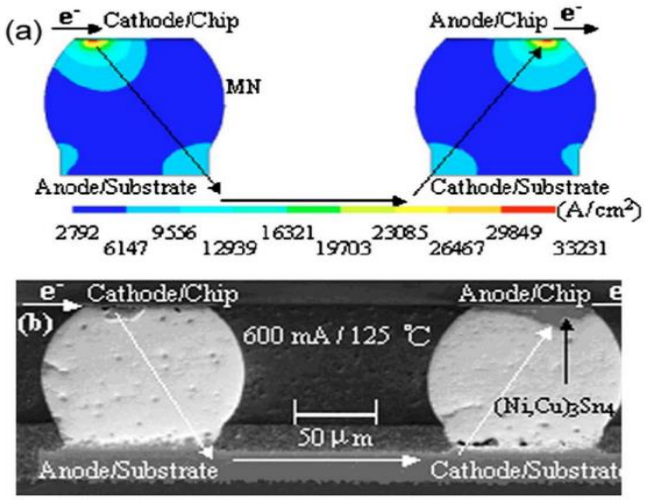

Figure 2.11 (a) Current density distribution in the solder bumps, (b) SEM images of solder bumps after stressed with a current of 1.68×10^4A/cm2 at 125 ℃ for 1431 h [98]

It can be seen that voids formed at the entry points of both the cathode/chip and the cathode/substrate sides of the solder bumps along the electron flow path. The IMC grew and accumulated at the outgoing points of both the anode/chip and anode/substrate sides along the electron flow path.

2.8.2 Voids formation and propagation in the interface

Another typical failure mode of EM is the propagation of voids across the contact interface between the solder bump and UBM. Chiu and Chen [99] investigated the void nucleation and propagation in solder joints during EM test by using X-ray microscopy. Figure 2.12 shows the X-ray images of the four samples stressed with 0.8 A current at 150 ℃ for 37.8 h, 110.2, 177.8 h, and 384.0 h, respectively. Larger voids formed with an increase of time, and the voids propagated from the left-hand side to the right-hand side.

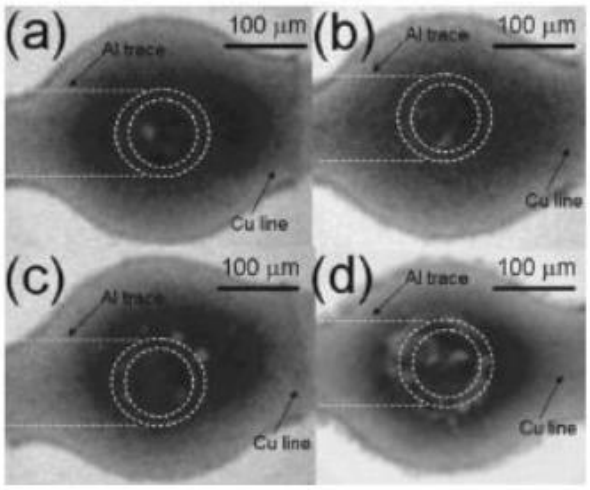

Figure 2.12 X-ray images of a Sn37Pb solder joint after stressing with 6.5×10^3A/cm^2 at 150 ^{o}C for (a) 37.8 h, (b) 110.2 h, (c) 177.8 h, and (d) 384.0 h [99]

They also found that voids started to form at approximately 10% of the failure time and grew for the remaining 80% of the failure time. Under this current stressing condition, the incubation time for void formation was about 20 hours and this was relatively short compared with the void propagation time. The void growth velocities in the initial stages increased from 1.3μm/h to 1.8μm/h with an increase of time, and it decreased to 0.3μm/h in the later stages. It must be stressed that the processes of voids incubation and growth always depend on the UBM, solder and the test conditions. So it was rational for different researchers to get different results in their test structures [99-100].

2.8.3 Joule heating enhanced dissolution of UBM and the metal trace

Joule heating enhanced dissolution of the UBM is another important failure mode of EM in solder joints. During current stressing, metal traces are the major heat source due to the small cross sectional area. Figure 2.13 shows the FEM simulation results of temperature distribution inside the solder when a joint was powered with a 0.59A current at 70℃ [101]. It was clear that the temperature of the Al trace is much higher than the solder. A hot spot was found in the entrance point of the Al traces.

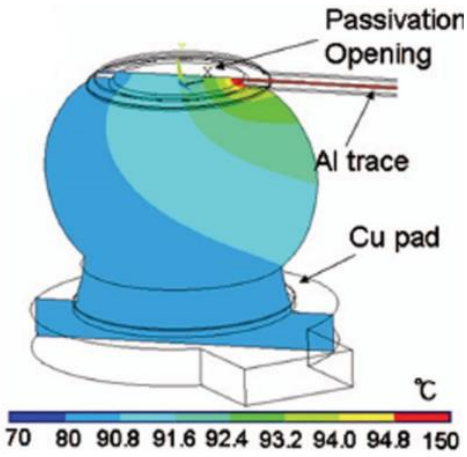

Figure 2.13 FEM simulation results of temperature distributions inside a solder joint [101]

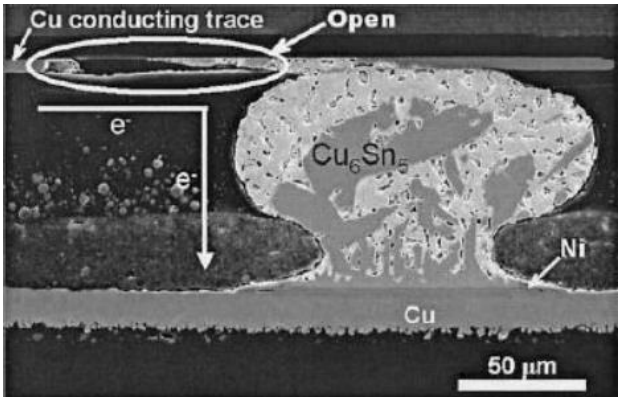

Figure 2.14 SEM image of a failed Sn37Pb solder joint [102]

Figure 2.14 is the real failure case of Joule heating enhanced dissolution of the UBM. It was obvious that the part of the Cu trace and the UBM were dissolved into the solder [102].

2.9 TM behaviour of solder joints

2.9.1 Thermal gradient in the flip chip solder joints

As mentioned above, TM is mass transport induced by a large thermal gradient. Obtaining the temperature distribution is important to understand the TM behaviour of solders joints. Ye et al. [103] obtained a temperature distribution map in a solder joint by FEM simulation. Their results showed that the thermal gradient was about 1500℃/cm when the solder joint stressed with a current density of $1.3\times10^4 A/cm^2$ at 23^oC.

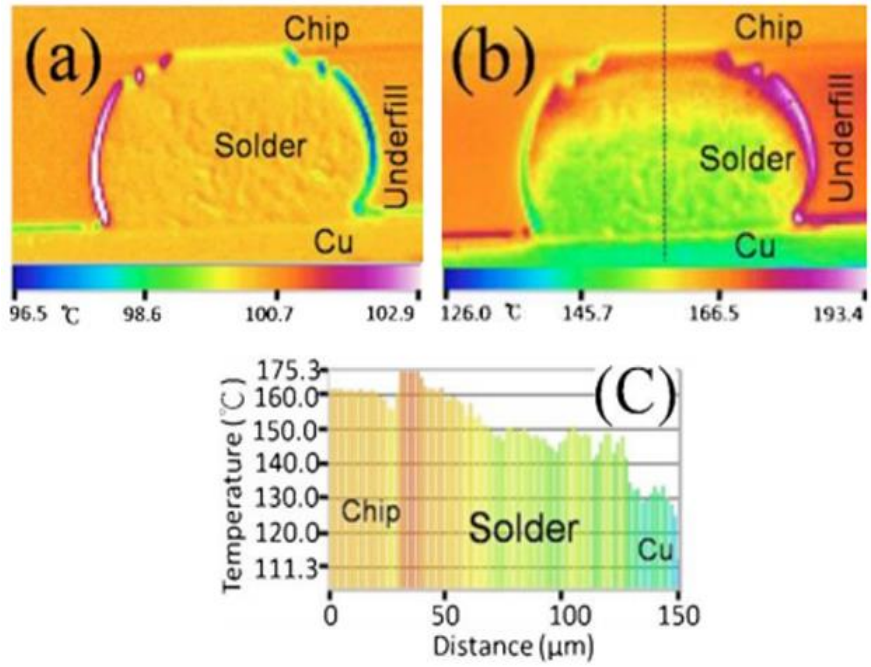

Figure 2.15 (a) Temperature distribution of the bump before current stressing, (b) temperature distribution in the bump powered by a current density of 9.2×10 A/cm^2, and (c) temperature profile along the dashed line in (b) [104]

By using infrared microscopy, Hsiao and Chen [104] measured the temperature gradient in a cross-sectioned solder joint when it was powered with an alternating current (AC) density of 9.2×10^4 A/cm^2 at 100 ℃. Before supplied with an AC current, temperature distribution in solder was uniform (as shown in Figure 2.15a), while after the solder joint supplied with an AC current the temperature gradient was created across the solder joint (as shown in Figure 2.15b). Figure 2.15c shows the temperature profile along the dashed line in Figure 2-14b. The thermal gradient was calculated to be 2143℃/cm. This study is important because it verified the existence of a large thermal gradient across real flip chip solder joints by the experiment instead of relying on simulation.

2.9.2 TM in tin-lead solder joints

Ye et al. [103] reported that TM accompanies EM in Sn37Pb FC solder joints, and they found that the Pb migrated towards the lower temperature side while Sn migrated towards the higher temperature side. TM may assist or counteract EM

depending on the direction of the thermal gradient. Huang and co-workers have carried out extensive studies on the TM in Sn-Pb solder joints [105-106]. They proposed a way to investigate the individual TM in FC solder joints. Also the atomic flux induced by TM was estimated. By measuring the net atomic flux from accumulation of Pb, the mole heat transport of Pb under a thermal gradient of 1000°C/cm was estimated to be -25.3kJ/mole.

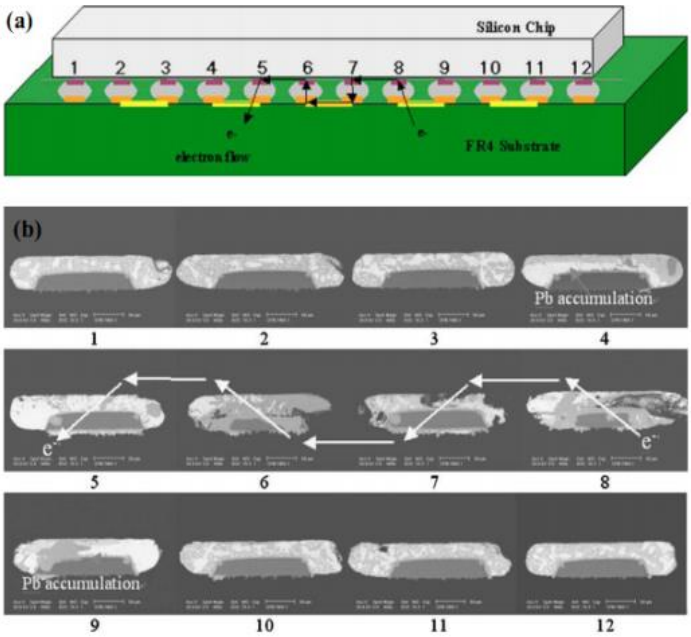

Figure 2.16 (a) Sketch of solder joints with four solder joints (5–8) under current stressing, (b) SEM images of a row of solder joints from joints 1 to 12, with solder joints from joints 5 to 8 under current stressing after 50 h at 150 ℃ [107]

Yang et al. [107] investigated the individual contribution of TM on microstructural evolution and atom migration in Sn37Pb solder joints. Figure 2.16a was a sketch of the FC solder joints used by them. Two pairs of solder joints (joints 5, 6, 7, and 8) were powered with a current of 1.8 A at 150 ℃. Unpowered solder joints, especially the most adjacent joints (joints 4 and 9) to the stressed joints, were investigated for the TM study. According to the cross-sectional observations (as shown in Figure 2.16b) after the current stressing, it is noticeable that in joints 4 and 9, the Pb-rich phase had accumulated at the substrate side (lower temperature). As the joints 4 and 9 were not powered, the driving force of the atomic transport comes from the thermal gradient created by the Joule heating.

Also, the driving force of TM was estimated to be of the order of 10^{-17} N, which reached the same order as that in EM under a current density of 10^4A/cm^2.

2.9.3 TM in lead-free solder joints

Although, many researchers have reported TM occurred in eutectic Sn-Ag solder and Sn-Ag-Cu solder, the mechanism of TM in lead-free solders is still unclear [108-113]. Mechanisms proposed by different researchers did not agree well with each other. Lin and Kuo reported the combined effects of EM and TM in Sn3.0Ag0.5Cu solder joints [108]. Regardless of the direction of electron flow, they found that voids formed at the interface on the chip side. Voids also formed at the interface even though the current flowed along the Al trace. They proposed that the solder mass (mainly Sn) moved from the higher temperature side to the lower temperature side. However, Hsiao and Chen found that Sn atoms migrated to the higher temperature side by stressing the Sn3.5Ag solder joints with a 1.01×10^4A/cm^2 AC current [109]. AC current eliminated the EM effect and creates a thermal gradient of 2829 ℃/cm, which facilitates the study of TM. Arrays of tiny markers fabricated by a focused ion beam were employed to measure the TM rate. The TM flux and molar heat of transport were measured to be 5.0×10^{12} atoms/cm^2 and 1.36 kJ/mol, respectively.

Chen et al. [110] reported the failure induced by TM with interstitial diffusion of Cu in Sn3.5Ag solder joints. As shown in Figure 2.17, it was noticeable that all the voids formed at the interface on the chip side of the powered bumps or the unpowered bumps, regardless the direction of the electric current. They proposed that the fast interstitial diffusion of Cu from the Cu UBM into Sn the solder left behind supersaturated vacancies for void formation. The driving force for the Cu diffusion was the large thermal gradient accredited to Joule heating across the solder bumps. A critical thermal gradient of approximately 400 ℃/cm was calculated, above which the TM force would be bigger than the EM force used in their study.

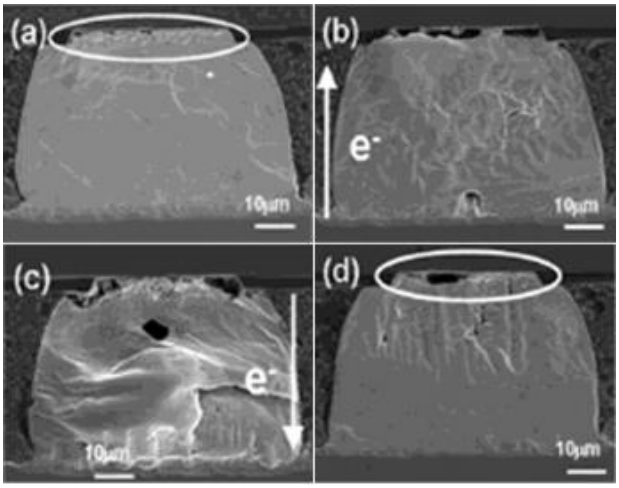

Figure 2.17 Cross-sectional SEM images showing the micro-structural changes of the joints after current stressing at 9×10^4A/cm^2 at 150 ℃ for 76 h: (a) and (d) unpowered solder joints, (b) and (c) powered joints [110]

In addition, Basaran et al. [111-113] conducted extensive studies on TM in Sn4.0Ag0.5Cu solder alloy, using a fully coupled thermo-mechanical-diffusion model with nonlinear material properties; they investigated the TM degradation mechanism in Sn4.0Ag0.5Cu solder alloy. Their results showed that grain coarsening effect played an important role in TM related phenomenon. TM-induced stresses were well above the yield stress. A damage evolution model using entropy production rate as a metric was utilized to evaluate the degradation in solder joints subjected to high temperature gradients. By applied Sn-Ag-Cu solder with 1000℃/cm thermal gradient driving force, the hardness degradation from the cold to the hot side was observed experimentally, while hardness degradation was not observed across the solder joint for isothermal ageing samples [113]. They proposed that hardness degradation could be attributed to Sn-grain coarsening at the hot side. Moreover, samples subjected to isothermal annealing exhibited IMC growth. In samples subjected to TM, the Cu concentration near the cold side was significantly higher than that near the hot one, which indicated the Cu atoms tended to migrate to the cold side during the TM testing.

Chapter 3 Preparation and Microstructures of Composite solders

3.1 Introduction

In this chapter, fullerene and TiC nanoparticles were chosen as the reinforcement to form composite solders. In addition, a novel composite reinforcement–Ni-coated graphene (NG)–was also synthesised through an electroless plating method. Then, the processing details of fabricating three composite solders with different reinforcement added were presented as well. After that, the composite solders were studied concerning about the retained ratios of the reinforcement added, microstructures, wettability, electrical resistance, CTE and melting points extensively.

3.2 Materials

3.2.1 SAC305 solder powder and paste

In this research, 96.5Sn–3Ag–0.5Cu (wt. %) alloy powder with average particle diameter of 35 μm (Beijing Compo, China) were used as matrix materials; as shown in Figure 3.1.

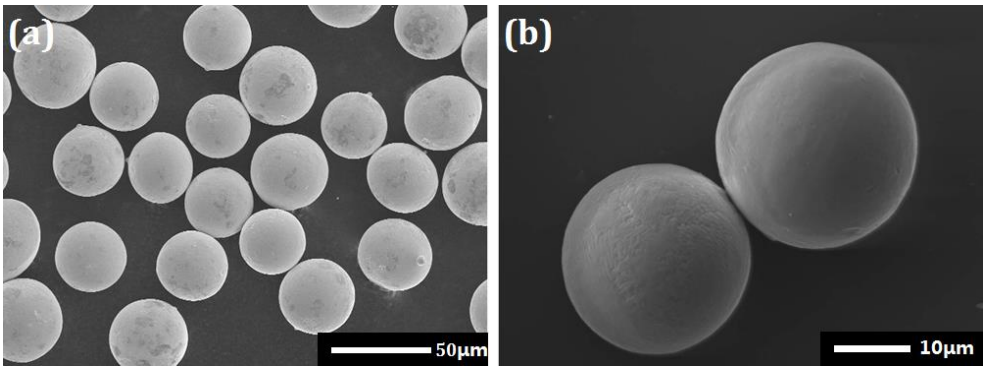

Figure 3.1 SEM images of SAC305 solder powder

3.2.2 Fullerene nano-particles

The Fullerene (FNS) nanoparticles (a mixture of approximately 80% C60 and 20% C70） utilized in this study, were purchased from JCNANO Materials Tech (China). Figures 3.2a and b shows the transmission electron microscope (TEM) images of the FNSs nanoparticles (with an average diameter of about 25-35nm). The X-ray diffraction (XRD) was carried out to identify the phase structure of the FNSs nanoparticles. As shown in Figures 3.2c, the XRD spectrum shows the FNSs nanoparticles appeared crystalline phase with characteristic peaks, which is in consistence with findings reported by Takashi et al [114].

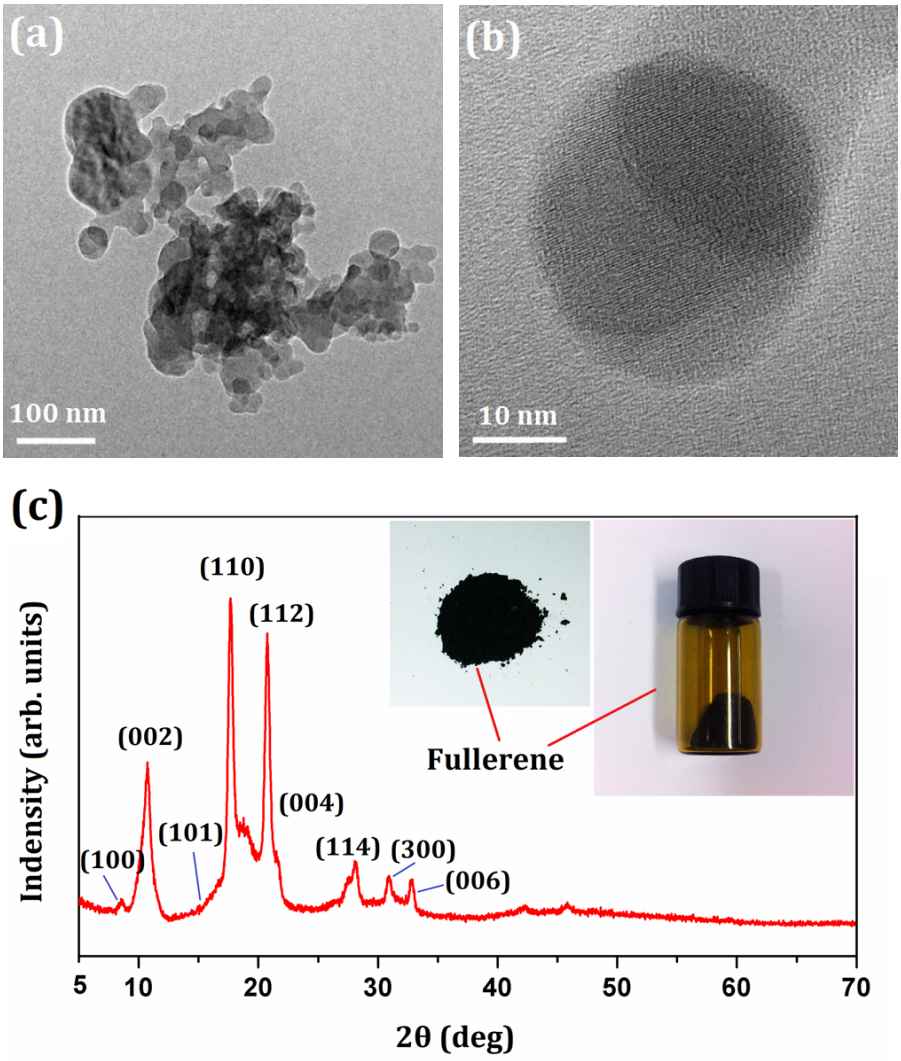

Figure 3.2 Bright field TEM image (a), HRTEM image (b) and XRD profile (c) of FNSs nanoparticles

3.2.3 Titanium carbide (TiC) nano-particles

TiC nanoparticles (with diameter in the range of 20-40 nm) used as reinforcement in the present work were provided by XFNANO Materials Tech (China); their TEM images are shown in Figure 3.3.

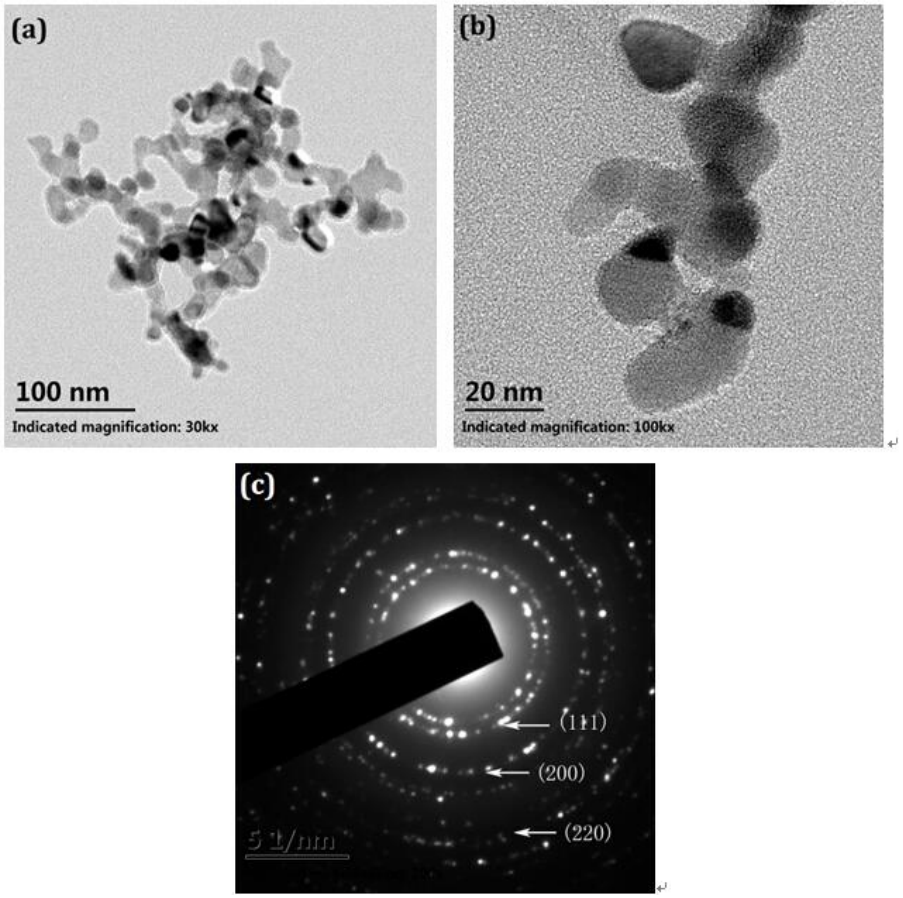

Figure 3.3 TEM images of the original TiC nanoparticles: (a) and (b) bright-field images: (c) selected area diffraction pattern

3.2.4 Synthesis and Characterization of NG

3.2.4.1 Synthesis of NG

For preparation of NG, the multi-layer graphene nanosheets provided by JCNANO Materials Tech (China) with size of 3-10μm and thickness of 5-10 nm, were used as the carrier for Ni plating; all chemistry reagents were purchased from Aladdin, China. The synthesis of NG process included three steps: (1) ultrasonic dispersion, (2) sensitization and activation, and (3) electroless Ni

plating. All these three steps are shown in a schematic diagram in Figure 3.4.

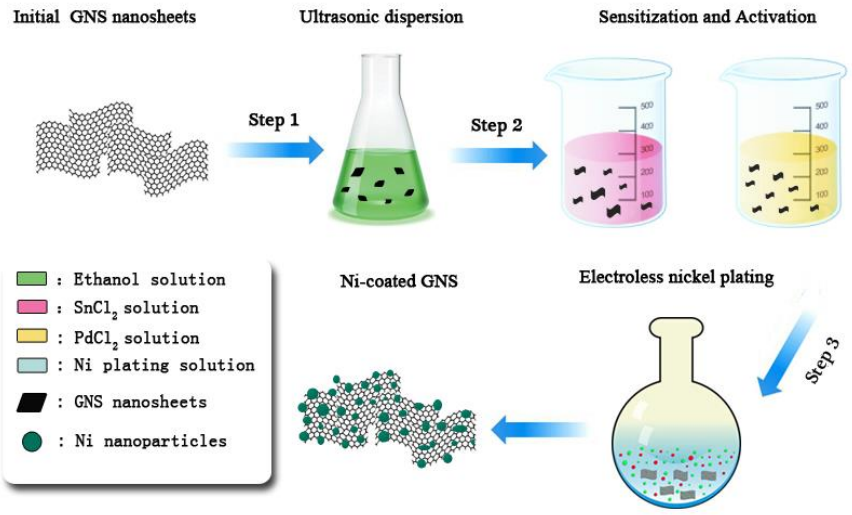

Figure 3.4 Schematic of preparation of Ni-decorated nano-sheets

In order to improve the dispersion of GNS nanosheets in chemical reagents, the as-purchased GNS nanosheets were first ultrasonically dispersed in ethanol solution (step 1). After that, the nanosheets were further sensitized and activated subsequently in $SnCl_2$ (10g/L) and $PdCl_2$ (0.5g/L) solutions (step 2). In the Ni-plating process (step 3), $NiSO_4$ was used as a source of Ni^{2+} while $N_2H_4{\cdot}H_2O$ was a reducing agent. After Ni plating, the NG were filtered in a centrifugal filter and dried in a vacuum furnace at 50 ℃ for 24 h.

Table 3.1 The components of plating solution and experimental condition

Bath composition		**Plating condition**	
$NiSO_4{\cdot}7H_2O$	25 g/L	pH	10
$N_2H_4{\cdot}H_2O$	30 g/L	Temperature (T)	90 ℃
Sodium tartrate	10 g/L	Ultrasonic power	90 W
Sodium citrate	30 g/L	Time	30 min
$(NH_4)_2SO_4$	50 g/L	GNS powder	0.5 g/L
$NH_3{\cdot}H_2O$	5%		

The components of the plating solution are listed in Table 3.1 together with experimental conditions. Morphology characterization of Ni-coated graphene nanosheets was performed with a FE-SEM (Sirion 200) system together with an Energy Disperse Spectroscopy (EDS).

3.2.4.2 Characterization of NG

As shown in Figure 3.5a, folds and wrinkles were observed on the surface of initial multi-layer GNSs, which are characteristic features of thin 2-D graphene [115]. After Ni plating, the surface of graphene nanosheets (see Figure 3.5b) exhibited a grainy morphology. From the magnified images (Figures 3.5c and d), it can be seen that Ni nanoparticles with an average diameter of 100 nm were successfully deposited on the surface of GNSs.

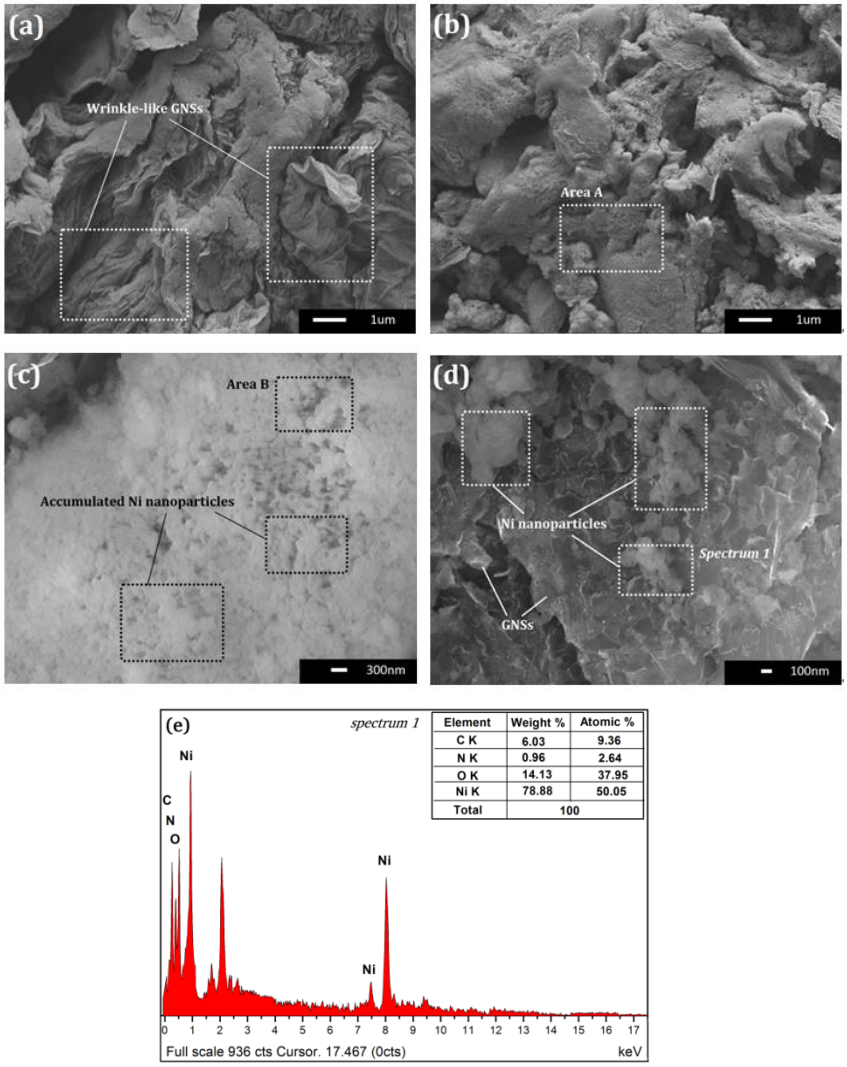

Figure 3.5 (a) Initial GNSs, (b) as-prepared NG, (c) magnified micrographs of Area A; (d) magnified micrographs of Area B

Results of EDS indicated weight fractions of C and Ni in the chosen location (marked in Figure 3.5d) - 6.03% and 78.88%, respectively. This result helped to confirm the existence of Ni nanoparticles on the GNS surface; the elements N and

O appeared in the EDS spectrum might be caused by residual reagents and oxidation.

Table 3.2 Elemental composition of the as-synthesised Ni-GNS

	C (wt. %)	Ni (wt. %)	Impurities (wt. %)
#1	34	44	22
#2	44	38	18
#3	41	40	19
#4	35	41	24
#5	43	39	18
Average	39.4	40.4	20.2

In addition, to further know the actual content of C and Ni in this newly synthesised NG, 5 samples (50mg for each sample) were tested using ICP-OES; the weight fractions of C and Ni in NG were also correspondingly calculated and presented in Table 3.2. As can be seen in Table 3.2, the average weight fractions of C and Ni in the initial NG composite are 39.4% and 40.4%, respectively. The average weight fraction ratio of C and Ni can be thus calculated as 0.98.

3.3 Preparation of composite solders

As mentioned in Chapter 1, there are two main methods to prepare composite solders, namely, the mechanical mixing and the *in-situ* methods. However, in consideration of many potential problems (e.g. coarsening of secondary phases during thermal ageing) existed in the *in-situ* method, only the mechanical methods were discussed in this part. For the mechanical methods, two commonly used approaches are mixing solder paste with reinforcement and the powder metallurgical route. To facilitate preparation of samples for different testing purposes in the later, the powder metallurgical route was selected as the method to preparation composite solders in this research. The main processing processes of the powder metallurgical route were shown in Figure 3.6.

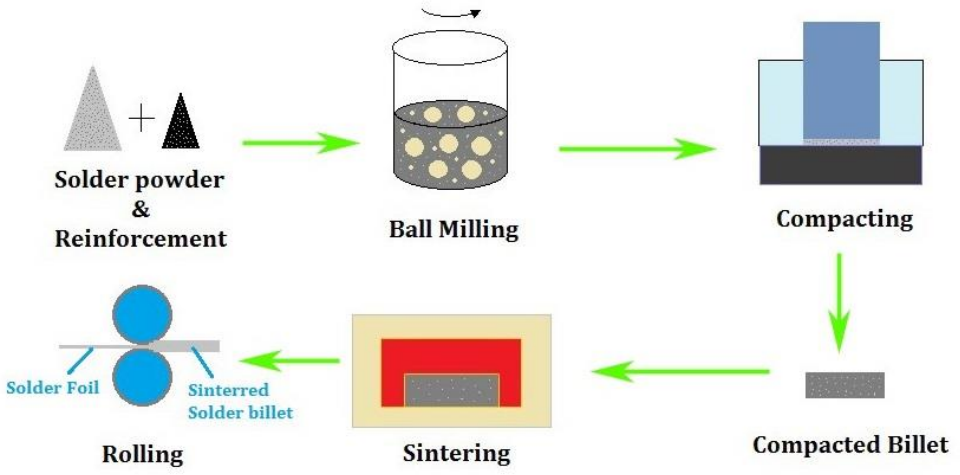

Figure 3.6 Schematic diagram of powder metallurgic method

Specifically, to prepare the composite solders for this study, reinforcements (FNS, TiC and NG) with different weight fractions (0%, 0.05%, 0.10% and 0.20%), were homogeneously blended with the as-purchased SAC305 lead-free solder powder using a planetary ball mill for 20 hours at speed of 180 rpm. Specifically, to avoid impurities (especially, other metal elements) introduced by mixing, milling jars and balls made of super-hard zirconia were employed as the milling media. Then, the ball-milled solder powder was uniaxially compacted into cuboid solder billets (with dimension of 24 mm × 8 mm × 4 mm) using a hydraulic compressor before sintered in a vacuum oven with sintering temperature of 180 ℃ for 3hrs. Finally, the sintered solder billets were rolled into solder foils with thickness of 200±20 μm or 100±10 μm at room temperature (≈20 ℃). The as-sintered solder billets were directly subjected to coefficient of thermal expansion (CTE) and electrical testing. For the convenience of wettability, melting behaviour, microstructural and mechanical analysis, the solder foils with thickness of 200μm were further formed into solder balls (800±10 μm in diameter) in a reflow oven. Specifically, the solder foils were first cut into small pieces with identical shape. Then, the cut solder pieces were placed on an Al2O3 plate coated with no washing flux. After that, the plate with solder pieces was put into a reflow oven to form solder balls needed. In addition, the solder foils with thickness of 100 μm were used to prepare the samples for EM and TM tests.

3.4 Experimental procedures

3.4.1 Microstructures

For microstructural observation, the as-prepared solder balls (both plain and composite) were firstly mounted in epoxy before grinding and polishing. The metallographic etching reagent was constituted by the mixture of ethanol and hydrochloric acid (99.5 vol. % ethanol and 0.5 vol. % hydrochloric acid). Then, the microstructures were observed using an environmental scanning electron microscope (ESEM Quanta 200). In addition, to deeply understand the effect of the doping of different reinforcement on morphologies of interfacial IMCs between Cu/solder joints, after etching in a 10 vol.% HNO_3 aqueous solution to remove the redundant solder joints, top-view morphology of interfacial IMCs between the Cu substrate and the solder joint was observed using SEM.

3.4.2 Solderability

Solderability consists of many aspects that determine the application of a solder. Usually, solderability of a solder was evaluated by testing its melting point and wettability. In this study, Differential scanning calorimeter (DSC) was employed to determine the melting points of plain and composite solders. Specifically, the solder foils (with thickness of 200 μm) whose weight ranges from 5mg to 10mg are used as specimens for DSC testing. The heating and cooling rate during the test were both 10℃/min. The dwell time was 30s, while the highest heating temperature reached up to 250℃.

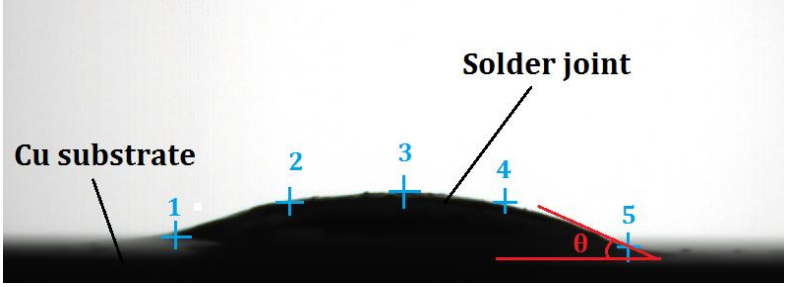

Figure 3.7 Schematic of contact angle test

In order to measure the wettability of solders, the contact angle between copper substrate and solder was tested. For wettability analysis, solder balls were placed on a polished Cu plate with no-wash flux and heated to a temperature of 250℃. After solidification, the contact angles were measured by a camera in the contact angle tester (as shown in Figure 3.7). For each solder, five specimens were tested, so that the reliability of the data could be ensured.

3.4.3 Physical properties

Thermo-stability and electrical resistance are two main physical properties for a solder alloy, which largely determine the electrical and thermal-mechanical properties of a solder joints. Thus, in this research, the coefficient of thermal expansion (CTE) and electrical resistance of the composite solders prepared were studied extensively. Specifically, a four-point probe system (as shown in Figure 3.8) was employed to measure the electrical resistivity of different solders. The as-sintered solder billets with dimension of 24 × 8 × 10mm were used as samples in electrical resistivity test. The dimension of sample was much larger than probe spacing; in this way, testing precision can be guaranteed. In accordance with previous researches, the testing current was set within the range of 100mA-1A.

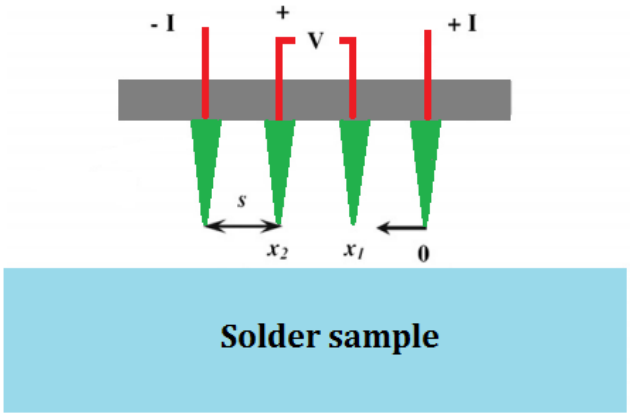

Figure 3.8 Schematic showing the four-point probe configuration used for the electrical resistivity measurements

The levels of CTE of the compacted solder billets after sintering were studied using a CTE analyzer (DIL 402C, NETZSCH, Germany) in the temperature range

of 50–120 ℃. The CTE value was obtained by calculating the linear length changes of solder billets at different temperature excursions; five samples were tested for each solder billet, so as to ensure the data reliability.

3.4.4 Actual content of reinforcement in composite solders

According to previous reports, no matter what method is used, most of the reinforcement added was excluded outside of solder joints in the soldering process [116]. In such a case, the amount of reinforcement retained in the final state of solder joints is quite different from the initial one, leading to reduction of an enhancing effect due to limited doping with reinforcement. To date, although the effect of foreign reinforcement on microstructure and performance of lead-free solders was widely studied, an actual content and distribution of reinforcement added in composite solder joints were rarely mentioned in previous works. Thus, in this study, the retained ratios of reinforcement (RRORs) in the composite solder under different processing stages were systematically investigated.

Specifically, to measure the extent of RRoRs in composite solder containing TiC and NG before soldering, 50mg specimen for each solder were ultrasonically dissolved in aqua regia; the resultant solutions were tested using an inductively coupled plasma optical emission spectroscopy (ICP-OES Varian-720) system with test precision at a ppm level. The RRoRs of composite solder reinforced with FNS nanoparticles was evaluated using a carbon and sulphur analyser (C-S analyser), which analytical precision is also 10^{-6}g. The RRoRs of reflowed solder joints were similarly tested using the ICP-OES and C-S analyser; 20 solder joints for each group were tested to ensure the reliability of testing data. The RRoRs were quantified based on the testing results of an atomic weight fraction of C, Ti and Ni.

3.4.5 Existence forms and locations of reinforcement in composite solders

To confirm the presence of reinforcement added in the composite solder

matrices, different testing approaches were adopted to study the existence form and locations of different reinforcement in composite solders. Specifically, XRD was carried out to verify the presence of reinforcement added in composite solders. Further, SEM, EDS and RAMAN were also employed cooperatively to study the actual locations of different reinforcement added in the composite solder matrices.

3.5 Results and Discussion

3.5.1 Microstructures

3.5.1.1 Microstructure in as-reflowed composite solder matrix

- **SAC/FNS and SAC/TiC composite solders**

The SEM images of two as-reflowed composite solders (including SAC305/FNSs and SAC305/TiC) are presented in Figure 3.9 and Figure 3.10, respectively; the microstructure of plain SAC305 is also shown in these figures for comparative analysis.

It can be seen from Figure 3.9a that three different phases, including β–Sn phase, Ag_3Sn intermetallic compounds (IMC) and Cu6Sn5 IMC can be observed in the plain SAC305 solder matrix. According to Figure 3.9 b-d, a small amount of FNSs nanoparticle addition can help to refine the microstructures of the composite solders. In particular, with an increase in the amount of the FNSs nanoparticles added (from 0 to 0.2 wt. %), both of the β-Sn and the IMCs showed a decreasing trend in average phase size. Compared to SAC305/FNSs composite solder, similar microstructural evolution was also observed in the TiC incorporating composite solders. With an increase in the amount of the TiC nanoparticles added (from 0 to 0.2 wt. %), the β-Sn and the IMCs also showed a decreasing trend in average phase size.

In order to precisely determine the effects of FNSs and TiC nanoparticles on the morphologies of β-Sn phase and IMCs, the grain sizes of the β-Sn and Ag_3Sn phases at 40 randomly selected locations were analysed for each solder sample.

The average values are presented in Table 3.3. As can be seen from the table, for both kinds of composite solders, the average grain size of β-Sn phase showed a considerable decreasing tendency with the addition amount of reinforcement increasing. In particular, the addition of 0.2 wt. % FNSs nanoparticles resulted in the finest β-Sn phase and eutectic areas among all samples.

The average size of the β-Sn phases in the SAC/0.2 FNSs composite solder matrix was 10.97±2.16μm, in comparison to 20.33±4.83μm of plain SAC305 solder. Similarly, the average size of the β-Sn phases in the SAC/0.2TiC composite solder matrix was 15.47±2.46μm, in comparison to 20.33±4.83μm of plain SAC305 solder. In terms of IMCs evolution, after FNSs addition, the rod-like Ag_3Sn IMC in the eutectic areas gradually converted to granulations. The statistical data of the Ag_3Sn IMC size shown in Table 3.3 also intuitively indicated that the FNSs nano-particles were effective to refine the morphology of Ag_3Sn IMC. Similarly, the statistical data of the Ag_3Sn IMC size shown in Table 3.3 intuitively indicated that the TiC nano-particles were also effective to refine the size of Ag_3Sn IMC.

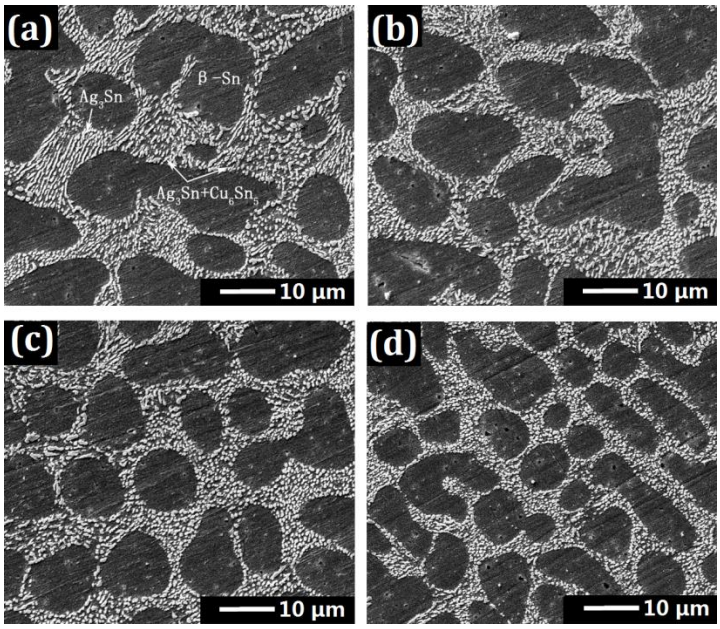

Figure 3.9 SEM images of as-reflowed (a) SAC305, (b) SAC305/0.05FNS, (c) SAC305/0.1 FNS and (d) SAC305/0.2 FNS

Both the microstructural images of the solders and the statistical grain-size data corresponding to the microstructures indicated that the addition of FNSs and

TiC nanoparticles impeded grain growth and gave rise to finer β-Sn phase and IMCs. The thermodynamics and kinetics of the grain growth could explain the grain refinement phenomenon in the composite solders. During the process of grain growth, the increasing interfacial energy between solder matrix and IMCs grains plays an important role in inhibiting the growth of the IMCs grains. When the IMC grains boundary encountered the added foreign nanoparticles in the grain growth process, the interfacial energy between them was increased and thus causes the enhanced thermodynamic resistance of grain growth. Moreover, given the inherent attributes of the foreign reinforcement, they also serve as a barrier and suppress the diffusion of metal atoms on the surface on the IMC phases. This process also hinders the growth of IMC grains, leading to finer IMCs.

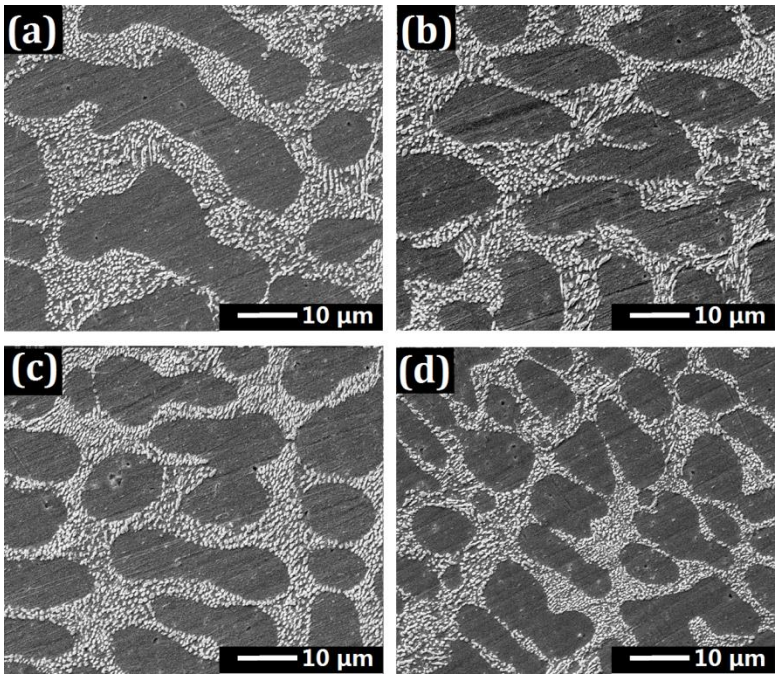

Figure 3.10 SEM images of as-reflowed (a) SAC305, (b) SAC305/0.05TiC, (c) SAC305/0.1 TiC and (d) SAC305/0.2 TiC

Table 3.3 Phase constituents and average phase size of the composite solders

Sample	Addition (wt. %)	Average size of β-Sn (μm)	Average length of Ag_3Sn (μm)
SAC	Nil	20.33±4.83	4.12±1.44
SAC/FNSs	0.05	19.30±1.72	2.53±0.67
SAC/FNSs	0.1	15.69±3.23	1.28±0.64
SAC/FNSs	0.2	10.97±2.16	0.67±0.22
SAC/TiC	0.05	20.13±2.33	2.93±0.52
SAC/TiC	0.1	18.99±2.67	1.88±0.47
SAC/TiC	0.2	15.47±2.46	0.93±0.34

- **SAC/NG composite solder**

Unlike microstructural changes in SAC/FNS and SAC/TiC composite solders, the microstructures in the NG reinforced composite solder matrices exhibited some differences. The SEM images of both as-reflowed plain SAC and composite solder containing NG reinforcement are shown in Figure 3.11. By comparing the microstructural images, two main phenomena can be easily observed in the composite solder matrice—the coarse Ag_3Sn IMC and the newly formed blocky IMCs. To measure the change of Ag_3Sn IMC in grain size, we likewise calculated this item and presented the result in Table 3.4. It is noticeable that the grain size of Ag_3Sn exhibited a increasing trend, from 1.22±0.34μm in the plain SAC solder to 2.35±0.46μm in the 0.2NG reinforced composite solder. The variation of Ag_3Sn IMC in grain size might be resulted from the change in undercooling during solidification, which caused by the doping of NG.

Table 3.4 Average grain size of Ag_3Sn IMC in SAC305/NG composite solders

Sample	Addition (wt. %)	Average size of Ag_3Sn (μm)
SAC	Nil	1.22±0.34
1	0.05	1.39±0.47
2	0.1	1.68±0.53
3	0.2	2.35±0.46

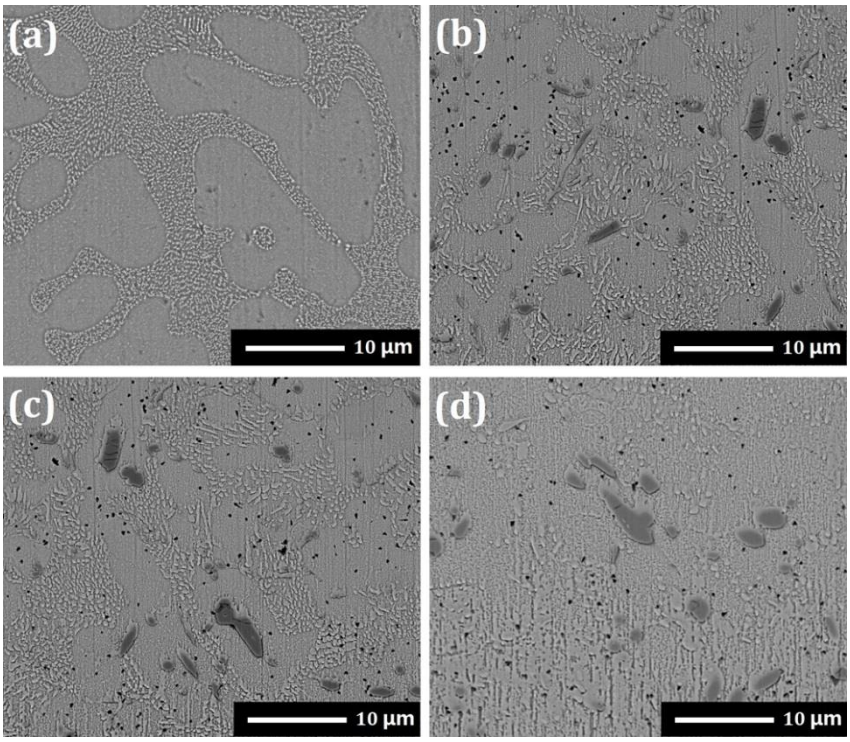

Figure 3.11 SEM images of as-reflowed solders: (a) SAC305, (b) SAC305/0.05NG, (c) SAC305/0.1 NG and (d) SAC305/0.2 NG

On the other hand, the newly formed blocky IMCs in the composite solder matrice were also studied. It can be found from Figures 3.11b-d that these IMCs with shape of sphere or short-rod were formed in the composite solder matrice after NG addition. In particular, with an increase in the amount of the NG added (from 0 to 0.2 wt.%), this IMC showed a increasing trend in both the quantity and volume.

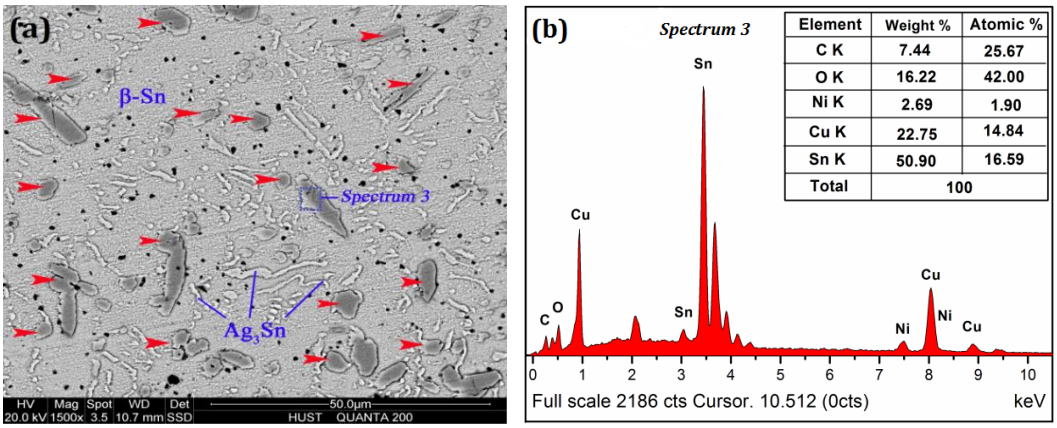

Figure 3.12 (a) Representative image of distribution of Cu-Ni-Sn in the SAC305/0.2NG solder matrix, (b) EDX spectrum in chosen location

In addition, in order to further understand the distribution and component of

this newly formed IMC in solder matrix, a representative SEM image of SAC/0.2NG solder alloy with corresponding EDX analysis were presented in Figure 3.12. From the SEM image, we found that this IMC phases (mentioned above) with dark colour (average size was 5.32±1.83μm), were relatively uniformly distributed in the solder matrix. EDX spectrum reveals that the atomic percentage of Ni, Cu, Sn in the chosen position were 1.9%, 14.84% and 16.59%; this result could help to prove the IMCs were $(Cu, Ni)_6Sn_5$ phase. In addition, the "C" and "O" tested might be introduced from impurities and oxides during experimental steps. A similar IMC phase has been reported by Yang et al. when studying the properties of SAC/CNT-Ni composite solder [28].

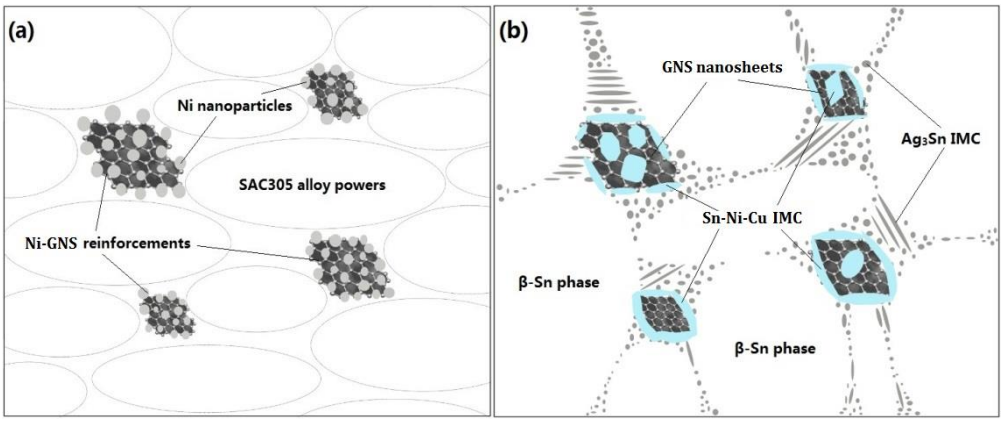

Figure 3.13 The suppositional existence form of NG in the solder matrix: (a) before and (b) after soldering

Moreover, it is also worthy to note the appearance of C element in the EDX spectrum (Figure 3.12b), which can be seen as an evidence of the exsistence of GNS reinforments. Hence, there is reason to believe that the deposited Ni nanoparticles were not completely broken away from the GNS surfaces during soldering process. As depicted in Figure 3.13, the Ni nanoparticles tend to act as a "bridge" that links the GNS nanosheets and the solder matrix by forming Ni-containing IMCs. This process would finally improve the retained ratio of GNS nanosheets in the solder joints. The influence of the deposited Ni nanoparticles on IMCs composition and the retained ratio of GNS nanosheets in solder alloy will be further studied in furture research.

3.5.1.2 Representative morphologies of interfacial IMCs from top-view

Generally, the addition of foreign reinforcement would not only affect the

microstructure of solder matrix, but also alter the morphology of interfacial IMCs between the substrate and composite solder joints.

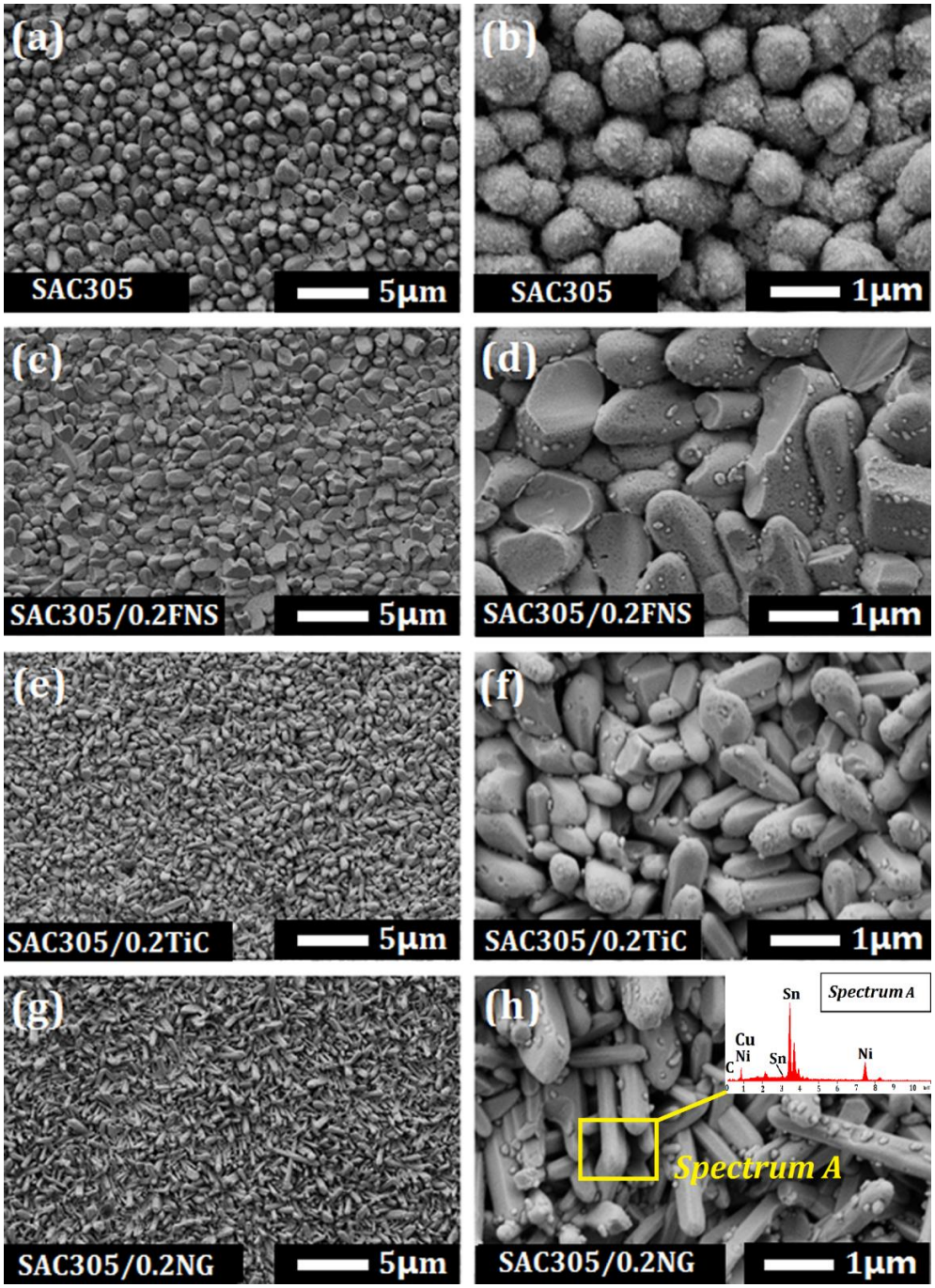

Figure 3.14 Top-view morphologies of interfacial IMCs of (a-b) SAC, (c-d) SAC/0.2FNS, (e-f) SAC/0.2TiC and (g-h) SAC/0.2NG

To understand the effect of the doping of three reinforcements on morphology of interfacial IMCs between the solder and the Cu substrate, the top-view SEM images of interfacial IMCs were obtained in this study. Typical SEM images of plain SAC, SAC/0.2FNS, SAC/0.2TiC and SAC/0.2NG are

presented in Figure 3.14.

Apparently, morphology of interfacial IMCs, namely Cu_6Sn_5, exhibited obvious changes after different reinforcement addition. Specifically, after FNS, addition, although no significant change was found in the grain size of Cu_6Sn_5, the morphology of this IMC was changed from circular granular to a short-rod-like; further, unlike IMCs with a round head in the plain SAC solder, some of these IMCs in SAC/FNSs solder showed a flat head. By contrast, after incorporation of TiC and NG, the morphologies of interfacial IMCs were both changed from the initial circular granular to interlaced polygon rods. Additionally, the EDX result shown in Figure 3.14(h) indicated that the interfacial IMC was actually Ni-Cu-Sn IMC. According to previous report [137-138], the diffusion coefficients of Ni in molten Sn is 2.3×10^{-4} cm^2/s which is higher than that of Cu (1.8×10^{-4} cm^2/s); further, the formation energy of $(Cu,Ni)_6Sn_5$ was 34.6 kJ/mol, which is much lower than that of Cu_6Sn_5 (58.6 kJ/mol). This indicates that some Ni atoms added would take the place of the original Cu, so as to form $(Cu,Ni)_6Sn_5$. However, the average diameter of the rods in SAC/0.2NG composite solder was smaller than that in SAC/0.2TiC composite solder. Specifically, compared to the average diameter of interfacial Cu_6Sn_5 grains in the SAC/Cu (1.75 ± 0.3 μm), the counterpart data for SAC/FNS, SAC/0.2TiC and SAC/0.2NG were 1.87 ± 0.2 μm, 0.86 ± 0.3 μm and 0.72 ± 0.2 μm, respectively.

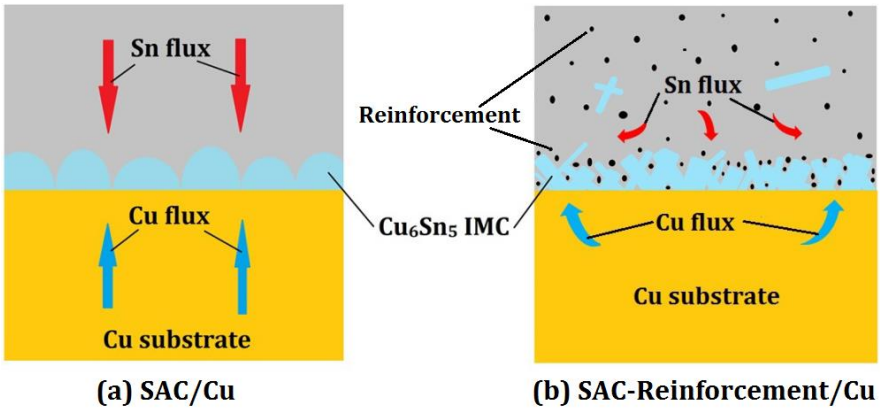

Figure 3.15 Schematic of Cu and Sn fluxes at interface of SAC/Cu (a) and (b) SAC-Reinforcement/Cu

These transformations in morphology and the grain size of the interfacial IMCs were defined by reaction kinetics; a schematic of Cu and Sn fluxes at the solder/Cu interface are shown in Figure 3.15. For the SAC/Cu system, fluxes of Cu and Sn atoms, coming from the Cu substrate and the molten solder, respectively, met directly at the Cu/solder interface, forming interfacial common Cu_6Sn_5 scallop-like or circular granular. However, the diffusional direction and the interfacial atomic concentration of Cu and Sn atoms in the SAC-reinforcement/Cu system might be influenced by foreign reinforcement. Specifically, as discussed in Chapter 2, foreign reinforcement added would be expelled out of a solder joint during the reflow process. The expelled foreign nanoparticles tend to accumulate at the solder/Cu interface, regarded as a main path for reinforcement exclusion [158]. In such case, the initial diffusional equilibrium for Sn and Cu atoms would be broken due to the presence of reinforcement, leading to variation in crystallization conditions of interfacial IMCs and resulting in new Cu_6Sn_5 with different morphology.

3.5.2 Solderabilities

3.5.2.1 DSC results

The melting point is a primary physical parameter to measure the availability of a solder alloy in the electronics packaging industry. In the present study, melting points of the plain and composite solders were identified by DSC endothermic curves.

Figures 3.16, 3.17 and 3.18 show the DSC curves of SAC/FNS, SAC/TiC and SAC/NG composite solders respectively. It can be seen from these results that all the endothermic peaks appeared within the range of 219.25℃ to 223.49℃. This result indicates that the addition of a small amount of foreign reinforcements had little impact on the melting point of the solder alloy. According to the Lindeman criterion [117], the melting point of a material is an intrinsic property that is determined by the atomic mean-square displacements and inter-atomic distance.

In this study, the addition of a small amount of foreign reinforcements can hardly break the balance between the atomic mean-square displacements and the inter-atomic distance of solder alloy. Therefore, there is no reason to believe that the addition of such foreign reinforcements limit the applicability of the SAC305 alloy by changing its melting point noticeably.

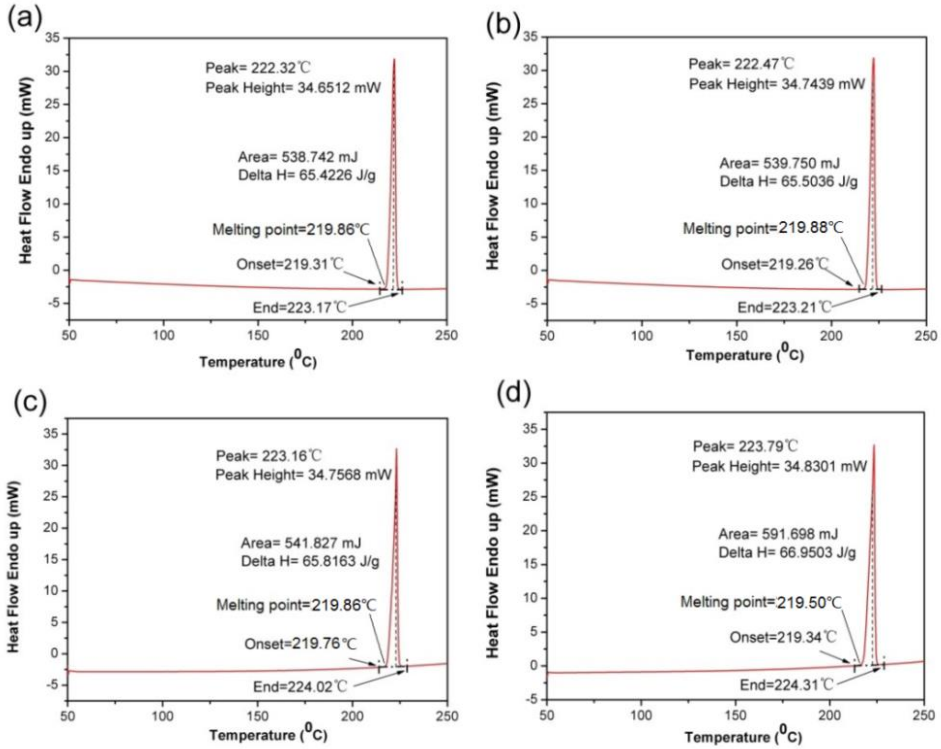

Figure 3.16 DSC curves for (a) SAC, (b) SAC/0.05FNSs (c) SAC/0.10FNSs and (d) SAC/0.20FNSs

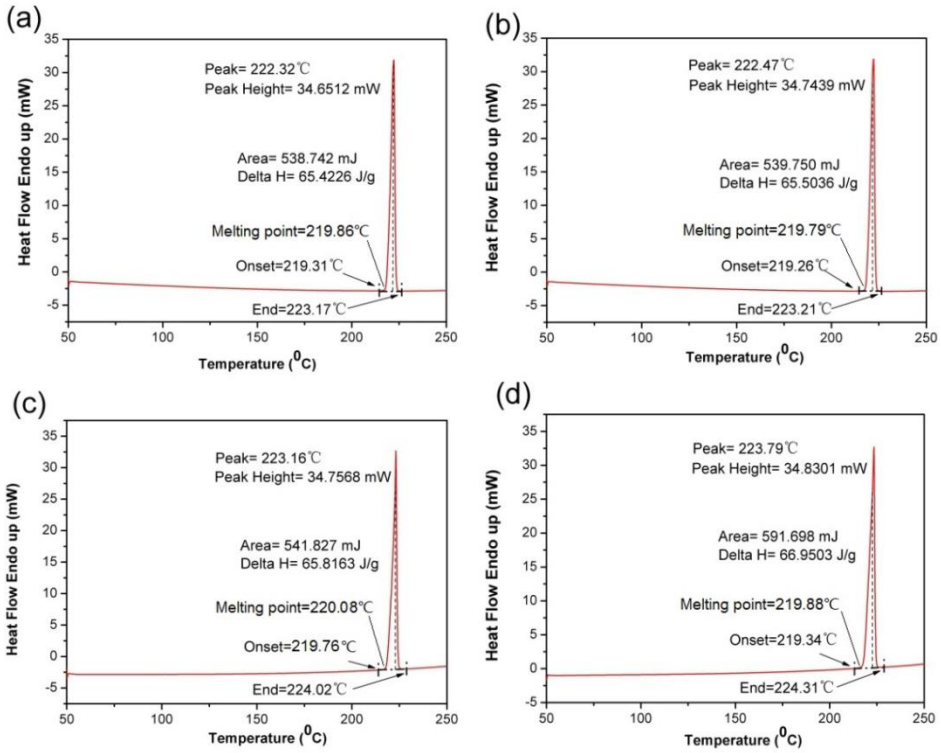

Figure 3.17 DSC curves for (a) SAC305（b）SAC305/0.05TiC（c）SAC305/0.1 TiC and （d）SAC305/0.2 TiC solders

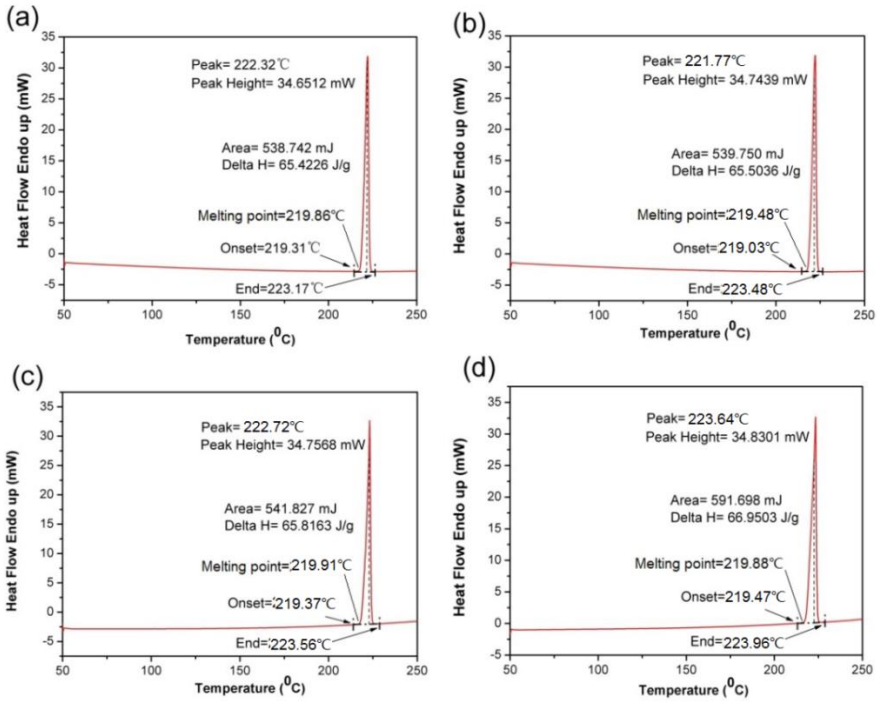

Figure 3.18 DSC curves for (a) SAC305（b）SAC305/0.05NG（c）SAC305/0.1 NG and （d）SAC305/0.2 NG solders

Table 3.5 Melting parameters of different solder alloys (in ℃)

Sample types	Onset T_M	End T_M	Melting range
SAC	219.31	223.17	3.86
SAC/0.05FNS	219.26	223.28	4.02
SAC/0.1FNS	219.56	223.76	4.2
SAC/0.2FNS	219.24	223.81	4.57
SAC/0.05TiC	219.26	223.21	3.95
SAC/0.1TiC	219.76	224.02	4.26
SAC/0.2TiC	219.34	224.31	4.97
SAC/0.05NG	219.48	223.48	4.11
SAC/0.1NG	219.37	223.56	4.19
SAC/0.2NG	219.47	223.96	4.49

However, after calculating the difference between the onset and end of melting for all the samples, it was found that the melting range of all composite solder alloys exhibits an upward trend with a growing amount of reinforcement. This data were listed in Table 3.5 for different solders; For example, for SAC/0.2TiC solder it is 28.8% higher - 4.97 ℃ - than that for the plain SAC solder. The reason for this phenomenon is concluded to be the difference in thermal conductivities of TiC (16.7 W/m K) and SAC solder (50 W/m K); lower thermal conductivity of reinforcement could reduce total thermal conductivity of SAC/TiC composite solder and cause the increase in its melting range. Thus, to improve solderability and applicability of SAC/TiC composite solders, an optimal addition amount of TiC needs to be further studied.

3.5.2.2 Wettability

Building a reliable bonding joint between the solder and substrate is critically

important in electronics packaging industry. The wettability of the solder alloy used largely determines the quality of such solder bonding [118]. Generally speaking, the solder alloy which has the smaller contact angle on the substrate also tends to offer more reliable interconnection in the soldering process.

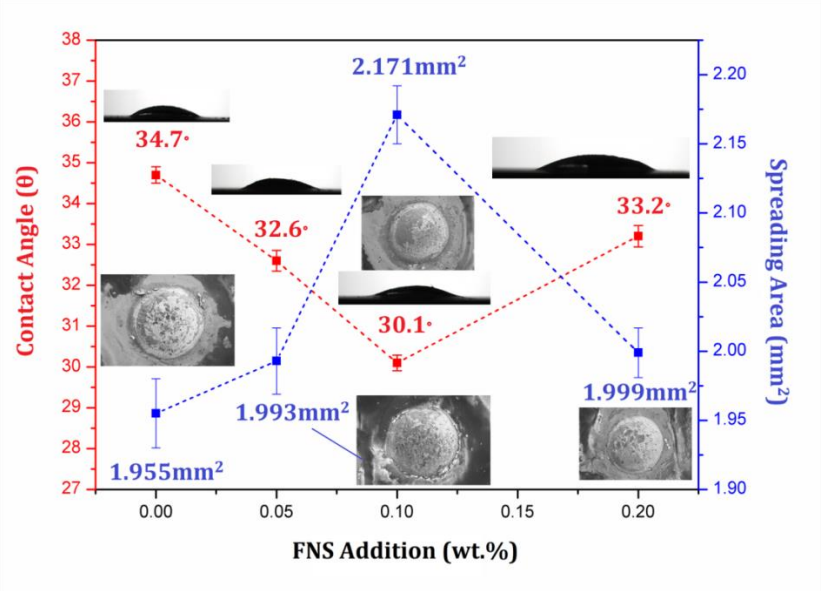

Figure 3.19 Graphical relationship between weight fractions of FNSs added to solder matrix and contact angle

As shown in Figure 3.19, the contact angle initially decreased with the addition of the FNSs nanoparticles (from 37.5 ° for the plain SAC alloy to 30.1 ° for the SAC with 0.1 wt% FNSs). However, the contact angle then increased with an increase in the amount of FNSs nanoparticles added, reaching 33.2 ° for the SAC with 0.2 wt% FNSs addition. These testing results indicate that the incorporation of FNSs nanoparticles helped improve the wettability of the SAC solder when the amount added was relatively small.

A possible reason for this phenomenon is that the added FNSs nanoparticles accumulated at the interface between the molten solder and the flux during soldering; the existence of these nanoparticles thus lowered the interfacial surface energy. This process decreased the interfacial tension between the flux and the solder, resulting in the formation of a smaller contact angle. On the other hand, carbon-based nano materials tend to absorb organic functional groups or small molecules (such as oxygen) from the flux or the air because of their unique

molecular structures [119-120]. Hence, a greater quantity of FNSs nanoparticles may result in the aggregation of modified reinforcements at the solder/flux interface, thus increasing the interfacial tension and leading to the increase in contact angle.

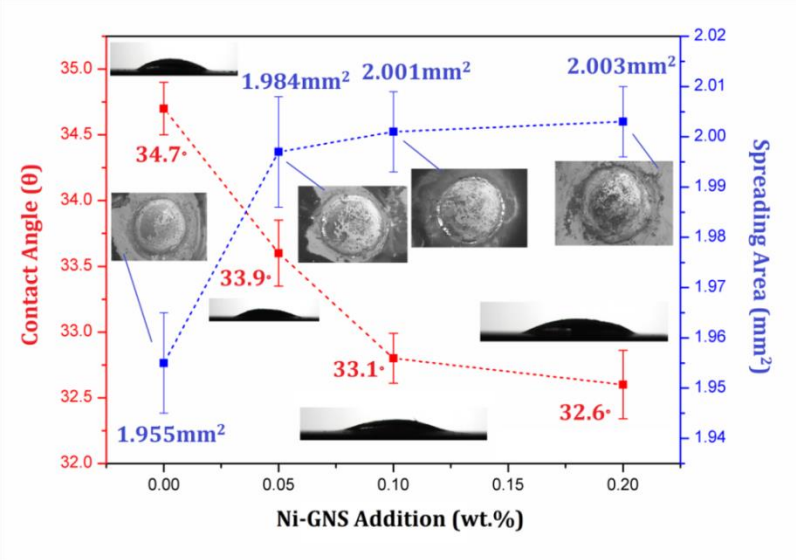

Figure 3.20 Graphical relationship between weight fractions of NG added to solder matrix and contact angle

As shown in Figure 3.20, the contact angle decreased with the addition of NG (from 37.5 ℃for the plain SAC to 32.6 ° for the SAC with 0.2 wt.% NG addition). These testing results indicate that the incorporation of NG reinforcements helped improve the wettability of the composite solders. Similarly, the possible reason for this phenomenon is that the added NG nanoparticles accumulated at the interface between the molten solder and the flux during soldering; the existence of these NG reinforcements thus lowered the interfacial surface energy. This process decreased the interfacial tension between the flux and the solder, resulting in the formation of a smaller contact angle. In addition, the incorporation of Ni element might make a contribution on the improvement in wettability as well.

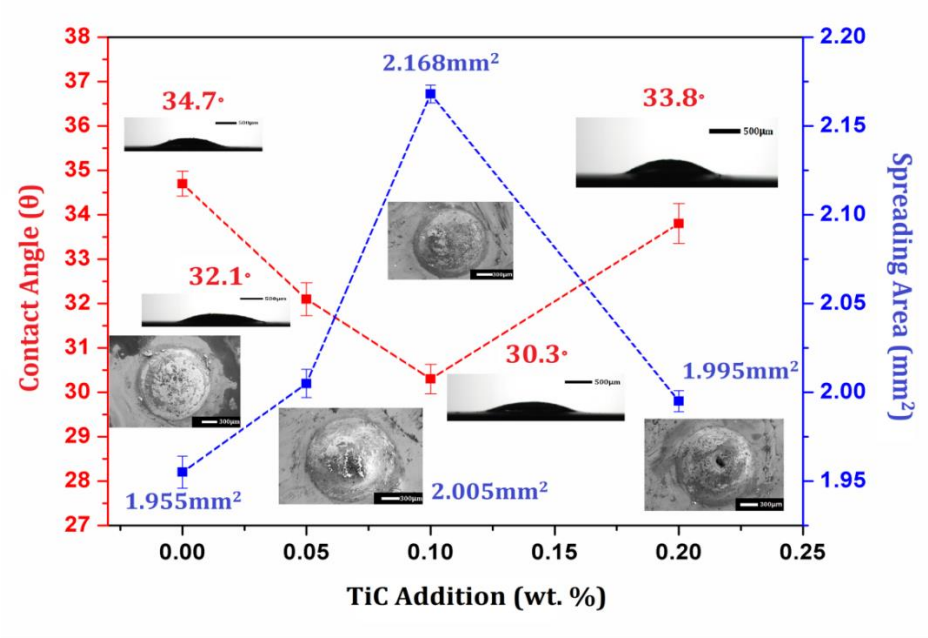

Figure 3.21 Effect of TiC content on contact angle and spreading area of SAC alloys

Wettability results of the SAC/TiC composite solders were presented in Figure 3.21. It was found that the contact angles of solders decreased firstly and then increased with the increasing content of TiC (Figure 3.20), with the data for the spreading area showing an opposite trend. Specifically, the contact angle firstly decreased - from 34.7 ° for the non-reinforced SAC to 30.3 ° for the composite solder with 0.1 wt. % TiC reinforcement, followed by an upward trend, with the contact angle increasing to 33.8 ° for 0.2 wt. % of TiC . Correspondingly, the spreading area of the composite solder reached the maximum value - 2.168 mm^2 when the content of TiC nanoparticles was 0.1 wt. %, which is 10.8% larger than that of plain SAC solder. However, it decreased to 1.995 mm^2 for 0.2 wt. % of nano-reinforcement. These results indicate that the relatively small addition of TiC nanoparticles into solder matrix contributes to improve wettability of the composite solder alloys. The possible reason for this phenomenon is that the appropriate TiC nanoparticles doped tend to accumulate at the interface between the flux and the molten solder during reflowing, lowering the interfacial surface energy and leading to reduced interfacial tension between them, forming eventually a smaller contact angle. Nevertheless, the excess of TiC reinforcement might increase viscosity of the molten solder, hindering its spreading.

Additionally, higher fractions of TiC nanoparticles may result in their aggregation at the solder/flux interface, increasing the interfacial tension and thus leading to the decrease in wettability.

3.5.3 Physical properties

3.5.3.1 Electrical resistance

The results of the electrical resistivity measurements of the composite solders are presented in Table 3.6, Table 3.7 and Table 3.8. The statistic data of electrical resistivity in Table 3.6 and Table 3.7 have clearly revealed that there is only a negligible difference between the plain solder and the FNSs and TiC nanoparticles reinforced composite solders. It has been reported previously that the electrical resistivity of a composite material is largely influenced by the type, size, shape, and volume fraction of reinforcements used [121-124]. According to the Matthiessen's rule, the total electrical resistivity of a material is comprised of three parts, namely, impurity resistivity, thermal resistivity and deformation resistivity [125]. These three types of resistivities disturb the normal electron motions by affecting the impurity scattering and lattice scattering. However, in the case of a composite solder alloy, the total electrical resistivity depends mainly on the impurity resistivity, in comparison to the monolithic solder alloys. Specifically, in a composite conductive system, the reinforcements (especially insulated foreign particles) usually act as electron scattering centres. When the volume fraction of these reinforcements is relatively high, it has a significant impact on the electrical resistivity value of the composite system.

Table 3.6 The resistivity of SAC plain and Fullerene doped solders

Sample #	FNS Addition (wt. %)	Electrical resistivity (μΩ·cm)
SAC	Nil	13.4 ± 0.2
1	0.05	13.5 ± 0.4
2	0.1	13.4 ± 0.3
3	0.2	13.6 ± 0.2

In this study, there was no notable change in electrical resistivity between all the FNSs and TiC nanoparticles reinforced composite solders, as the amount of

reinforcements added was very small. Using a similar approach, Nai et al. [126] measured the electrical resistivity of a MWCNTs doped lead-free solder alloy. They also found no evidence of dramatic changes in the electrical resistivity of the solder alloy after the addition of a small amount of the MWCNTs as reinforcements. Thus, the findings of the present study are consistent with those reported previously by other researchers.

Table 3.7 The resistivity of SAC plain and TiC doped solders

Sample #	TiC Addition (wt. %)	Electrical resistivity (μΩ·cm)
SAC	Nil	13.8 ± 0.3
1	0.05	14.0 ± 0.2
2	0.1	14.3 ± 0.2
3	0.2	15.1 ± 0.3

However, for the NG incorporating composite solders, The testing data of electrical resistivity showed a slightly decreasing trend with the increasing amount of the NG reinforcements.

Table 3.8 The resistivity of SAC plain and NG doped solders

Sample #	FNS Addition (wt. %)	Electrical resistivity (μΩ·cm)
SAC	Nil	13.8 ± 0.3
1	0.05	13.5 ± 0.2
2	0.1	13.2 ± 0.3
3	0.2	12.9 ± 0.2

This phenomenon can be interpreted from both the effect of reinforcement's electrical resistivity and the amount of the NG added. On the one hand, the electrical resistivities of Ni (6.84 μΩ·cm) and GNS (~10 μΩ·cm) were both much smaller than that of SAC solder (12.9μΩ·cm). Thus, the addition of NG helped lower the electrical resistivity of the composite slder. On the other hand, as mentioned above, the volume fraction of reinforcements also have considerable influence on resistivity of composites. However, in this study, the relatively small amount of the NG add can hardly affect the resistivity of solder systems significantly.

3.5.3.2 CTE results

The effects of foreign reinforcement on a magnitude of CTE of the composite solder alloys for a broad range of temperature was widely reported [127-128]. To understand thermal-expansion behaviour of composite solders, in the present work, the effect of TiC reinforcement on the instantaneous CTE of composite solders was studied. Evolution of CTE with temperature curves in the range from 50-120 ℃ is presented in Figure 3.22 for plain and composite solders. Apparently, the CTE values increased with increasing temperature for all the studied compositions; all the composite solders exhibiting lower CTEs than that of the SAC solder without reinforcement. In particular, the CTE of the composite colder with the highest fraction of reinforcement - SAC/0.2TiC – was some 8-10% lower than that of the plain SAC throughout the whole studied temperature range. The obtained results illustrate that addition of TiC reinforcement facilitated improvement of dimensional stability of the composite solders in this temperature range. This phenomenon could be explained by a significantly lower CTE magnitude of TiC - 7. 4×10^{-6}/K - compared to that of the SAC solder alloy - 29.1×10^{-6}/K [129-130]. During heating, thermal expansion of the SAC solder matrix could be restricted by TiC reinforcement and effective bonding between it and the matrix.

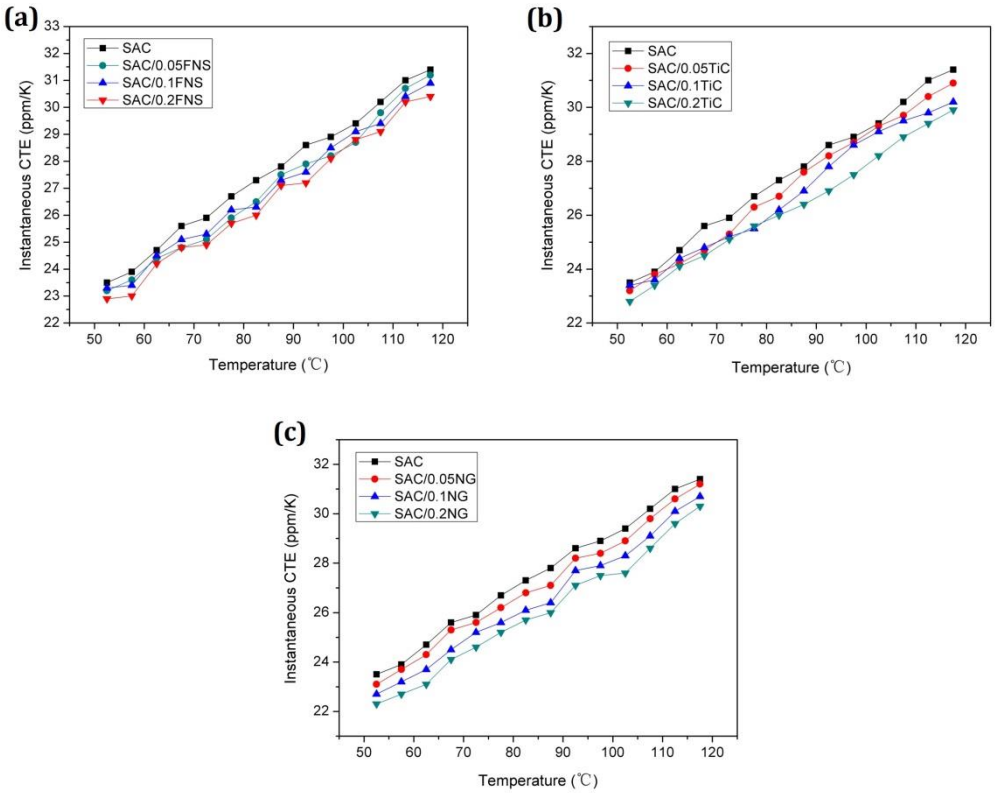

Figure 3.22 Effect of temperature of instantaneous CTE for plain and composite solders

3.5.4 Retained ratio and presence form of reinforcement added

3.5.4.1 Retained ratio of reinforcement added

As shown in Figure 3.23a, after the reflow process, most of the added FNSs reinforcements were found expelled out of the solder ball. This phenomenon resulted from flux volatilization during soldering process and the non-wetted interface between reinforcements and the molten solder. After ultrasonically cleaned the flux residuals, the actual retained ratio of fullerene reinforcements (namely, the weight fraction of C element) in the composite solder balls were tested in a C-S analyzer, and the experimental results were shown in Figure 3-23b. It is notable that the retained ratios of reinforcements in all kinds of composite solder joints showed a considerable decrease trend with the reflow cycles increase. It is also easy to find that the first reflow process has most serious impact on the retained ratio of reinforcements. After the first reflow, the retained ratios of reinforcements of all these three composite systems saw a decrease in a

large degree, from 0.05%, 0.1% and 0.2% to 0.012%, 0.021% and 0.036%. Although the retained ratio of reinforcements keeps decreasing with reflow cycle increases, the drop rate of retained ratio tended to be slow down.

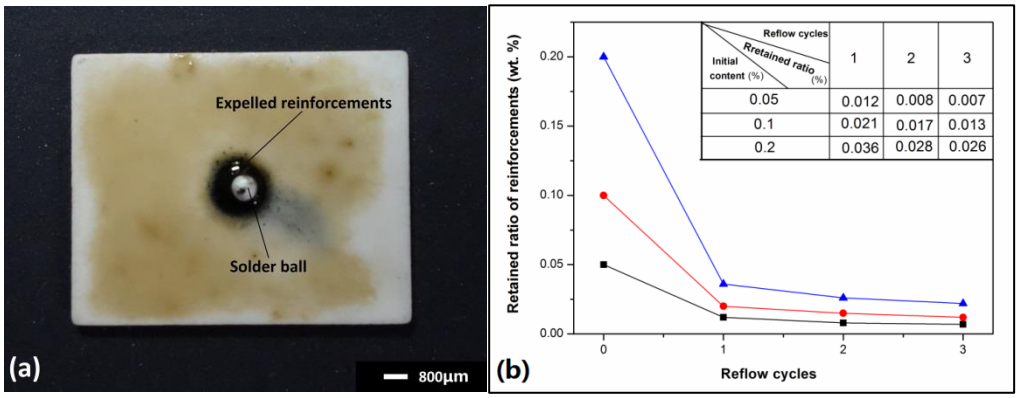

Figure 3.23 (a) Digital image of composite solder after reflow; (b) effect of reflow cycles on retained ratio of FNS reinforcements in solder balls

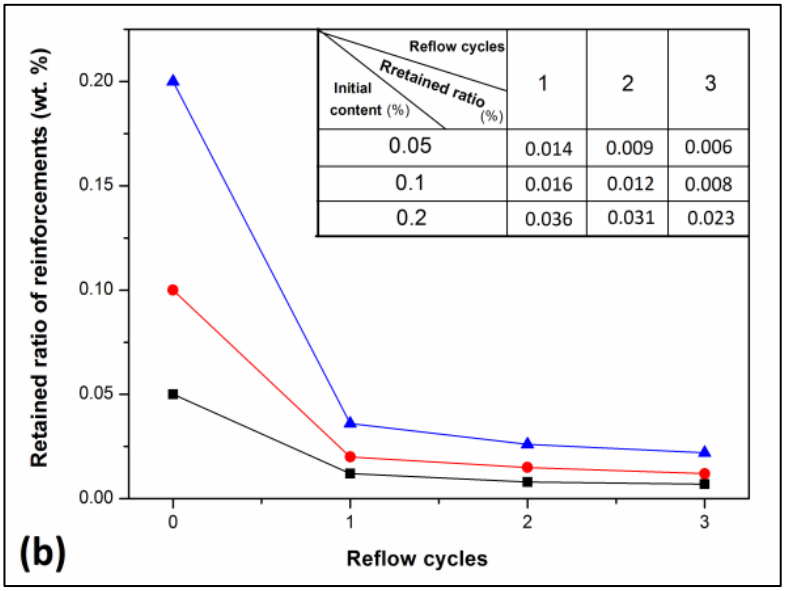

Figure 3.24Effect of reflow cycles on retained ratio of TiC reinforcements in solder balls

The retained ratios of TiC reinforcements in the solder balls after different reflow cycles are shown in Figure 3.24; it is also known that the retained ratios of TiC reinforcements solder joints showed a similar decreasing trend with the increase in reflow cycles. After the first reflow cycle, the retained ratios of reinforcements of all these three composite systems saw a decrease by a large degree (from 0.05%, 0.1% and 0.2% to 0.014%, 0.016% and 0.036%). Like what happens in SAC/FNS composite solders, the retained ratio of TiC reinforcements

kept decreasing with reflow cycles and the drop rate of the retained ratio tended to slow down. According to retained ratio data shown in Figure 3.23 and Figure 3.24, it is necessary to point out that the average retained ratio of FNS or TiC reinforcement added in the composite solder joints after 1 reflow cycle was approximately 20%; this average ratio for both two reinforcements even drop to 10%, when the solder joints experienced two reflow cycles.

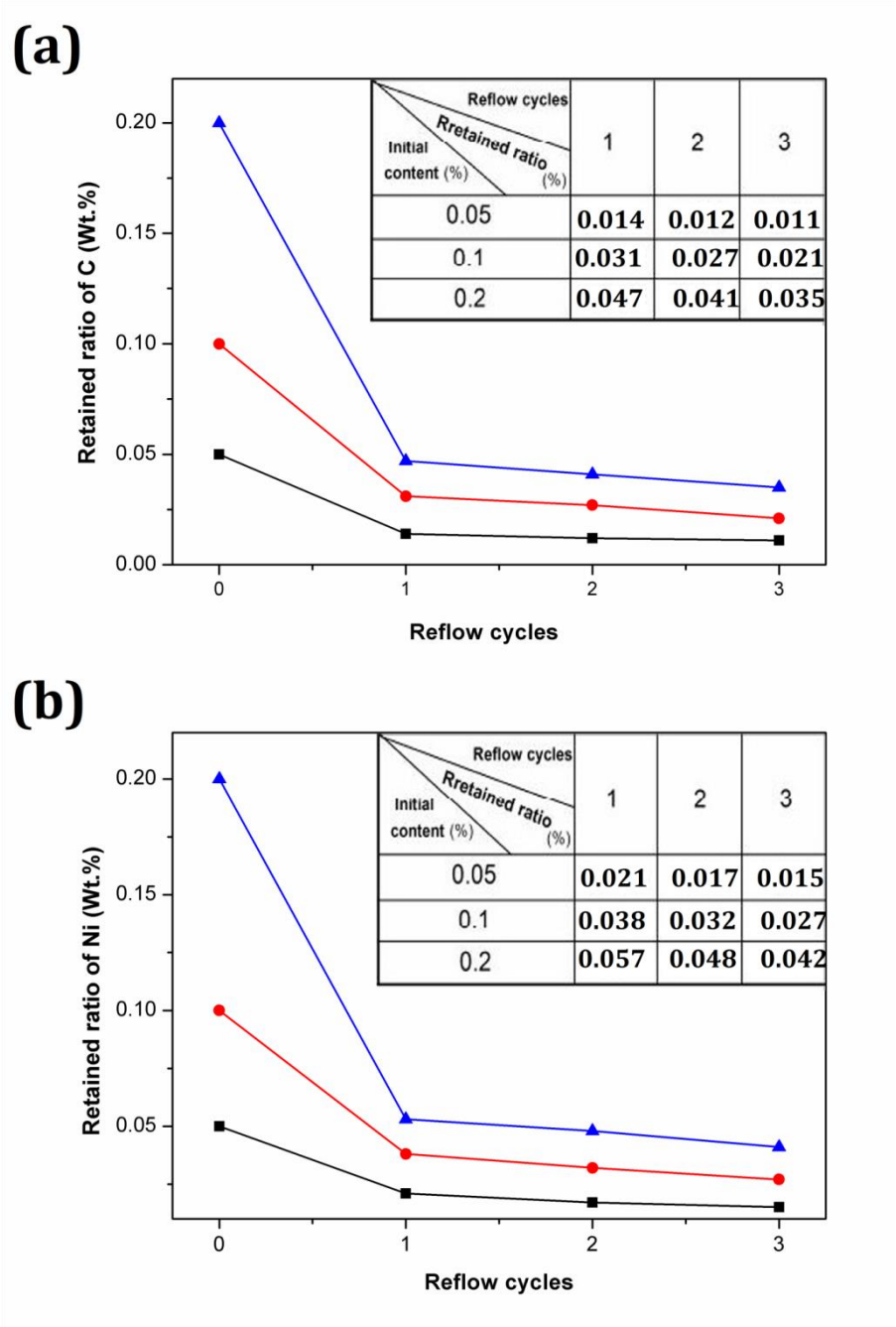

Figure 3.25 Effect of reflow cycles on retained ratio of (a) C and (b) Ni in solder balls

As to the retained ratio of NG added in solder balls after different reflow

cycles, the weight fractions of C and Ni in solder balls were separately measured using C-S analyser and ICP-OES; the obtained results are presented in Figure 3.25. According to the result shown in Figure 3.25, the content of C and Ni in reflowed solder balls showed a decreasing trend with reflow cycles increase. Although the variation of weight fraction of C and Ni in SAC/NG solder balls showed a similar trend to that C and Ti in SAC/FNS and SAC/TiC composite solders, the actual retained ratio of C and Ni in SAC/NG solder balls showed a considerable increase. In addition, in contrast to data presented in Figure 3.23 and Figure 3.24, it is interesting to find that the incorporation of Ni coating considerably improved the retained ratio of C (namely, GNS) in solder joints. Unlike the results shown in Figure 3.23 and Figure 3.24, there was a considerable part of C and Ni (especially, C) added were found to be retained in SAC/NG composite solder joints after different reflow cycles. The average weight fractions of NG in composite solder joints after 1 and 3 reflow cycles were calculated to be 65% and 45%, respectively; these data were much higher than their counterparts for SAC/FNS and SAC/TiC.

Further, as mentioned in section 3.2.4.2, the average weight fraction ratio of C and Ni in the initial NG is approximately 0.98. In consideration of the fact that the NG sheets is a composite reinforcement which consist of the GNS carrier and the decorated Ni nanoparticle, the tested weight fraction ratio of C/Ni in solder balls after different reflow cycles could be able somewhat reflect the effect of Ni coating on the retained ratio of GNS in solder balls after soldering process. The Weight fraction ratios of C/Ni in SAC/NG solder joint after different reflow cycles were calculated based on experimental data shown in Figure 3.25 and listed in Table 3.9.

Table 3.9 Weight fraction ratio of C/Ni in SAC/NG solder after different reflow cycles

Initial addition amount of NG (wt. %)	Reflow Cycles		
	1	2	3
0.05	0.74	0.71	0.73
0.1	0.82	0.84	0.78
0.2	0.82	0.85	0.83

It can be seen from Table 3.9 that the average weight fraction ratios of C and Ni in SAC/NG solder joints show a slight decline compared with the initial data (0.98), which indicates that a small part of GNS added could not be retained in the solder joint during reflow process. This phenomenon could be explained by the inhomogeneity of Ni nanoparticles on the GNS sheets; those GNS nano-sheets with fewer Ni nanoparticles might not form a stable bonding with solder matrix, leading to a loss of the retained ratio of C in the final solder joints. Additionally, it can be found that the average weight fraction ratio of C and Ni in SAC/NG solder joints kept stable (approximately, 0.8) even if the reflow cycles continue to increase.

The findings in retained ratio of NG in SAC/NG composite solder indicate that the Ni nanoparticles decorated are helpful to form a reliable bonding between GNS sheets and Sn-based solder matrix, improving the retained ratio of GNS in the final solder joints. The relatively stable weight fraction ration of C/Ni also reveal that there would be still a relatively strong bonding existed between Ni nanoparticles and GNS carriers during reflow process.

3.5.4.2 Existence forms and locations of reinforcement in composite solders

The verification of existence, structural attributes characterization and actual position of reinforcements in the solder matrix are always the main focus of composite solders research. It has been reported previously that shear fractures occur mostly at the intermetallic phase/solder interface [131-132]; in addition, according to the microstructural analysis in section 3.5.1, the reinforcements are more likely enriched at IMC surface or phase interfaces, leading to a finer

microstructure. Hence, the foreign reinforcements can readily be observed at the shear-fracture areas. In the present study, observations were made at the surfaces of the shear-fractured joints to verify the existence of the added FNSs nanoparticles and to determine their locations.

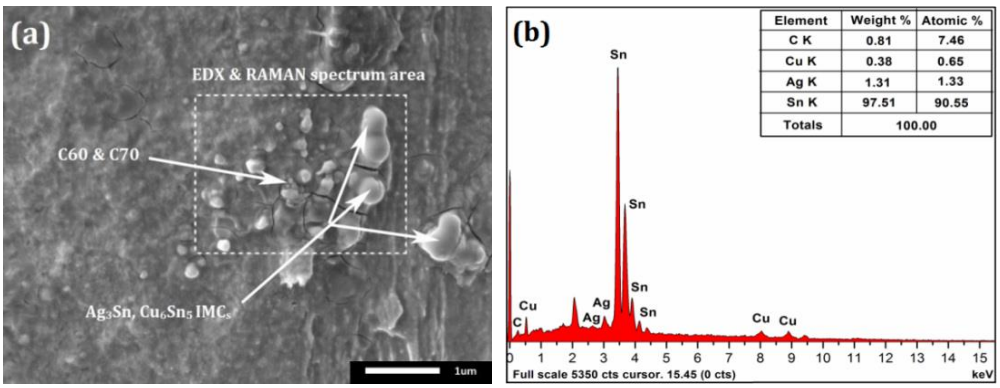

Figure 3.26 (a) Representative SEM image of FNSs agglomeration located at the bottom of dimple after shear test, (b) EDX spectra for the selected area marked in (a)

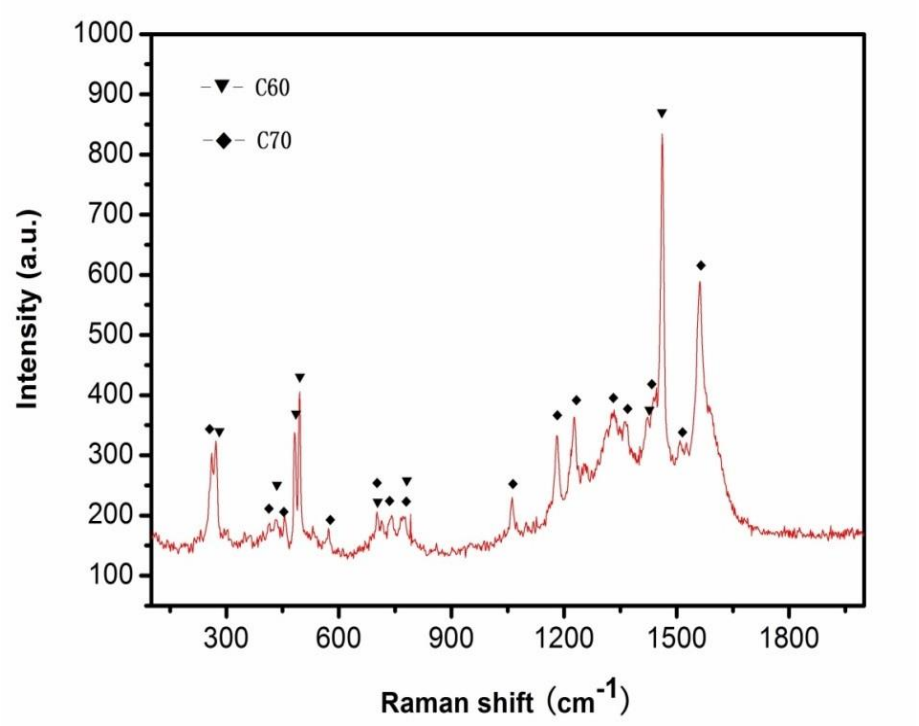

Figure 3.27 Raman spectrum of FNSs in Fig. 15 (a)

Figure 3.26a and b show a representative SEM image taken from a dimple bottom and the EDX spectrum of a selected area respectively. According to the EDX spectrum, carbon atoms were indeed present in the solder matrix, with a weight ratio of 0.81% and atomic ratio of 7.46%. Further, as can be seen from the

SEM image in Figure 3.26a, in addition to the Ag_3Sn and Cu_6Sn_5 phases, nano-sized particles of an unknown material were found around the IMC phases. In order to identify these unknown particles, Raman spectroscopy was used to analyse the area where these nanoparticles had aggregated; the result of Raman spectrum is shown in Figure 3.27. In keeping with the results reported by Ferrari et al. [133], the characteristic frequency shifts observed in this study and their qualitative types are listed in Table 3.10. The obtained results confirmed that the unknown particles were FNSs nanoparticles (a mixture of C60 and C70). Thus, the Raman spectrum together with the results of the SEM and EDX analyses confirmed the presence of the FNSs nanoparticles in the matrices of the composite solders.

Table 3.10 The observed peaks and their qualitative classification

ν(cm^{-1})	C60	C70	ν(cm^{-1})	C60	C70
254		✓	770	✓	✓
270	✓		1062		✓
410		✓	1185		✓
432	✓		1230		✓
450		✓	1334		✓
486	✓		1368		✓
494	✓		1426	✓	
570		✓	1446		✓
704		✓	1468	✓	
710	✓		1514		✓
736		✓	1564		✓

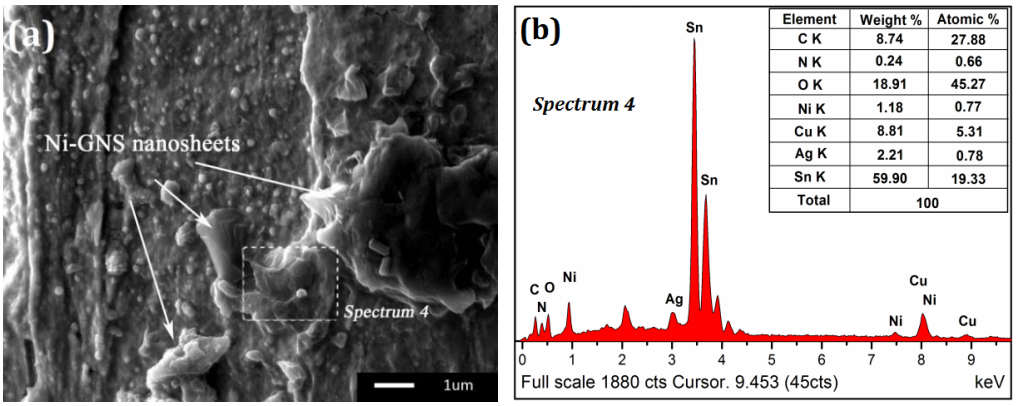

Figure 3.28 (a) Representative SEM image of NG agglomeration located at the bottom of dimple after shear test, (b) corresponding EDX spectra for the selected area marked in (a)

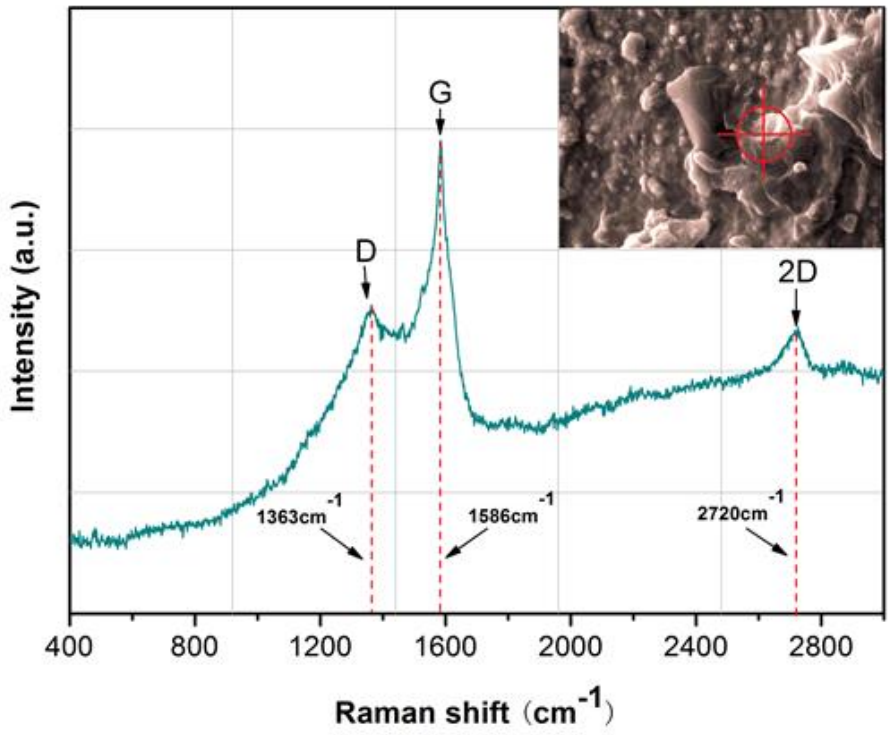

Figure 3.29 Raman spectrum of chosen area in Figure 3-30a

Figures 3.28a and b show the representative SEM image taken from a fracture surface and the EDX spectrum of a selected area respectively. It can be seen from the chosen position that there were some sheet-like substances embeding in the solder matrix. According to the EDX spectrum, carbon and Ni atoms were indeed present in the chosen position, with a weight ratio of 8.74% and 1.18%. To identify these sheet-like substances, Raman spectroscopy was employed to further analyze the area where these sheets aggregated; the result of Raman spectrum is shown in Figure 3.29. From the Raman spectrum, it was clearly to find three notable peaks in 1363cm^{-1}, 1586cm^{-1} and 2720cm^{-1}, which were characteristic frequency shifts of GNS [133]. Thus, the Raman spectrum together with the results of the SEM and EDX analyses confirmed the presence of the NG reinforcements in the matrices of the composite solders.

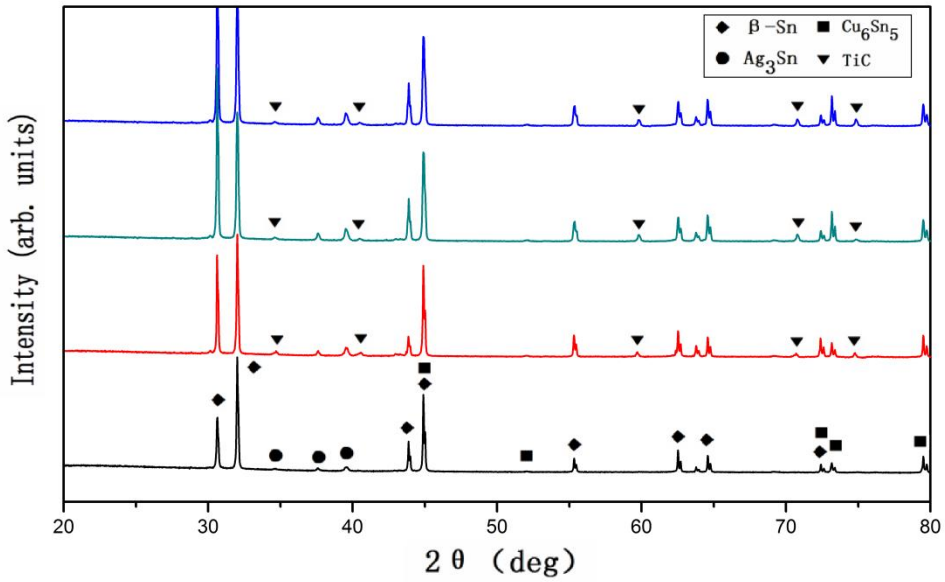

Figure 3.30 XRD spectrum of both the plain and TiC reinforced composite solders

To verify the exsitence of TiC added in the solder matrix, XRD spectrum were employed in this section. Figure 3.30 shows the XRD spectrums of both the plain and composite solders. After phase identification, we confirmed the exsitence of TiC in the composite solder matrix; and the characteristic peaks of TiC were marked using a triangle symbol which can be seen in Figure 3.30. In addition, in order to further understand the exsitence and distribution of the added TiC reinforcements in the solder matrix, microstructures of the TiC incorporating composite solder were observed using an ESEM (QUATA 200).

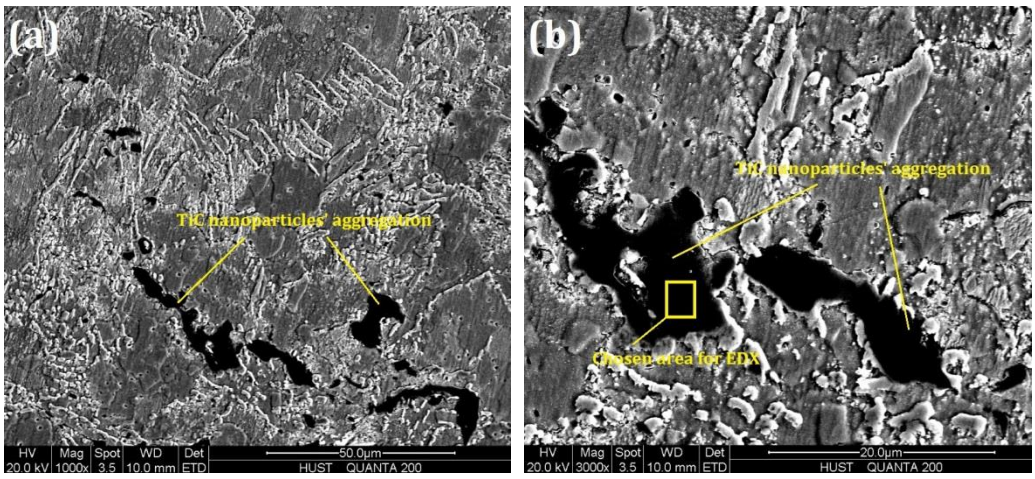

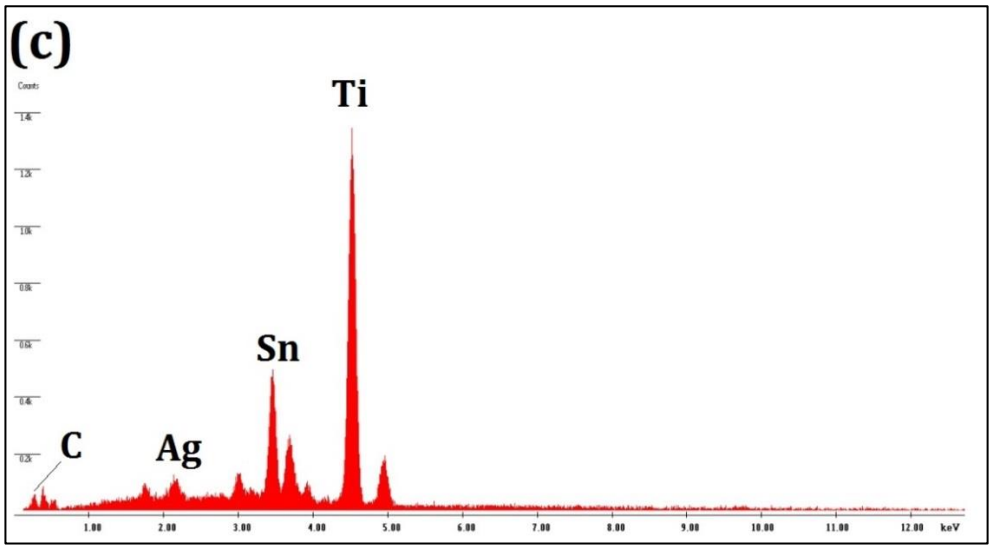

Figure 3.31 (a) and (b) Aggregation of TiC nanoparticles in the solder matrix, (c) EDX spectrum for the chosen area

As shown in Figure 3.31a and b, an aggregation of TiC nanoparticles were found in the solder matrix, the corresponding EDX spectrum shown in Figure 3.31c also hleps to confirm the exsitence of TiC reinforcement. Although the results of XRD toghther with SEM images could confirm the exsitence of the added TiC (mostly in the form of aggregation) in the solder matrix, it still needs much work to do to further understand the distribution of other TiC reinforcements which exist in other forms.

3.6 Summary

In this Chapter, FNSs and TiC nanoparticles were chosen as reinforcement. Further, GNS nano-sheets decorated with Ni nanoparticles (NG) were also prepared with the chemical reduction method. Then, SAC305 composite solders reinforced with different fractions of FNS, TiC and NG nanoparticles were prepared using a powder metallurgical method. In addition to their physical properties and solderability, microstructural evolution of interfacial IMCs was systematically studied. In addition, the presence and locations of different reinforcement in different composite solder matrices were also comprehensively investigated.

According to experimental results, the addition of FNS and TiC can effectively refine the β-Sn and Ag3S IMCs; the shape of Ag3Sn changed from short-rod to granular-like. After the addition of NG reinforcement, the newly formed $(Cu, Ni)_6Sn_5$ IMCs were observed in the SAC/NG composite solder joint. The appropriate addition of foreign reinforcement (FNS, NG and TiC) could effectively improve the wettability of SAC305 solder alloy without obviously affect the melting point and electrical resistance of the solder alloy. Under testing conditions, the addition of three reinforcements can lower the CTE of solder alloy. The results of retained ratio indicate that the average loss ratio of FNS and TiC is approximately 80% after the first reflow cycle, while this data for NG reinforcement is only 40%; this phenomenon shows that the Ni layer prepared can effectively improve the retained ratio of GNS in solder joints.

Chapter 4 Microstructural and mechanical evolution of composite solders under thermal ageing

4.1 Introduction

The thermal ageing test under high temperature is a main approach to evaluate the reliability of solder joints since the microstructure and mechanical properties of solder joints will degraded under a relatively high service temperature. In this chapter, to understand the performance of composite solders prepared under the isothermal ageing condition, microstructural (including solder matrices and interfacial IMCs) and mechanical evolution (e.g. micro-hardness and shear strength) were evaluated and discussed.

4.2 Experimental procedures

4.2.1 Preparation of samples for thermal ageing

To perform the thermal ageing test, composite solder balls (800 μm in diameter) containing three different reinforcements were soldered onto experimental chips with Cu pads (with diameter of 600μm). These three kinds of composite solder were SAC/FNS, SAC/TiC and SAC/NG, while plain SAC solder balls were used as control group. After reflow process, all solder balls in experimental and control groups were soldered onto Cu pads. After ultrasonically cleaning, these chips were placed in a vacuum oven. When conducted thermal ageing test, the thermal ageing temperature was set to 150℃, while thermal ageing time were 0h, 200h, 400h and 600h, respectively. The detail of experimental conditions can be seen in Table 4.1. Different samples that experience different thermal ageing time were studied concerning their

microstructures evolution and mechanical properties.

Table 4.1 Experimental design of isothermal ageing test

Atmosphere	Vacuum			
Temperature	150℃			
Target 1	Microstructures at interfaces and matric			
Target 2	Microhardness			
Target 3	Shear strength			
Ageing Time	0h	200h	400h	600h
SAC				
SAC/0.05FNS				
SAC/0.1FNS				
SAC/0.2FNS				
SAC/ 0.05TiC				
SAC/ 0.1TiC				
SAC/ 0.2TiC				
SAC/ 0.05NG				
SAC/ 0.1NG				
SAC/ 0.2NG				

4.2.2 Microstructural observation

For microstructural observation, different solder samples after different ageing time were firstly mounted in epoxy before grinding and polishing. The preparation process of solder samples for microstructural analysis was presented in Figure 4.1. To obtain a clear microstructural morphology, all samples polished were etched using a lab-made etching reagent; the metallographic etching reagent is constituted by the mixture of ethanol and hydrochloric acid (99.5 vol. % ethanol and 0.5 vol. % hydrochloric acid).

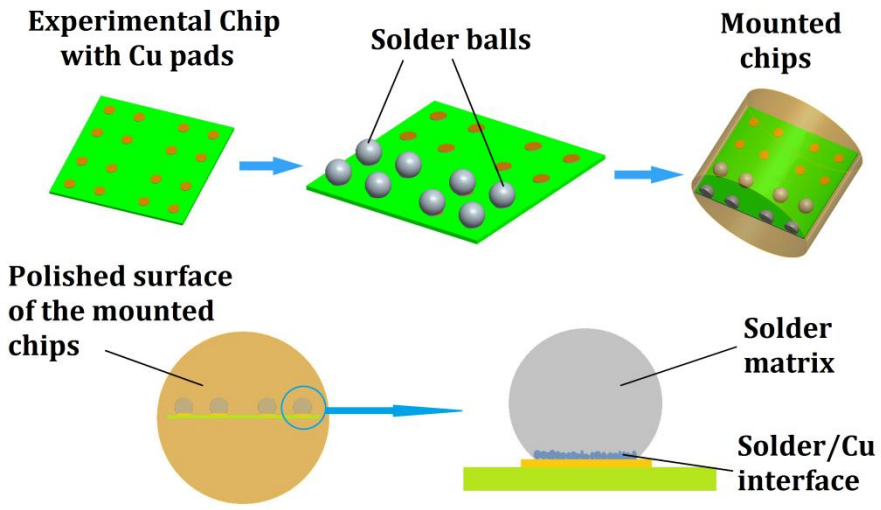

Figure 4.1 preparation process of solder samples for microstructural analysis

The microstructural morphologies of solder joints at the solder/Cu interface (or in the solder matrices) were observed using an environmental scanning electron microscope (ESEM Quanta 200).

4.2.3 Mechanical tests

To evaluate the effect of thermal ageing on mechanical strength of solder joints, micro-hardness and shear strength of solder joints reinforced with different reinforcement experienced different ageing time were comparatively analysed. Specifically, the micro-hardness test was carried out using a Vickers hardness tester (M-CT) at room temperature; the process in detail is shown in a schematic diagram (see Figure 4.2). During hardness test, the applied load was 100g while the dwell time was 20s. For each solder sample, thirty points were tested with the minimum and maximum values removed. By measuring the size of impression diagonals, the micro-hardness data of different samples was calculated using Equation 4-1 and Equation 4-2:

$$HV = 0.102 \times 2\frac{F \sin 68^0}{d^2} \tag{4-1}$$

$$d = \frac{(d_1+d_2)}{2} \tag{4-2}$$

where HV is the data of Vickers hardness, F is the loading force and d is the arithmetic mean value of d_1 and d_2.

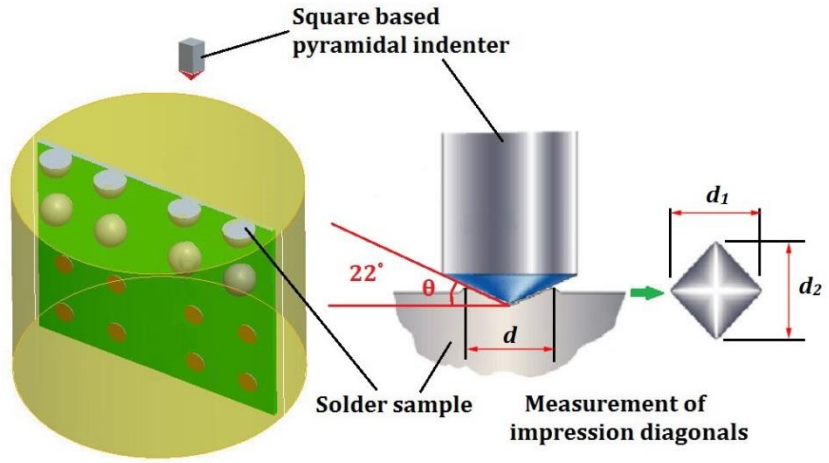

Figure 4.2 Schematic diagram of microhardness test

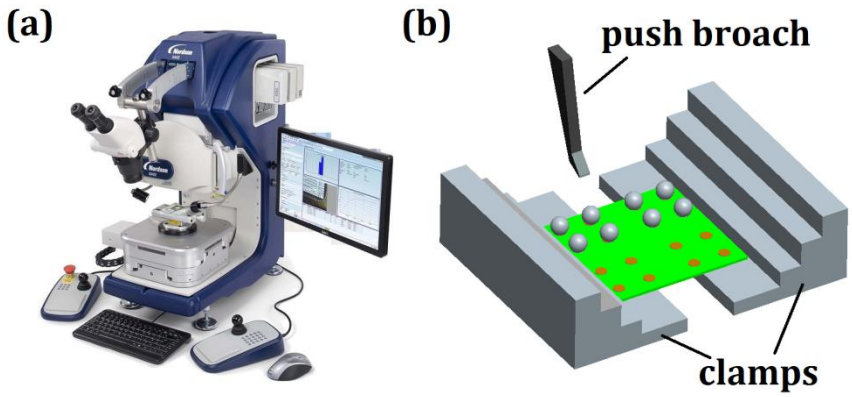

Figure 4.3 (a) DAGE tester and (b) Schematic diagram of shear test

The solder balls with diameter of 800 μm were also utilized for ball shear test. These solder balls, by using a reflow oven, were soldered on an experimental chip, which have copper soldering pads (with diameter of 600μm). The ball shear test was conducted on a Multi-function push pull tester (DAGE 4000-plus, Nordson Co. Ltd., U.S., shown in Figure 4.3a) with shear height of 50μm and shear speed of 25mm/s; the schematic diagram of shear test is shown in Figure 4.3b. In order to ensure the reliability of experimental data, shear strength values of thirty solder balls with the abnormal data (the data those greater or less than the half of the average value tested) removed were recorded for each kind of solder.

4.3 Results and Discussion

4.3.1 Microstructural evolution at solder/Cu interface

The microstructure and mechanical properties of interfacial IMC are main factors that considerably affect the reliability of solder joint. In general, the thickness of interfacial IMC would increase continuously during thermal ageing. In view of the interfacial IMCs are mostly consist of brittle phase, the extensive growth of interfacial IMCs would seriously threaten the service reliability of solder joints. In this part, the microstructural evolution of interfacial IMCs of both plain and composite solder joints are observed using SEM. The obtained SEM images of SAC, SAC/FNS, SAC/TiC and SAC/NG solder joints experienced different ageing times are shown in Figures 4.4, 4.5, 4.7 and 4.8, while the thickness data of all samples are presented in Figures 4.9, 4.10 and Table 4.2, 4.3, respectively.

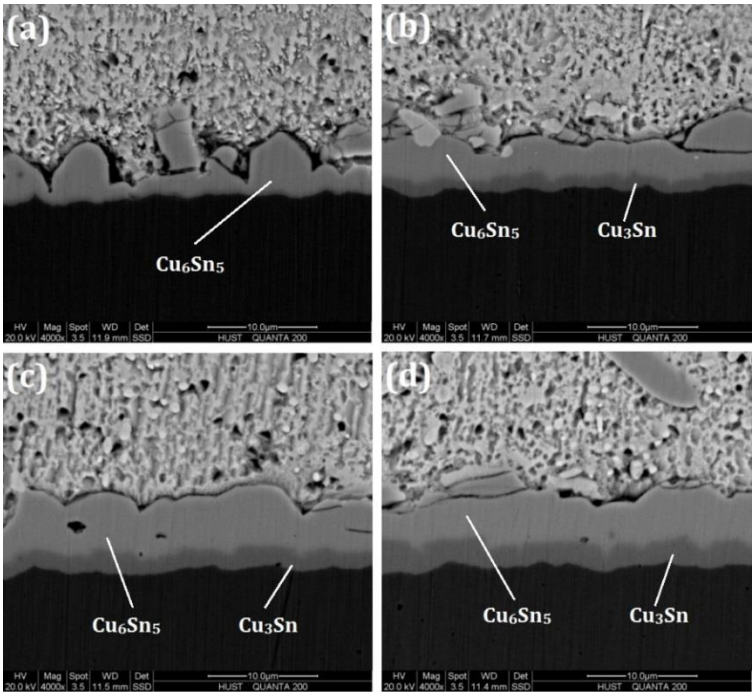

Figure 4.4 Microstructure of interfacial IMC in SAC: (a) 0h; (b) 169h; (c) 324h and (d) 484h

The microstructural evolution of interfacial IMC of plain SAC solder joint is shown in Fig 4.4. It can be found that scallop-like Cu_6Sn_5 IMC was formed at

Cu/solder interface after reflow process. In addition, the Cu_3Sn IMC was formed under Cu_6Sn_5 IMC with ageing time increases while the thickness of Cu_3Sn IMC also showed a continuous increase during ageing period (see Fig. 4.4b-d). In the condition of thermal ageing, the growth of Cu_6Sn_5 IMC was based on the inter-diffusion between Cu and Sn atoms that come from Cu substrate and solder joint, while the growth of Cu_3Sn IMC was based on the reaction between Cu substrate and Cu_6Sn_5 IMC: $Cu_6Sn_5 + Cu \rightarrow Cu_3Sn$. Since the diffusion rate of Sn atom is much higher than that of Cu atom, the Cu_6Sn_5 IMC is more easily formed at solder side, while Cu_3Sn IMC is more easily formed at Cu substrate side.

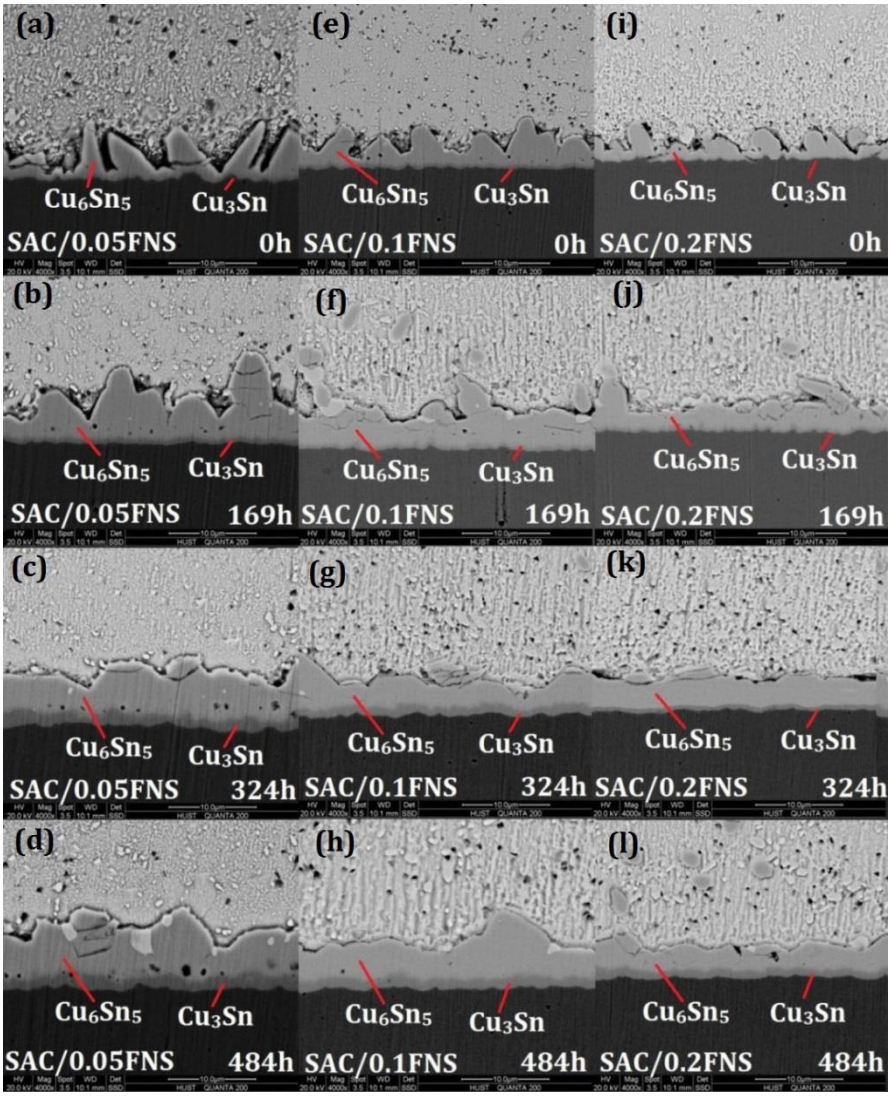

Figure 4.5 Microstructure of interfacial IMC in SAC/FNS: (a) 0h; (b) 169h; (c) 324h and (d) 484h

It can also be found from Figure 4.4 that the thickness of both of two

interfacial IMCs (Cu_6Sn_5 and Cu_3Sn) showed a continuous increase with thermal ageing time increases. The morphology of initial scallop-like Cu_6Sn_5 IMC was gradually flattened over ageing time. This phenomenon is attributed to the decreasing free energy between the solder/IMCs interface during thermal ageing [134]. This change observed in morphology of Cu_6Sn_5 IMC is well agreed with the research result proposed by Choi et al [135]. Specifically, the thickness data of two IMCs listed in Table 4.2 and 4.3 also showed that the thickness of Cu_6Sn_5 and Cu_3Sn IMC reached 9.32 μm and 3.42 μm, respectively, after 600h ageing. Compared to their initial thickness, the thickness data of two IMCs in the thermal aged sample were grown by two and ten times, respectively.

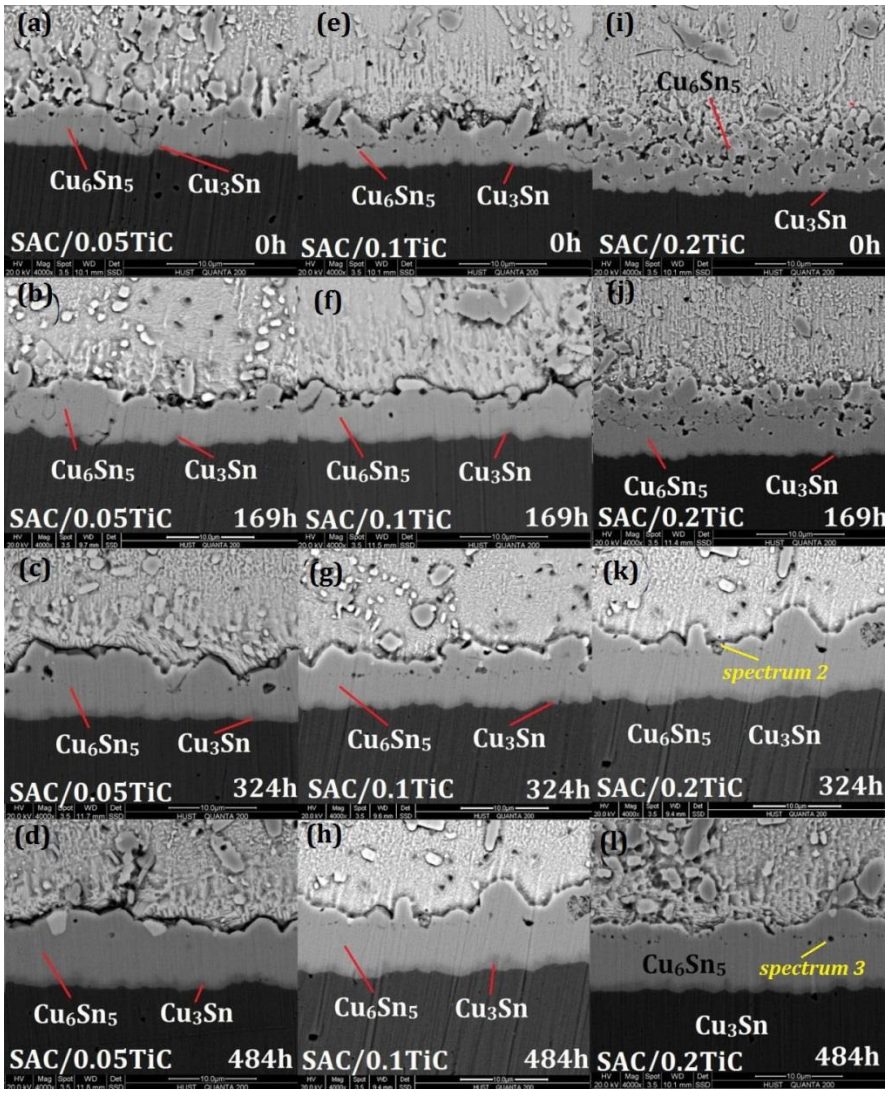

Figure 4.6 Microstructure of interfacial IMC in SAC/TiC: (a) 0h; (b) 169h; (c) 324h and (d) 484h

Under the same aging conditions, after different periods of aging time, IMC microstructure changes in the sample interface of different contents of FNS(0.05 %、0.1 % and 0.2 %) are shown in Figure.4.5. According to observed results on interfacial IMC of the initial SAC/FNS solder joints, it can be seen that adding FNS did not significantly impact the interfacial microstructure. However, by comparing the initial thickness of the interfacial IMC layer in SAC and SAC/FNS solder joints, it was found that after adding FNS reinforcement, the average thickness of IMC layers in composite solder joints' interface was less than that in the plain SAC sample. As the amount of FNS added increases, thickness of initial IMC became thinner. Observed results indicated that initial thicknesses of the Cu_6Sn_5 IMC layer in solder joints with 0.05%, 0.1% and 0.2 % added FNS were about 3.92μm, 3.75μm and 3.27μm respectively. The initial thicknesses of the Cu_3Sn IMC layer were about 0.16μm, 0.18μm and 0.17μm. The thickness data were obviously less than that in SAC solder joints. This phenomenon can be explained that in the process of reflow, some FNS reinforcement was discharged and concentrated on the interface of solder joint and Cu pad, reducing inter-diffusion between Cu atoms and Sn atoms, thus forming the relatively thin IMC layer.

On the other hand, after ageing periods of 169 hours, 324 hours and 484 hours, thicknesses of two types of IMCs (Cu_6Sn_5 and Cu_3Sn) at the SAC/FNS solder joints and Cu pad interfaces were also found to significantly increase as aging time increases. However, compared with the plain SAC solder, the growth rate of two types of IMCs in the SAC/FNS composite solder was obviously lower. After 484 hours, thicknesses of Cu_6Sn_5 IMC in composite solder with 0.05%, 0.1% and 0.2% of FNS were 9.12μm, 7.33μm and 5.96μm, while thicknesses of Cu_3Sn IMC were 2.86μm, 2.43μm and 2.17μm; the increase in thickness data of two IMCs were both significantly lower than that in the SAC solder joint. This phenomenon indicates that adding FNS reinforcement is effective to restrain the growth of IMC layer in interface under thermal ageing.

The interfacial morphology of SAC/TiC composite solder with different contents of TiC reinforcements (0.05 %、0.1 % and 0.2%) after different periods of aging time are shown in Figure. 4.6. Based on microstructural observations, it was found that the interfacial morphology of initial SAC/TiC solder joint was different with the SAC and the SAC/FNS solder joints. Specifically, The SAC/TiC solder joints showed a "porous" interface, further, the degree of "porous" increases as the amount of TiC addition increases. According to observed results on interfacial IMC of various composite solders from top-view in Figure 3.14, it can be seen that the "porous" feature observed here was actually the observation results from the side of rod-like IMC in interfaces. According to EDX results (shown in Figure.4.7a), TiC can be found in these "holes"; this phenomenon was caused by TiC gathered in interface between solder joint and Cu pad, which was discharged during reflow process. As aging time increases, it was found that thicknesses of two IMC interfaces in SAC/TiC composite solders also increased constantly. From the perspective of morphology, as aging time lengthens, initial "porous" features gradually vanish and become increasingly smooth. The quantity of "Holes" in the IMC layer also decreased, and transferred to the top of IMC layer (this phenomenon was particularly obvious in SAC/0.2TiC). According to results in Figure.4-4b EDX, it was found out that TiC still existed in these residual holes; It shows that TiC reinforcements, which initially gathered in the interface, may change their position due to the growth of IMC.

Image J was used to measure the thicknesses of interface IMC of SAC/TiC after different ageing times. Here, it should be specifically pointed out that when measuring the thicknesses of interface IMC, the area of "porous" position was ignored, in order to ensure actual IMC thickness was measured. According to test results, it finds out that as the time of thermal ageing increases, although IMC thickness of SAC/TiC composite solder interfaces also showed an increase trend, the growth rate was lower than the SAC solder. Specifically, after 484 hours of ageing, growth rates of Cu_6Sn_5 IMC thicknesses in composite solders of SAC/0.05TiC, SAC/0.1TiC and SAC/0.2TiC were 69.4%, 22.5% and 5.8%

respectively. This data were far less than growth rates of thickness of Cu_6Sn_5 IMC in the SAC sample. Similar to what happened in the SAC/FNS composite solders, TiC reinforcements also restrains the growth of Cu_3Sn IMC during ageing period to a great extent. Tests results showed that when 0.1 wt. % TiC is added, growth rates of Cu_3Sn IMC in composite solder were the lowest during ageing period. After 484 hours, thickness of Cu_3Sn IMC in SAC/0.1TiC composite solder interface increases by about 1.06 times; this data was far less than the SAC solder.

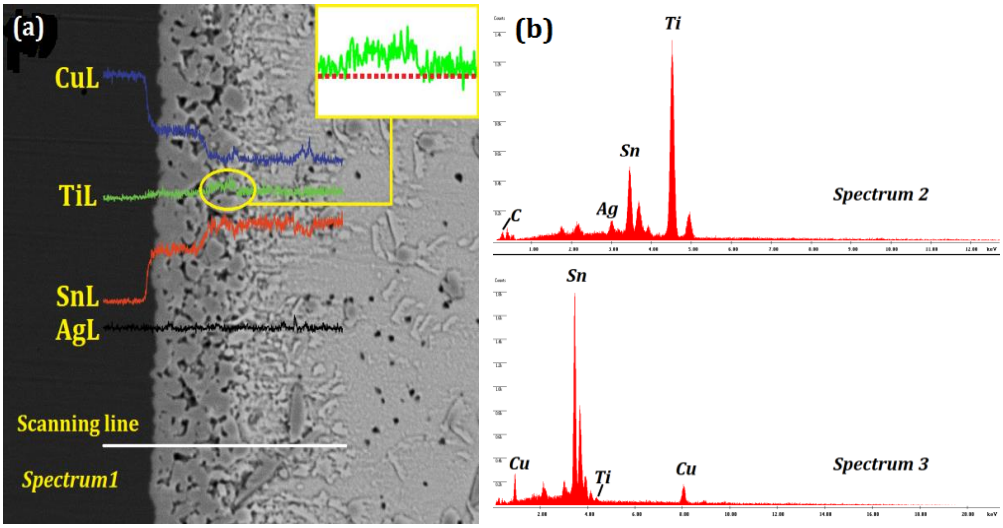

Figure 4.7 (a) EDX result of SAC/0.2TiC interface and (b) selected area in Figure. 4-3 (k) and (l)

According to observation results of SEM and EDX above mentioned, it can be seen that restraint of growth in two IMCs is mainly caused by decrease in diffusion rate of metal atoms during ageing period, which is induced by external reinforcements enriched at interfaces. On one hand, reinforcements tend to cling to surface of IMC interfaces; they may hinder diffusion of metal atoms between IMC and solders, thus limiting the growth of interfacial IMC [136]. On the other hand, foreign reinforcements gathered in interfaces may disrupt concentration gradient of Sn atoms, thus impacting the growth rate of interfacial IMCs. Besides, it was also found that after 484 hours of ageing, the thickness of Cu_3Sn in SAC/0.2TiC solder interface was greater than other two types of solders. It is because that the thermal conductivity of TiC is relatively worse. Excessive TiC might increase the temperature in interface between TiC and solder matrix, which might accelerate the diffusion of tin atoms in these interfaces, thus promoting the growth of IMC interface to some extent.

The Interfacial morphology of SAC/NG composite solder with different contents of NG reinforcements (0.05 %、0.1 % and 0.2%) after different periods of ageing time are shown in Figure. 4.8. By comparing with the SAC solder, it can be found that addition of NG changed the morphology of interfacial IMC to some extent. According to observation results, it can be seen that after adding NG, the interfacial IMC demonstrated a cauliflower-like structures. In addition, in order to evaluate thickness data of interfacial IMC during ageing period, Image J was also used to measure thicknesses of IMC in SAC/ NG solder interfaces after different ageing time. Specifically, by observing the initial morphology of interfacial IMC of SAC/NG solder, it can be seen that thickness of initial interfacial IMC was in direct proportion of adding amount of NG. For instance, the thickness of initial interfacial IMC in plain SAC solder was 4.22±0.27μm, while the data in 0.2NG solder was 4.79±0.21μm. According to relevant research, formation activation energy of $(Cu,Ni)_6Sn_5$ is about 34.6 kJ/mol, while the formation activation energy of Cu_6Sn_5 is about 58.6 kJ/mol [137]. Additionally, coefficients of diffusion of copper atoms and nickel atoms in molten tin are 1.8×10^{-4} cm^2/s and 2.3×10^{-4} cm^2/s, respectively [138]. Therefore, it can be seen that for solder that contains nickel, $(Cu,Ni)_6Sn_5$ is more likely to form than Cu_6Sn_5. In this study, nickel atoms that come from NG added diffuse to interfaces between solder and Cu pad during reflow process, thus leading to the formation of $(Cu,Ni)_6Sn_5$ IMC. Hence, changes in morphology and thickness of SAC/NG solder interface were mainly caused by Ni introduced.

According to observation results, thicknesses of interfacial IMC in SAC/NG composite solders with different amount of NG also showed an increase trend as ageing time increases. Similar to cases in SAC/FNS and SAC/TiC solders, growth rate of Cu_6Sn_5 IMC was obviously lower than the plain SAC; In particular, the growth of Cu_3Sn IMC was limited to a great extent. Likewise, the mechanism that limits IMC growth in SAC/FNS and SAC/TiC solder interfaces, which is discussed previously, can also be used to explain the growth of IMC in SAC/ NG solder interfaces. Besides, according to relevant literatures [13, 20-21], the addition of Ni element also poses apparent impacts on growth of IMC interface. Yoon et al. [138] reported that the diffusion coefficient of $(Cu,Ni)_6Sn_5$ IMC interface was

increased after adding appropriate amount of Ni reinforcement.

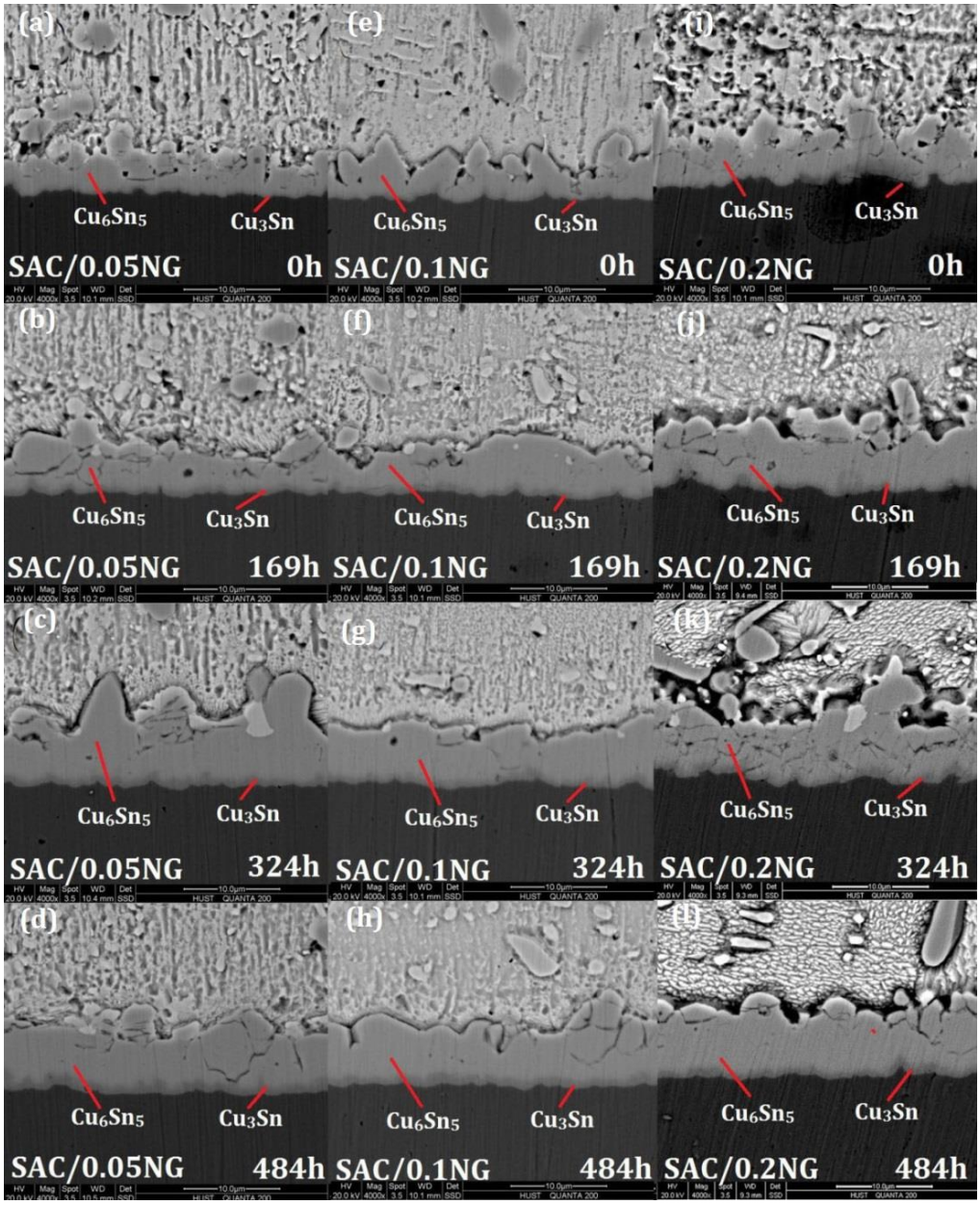

Figure 4.8 Microstructure of interfacial IMC in SAC/NG: (a) 0h; (b) 200h; (c) 400h and (d) 600h

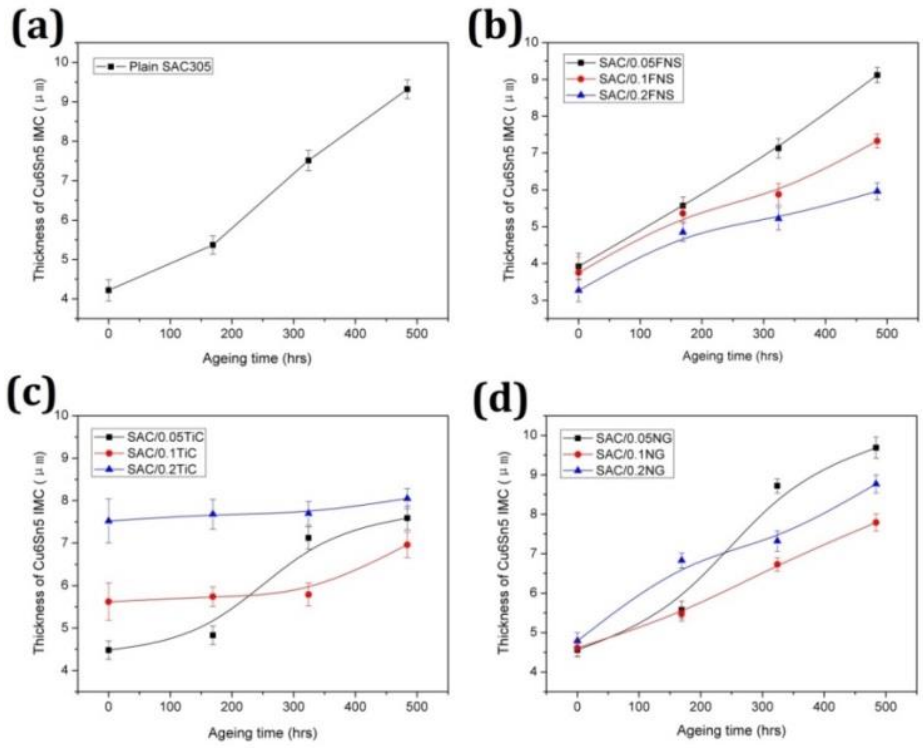

Figure 4.9 The thickness of Cu_6Sn_5 IMC: (a) SAC; (b) SAC/FNS; (c) SAC/TiC and (d) SAC/NG

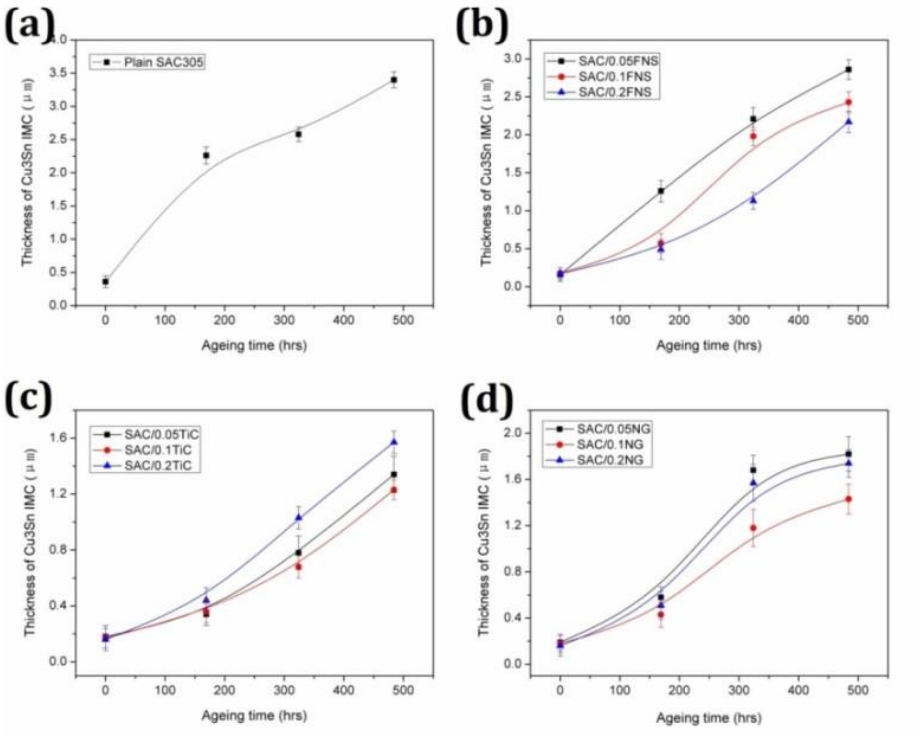

Figure 4.10 The thickness of Cu_3Sn IMC: (a) SAC; (b) SAC/FNS; (c) SAC/TiC and (d) SAC/NG

Table 4.2 Thickness data of Cu_6Sn_5 IMC in solder joint after different ageing time

	Thickness of Cu_6Sn_5 IMC (μm)			
	0h	**169h**	**324h**	**484h**
SAC	4.22±0.27	5.37±0.23	7.51±0.26	9.32±0.24
SAC/0.05FNS	3.92±0.36	5.57±0.24	7.13±0.26	9.12±0.21
SAC/0.1FNS	3.75±0.43	5.36±0.22	5.88±0.29	7.33±0.19
SAC/0.2FNS	3.27±0.31	4.85±0.25	5.22±0.31	5.96±0.23
SAC/0.05TiC	4.48±0.32	4.83±0.23	7.12±0.26	7.59±0.28
SAC/0.1TiC	5.62±0.44	5.74±0.23	5.79±0.27	6.96±0.31
SAC/0.2TiC	7.52±0.52	7.68±0.35	7.71±0.28	8.05±0.25
SAC/0.05NG	4.56±0.17	5.58±0.22	8.72±0.18	9.69±0.27
SAC/0.1NG	4.61±0.2	5.47±0.18	6.73±0.17	7.79±0.22
SAC/0.2NG	4.79±0.21	6.83±0.19	7.32±0.26	8.77±0.23

Table 4.3 Thickness data of Cu_3Sn IMC in solder joint after different ageing time

	Thickness of Cu_3Sn IMC (μm)			
	0h	**169h**	**324h**	**484h**
SAC	0.36±0.09	2.26±0.13	2.58±0.11	3.42±0.12
SAC/0.05FNS	0.16±0.09	1.26±0.14	2.21±0.15	2.86±0.13
SAC/0.1FNS	0.18±0.07	0.57±0.13	1.98±0.12	2.43±0.14
SAC/0.2FNS	0.17±0.08	0.49±0.13	1.13±0.11	2.17±0.14
SAC/0.05TiC	0.18±0.08	0.34±0.11	0.78±0.12	1.34±0.13
SAC/0.1TiC	0.17±0.09	0.36±0.08	0.68±0.07	1.23±0.08
SAC/0.2TiC	0.16±0.08	0.44±0.09	1.03±0.14	1.57±0.15
SAC/0.05NG	0.19±0.07	0.58±0.09	1.68±0.13	1.82±0.15
SAC/0.1NG	0.18±0.08	0.43±0.11	1.18±0.16	1.43±0.13
SAC/0.2NG	0.17±0.08	0.51±0.12	1.57±0.16	1.74±0.12

In general, the growth of interfacial IMCs under isothermal ageing can be described using the following empirical equation:

$$X = (Dt)^n \tag{4-3}$$

in which X is the thickness of IMC layer at the time of t, D is the diffusion constant that decides the growth rate of IMC layer, n is time coefficient. In this study, IMC growth during ageing process is mainly determined by diffusion of Sn, Cu （or Ni） atomic. The "n" can be obtained using linear fitting from the functional relationship between Ln (X) v.s. Ln (t); these functional curves for SAC305/FNS, SAC305/TiC and SAC305/NG compared with SAC305 are shown in Fig.4.10. According to the linear fitting results, n for SAC305 is 0.416, while average n for SAC305/FNS, SAC305/TiC and SAC305/NG are 0.404, 0.343 and 0.418, respectively. . Thus the diffusion coefficients for different dolders can be calculated based on (4-3); the calculated diffusion coefficients of various solder joints and factors of linear fitting are shown in Table 4.4.

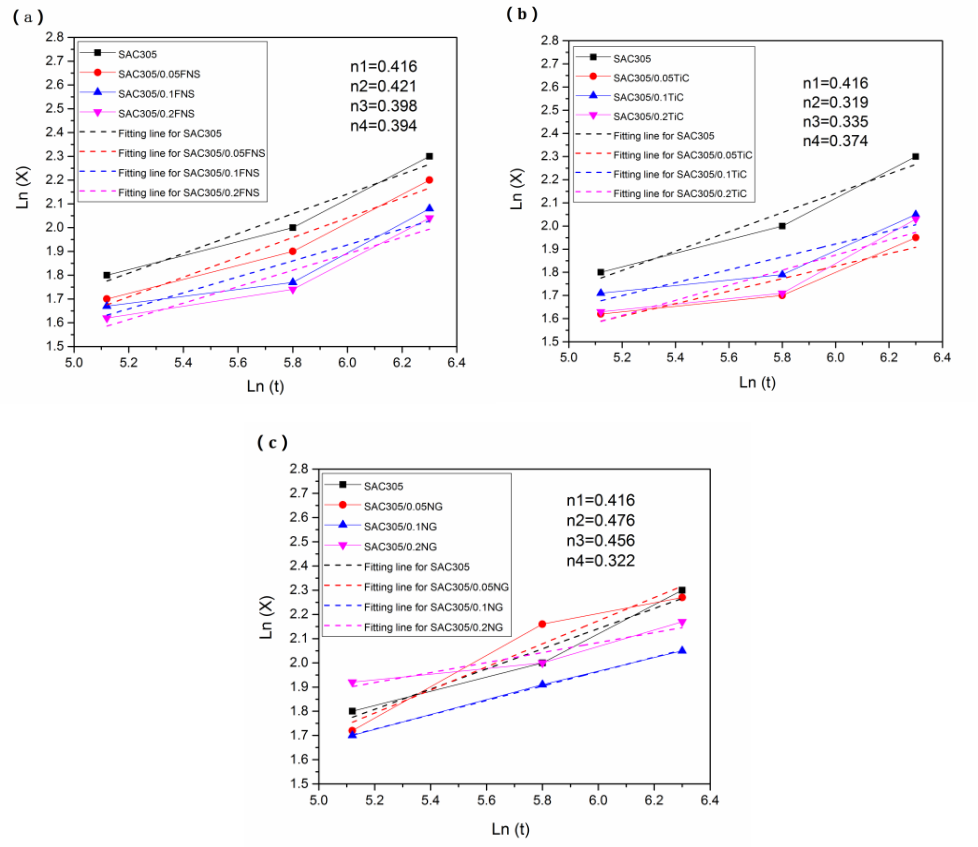

Figure 4.11 Functional relationship of Ln(X) v.s. Ln(t) for: (a) SAC305/FNS; (b) SAC305/TiC; (c) SAC305/NG

Table 4.4 Diffusion coefficient in different solder joint under isothermal ageing

Solder	D（$\times 10^{-15}$ cm^2/s）	R^2
SAC	9.4	0.914
SAC/0.05FNS	8.7	0.939
SAC/0.1FNS	7.4	0.923
SAC/0.2FNS	7.1	0.934
SAC/0.05TiC	7.8	0.913
SAC/0.1TiC	6.2	0.933
SAC/0.2TiC	5.9	0.967
SAC/0.05NG	7.6	0.918
SAC/0.1NG	6.4	0.929
SAC/0.2NG	5.3	0.954

It can be seen from Table 4.4 that compared with diffusion coefficients of the plain SAC305 solder, all three composite solders show lower diffusion coefficients. Regardless of what type of composite solders, diffusion coefficients of solder joints under isothermal ageing decrease as the addition amount of reinforcements increase. In particular, if 0.2 wt.% of TiC and NG is added, decrease in diffusion coefficients of solder joints is the most significant, reaching 5.9×10^{-15} cm^2/s and 5.3×10^{-15} cm^2/s, respectively. It indicates that addition of particles of FNS, TiC and NG into SAC305 can effectively lower the growth of IMC layer under isothermal ageing condition.

4.2.2 Microstructural evolution in solder matrix

In addition to observing the morphology of interfacial IMCs, the microstructural evolution in different solder matrix after 484h was also studied. In this section, all three composite solders with 0.2 wt. % reinforcement together with the SAC solder were selected to comparatively study the microstructural evolution in solder matrix; the morphologies of matrix structures of various solder joints before and after 484h ageing are shown in Figure.4.12.

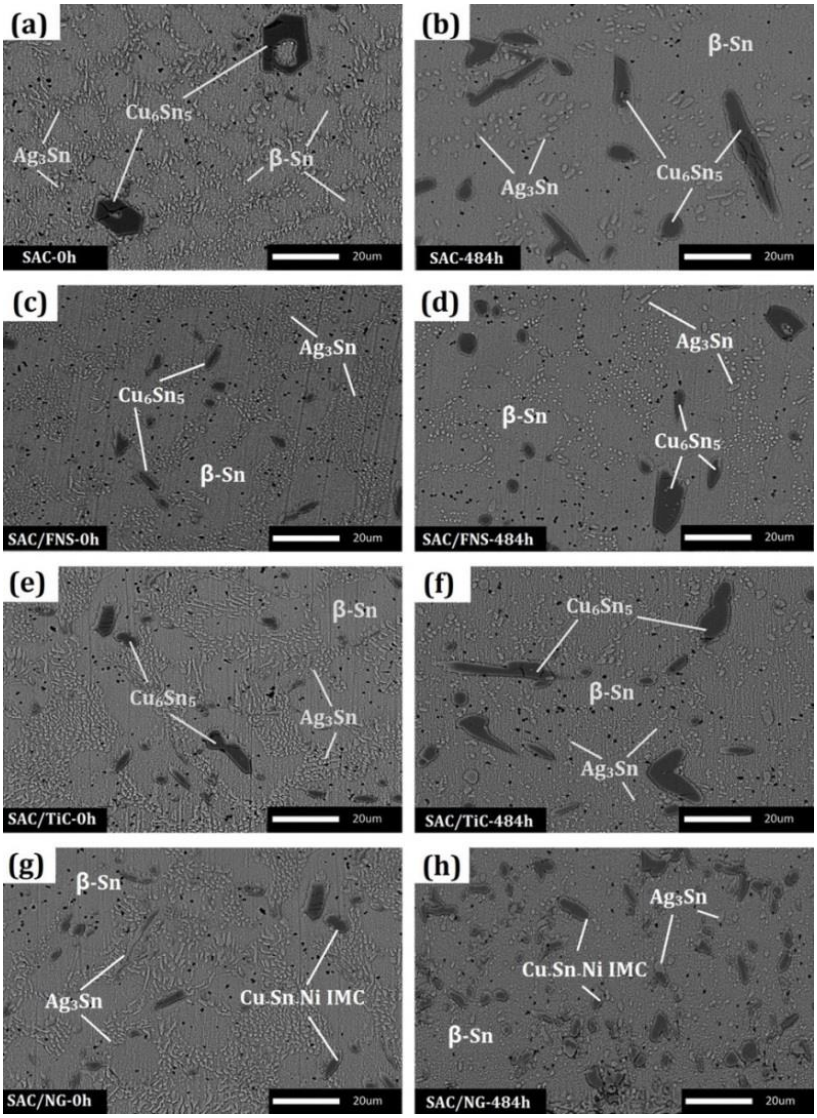

Figure 4.12 Typical microstructure in solder matrix before and after 484h ageing: (a) and (b) SAC305; (c) and (d) SAC305/0.2FNS; (e) and (f) SAC305/0.2TiC; (g) and (h) SAC305/0.2NG

It can be seen from Figure.4.12a and b that the initial plain SAC solder matrix mainly contains β-Sn phase, short rod-like Ag_3Sn IMC and polygonal Cu_6Sn_5 IMC. After 484 h, it can be found that the grain boundary of β-Sn phase in the plain SAC solder matrix almost disappeared, while Ag_3Sn IMC showed an obvious coarsening; it also transforms from initially grains or short rod-like to circular or oval grains. In addition, as for Cu_6Sn_5 IMC, both volume and quantity were apparently increased after 484h of thermal ageing.

Compared with the SAC solder, it can be found from the initial SAC/0.2FNS solder matrix that after adding FNS reinforcement, the size of Ag_3Sn IMC and

Cu_6Sn_5 IMC in initial SAC/FNS solder matrix was significantly decreased compared with the SAC solder. As analysed in Section 3.5.1, foreign reinforcements added tend to adsorb on surface of IMC during the solidification process; atomic inter-diffusion is thus reduced. After 484h ageing, the grain boundary of β-Sn phase in the matrix of SAC/0.2FNS also becomes fuzzy; however, the overall range of variation was less than that in the SAC. Besides, although the size of Ag_3Sn and Cu_6Sn_5 IMC showed an increase in the aged composite solder matrix, the degree of increase was less than the SAC sample. In particular, the average size of Ag_3Sn IMC in aged SAC/0.2FNS was only 1/5 of the size in the SAC solder. Likewise, it was also observed in the matrix of aged SAC/0.2TiC that the growth of Ag_3Sn and Cu_6Sn_5 IMC was suppressed, and their size was less than that in the SAC solder. For SAC/0.2NG, the most obvious phenomenon is that abundant bulky Cu-Ni-Sn IMCs were formed in the solder matrix after 484h ageing. The possible reason is that during reflow process, nickel atoms, which were not totally involved in reaction of solder matrix, continue to be involved in inter-diffusion reaction with copper and tin atoms in the ageing process, thus leading to the abundant bulk-like Cu-Ni-Sn IMCs formed.

4.3 Mechanical Properties

4.3.1 Micro-hardness

Micro-hardness test data of all samples after different ageing time is shown in Table 4.5. To facilitate contrastive analysis, hardness data of SAC samples obtained in the same conditions is also added to test results.

Table 4.5 Micro-hardness data of different solder alloy after different ageing time at 150℃

Solder	Micro-hardness（HV）			
	0h	169h	324h	484h
SAC	13.04±0.16	12.63±0.14	12.12±0.18	11.86±0.19
SAC/0.05FNS	13.33±0.15	13.16±0.18	12.89±0.13	12.47±0.19
SAC/0.1FNS	13.47±0.25	13.18±0.19	12.76±0.16	12.53±0.21
SAC/0.2FNS	13.68±0.19	13.24±0.21	12.95±0.23	12.55±0.18
SAC/0.05NG	13.72±0.15	13.61±0.18	13.19±0.17	12.96±0.16
SAC/0.1 NG	14.17±0.18	13.94±0.21	13.43±0.17	13.06±0.18
SAC/0.2 NG	14.38±0.21	14.19±0.18	13.77±0.16	13.18±0.19
SAC/0.05TiC	14.06±0.16	13.58±0.14	13.12±0.18	13.03±0.18
SAC/0.1 TiC	14.39±0.21	13.77±0.18	13.52±0.16	13.36±0.18
SAC/0.2 TiC	14.52±0.22	14.09±0.19	13.94±0.23	13.52±0.2

According to test results of micro-hardness of samples before thermal ageing, the addition of different foreign reinforcement can enhance the micro-hardness of SAC solder alloy to varying degrees. Besides, hardness of each composite solder alloy increased as the quantity of addition increases. For instance, before ageing, average micro-hardness of the SAC sample was about 13.14 HV, while hardness data of SAC/0.2FNS、SAC/0.2NG and SAC/0.2TiC were 13.68HV、14.38HV and 14.42HV, respectively. Among them, hardness of composite solder with 0.2 wt. % TiC addition presents the most significant increase, reaching 11.3%. As ageing time increases, micro-hardness of the SAC solder decreased obviously; after 484 hours ageing, its hardness decreased to 11.86HV. In comparison, although hardness data of all composite solders also decreased as ageing time increases, after the same length of ageing time, micro-hardness data of all composite solder alloys were higher than the SAC solder alloy. After 484 hours ageing, average decreasing amplitudes in hardness of composite solder alloys with FNS、NG and TiC reinforcements are 5.7%、7.2% and 6.9%, which were lower than that of the

SAC solder alloy.

Improvement in hardness of composite solder alloys can be explained with refined crystalline strengthening caused by adding reinforcements. According to microstructure analysis of solder alloys in Section 3.5.1, β-Sn and IMC phases in composite solder were gradually refined as the amount of reinforcement particles increases (especially FNS and TiC). This refinement phenomenon can also be observed in composite solders after ageing. In general, grain refinement and improvement in micro-hardness are internally related, and conform to the Hall-Petch relationship:

$$\sigma_\gamma = \sigma_0 + \frac{K}{\sqrt{d}} \tag{4-4}$$

Here, σ_γ is the yield strength of materials; σ_0 and K are constants related to materials; d is the average grain size of materials. In general, the main barrier of dislocation motion in alloy is grain boundary. When dislocation gathers at grain boundary, stress also concentrates on the front of gliding surface, and grain boundary eventually yields; deformation movement then transfers to the next grain boundary. Therefore, grain refinement may lead to increase in the number of grain boundary, thus increasing the yield strength of alloy materials.

On the other hand, the Shear lag theory [140] can also be used to analyze the increase of micro-hardness. According to the theory, in composite materials, the contribution of reinforcement to matrix strength can be expressed as:

$$\sigma_{mmc} = \sigma_m\left[V_f\left((s+4)/4\right) + \left(1 - V_f\right)\right] \tag{4-5}$$

where σ_m is the strength of matrix alloy, V_f is the volume fraction of reinforcement, s is the aspect ratio of reinforcement. For FNS and TiC particles, it can be assumed that s=1, hence concluding:

$$\sigma_m = \sigma_m\left(1 + \frac{V_f}{4}\right) \tag{4-6}$$

As additive amount of reinforcements in this study were relatively small, the strengthening effects caused by reinforcement particles were limited. Strengthening effects are mainly related to dispersion strengthening of Ag_3Sn、

Cu_6Sn_5 and（Cu, Ni）$_6Sn_5$ IMCs in solder materials. This strengthening effect can be explained using dislocation bypass mechanism [141]. According to this mechanism, there has stress field and lattice distortion existed in the interface between matrix and second phase. During the process of deformation, the second phases could enhance the strength of alloy by hindering glide of grain boundary and dislocation. In general, when dislocation bypasses particles dispersed in matrix, as foreign shear strength increases, the curvature of dislocation increases and gradually becomes ring-like. Every dislocation passed the particle leaves a dislocation loop. These dislocation loops formed pose resistance to other dislocations which also want to pass the particle. Moreover, as more dislocation loops accumulates around particles, the resistance to other dislocations also increases; the strength of material is thus increased [142]. As mentioned in Section 3.5.1, addition of FNS and TiC could refine Ag_3Sn IMC to some extent. In contrast, although adding NG reinforcements may coarsen Ag_3Sn IMC, a mass of （Cu, Ni）$_6Sn_5$ IMC can be formed in the matrix. According to the above analysis, the refined IMCs and foreign reinforcement dispersed in solder matrix collectively enhance the micro-hardness of composite solders.

4.3.2 Shear strength

Shear strength test results of three composite solders are shown in Table 4.6. Likewise, to be convenient for comparative analysis, shear strength data of SAC sample were also added in each test result.

According to the testing results, the addition of FNS and NG can enhance shear strength of solder alloy to some extent. Specifically, after adding 0.2 wt. % amount of reinforcement, shear strength values of SAC/FNS and SAC/NG solder alloys were increased from the initial 48.8 MPa to 56.8 MPa and 58.4 MPa respectively, improvement in shear strength of these two composite solders reached 16.3% and 19.6%. Improvement in shear strengthen of the two composite alloys is also mainly attributed to reinforcement added and refined IMC in solder

matrix. The “pinning effects” produced by these second phases could hinder dislocation glide in the shear direction to a large extent. In addition, in composite solders, dislocation produced by elastic modulus mismatch and thermal mismatch, as well as load transfers induced by the existence of reinforcements are also reasons for the improvement in shear strengthen. In contrast, the doping of TiC leads to slight decrease in shear strengthen of SAC/TiC solder. According to observation results of SAC/TiC solder joints in Section 3.4.5, it is assumed that this phenomenon can be explained by the agglomeration of reinforcements formed in SAC/TiC matrix. This agglomeration of foreign reinforcement may cause stress concentration within solder joints, leading to crack or other defects when the solder joint under shear force and thus lower the shear strength of solder joint.

Table 4.6 Shear strength of different solder alloy after different ageing time

Solder	Shear strength（MPa）			
	0h	169h	324h	484h
SAC	48.8±1.8	43.4±1.6	40.7±1.9	38.2±2.5
SAC/0.05FNS	52.3±2.1	48.6±1.8	44.3±2.3	40.1±1.5
SAC/0.1FNS	55.7±1.8	48.8±2.1	46.3±1.9	42.7±2.1
SAC/0.2FNS	56.8±2.4	51.2±2.6	48.8±2.6	43.6±2.6
SAC/0.05NG	52.7±2.6	50.3±2.8	46.7±2.8	44.8±2.7
SAC/0.1 NG	56.4±1.9	53.6±2.6	50.7±1.9	47.3±2.2
SAC/0.2 NG	58.4±2.2	53.8±1.8	51.4±2.5	48.6±2.1
SAC/0.05TiC	48.5±2.5	44.2±2.6	42.3±2.3	40.7±1.9
SAC/0.1 TiC	47.2±1.9	44.7±2.2	42.9±2.1	42.6±2.4
SAC/0.2 TiC	46.7±2.7	45.1±2.8	43.2±2.2	41.8±2.6

As ageing time increases, average shear strengthen of the SAC sample showed an obvious decrease from the initial 48.8MPa to 38.2MPa, the decreasing rate was 21.7%. In contrast, although shear strengthen of three composite solder alloys also gradually decreased during ageing process, the shear strengthen values were higher than the SAC composite alloys under the same condition. It is worth

noticing that although initial shear strengthen of SAC/TiC solder alloys was slightly lower than the SAC, the shear strengthen of the aged SAC/TiC sample begins to higher than the SAC sample. This phenomenon was directly related to the process that the "porous" IMC at the interface was gradually compacted during ageing process. Among three reinforcements, NG is more effective on improving shear strengthen of solder alloy. After 484 hours ageing, SAC/NG still maintains highest shear strengthen among the three composite solders. Specifically, after 484h ageing, the average shear strengthen of solder alloy with 0.2 wt. % NG addition was 48.6 MPa; this data was 27.2% higher than SAC samples in the same condition. Here, the improvement in shear strength of composite solders are mainly attributed to the following reasons: 1) "pinning" effects caused by reinforcement added and refined IMC particles; 2) the growth of interfacial IMCs (Cu_3Sn and Cu_6Sn_5) was suppressed.

4.4 Summary

In this chapter, the microstructural and mechanical evolution of three composite solders under thermal ageing was comparatively studied. According to experimental result, three reinforcements mentioned in this thesis can all effectively suppress the growth of Cu_6Sn_5 and Cu_3Sn IMCs under thermal ageing, while the addition of FNS and TiC can retard the coarsening of Ag_3Sn and Cu_6Sn_5 IMCs during thermal ageing. In addition, the doping of three reinforcements improved the mechanical strength of SAC solder alloy to some extent. Specifically, the TiC reinforcement is more effective for the improvement of harness, while the addition of FNS and NG is more positive for improving the shear strength of solder joints.

Chapter 5 Electro-migration Behaviour of Composite Solder Joints

5.1 Introduction

Electro-migration (EM) of solder joint is the directional migration of atoms in solder joints under high current density due to the effect of electron wind. In some conditions, electro-migration can lead to a rapid growth or consumption of IMC at the interface of an interconnection structure, resulting in thick IMC or defects such as voids on interfaces. In addition, electro-migration may cause composition segregation of elements within solder joints, leading to uneven distribution of stresses in them. For currents of high density, Joule heat generated accelerates void formation and crack growth in solder joints. At present, as a result of microminiaturization and multi-functionalization of electronic products, a size of micro solder joints and an interconnection height of electronics packages are greatly reduced, leading to a sharp rise in current density affecting solder joints in service, under these conditions, failure of solder joint caused by electro-migration can lead to severe threat of service reliability of such joints.

Some researchers found that compounding or alloying of solder joints can effectively relieve or restrain the electro-migration in condition of large EM stressing. For example, addition of metal elements such as Ni, Co, Zn and Sb and nonmetal nano-particles such as ZnO, Al_2O_3, carbon nano-tubes (CNT) and graphenes (GNS) in solders was proved to restrain electro-migration in solder joint to a certain extent[13, 143-144]. In order to verify the effect of three different reinforcements -FNS, TiC and NG- on electro-migration in solder joints, in this chapter, the reliability of newly prepared composite solder alloys is evaluated under EM stressing. Microstructural evolution and mechanical properties of different solder systems exposed to different times of EM stressing are studied. Surface conditions of as-stressed samples are tested using a surface profiler. In

addition, the service life of different solder joints is assessed and comparatively analysed. The failure mechanism of different composite solder joints under EM stressing is analysed as well.

5.2 Experimental procedures

5.2.1 Design and preparation of EM samples

A U-type sample structure for EM tests was designed and prepared. As shown in Figures 5.1a and b, two L-shape copper plates were welded together to form a U-shape sample using a clamp and a reflow oven; the dimensional details of the sample are presented in Figure 5.1c. A current density used in EM tests in this chapter was about 1.5×10^4 A/cm^2, with tests performed of room temperature. After different stressing times, samples were analysed to understand the microstructural evolution in solder joints. Additionally, the mechanical properties, including micro-hardness and the elasticity modulus were evaluated employing a nano-indentor.

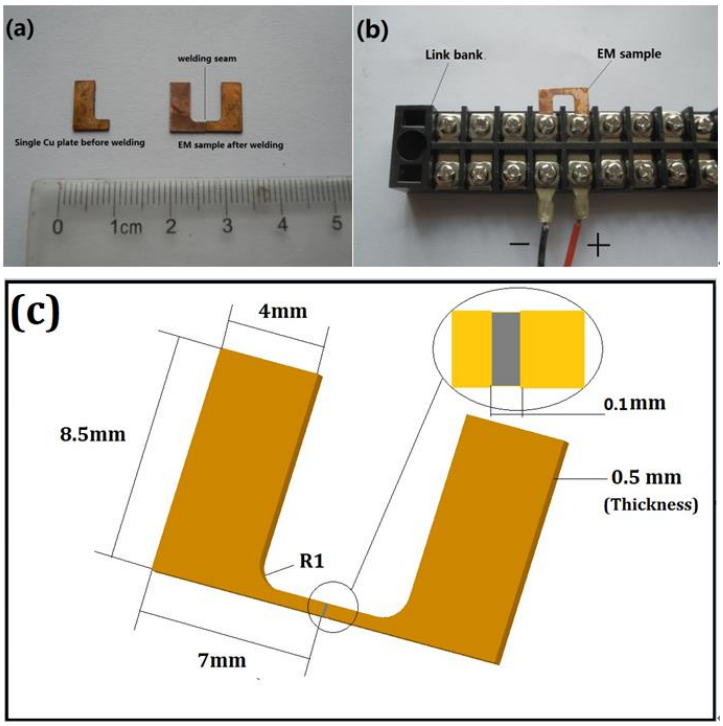

Figure 5.1 (a) and (b) Digital photographs of EM sample; (c) 3D dimensions of EM sample

5.2.2 Microstructure

In the EM tests, 10 samples for each kind of solder (plain and composite) were tested to satisfy different testing purposes. Specifically, microstructural evolution of one selected sample for each kind of solder was continuously observed using a scanning electron microscope (SEM QURTA 200) every 120 hours; the total stressing time of the TM tests was designed as 360 h. The rest of samples that experienced the same TM stressing process were used for mechanical and compositional analyses. Surface parameters of the as-stressed samples were tested using a surface profiler ZYGO.

5.2.3 Mechanical properties

Mechanical properties of all samples before and after TM tests were evaluated with a nano-indenter Hysitron Ti750 at a constant load rate of 10 mN and a dwell time of 5 s. To assess the difference in mechanical properties in various areas of the samples, each solder seam was evenly divided into three areas, denoted as Area Anode, Area Centre and Area Cathode, at different positions between cold and hot ends. Five randomly selected locations for each area were tested to ensure reliability of the test results (Fig. 5.2).

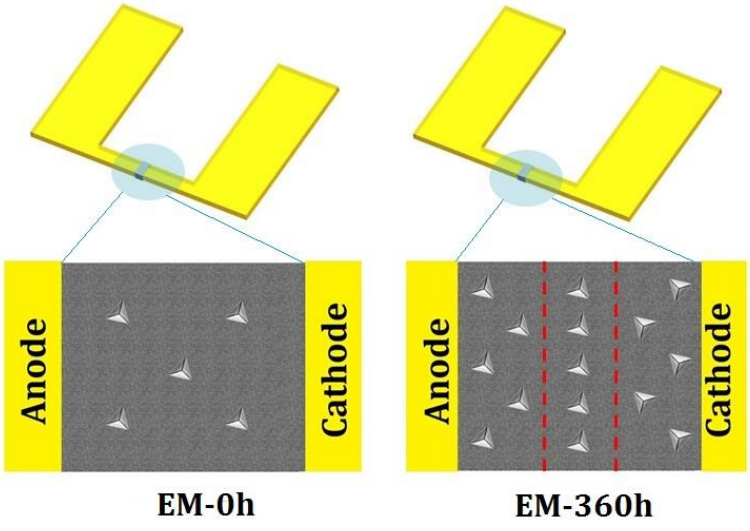

Figure 5.2 Schematic diagram of indentation positions in EM samples

A level of hardness (H) was calculated from the obtained load–displacement data. As the indenter was allowed to penetrate into the specimen, both elastic and plastic deformation occurred, and only the elastic portion of the displacement was recovered during unloading. Nano-indentation hardness is defined as follows:

$$\mathrm{H} = \frac{P_{max}}{A} = \frac{P_{max}}{24.5 h_c^2} \tag{5-1}$$

where P_{max} is the load measured at the maximum depth of penetration (h) in an indentation cycle, A is the projected contact area, and h_c is the contact depth of the indentation, which is given by

$$h_c = h - 0.75 \frac{P_{max}}{S}, \tag{5-2}$$

where S is the slope (dp/dh) of the initial portion of the unloading curve at $h=h_{max}$, and 0.75 is a constant that depends on the indenter geometry.

5.2.4 Service life

In addition, to evaluate the service life of composite solder joints under EM stressing, ten EM samples for each solder were measured at the above-mentioned current density. The solder joints were regarded failed when the change in electrical resistance of an EM sample achieved 15%, the service life was thus obtained. For the EM test, the samples were linked in series, as shown in Figure 5.3.

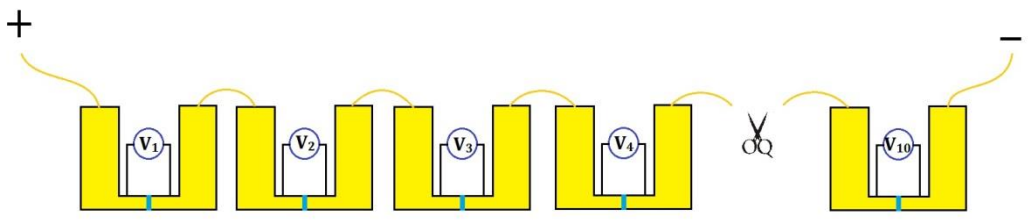

Figure 5.3 Schematic diagram of connection of EM samples

5.3 Results and Discussion

5.3.1 Surface characteristics of EM samples after current stressing

A ZYGO laser profiler was employed to measure surface profile of different solder joints before EM stressing and after 360 hours of stressing. The pseudo colour images of the surface profile of solder joints are shown in Figure 5.4; average profiles acquired linear based on scanning of 300 lines of cross-solder joint on the each sample are shown in Figure 5.5.

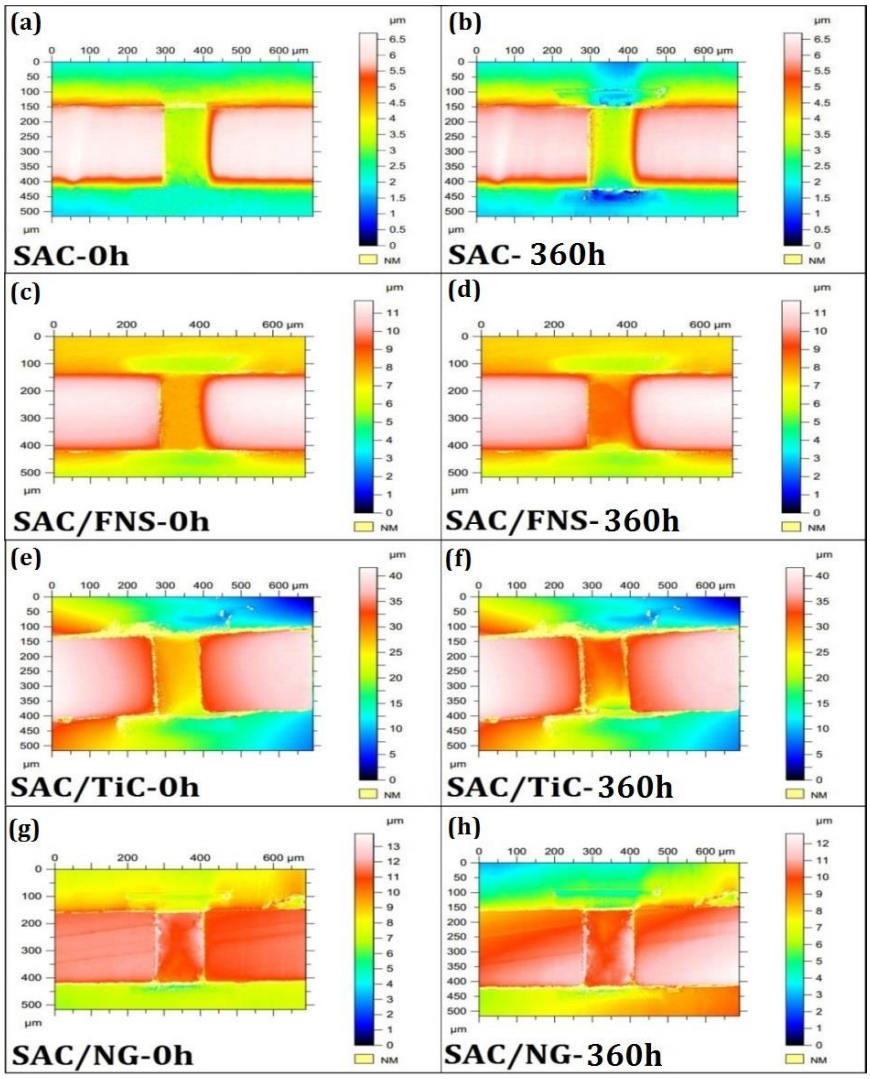

Figure 5.4 Results of Surface scanning of different solder joints before and after 360 h stressing: (a-b) SAC; (c-d) SAC/0.2FNS; (e-f) SAC/0.2TiC; (g-h) SAC/0.2NG

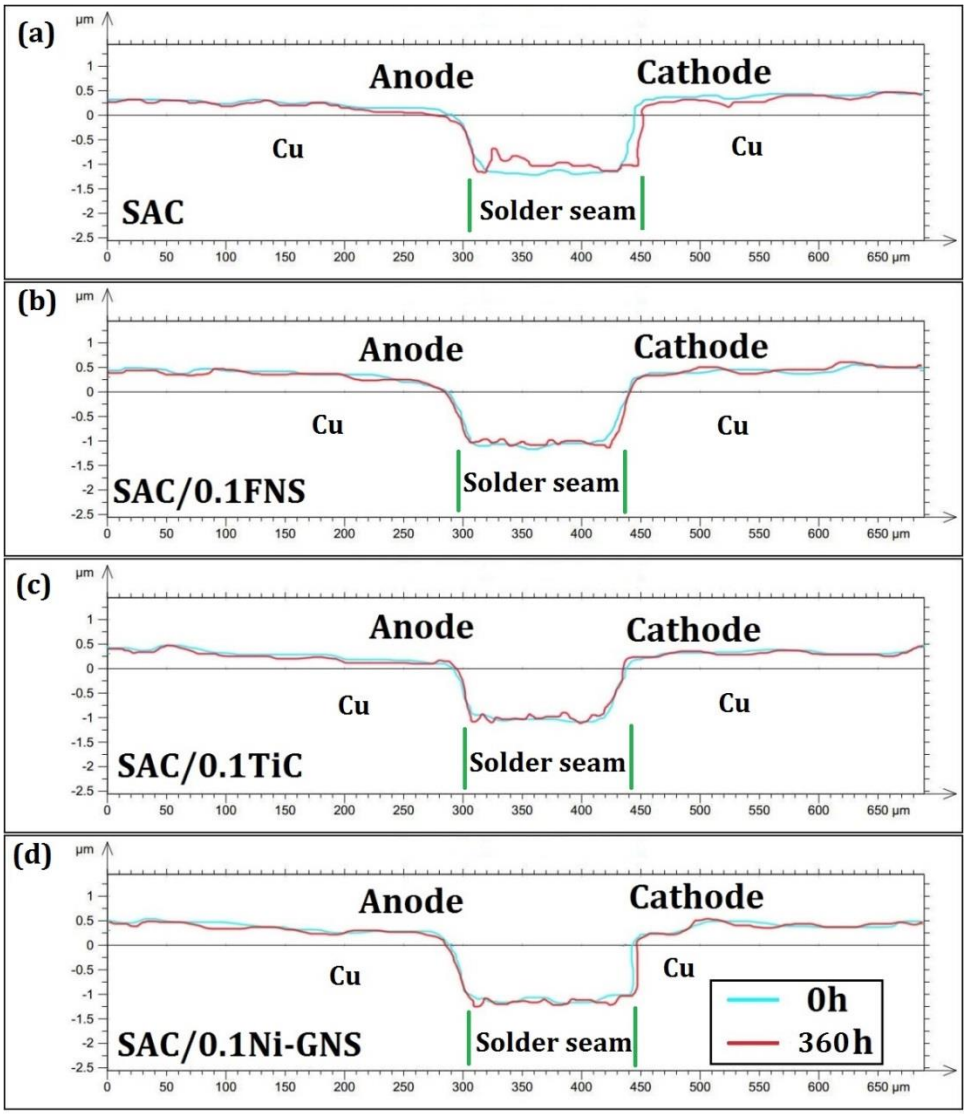

Figure 5.5 Side profiles of different solder joints before and after 360h current stressing

According to the obtained test results, after 360 hours EM stressing, significant extrusions were formed at the anode side of the SAC solder joint; these extrusions were caused by migration and accumulation of metal atoms (such as tin atoms) in solder or oxidation on the surface of solder joints. By contrast, three composite solder joints with foreign reinforcements were generally stable on the whole although there are some fluctuations on the surface. According to the average profile curve of different solder joints shown in Figure 5.5, small hills were found in the area on the side near to the anode side of SAC solder joints after 360 hours EM stressing, with average height of the extrusion of 0.42 micrometres. In contrast, after the same time of EM stressing, the extrusions were distributed

dispersedly in the solder joints, without concentration on one side although there are some fluctuations and roughness on surface of the three composite solder joints. Besides, according to the data measured, the average height of the extrusions of the three composite solders was only 0.18 micrometres. It can be inferred that the extrusions around the anode side of the SAC solder joints might be caused by the pressure difference on the anode side, due to different migration rates of various metal atoms in the solder joint. This lead to some metal atoms (e.g. Sn) enriched at the anode side; in contrast, surface roughness in three composite solders was mainly caused by surface oxidation during EM stressing. Therefore, the appropriate addition of foreign reinforcements can effectively suppress electro-migration in solder joints.

5.3.2 Microstructural evolution of solder joints under EM stressing

SEM images of SAC, SAC/FNS, SAC/TiC and SAC/NG solders after 120, 240 and 360 hours of EM stressing are shown in Figure 5.6, 5.7, 5.8 and 5.9, respectively. The measured thicknesses of interfacial IMCs (cathode and anode) of different solder joints are shown in Figure 5.10 and Table 5.1.

According to the observations of microstructures of different solders after various times of EM stressing, the extension of EM stressing time, led to gradually coarsening of the microstructure of SAC solder joint. At the same time, dark grey bulky Cu_6Sn_5 IMC started to form in solder joints near to the cathode side (Figure 5.6g); after 360 hours, both the quantity and volume of these bulky IMCs increased significantly and mainly enriched at the anode side. According to the thickness data of SAC solder joint, the IMC layer at the cathode interface became thicker first and then thinner (its thickness increased from 2.18 ± 0.13 μm to 2.46 ± 0.15 μm, and then decreased to 1.38 ± 0.21 μm after 360 hours). With the extension of the stressing time, the IMC at the cathode interface changed from scallop-like to flat gradually; after 360 hours of stressing, thickness of the interfacial IMC at the cathode decreased significantly. At the same time, a part of

copper substrate was dissolved and discontinuous voids also formed on the interface between the solders and the IMC. Besides, it was found that thickness of the IMC layer at the cathode side increased gradually with the stressing time (from 2.21±0.21 μm to 5.67±0.12 μm after 360 hours of stressing); dark Cu_3Sn IMC formed at the bottom of the Cu_6Sn_5 IMC layer. In addition, after 360 hours of stressing, light-grey Ag_3Sn IMC particles can be found in the anode IMC layer.

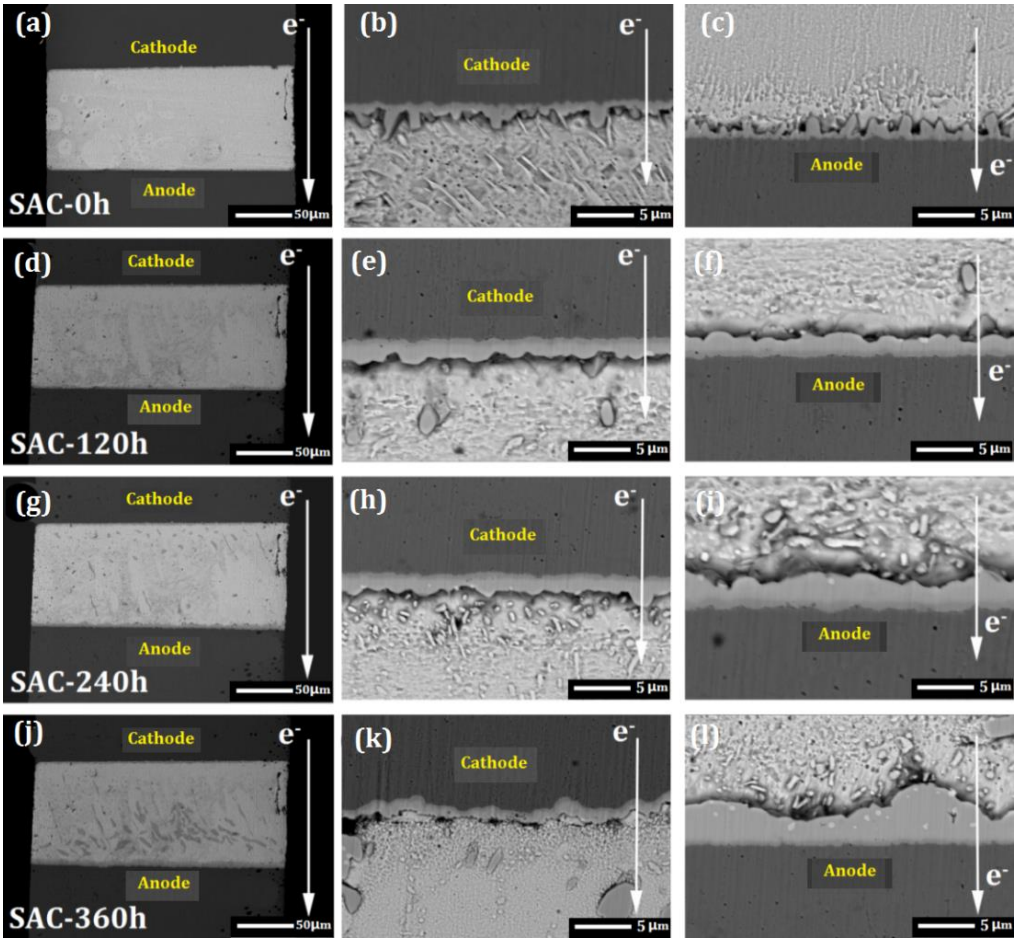

Figure 5.6 Microstructural evolution in SAC solder joints after different stressing times

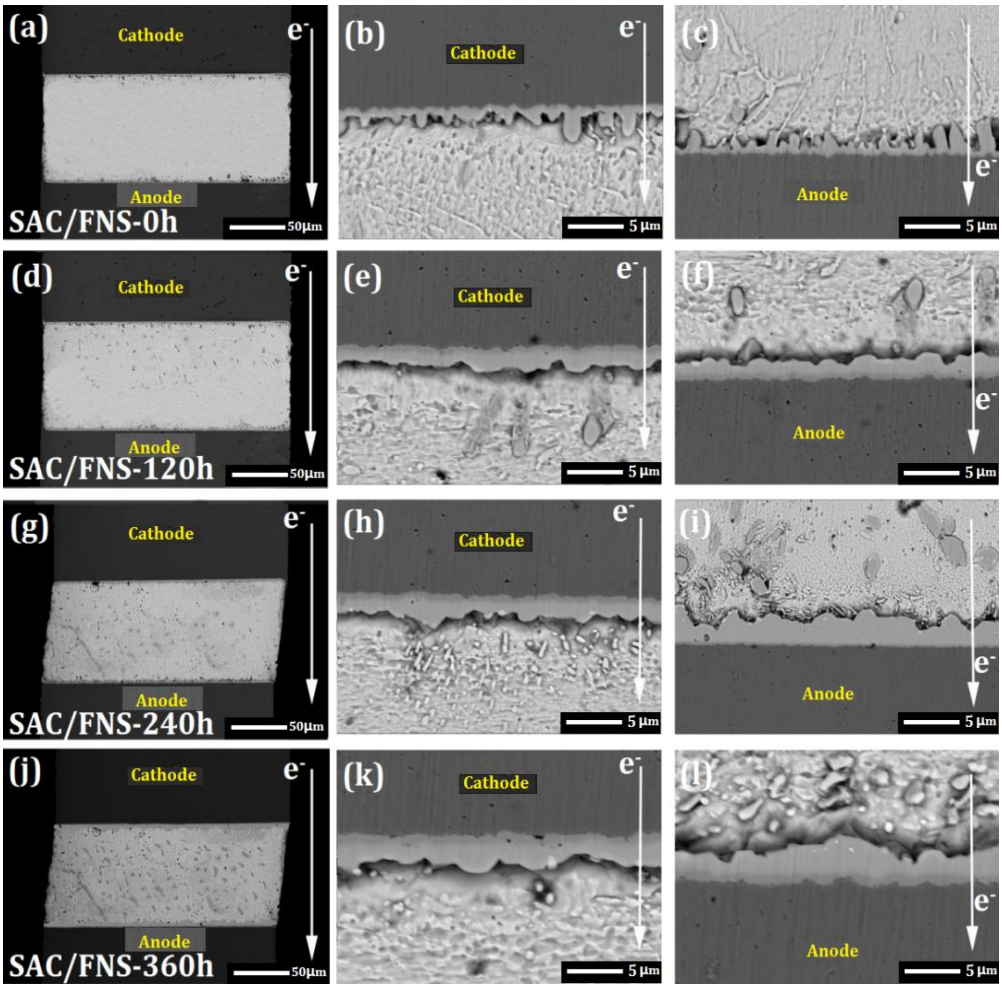

Figure 5.7 Microstructural evolution in SAC/FNS solder joints after different stressing times

From the obtained results for SAC/FNS solder joints after different EM stressing times, after the EM stressing for 120 hours, changes similar to those in SAC solder joints can be found, i.e., formation of the dark bulk Cu_6Sn_5 IMC in the solder joints near to the cathode region. However, unlike SAC, with the extension of the stressing time, IMCs were not enriched at the anode side, although they increased in quantity and volume; these IMCs were dispersively distributed all over whole solder joints. In addition, the growth mode of interfacial IMCs was also different from that in SAC solders. Thickness of the IMC at the cathode side of this type of solder joints increased continuously during the stressing period (from 2.16±0.18 μm to 3.13±0.16 μm). After 120 hours stressing, formation of Cu_3Sn IMCs was also observed in the interfacial IMC layer. Besides, although several voids were also formed at the bottom of the interfacial IMC after

360 hours stressing, their volume and quantity were far smaller those that of SAC samples under the same conditions. On the other hand, thickness of the interfacial IMC layer at the anode side increased gradually during the whole EM stressing period- from 2.24±0.24 μm to 4.07±0.15 μm.

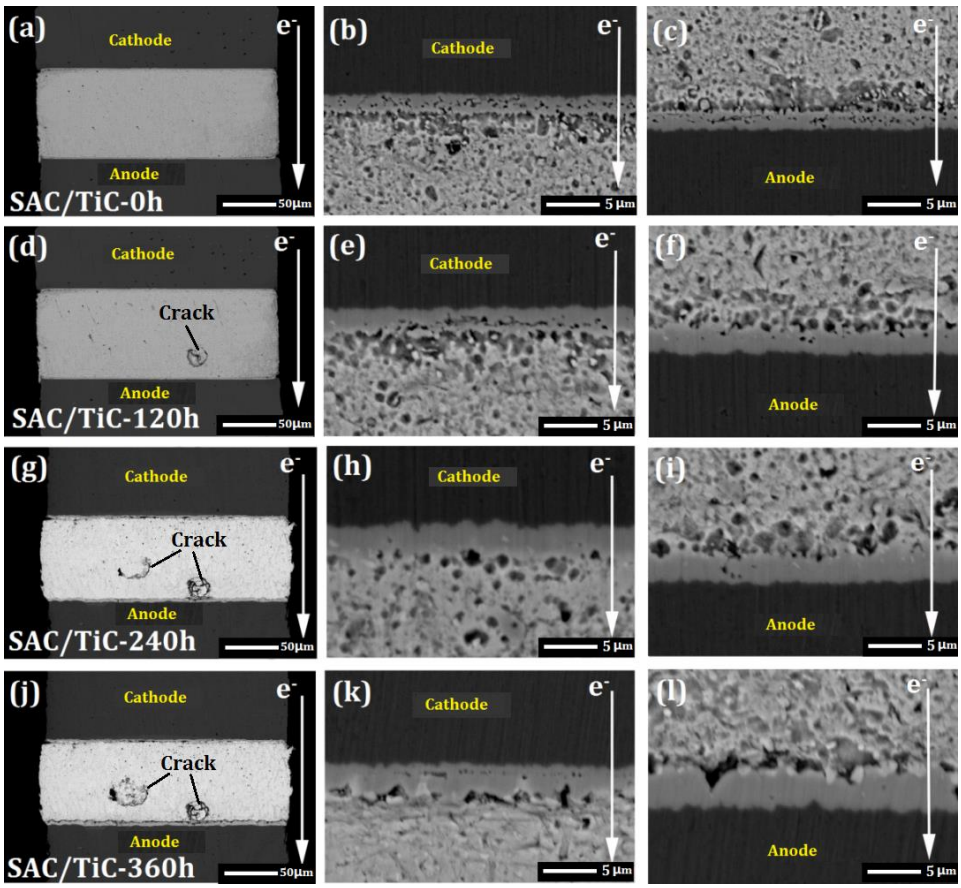

Figure 5.8 Microstructural evolution in SAC/TiC sample after different stressing times

The results obtained for SAC/TiC solder joints after different EM stressing time demonstrate that small blocky Cu_6Sn_5 IMCs were gradually formed around the cathode side with the increase in the stressing time; however, these IMCs were mainly distributed in the central regions and around the cathode areas of solder joints during the whole stressing period, not migrating to the anode region after long-time stressing. After 120 hours of stressing, some cracks in the central regions of solder joints were observed, proving agglomeration of TiC reinforcement; Cu_6Sn_5 IMCs were also found around these TiC reinforcement. It can be explained by heat concentration caused by low thermal conductivity of TiC, which intensified diffusion of metal atom and promoted the formation of Cu_6Sn_5

IMC. In addition, thickness of the interfacial IMC at both cathode and anode sides exhibited a continuous increase with the extension of the stressing time (from 2.48±0.13 μm to 2.92±0.14 μm). Similar to SAC/FNS samples, after 324 hours of stressing, there were some voids formed in the interfacial IMC layer at the cathode side. As for the anode side, thickness of the IMC layer also shows an increasing trend during the stressing period, increasing from 2.51±0.14 μm to 4.36±0.21μm; the initial porous structure gradually disappeared. After 360 hours of stressing, there were no voids or crack formed in the IMC layer. Unlike SAC and SAC/FNS samples, during the whole stressing period, no significantly thickened Cu_3Sn IMCs were observed at bottom of the Cu_6Sn_5 IMC in SAC/TiC samples. This indicates that addition of TiC was helpful to suppress the growth of Cu_3Sn IMCs in solder joints under EM stressing.

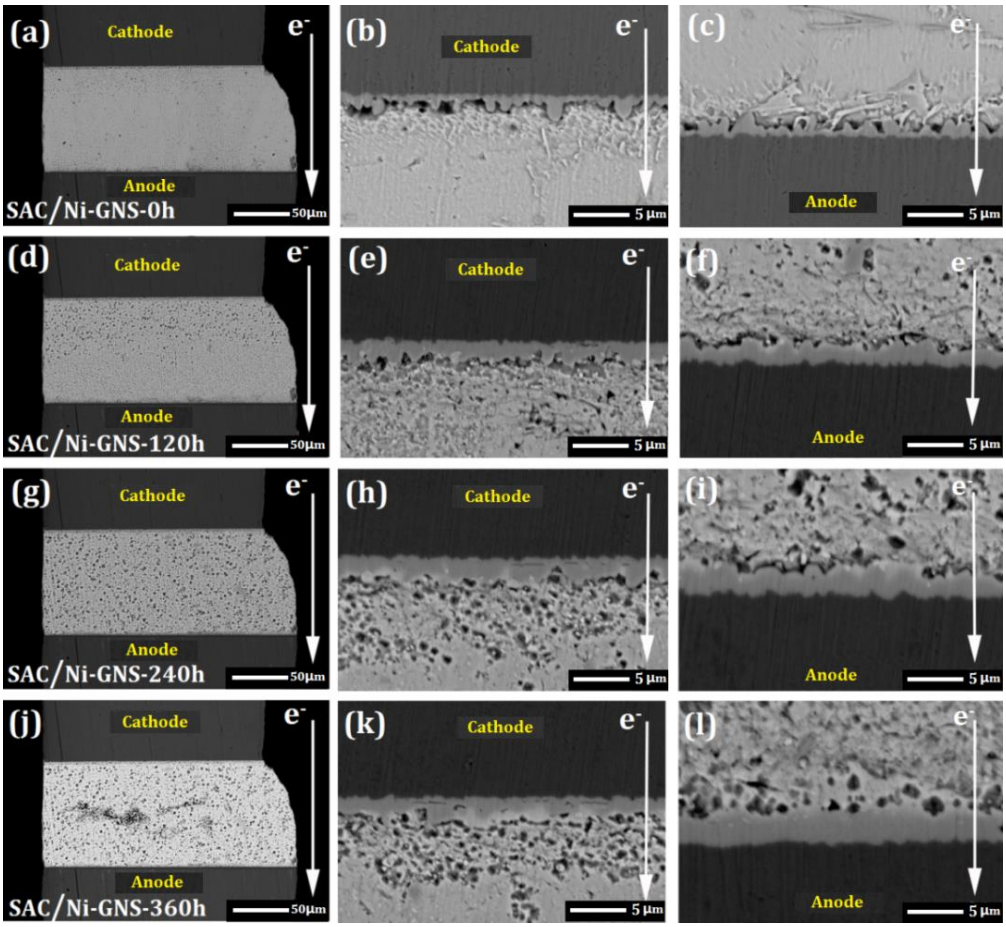

Figure 5.9 Microstructural evolution in SAC/NG solder joint after different stressing times

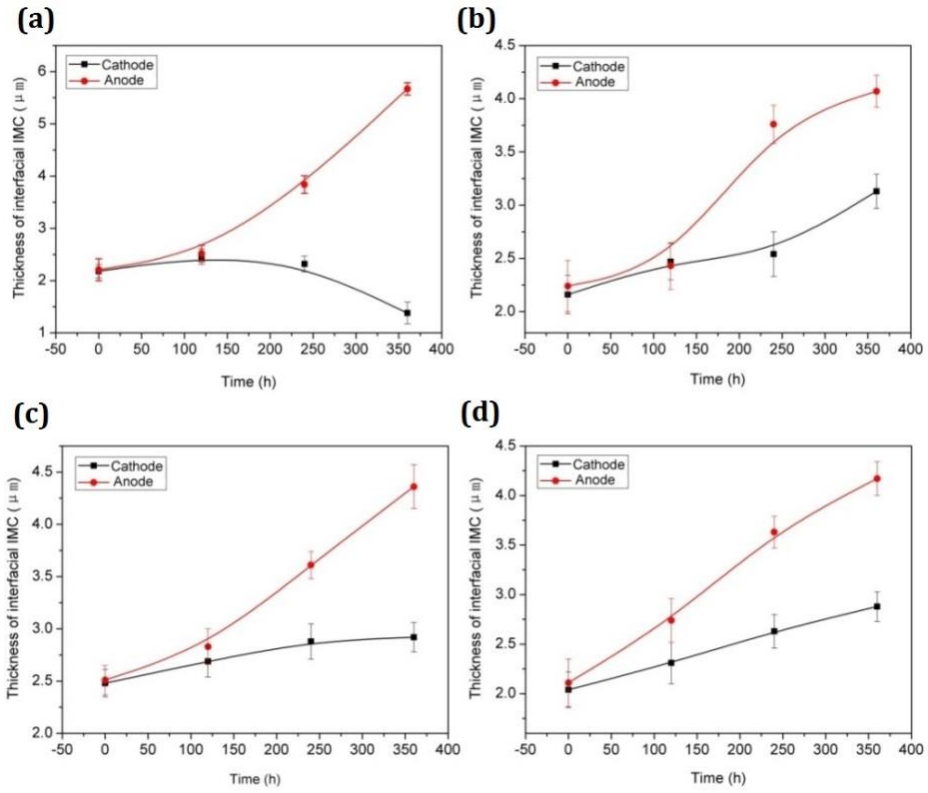

Figure 5.10 Evolution of thickness curves of interfacial IMC in different solder joints: (a) SAC; (b) SAC/FNS; (c) SAC/TiC; (d) SAC/NG

The microstructural evolution in SAC/NG solder joint was similar to that in SAC/FNS samples. After 120 hours stressing, small blocky IMCs started to form around the cathode side; with the extension of times, 240 hours later, these IMCs were gradually dispersively distributed all around the whole solder joints. The quantity and volumes of IMCs in this solder joints were larger than in SAC/FNS samples, and the distribution was also more homogeneous (Figure 5.9g). Analysis of the microstructure of SAC/NG solders showed that the IMCs in the solder joints were (Cu, Ni) $_6Sn_5$ IMC. After 360 hours stressing, IMCs with large volume were observed in the solder joints, which may be caused by over-growth of local IMCs due to uneven temperature distribution related to the non-uniform distribution of the reinforcement in solder joints. On the other hand, according to the obtained thickness data, thickness of interfacial IMCs at both cathode-side and anode side interfaces increased continuously during the stressing period, from 2.04±0.18 μm (cathode) and 2.11±0.24 μm (anode) to 2.88±0.17 μm (cathode)

and 4.17±0.17 μm (anode) after 360 hours stressing. In addition, no significantly thickened Cu_3Sn IMC was found at the bottom of the interfacial IMC in both sides during the whole stressing period. This illustrates that the growth of Cu_3Sn IMC under EM stressing conditions was also effectively restrained after the doping with NG reinforcement.

Table 5.1 Thickness data for interfacial IMCs in different solder joints

		Thickness of interfacial IMC (μm)			
		SAC	**SAC/FNS**	**SAC/TiC**	**SAC/NG**
Cathode	**0h**	2.18±0.13	2.16±0.18	2.48±0.13	2.04±0.18
	120h	2.46±0.15	2.47±0.17	2.69±0.15	2.31±0.21
	240h	2.32±0.15	2.54±0.21	2.88±0.17	2.63±0.15
	360h	1.38±0.21	3.13±0.16	2.92±0.14	2.88±0.17
Anode	**0h**	2.21±0.21	2.24±0.24	2.51±0.14	2.11±0.24
	120h	2.52±0.16	2.43±0.22	2.83±0.17	2.74±0.22
	240h	3.84±0.17	3.76±0.18	3.61±0.13	3.63±0.16
	360h	5.67±0.12	4.07±0.15	4.36±0.21	4.17±0.17

Based on the microstructural analysis of both plain and composite solder joints under EM stressing, the following two points can be concluded: 1) Thickness of interfacial IMC layer at the anode side of all the samples shows a continuous increase during the stressing period. There was also a continuous increase of thickness of the interfacial IMC at the cathode side of three composite solder joints, except for the trend of an initial increase followed by a decrease of thickness of SAC; the growth rates of IMCs on the anode side of all the samples were much higher than that on the cathode side. 2) Regarding solder matrix, after 360 hours stressing, most of Cu_6Sn_5 IMCs formed in SAC solder joints were distributed at their anode side, while Cu_6Sn_5 and $(Cu, Ni)_6Sn_5$ IMC formed in SAC/FNS and SAC/NG sample solder joints were distributed all around the whole solder joints. Most of Cu_6Sn_5 IMCs formed in SAC/TiC solders were located at the cathode side and the central regions, illustrating that the addition of

the TiC reinforcement was positive for suppression of the migration of IMCs.

In general, the growth of interfacial IMCs under EM stressing is mainly caused by two driving forces: the chemical gradient and the electron wind. The diffusion flux equation for transfer of metal atoms is shown in Formula 5-3

$$J = J_{chem} + J_{em} = C\frac{D}{kT}\left(\frac{\partial \mu}{\partial x}\right) + C\frac{D}{kT}Z^{*}ej\rho \ . \qquad (5\text{-}3)$$

Here, J is the total diffusion flux, J_{chem} is the diffusion flux generated by the chemical potential, J_{em} is the diffusion flux caused by the electro-migration, C is atomic concentration, D is the diffusion coefficient, k is the Boltzmann constant, T is the thermodynamic temperature, $\partial\mu/\partial x$ is the chemical-potential gradient, Z* is the number of effective charges, e is the electron charge, ρ is resistance and j is the current density. It is generally considered that the growth and decrease of thickness of interfacial IMCs are jointly determined by the atomic migration caused by two driving forces. In the anode side, the effect of chemical-potential gradient and the electro-migration driving force are the same, both facilitating the growth of interfacial IMCs. In the cathode side, they have opposite effects; the driving force of chemical potential promotes the growth of IMCs, and the driving force of electro-migration facilitates the dissolution of IMCs [85]. It explains the phenomenon of increase in thickness of interfacial IMCs in the anode side of SAC solder joint, and decrease in the cathode side. As for three other composite solders, the addition of foreign reinforcement can change the chemical potential at the interface of the solder joints to a great extent, and can also affect the atomic diffusion flux caused by electro-migration by changing the current-density distribution in the whole solder joints. Therefore, formation and migration modes of IMC in three composite solder joints differed significantly from that in SAC solder joints. In addition, foreign reinforcements added in the solder joints may reduce this atomic diffusion flux to different extents and change the chemical potential at the interface.

5.3.3 Evolution of mechanical properties of solder joints under EM stressing

As mentioned in Section 5.2.3, hardness values of different solder joints after different stressing times were measured using the nano-indentation tester Hysitron Ti750. Previous researchers tested hardness of the composite solder alloy using mostly a Vickers hardness tester [145-148], while some others evaluated the hardness and the modulus of the solder joints with a nano-indentation tester [149-150]. Analysing hardness of solder joints after long-term current stressing with a nano-indentation tester, Ren et al. [151] found that the hardness values of the solder joints were distributed in a gradient way from the anode side to the cathode side.

Currently, there are few reports on evolution of mechanical properties of composite solder joints with foreign reinforcement after long-term EM stressing. Therefore, in this research, hardness of different solder joints before and after 360 hours of EM stressing was tested using a nano-indentation tester; specific testing methods and testing regions are shown in the experimental part (Section 5.2). The loading and unloading curves of all the samples are shown in Figure 5-11, while the average indentation depths at different positions tested are shown in Table 5.2; besides, the average hardness values of various regions are shown in Figure 5.12 and Table 5.3.

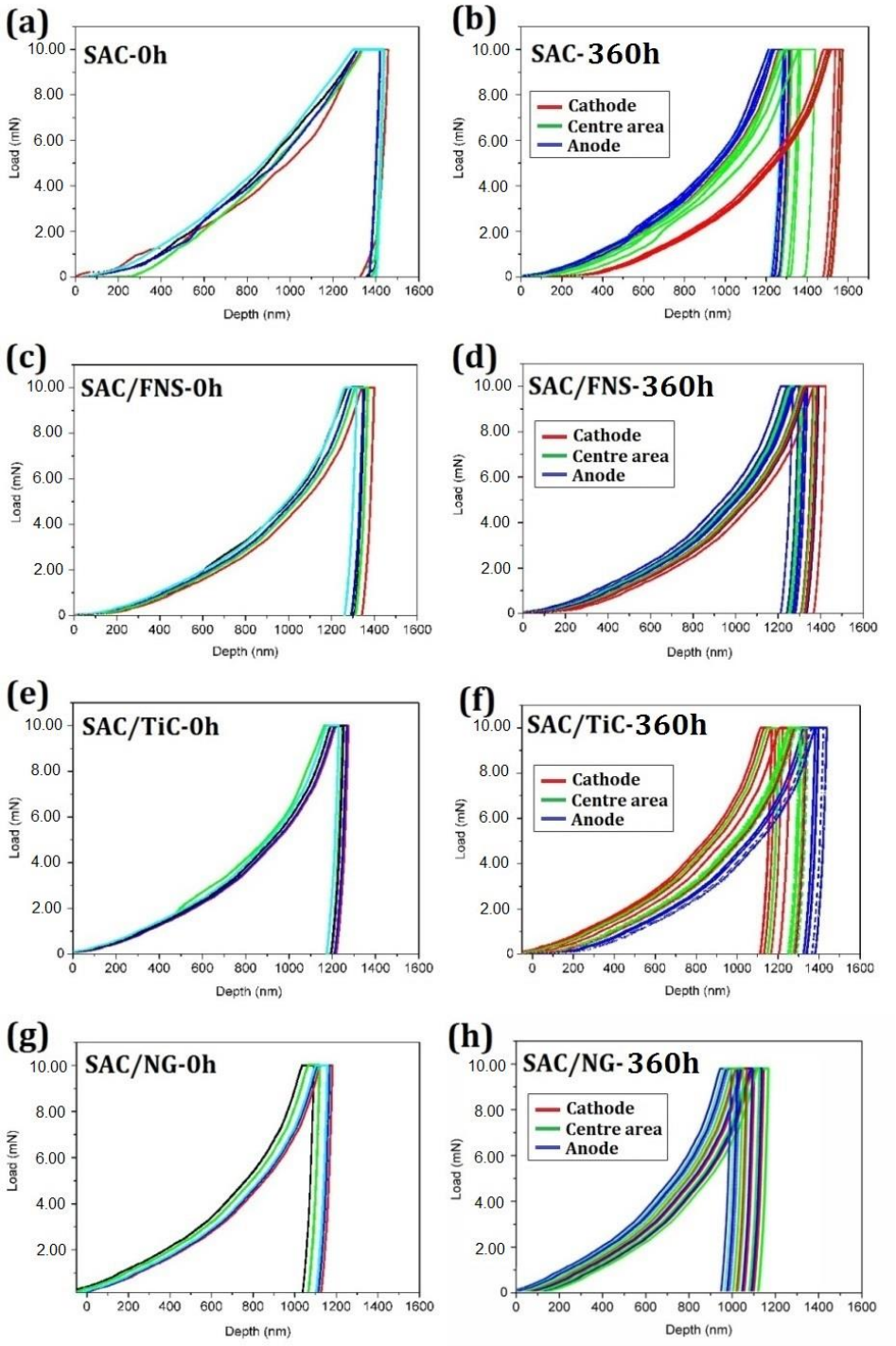

Figure 5.11 Test results for indentation before and after EM for 360 h: (a-b) SAC; (c-d) SAC/FNS; (e-f) SAC/TiC; (g-h) SAC/NG

Table 5.2 Average indentation depth for different samples at different regions

Solder	Stressing time	Average indentation depth (nm)		
SAC	0h		1389	
	600h	cathode	central	anode
		1508	1317	1243
SAC/FNS	0h		1314	
	600h	cathode	central	anode
		1347	1253	1264
SAC/TiC	0h		1211	
	600h	cathode	central	anode
		1184	1275	1348
SAC/NG	0h		1098	
	600h	cathode	central	anode
		1064	1071	1029

According to the nano-indentation curves in Figure 5.11 and the average indentation depth shown in Table 5.2, hardness of the SAC solder samples was lowest (with an average indentation depth of 1389 nm) before EM stressing. By contrast, the hardness values of three composite solder joints were somewhat higher. Specifically, the initial average indentation depths of SAC/FNS, SAC/TiC and SAC/NG were 1314 nm, 1211 nm and 1098 nm, respectively. Initial hardness of SAC samples was about 0.2021 GPa, while the initial hardness values of the three composite solders were 0.2156 GPa, 0.2327 GPa and 0.2614 GPa, respectively; in particular, hardness of the composite solder with 0.1 wt. % NG addition was about 29.3% higher than that of SAC solders. This illustrates that addition of foreign reinforcement can effectively improve the hardness of solder alloys. In addition to the strengthening effect on solders caused by the dispersive distribution of the reinforcement, refined crystalline strengthening caused by addition of reinforcement is another reason for the improvement of their

mechanical properties. Besides, according to the nano-indentation curves and hardness data obtained, the spread of hardness data of SAC samples was smaller than that of three composite solders. This indicates that the foreign reinforcements added were not evenly distributed in the whole solder joints. As mentioned in Section 3.5, the foreign reinforcement added (especially the non-reactive ones) are likely to be discharged out of the solder joints during the reflow process, which not only leads to the exclusion of the reinforcements, but also can result in the uneven distribution of the reinforcements in the solder joints. In such a case, hardness is higher in areas with more reinforcements, and it is relatively low in positions with fewer reinforcements, which results in the large dispersion of the hardness data for composite solder samples.

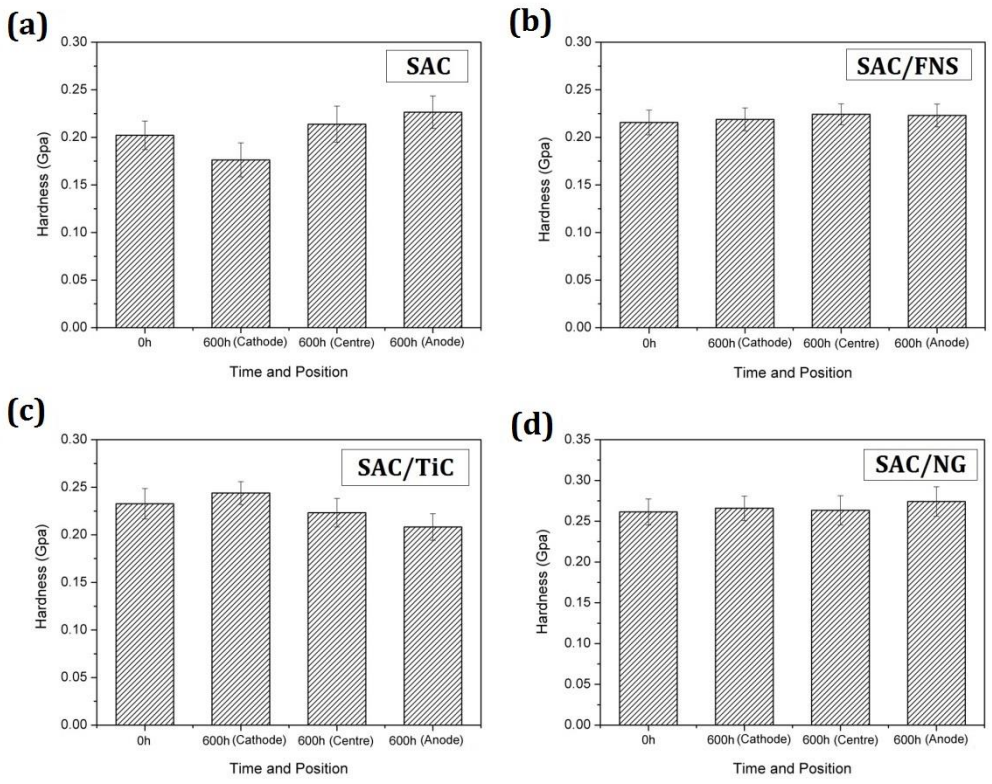

Figure 5.12 Distribution of average hardness in solder joints before and after current stressing

According to the results for different samples after 360 hours stressing, the curves of all solder joints after EM stressing show a greater difference compared with their initial forms. For SAC samples, after 360 hours of stressing, hardness in

the solder joints was obviously distributed in a gradient direction; specifically, the anode region was harder (with average indentation depth of 1243 nm and average hardness of 0.2264 GPa), at the same time, the cathode side region was softer (with an average indentation depth of 1508 nm and average hardness of 0.1763 GPa) and the central areas were moderate with average hardness of 0.2138 GPa. Thus, hardness of the solder joints declined from the anode side to the cathode side. This phenomenon can be explained by microstructural evolution of solder joints. According to the microstructures of stressed SAC solder joints shown in Section 5.3.2, large quantities of Cu_6Sn_5 IMCs enriched at the anode side of the solder joints after 360 hours stressing. According to the related literatures [152-154], hardness of Cu_6Sn_5 IMCs was higher than that of SAC solder alloy (hardness of Cu_6Sn_5 IMC was about 6.10 ± 0.53 GPa), resulting in higher hardness in the anode side. Meanwhile, migration of large quantities of copper atoms to the anode side and relative enrichment of the tin atoms in the cathode led to the decrease in hardness in the cathode side; this result is basically consistent with the research results of Ren et al. [151]

Table 5.3 Average hardness data for solder joints before and after current stressing

	Average hardness (GPa)			
	0h	**600 h (Cathode)**	**600 h(Central)**	**600 h (Anode)**
SAC	0.2021	0.1763	0.2138	0.2264
SAC /FNS	0.2156	0.2189	0.2243	0.2231
SAC /TiC	0.2327	0.2439	0.2232	0.2082
SAC /NG	0.2614	0.2659	0.2633	0.2742

By contrast, according to the test results for SAC/FNS samples after stressing, there was no significant difference in average hardness between different tested

regions. Specifically, after 360 hours of EM stressing, hardness in the anode and central regions of the SAC/FNS sample increased slightly (from 0.2156 GPa to 0.2237GPa, an increase of only about 4%), while that of the anode region decreased slightly to 0.2189 GPa, only by 1.5%. Therefore, although average hardness of SAC/FNS solder joints after EM stressing was decreased slightly, the hardness distribution was relatively even, without a significant gradient observed in the solder joints. The hardness-test results for SAC/FNS correspond to the microstructural observations. The decrease in hardness caused by grain coarsening during the EM stressing period and the increase in hardness caused by the dispersive distribution of Cu_6Sn_5 IMCs led jointly to only a slight decrease in average hardness of the stressed solder. This indicates that addition of FNS could effectively restrain migration of metal atoms (mainly, copper atoms and tin atoms) in solder joints under condition of EM stressing, and helped to improve the stability of mechanical properties of the entire solder joints.

The nano-indentation results for SAC/TiC solder joints after 360 hours EM stressing were also different from those for SAC solder joints. Specifically, hardness of SAC/TiC solder joints after EM stressing was also distributed in a gradient direction. However, unlike the SAC samples, the high-hardness region of SAC/TiC samples was in the cathode area (with the average hardness of 0.2439 GPa, about 5% higher than its initial hardness), while low hardness was found in the anode area (with the average hardness of 0.2082, about 10.5% lower than its initial hardness); this result is totally opposite to that of the SAC samples. Compared with SAC and SAC/FNS solders, the change in hardness of solder joints of SAC/TiC samples was also closely related to formation and distribution of Cu_6Sn_5 IMCs during the stressing period. After 360 hours of stressing, large quantities of Cu_6Sn_5 IMCs were enriched in the cathode side of SAC/TiC solder joints, while less of them concentrated on the anode side; this morphology is fully opposite to microstructures of SAC samples. Considering both the results for microstructures in Section 5.3 and the hardness-test result in this section, it can be found that although addition of TiC reinforcement gave a rise to the redistribution

of hardness in solder joints (this can also cause the redistribution of stresses in solder joints, threatening their reliability), it restrained the migration of metal atoms under EM stressing to a certain extent.

As for SAC/NG samples, after 360 hours of stressing, hardness distribution in them showed the characteristics similar to those in SAC/FNS samples: the hardness data of the stressed sample does not show any gradient distribution, but a relatively dispersive one. However, unlike SAC/FNS samples, average hardness of stressed SAC/NG sample increased slightly; after stressing it was 0.2678 GPa, about 0.64% higher than the initial hardness of 0.2614 GPa. This was due to higher hardness of $(Cu, Ni)_6Sn_5$ IMCs newly formed in solder joints than Cu_6Sn_5 IMCs, leading to the increase in hardness of solder joints caused by a dispersive distribution of IMC than the decrease of hardness caused by coarsening of grains in solder joints during the EM stressing period; therefore, hardness of SAC/NG samples slightly increased after EM stressing. Since hardness of solder joints after EM stressing was relatively even, it can be concluded that addition of NG reinforcement was also helpful to maintain stability of the mechanical properties of solder joints during EM stressing.

5.3.4 Failure life of solder joints under EM stressing

The failure life of solder joints under EM stressing was evaluated by measuring the change in electrical resistance during the stressing period; the sample was regarded failed when the real-time recorded resistance of the sample was 15% higher than the initial resistance. In order to ensure the reliability of data, ten samples of each type of solders were selected for resistance recording; the resistance curves obtained for different samples during the EM stressing period are shown in Figure 5.13. In addition, the statistic data for failure life of all the samples are shown in Figure 5.14.

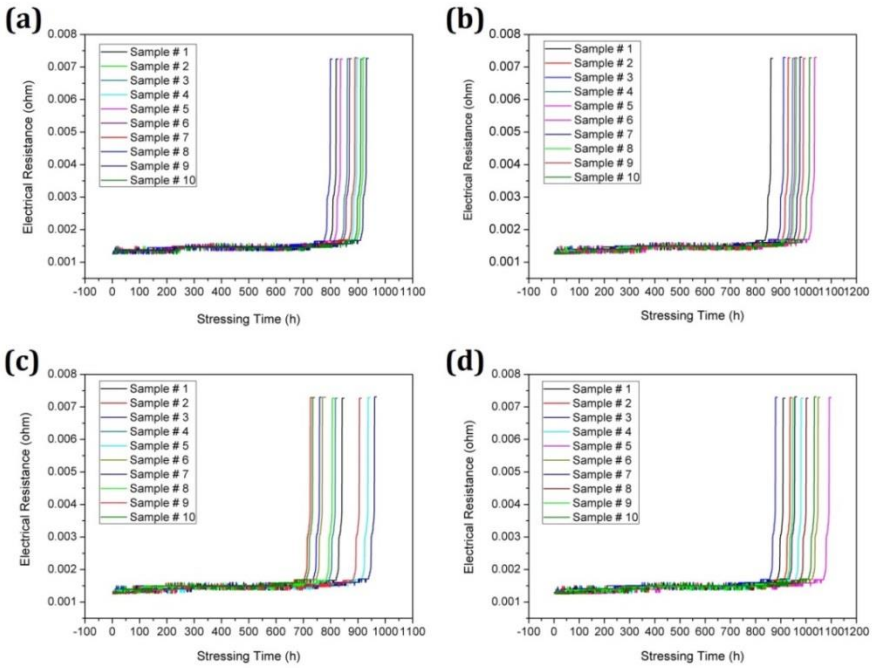

Figure 5.13 Electrical resistance of solder joints: (a) SAC; (b) SAC/FNS; (c) SAC/TiC; (b) SAC/NG

According to Figure 5.13, the resistance values of almost all the samples before current stressing were within the range of 1.36-1.49 mΩ. With the extension of stressing time, resistance of all the samples rose, increasing greatly before failure. It should be explained that slight fluctuations of resistance before failure was due to daily fluctuations of temperature. Apparently, a spread in resistance data for of SAC samples is lower than that of three composite solder samples (especially for the stage near to failure). It shows that the variance for failure-life data for SAC samples is smaller.

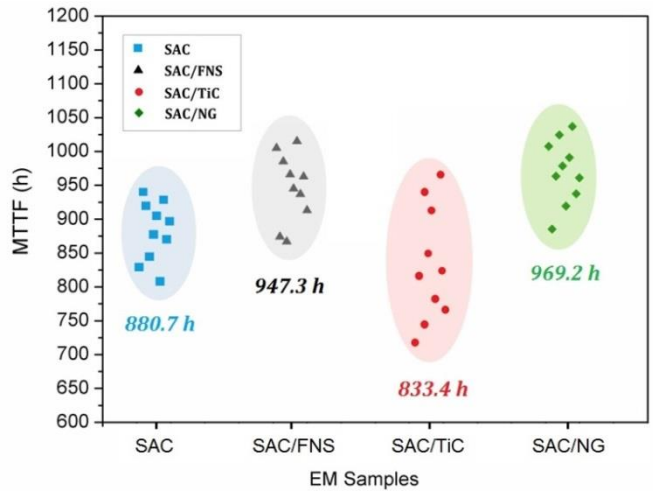

Figure 5.14 Average failure life of different solder joints

It can also be found from Figure 5.14 that the failure life values of the ten samples of SAC solders are very close, with the standard deviation of 44.09 h. By contrast, the values for three composite solders show a higher dispersion: the standard deviations for SAC/FNS, SAC/TiC and SAC/NG solder samples were 50.59 h, 84.99 h and 47.91 h, respectively. This might be caused by uneven distribution of reinforcements in these composite samples; agglomerations of reinforcements in solder joints can cause defects such as cracks around them, leading to early failure of samples. The average failure life of SAC solder samples under the EM stressing was about 880.7 hours, while that of SAC/FNS and SAC/NG solder samples was 947.3 hours and 969.2 hours, respectively. This parameter for two kinds of samples increased by 7.6% and 10.4%, respectively, compared with SAC samples. This illustrates that addition of reinforcements with FNS and NG is helpful for the improvement of the failure life of solder alloys under the stressing conditions. However, the average failure life of SAC/TiC samples is relatively low, only as 833.4 hours, about 5.4% lower than that of SAC samples. The coefficients of heat conduction and electric conduction are the lowest for TiC among the three studied reinforcements, Thus, it was easy to generate concentrated Joule heat and current density around TiC reinforcements (especially, in case of their agglomerations of) during EM stressing, leading to early failures of samples due to formation of such defects.

5.4 Summary

The U-shape Cu/solder/Cu samples were designed and prepared to study research on electro-migration in solders. The surface morphology of different solder joints was observed before and after EM stressing, microstructural evolution of the solder matrix and interfacial IMCs in different solders were studied after different EM stressing times; Mechanical performance of different solder joints was also analysed using nano-indentation; the failure life of different solders under EM stressing was also measured.

According to the experimental results, the appropriate addition of foreign reinforcement (FNS, NG and TiC) could effectively suppress the formation and migration of Cu6Sn5 and (Cu，Ni)6Sn5 IMCs in composite solder joints during EM stressing. Further, in addition to retard the growth of Cu3Sn IMC during EM stressing, the addition of three reinforcements is also helpful to maintain the interfacial integrity of solder joints. The hardness value of solder joints of SAC samples after EM stressing gradually decreases from anode side to cathode side, while the distribution of hardness value in SAC/FNS and SAC/NG samples after stressing is more homogeneous, without significant gradient distribution. The hardness value of solder joints in SAC/TiC samples after stressing also distributes in a gradient way; however, opposite to that of SAC samples, the hardness value gradually increases from anode side to cathode side. The failure life of SAC solder alloys under experimental condition can be improved by 7.6% and 10.4% with 0.1 wt. % addition of FNS and NG, respectively. The addition of TiC may threaten the failure life of solder alloys.

Chapter 6 Thermo-migration behaviours of composite solder joints

6.1 Introduction

With the decrease in the IC size and increase in the packaging density, both the current density and temperature of ICs grow. With respect to solder joints, a reduction in their diameter and spacing results in a current density close to, or above, 10^4 A/cm^2 [3-4]. Joule heat is generated when a current flows through the conductive material, and a high service current generates a large amount of such heat in a micro-interconnection structure. Because of a difference in thermal conductivity of a material, a large temperature gradient can be formed across a solder joint. As a result, metal atoms in the solder joint move along the direction of the temperature gradient, this process is known as thermo-migration (TM). Similar to electro-migration, TM is also characterized by mass migration of metal atoms at macroscopic level. Normally, TM of the metal atoms in a joint is also likely to cause elemental segregation, an excessive growth of interface IMC and dissolution of an UBM layer, which may ultimately and seriously affect in service reliability of the solder joint. Therefore, TM is also one of the main reasons for failures of interconnections [82]. At present, TM is separated from EM as a new research direction of IC reliability. Microstructural evolution, a change in mechanical properties, an atomic migration rate and a failure mode of solder joints under TM stressing are problems that should be solved.

According to previous reports [40, 42],addition of some alloying elements or foreign reinforcement can improve mechanical properties of solder joints and inhibit occurrence of the EM under high current density stressing to a certain extent. The current research on migration behaviour in composite solders focuses mainly on electro-migration; most researchers combine simply TM and EM together to discuss, and studying of TM is rarely carried out. In this chapter, a TM

set-up is designed and prepared, while TM behaviours of the newly prepared composite solders are studied. Evolution of microstructure and mechanical properties of the composite solders under the large temperature gradient and the element migration in solder joints are investigated systematically.

6.2 Experimental procedures

6.2.1 Design and preparation of TM setup and sample

To achieve a large enough thermal gradient across solder joints, a lab-made thermo-migration test setup was designed and prepared (Figure 6-1a). This setup consisted of a constant-temperature heating plate with a temperature of 250 ℃±5 ℃ as the heat source and a Peltier thermoelectric cooler. A stable initial temperature (0 ℃±2 ℃) of the thermoelectric cooler was guaranteed by a temperature controller, while a heat sink and a cooling fan were used to ensure its proper functioning during current stressing. The heating and cooling components were fixed on corresponding Cu bases with grooves (they were also the hot and cold sides in the TM tests). The spacing between two Cu bases was kept as 10 mm, while rectangular grooves with depth of 1 mm for placing TM samples were also produced on both hot and cold Cu bases with wire-electrode cutting. Due to the difference of heat conductivity of different materials, samples for TM are designed as an asymmetrical structure with a shorter hot end (2 mm) and a longer cold end (10 mm); a Cu plate (with thickness of 1 mm and width of 5 mm) was used as substrate material for both hot and cold sides of the sample. For sample preparation, end surfaces of Cu substrates of both sides were well polished before soldering. A solder foil with dimensions of 5 mm×1 mm×0.1 mm was then clamped between two Cu substrates; finally, the clamped Cu substrates and the solder foil together with the clamp were placed in a reflow oven to prepare a sample of Cu/solder/Cu sandwich-like structure. The width of solder joints in reflowed solder samples remained similar to the thickness of the initial solder foils (namely, 100 μm); a

schematic diagram of the reflowed sample is shown in Figure 6-1b. For the TM tests, the hot and cold ends of the prepared sample were placed correspondingly in the above-mentioned grooves on both hot and cold Cu bases; the embedded depth was approximately 1 mm. To ensure good thermal conduction, thermal silicone grease was applied on each contact surface between different parts in the tests.

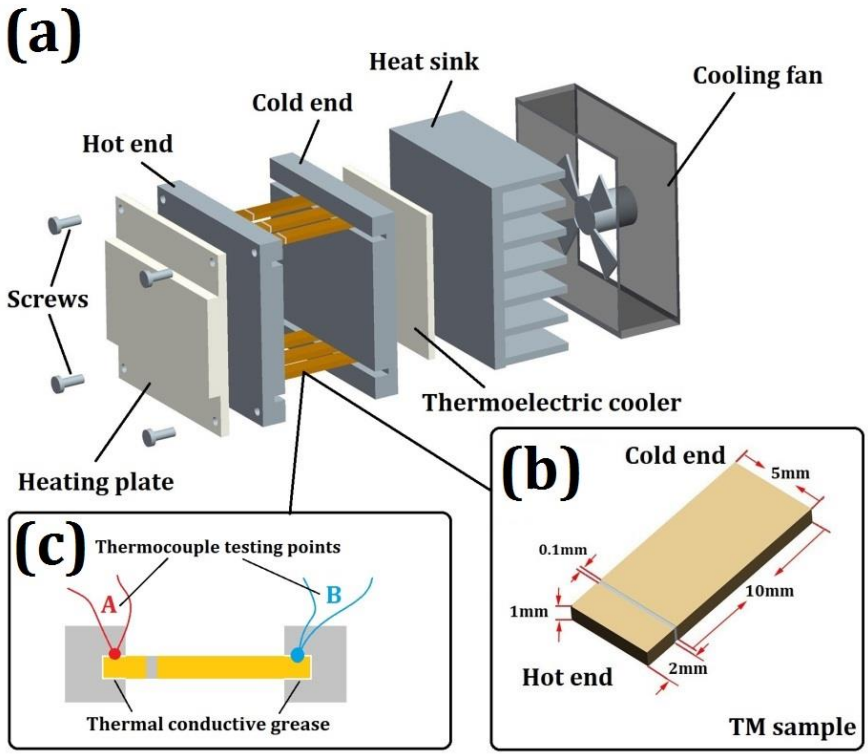

Figure 6.1 Schematic diagram of TM setup (a), TM samples (b) and thermocouple positions (c)

In order to assess the levels of temperature gradient and environmental temperature in a solder seam, experimental measurements and finite-element modelling were employed to evaluate the feasibility of the TM setup and the samples. A finite-element model was built with ANSYS 15.0 according to the actual dimensions of the setup and the sample. To get good modelling results for a temperature distribution across the solder seam, thermocouples were first utilized to obtain the real temperature at points A and B during current stressing (the distances from A and B to the solder seam were 1 mm and 9 mm, respectively, as illustrated in Figure 6.1c). The obtained average temperatures for points A and B were recorded when the temperature difference reached a balance; the recorded

data were then set as the stressing temperatures of the two ends for the subsequent modelling. Moreover, a high-precision infrared microscopy (QFI, MWIR-SE) with a self-calibration system was also employed to directly observe a temperature distribution in the solder seam of the TM sample.

6.2.2 TM tests and characterization

In the TM tests, five samples for each kind of solder (plain and composite) were tested to satisfy different testing purposes. Specifically, microstructural evolution of one selected sample for each kind of solder was continuously observed using a scanning electron microscope (SEM QURTA 200) every 200 hours; the total stressing time of TM tests was designed as 600 h. The rest of samples that experienced the same TM stressing process were used for mechanical and compositional studies. A focused ion beam (FIB) system was employed to analyse the distributions of Cu-Sn IMCs in a subsurface layer of the studied solder joints, while features of the inner structure were studied with an X-ray Micro-CT scanner (Metris XT H 160Xi) before and after the TM tests. Mechanical properties of solder joints were also evaluated with a nano-indenter (Hysitron Ti750) before and after the TM tests at a constant load rate of 10 mN and a dwell time of 5 s. To assess the difference in mechanical properties in different areas, in nano-indentation tests, each solder seam was evenly divided into three areas, denoted as A, B and C at various positions between cold and hot ends. Five randomly selected locations were tested for each area to ensure reliability of the test results. In addition, to evaluate quantitatively the process of dissolution of Cu atoms into the solder joints under a large temperature gradient, the joints were removed from TM samples after different TM stressing times. After that, residual Cu at the surface of solder joints was removed by fine polishing. The treated solder joints were then ultrasonically dissolved in solution of aqua regia for elemental analysis using an inductively coupled plasma optical emission spectroscopy (ICP-OES, Varian-720) with test precision at PPM level.

6.3 Results and Discussion

6.3.1 Feasibility of TM set-up and sample

The Feasibility of the designed TM set-up and sample was first evaluated using a thermocouple under the actual stressing condition. Figure 6.2 shows the thermocouple temperatures recorded at both ends of the sample, from the start of power-on to temperature stabilization to a switch off. It can be seen from the test results that the hot-end temperature of the sample continued to rise and the cold end temperature rose after a slight decrease. The temperature difference between the cold and hot ends was stable after about 7 minutes of stressing. The average temperatures at the hot and cold ends of the sample were about 206.7 ℃ and 40.3 ℃, respectively.

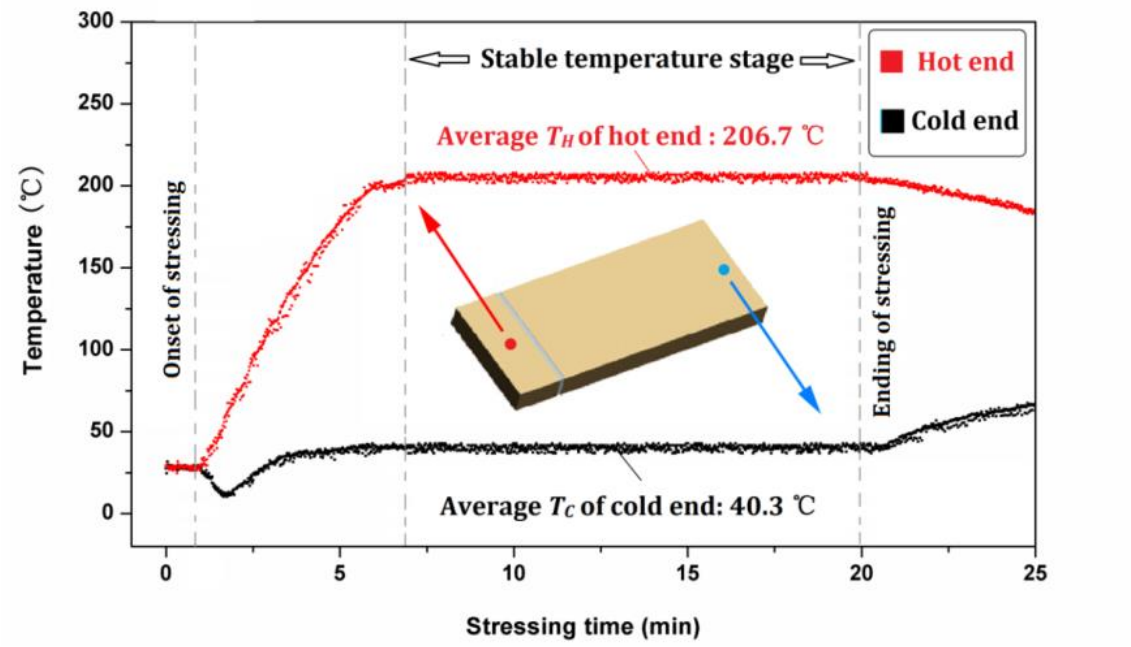

Figure 6.2 Evolution of temperature at cold and hot ends with stressing time

The test results for both ends of the specimen were set as input parameters for the subsequent FE modelling, and the temperature distribution and temperature gradient in the solder joint are thus further calculated; these calculation results of the FEM are shown in Figure 6.3.

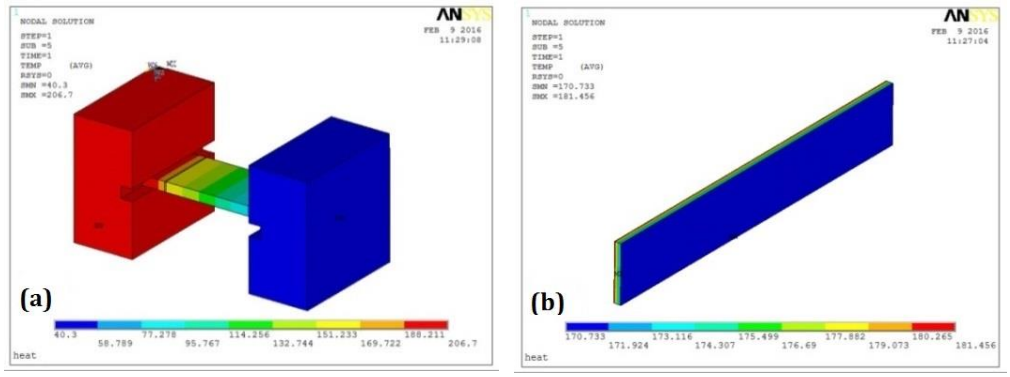

Figure 6.3 Temperature distributions in TM setup (a) and solder seam (b)

According to the simulation results, temperature of the hot side can reach 181.4 ℃, while of the cold side 170.7 ℃, and the average temperature of the solder joint area is about 176 ℃. Considering that the width of the solder joint is about 100 μm, its temperature gradient is 1070 K / cm in this case. According to the existing literature [155], the ambient temperature of TM in lead-free solder exceeds 100 ℃ and the actual temperature gradient in solder joints is higher 1000 K / cm. Therefore, based on the temperature test and simulation results, the designed TM set-up and the sample meet the requirements for TM research.

On the other hand, in order to measure the actual temperature gradient in the solder joint, the temperature distribution of the solder joint region was measured with another method; it was directly observed using a high-resolution infrared imaging system. The results observed are shown in Figure 6.4.

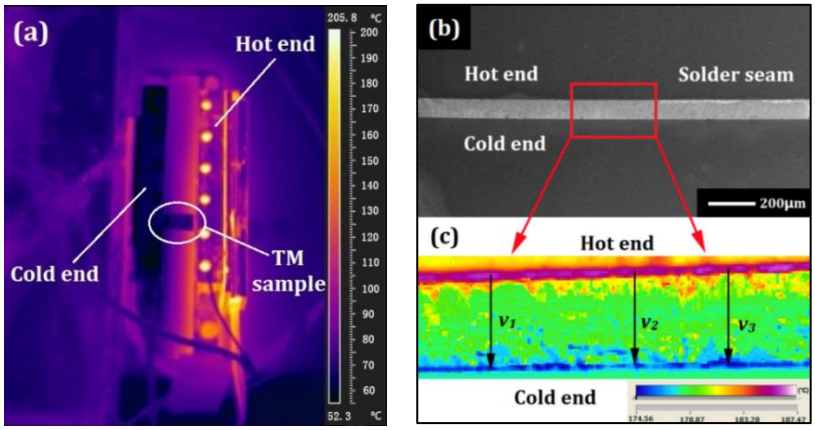

Figure 6.4 Temperature distributions in TM setup (a) and solder seam (b) and (c)

The results show that the average temperature of two Cu bases can reach 205.8 ℃ and 52.3 ℃, respectively. According to Figure 6.4b, the high- and

low-temperature areas of solder joints were mainly concentrated at the interface between the solder joint and the Cu substrate; the highest and the lowest temperatures at the hot end of solder joints can reach 187.5 ℃ and 174.6 ℃, respectively, and the average temperature of the solder joints was about 181.1 ℃. In order to further analyse the temperature gradient in the solder joints, three line scanning tests (i.e. V_1, V_2 and V_3) were carried out across the solder joints; the temperature data along the three lines are shown in Figure 6.5.

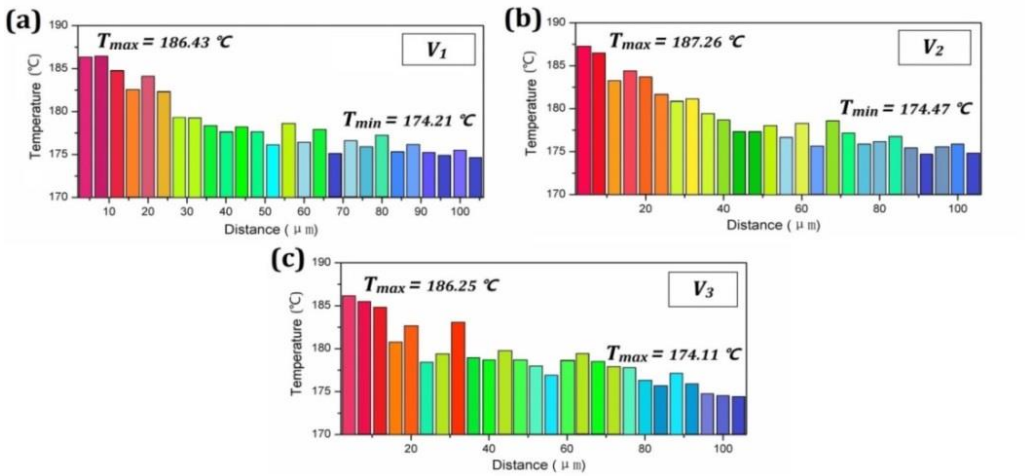

Figure 6.5 Actual temperature distributions along (a) V_1, *(b)* V_2 and (c) V_3 in Figure. 6.3

From Figure 6.5 it can be found that the temperature decreased from the hot end to the cold end; the maximum temperatures of V_1, V_2, and V_3 were 186.4 ℃, 187.3 ℃, and 186.3 ℃, respectively, while the lowest temperatures are 174.2 ℃, 174.5 ℃, and 174.1 ℃, respectively. In this case, the temperature gradients along the direction of the three marker lines were 1220 K / cm, 1280 K / cm and 1220 K / cm, respectively. The average temperature gradient in the solder joint can be thus estimated to be 1240 K/cm. This temperature gradient is very close to the simulation result obtained in the previous section; in this research, the experimental observations of (1240 K/cm) was taken as the average temperature gradient for the solder joints.

From the above analysis, it can be seen that the TM set-up designed is able to achieve a temperature gradient in excess of 1000 K / cm in the solder joint and to ensure that the temperature of the solder joint region is higher than 100 ℃. Therefore, the set-up and the sample in this study can fully satisfy the requirements of TM research.

6.3.2 Microstructural evolution

6.3.2.1 Surface morphology of solder joints

In order to understand the influence of service conditions on the surface morphology of solder joints, a group of samples was selected to study the morphological changes of solder joints before and after 600 hours of thermal stressing; the results observed for SAC, SAC/NG, SAC/FNS, and SAC/TiC are shown in Figures 6.6, 6.8, 6.9 and 6.10, respectively.

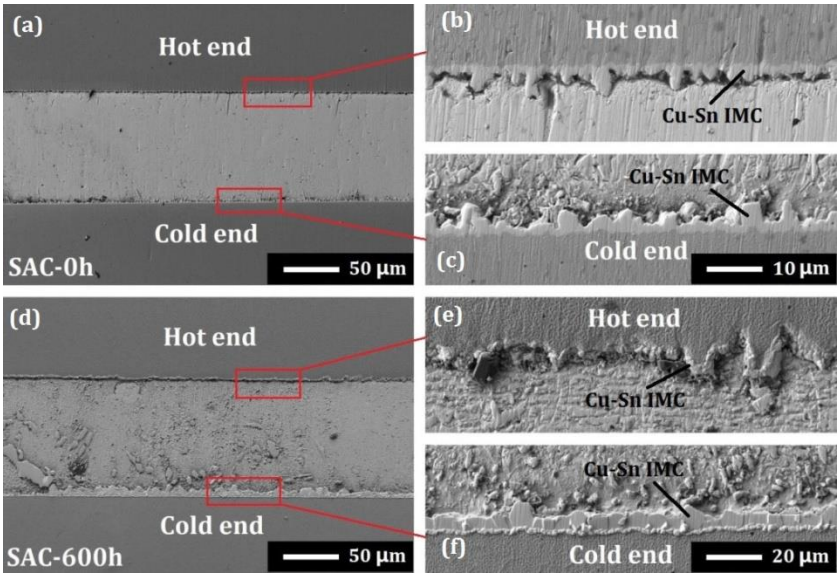

Figure 6.6 SAC solder joint before (a-c) and after (d-f) 600 h TM stressing

Apparently, after 600 hours stressing, thickness of the IMC layer at the cold end of the SAC solder joint increased significantly and the interface of hot-end was damaged severely. An initially flat surface of the entire solder joint also became rough after stressing, with larger blocks of IMCs found in its central and cold. In addition, it is worth noting that a very thin layer of protrusions was formed at the interface between the Cu-Sn IMC layer and the copper substrate at the cold end of the sample after 600 hours of stressing (Figure 6.5f); the enlarged view is shown in Figure 6.8 and the corresponding EDX results are given in Table 6.1.

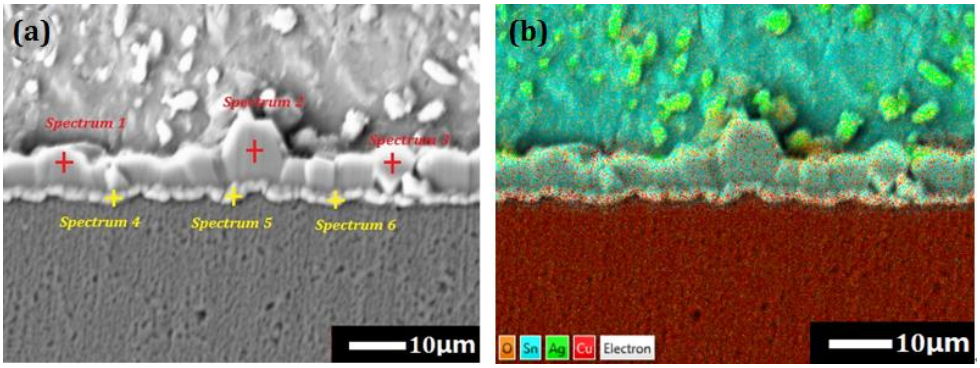

Figure 6.7 (a) SEM image of selected cold interface of SAC solder seam after 600 h of TM stressing; (b) corresponding results of EDS mapping

Table 6.1 Elemental composition (at %) of selected points in Figure. 6-7a

	Sn	Ag	Cu	O
Spectrum1	41.3	0.3	47.6	10.8
Spectrum2	41.7	0.2	47.9	10.2
Spectrum3	40.8	0.4	46.5	12.3
Spectrum4	21.7	0.2	56.9	21.2
Spectrum5	22.4	0.1	58.7	18.8
Spectrum6	24.3	0.3	63.6	11.8

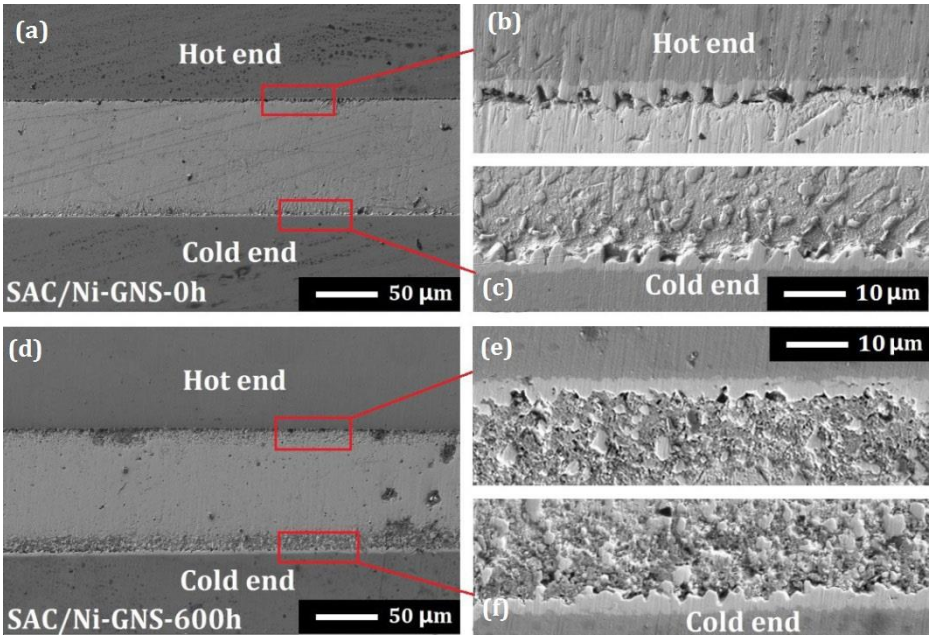

Figure 6.8 SAC/NG solder joint before (a-c) and after (d-f) 600 h of TM stressing

The EDX analysis demonstrated that the thin-layer protrusions mainly consisted of Cu, Sn and O. The data of element composition in Table 6.1 shows that the protrusions were Cu_3Sn IMCs; this can be explained by different transport rates of atoms. According to the previous reports [156], under large temperature gradients, tin atoms in tin-based solder moved from its cold end to the hot end, while copper, nickel and silver atoms migrated from the hot side to the cold one. Based on this observation and the experimental results of this research, it can be concluded that compressive stresses caused by the migration of copper and silver atoms to the cold end were much larger than those due to the moving tin atoms to the hot end. So, the cold end was generally subjected to compressive stresses, while the interface of the hot end was exposed to tensile stresses. Different stresses on the interface might exacerbate extrusion of the Cu_3Sn IMC layer at the cold end and accelerated dissolution of the interface at the hot end.

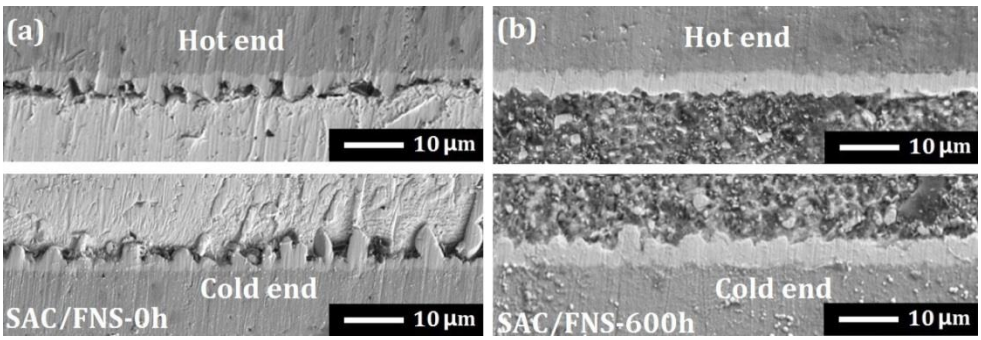

Figure 6.9 SAC/FNS solder joint before (a) and after (b) 600h TM stressing

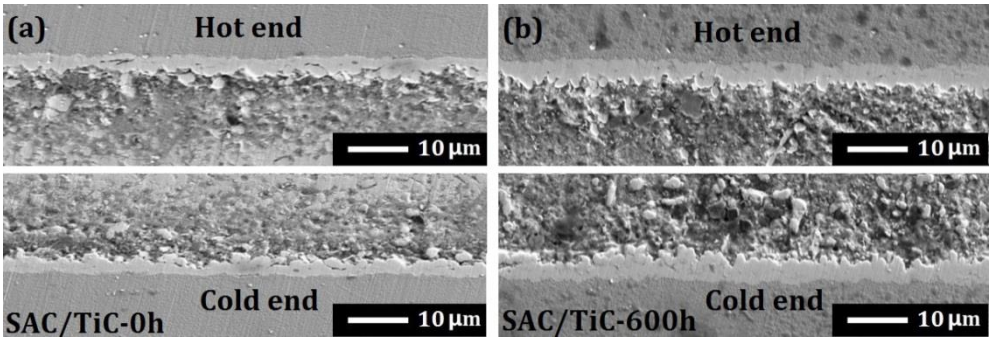

Figure 6.10 SAC/TiC solder joint before (a) and after (b) 600 h of TM stressing

Comparing morphology of SAC/NG，SAC/FNS and SAC/TiC solder joints before and after 600 h of stressing, it was found that the interfacial IMC layers of the three kinds of solder joints were also affected by the TM stressing (IMC thickening at the interface of SAC / FNS was the most obvious). However, the

growth rate of the IMC layer was much lower than that of the SAC solder joint. The extrusion of thin IMCs was not found at the cold ends of three kinds of composite solder joints and no serious damage was observed at the hot ends. This showed that the three kinds of reinforcement particles employed in this research can effectively lower the migration rate of metal atoms in the solder joints under a large temperature gradient and alleviate tensile stresses at the interface of the solder joints to some extent.

6.3.2.2 Microstructural evolution in solder matrix before and after TM

The microstructural evolution of different solder joints subjected to varying times of TM stressing are shown in Figures 6.11, 6.12, 6.13 and 6.14. The thickness curves of interfacial IMC and corresponding thickness data for different solder joints are shown in Figures 6.15 and Table 6.2, respectively. For the SAC solder, the initial microstructure of the solder joint was composed of β-Sn phases, Ag_3Sn and Cu_6Sn_5 IMCs. After 200 hours of TM stressing, it was found that bulk Cu-Sn IMCs began to form in the hot region of the solder joint; Cu-Sn IMCs (Cu_6Sn_5) actually contained two parts: 1) the initial Cu_6Sn_5 IMCs in the solder; 2) the Cu_6Sn_5 phase formed during the stressing process. As the stressing time continued to increase, the bulk IMCs in the solder joints began to be dispersed throughout the solder joint (after 400 hours). And at the later stage of the stressing process (after 600 hours), Sn IMCs were mainly concentrated at the cold end of the solder joint and the IMC layer at the cold end thickened significantly.

As for the interfacial IMCs, the thickness of IMC layer at the cold end of the SAC solder joint increased with the increase in the stressing time. After 600 hours, thickness increased from 2.12 μm to 8.96 μm; the increment was 323%. In addition, granular Ag_3Sn IMCs were also found in the IMC layer of the cold end. Thickness of the IMC at the hot end is thinned seriously with the increase in the stressing time. Even the copper substrate dissolved locally with continuous voids and cracks formed between the solder and the substrate. This can be attributed in large part to migration of copper atoms from the substrate to the solder joint

during thermal stressing. The processes of formation and migration of Cu-Sn and Sn-Ag IMCs in SAC solder joints indicated that Cu and Ag atoms migrated from the hot end to the cold one at a large temperature gradient; this result is consistent with the previous reports [156-157].

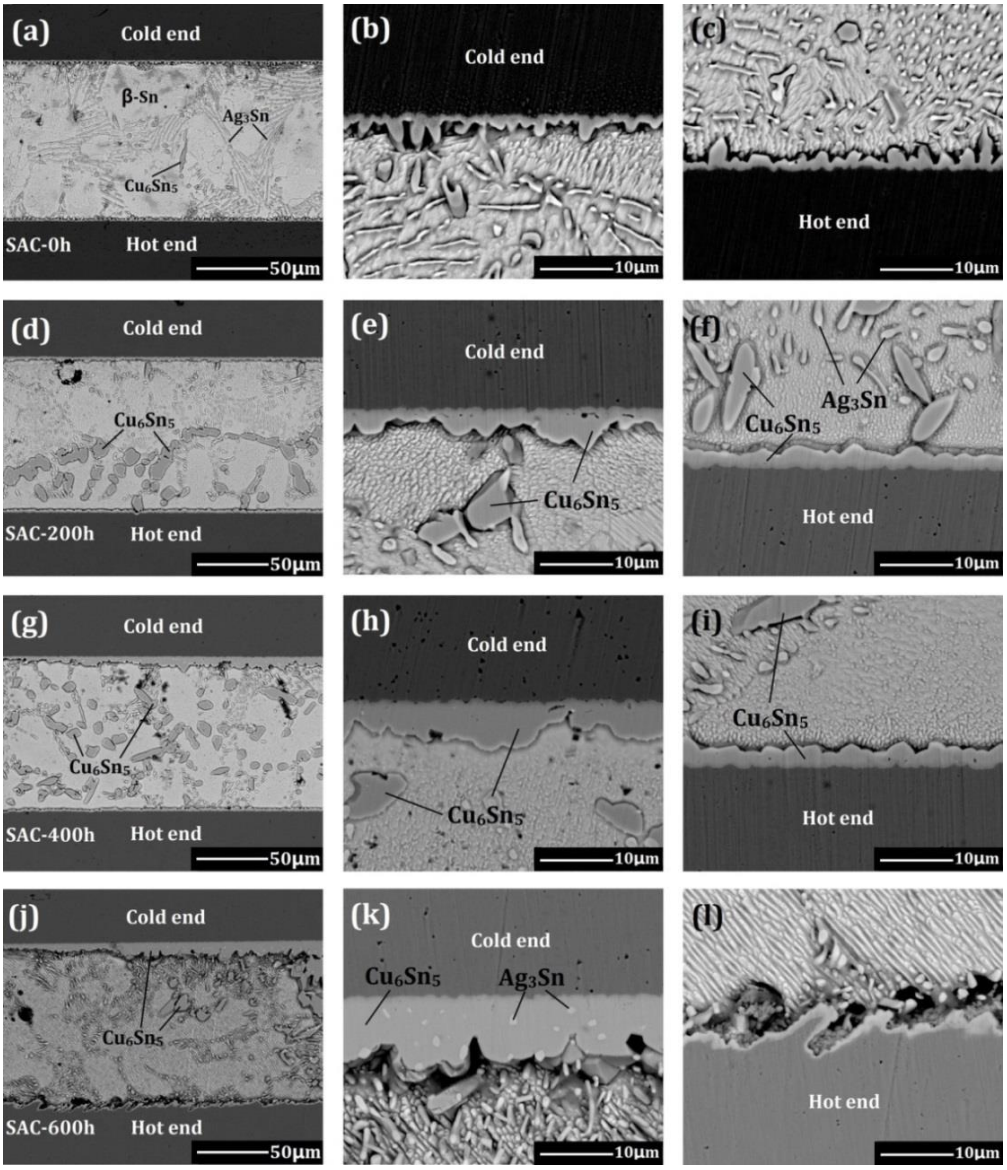

Figure 6.11 Microstructural evolution of SAC solder joint: (a)-(c) 0 h; (d)-(f) 200 h; (g)-(i) 400 h; (j)-(l) 600 h

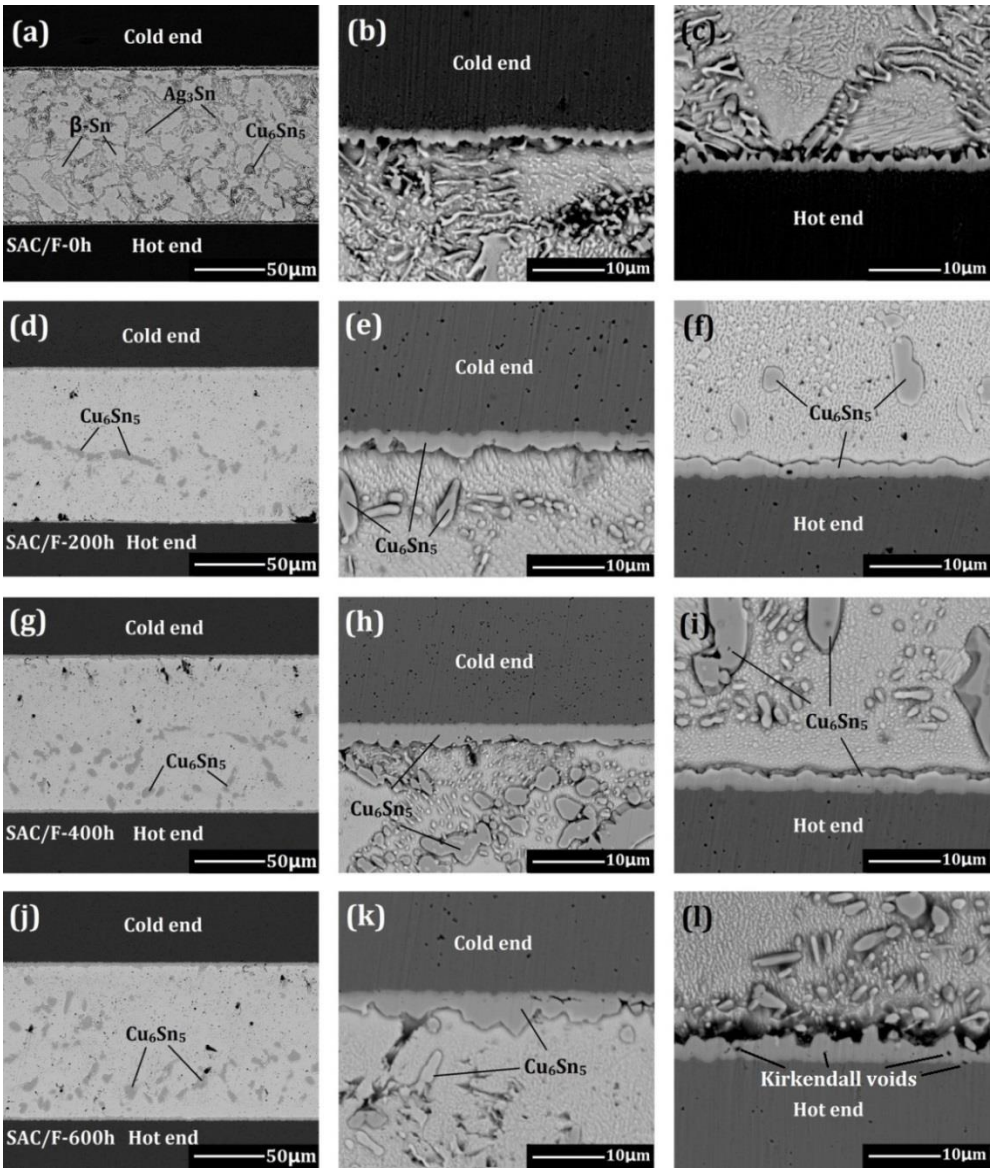

Figure 6.12 Microstructural evolution of SAC/FNS solder joint: (a)-(c) 0 h; (d)-(f) 200 h; (g)-(i) 400 h; (j)-(l) 600 h

There are some similarities as well as differences in the microstructural evolution of SAC/ FNS solder joints under the same thermal stressing conditions compared with SAC solder joints. Similarly, after 200 hours, some bulk Cu-Sn IMCs also began to form at the hot ends of the SAC / FNS joints, but these newly formed IMCs were much smaller than in SAC in terms of both volume and quantity; Unlike the SAC solder joints, these newly formed IMCs did not diffuse throughout the solder joint and eventually enrich at the cold end of the solder joint as the stressing time continued to increase. After 600 hours, Cu-Sn IMCs in the solder joints were mostly distributed at the hot end and central regions of the

solder joints, and only a small part of them was located at the cold; this might be caused by the uneven distribution of reinforcement. The number of Cu-Sn IMCs newly formed was also significantly lower than that in the SAC solder joints. On the other hand, the growth curve and the thickness data of interfacial IMCs in SAC/FNS also had some similarities and differences compared with the SAC sample. Specifically, thickness of the IMC layer of the SAC/FNS sample at the cold end increased with the stressing time-from 1.86 μm to 4.07 μm, an increase of 119%, which was much lower than that in the SAC solder joint. In addition, granular Ag_3Sn IMCs were also observed in the cold-end IMC layer after 600 of hours stressing. Thickness of the IMC at the hot end also increased gradually from 2.14 μm to 3.52 μm; the increase was only 64.5%, much lower than that of IMC at the cold end. In addition, the SAC/FNS sample was more stable during the entire stressing process, and there was no serious damage due to the copper substrate dissolution or IMC migration (only a few Kirkendall voids were found). These results show that addition of FNS lowered the migration rate of metal atoms in the solder joint effectively and reduced the growth and migration rate of IMCs in the interface and matrix; it helped to maintain microstructural stability of the whole solder joint under TM stressing. This is mainly caused by the physical properties of FNS and the character of its distribution in the solder matrix. Based on the analysis in Chapter 3, the reinforcement was more likely to concentrate around IMC grains and interfacial IMC grains. Since the reinforcement does not react with the molten solder and did not coarsen during the stressing process it could prevent the diffusion of metal atoms to a certain extent and further hinder the process of formation, growth and migration of IMCs.

According to Figure 6.13, small (or large) Cu-Ni-Sn IMC phases were observed in the initial SAC / NG sample; the grain size of the β-Sn phase in this solder joint was smaller than that of the SAC sample. In addition, morphology of Ag_3Sn IMCs in this solder joint also changed from needle-like to granular or short-rod-like compared to that in the SAC solder; these observations are also consistent with those of Section 3.4.1. The volume and quantity of Cu-Ni-Sn IMC

phases in the solder joint also increased to some extent with the increase in the stressing time. The growth trend of Cu-Ni-Sn IMC in bulk was the most obvious; its growth can be attributed to diffusion of nickel atoms, which not completely reacted with the substrate during the reflow process and continued to react with the solder matrix during the thermal stressing process, thus forming new Cu-Ni -Sn IMCs. In this process, original copper atoms in the solder joints and those diffused from the substrate to the solder joints during the stressing process also contributed to the continuous growth of Cu-Ni-Sn IMCs. Although the number and volume of Cu-Ni-Sn IMCs increased with the stressing time, the positional change of Cu-Ni-Sn IMCs was not obvious during the whole stressing period, and there was no obvious IMC migration compared with the SAC sample. On the other hand, addition of NG could also play a role in inhibiting the excessive growth of interfacial IMC and maintaining stability of the interface. Specifically, the IMC layers at both ends thickened during the whole stressing period. As shown in Table 6-2, the growth rates of interfacial IMCs at the hot and cold ends were only 131% and 133%, respectively; the growth rate of interfacial IMCs in SAC/NG was much lower than that in SAC. In addition, the thickening rate of IMCs at the both ends of the sample was almost the same; this also suggests that the interface of this composite solder joint was more stable than for SAC and SAC/FNS under TM stressing. Moreover, granular Ag_3Sn IMC were not observed in the cold-end IMC layer of the solder joint and IMCs at the hot-end also maintained good integrity during the entire stressing. Since NG is a composite reinforcement, Ni atoms on the surface of the graphene could react with Sn and Cu atoms (including original copper atoms and those diffused into the solder joints during stressing) in the solder to form a new Cu-Ni-Sn IMC phase during the thermal stressing process. It is worth noting that formation of new Cu-Ni-Sn IMC can consume a part of Cu atoms diffused from the Cu substrate and, thus, suppress diffusion of Cu atoms from the hot side to the cold side. Further, graphene itself can also act as a barrier to reduce diffusion of atoms so as to reduce the migration rate of the metal atoms during migration process. Based on

these phenomena observed, it is reasonable to believe that addition of the NG reinforcement can effectively suppress the growth of the IMC layer and migration of IMCs in the solder joint under TM stressing.

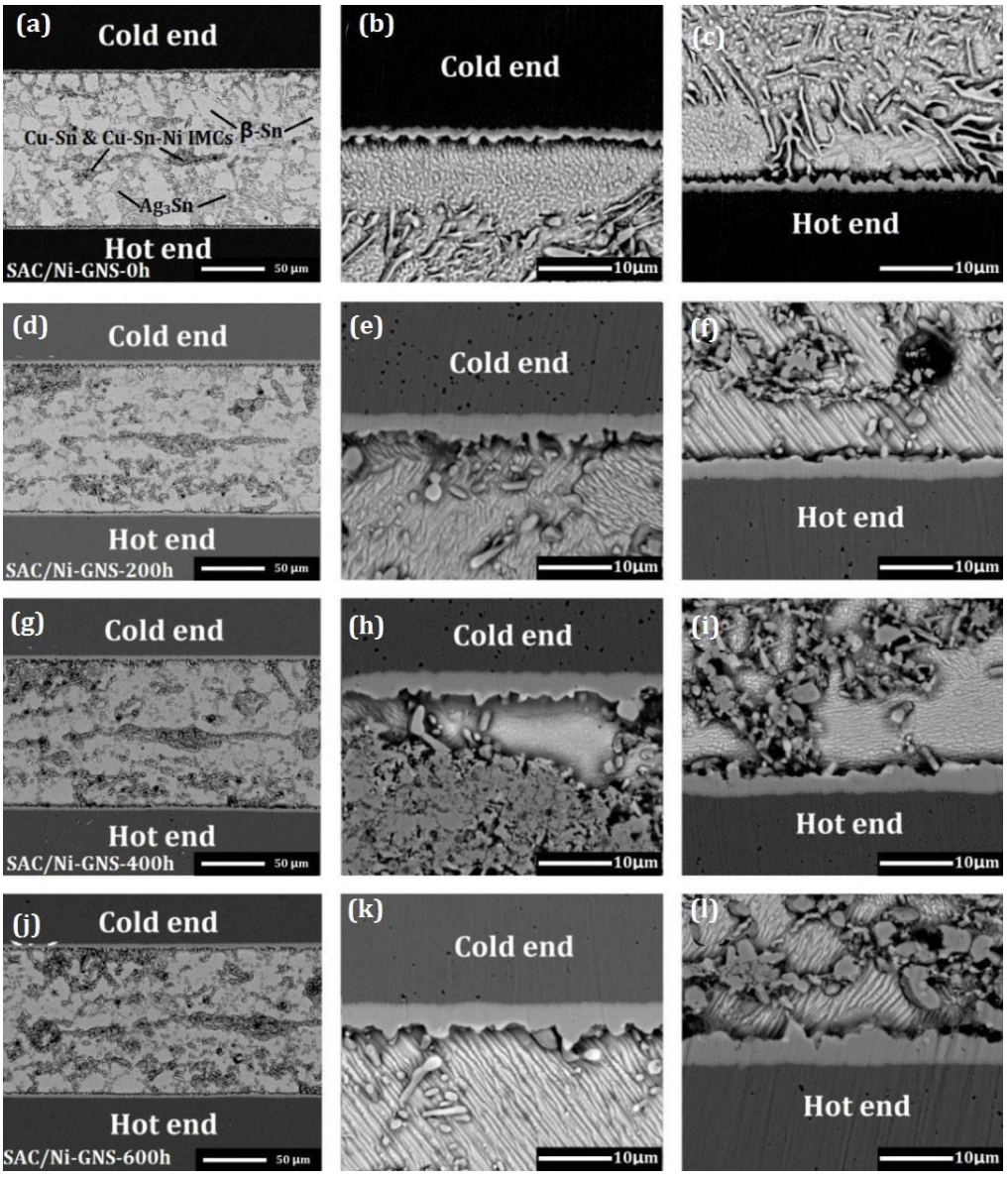

Figure 6.13 Microstructural evolution of SAC/NG solder joint: (a)-(c) 0 h; (d)-(f) 200 h; (g)-(i) 400 h; (j)-(l) 600 h

The results for SAC/TiC sample shown in Figure 6.14 demonstrate that some bulk IMCs also began to form at the initial stage of thermal stressing (after 200 hours). As the stressing time increased, the number and volume of IMCs in the solder joints also increased and gradually dispersed throughout the solder joint (after 400 hours of stressing). Unlike the SAC sample, the number and volume of

newly formed IMCs increased in the solder joint but they did not continue to migrate to the cold end, remaining almost unchanged and eventually distributed throughout the solder joint. This might be caused by relatively poor thermal conductivity of TiC that could cause excessive heat generation in TiC aggregation area. The increase of local temperature could accelerate the process of diffusion and reaction of metal atoms to form a large amount of dispersed IMCs around TiC reinforcement. At the same time, copper atoms diffused from the Cu substrate to the solder joints were fixed in the solder joints in the form of Cu-Sn IMCs to some extent, preventing the further migration of Cu atoms to the cold end. On the other hand, the growth mode of interfacial IMCs at the both ends of the solder joint was similar to that in SAC / NG, namely, thickness of the IMC layers increased with the increasing stressing time. After 600 hours, the increase in thickness at the cold and hot ends was 97% and 112%, respectively; the average growth rate of IMCs at the hot end was higher than that of the cold end. In addition, the interfacial IMCs were relatively intact, and no serious damage occurred after 600 hours of stressing, but a considerable number of Kirkendall voids were formed at the both ends. Based on these observations, it can be concluded that the addition of TiC reinforcement can also effectively suppress migration of Cu atoms from the hot end to the cold end to a certain extent. However, bulky IMCs and the Kirkendall voids formed during the stressing process may seriously affect in-service reliability of the solder joint.

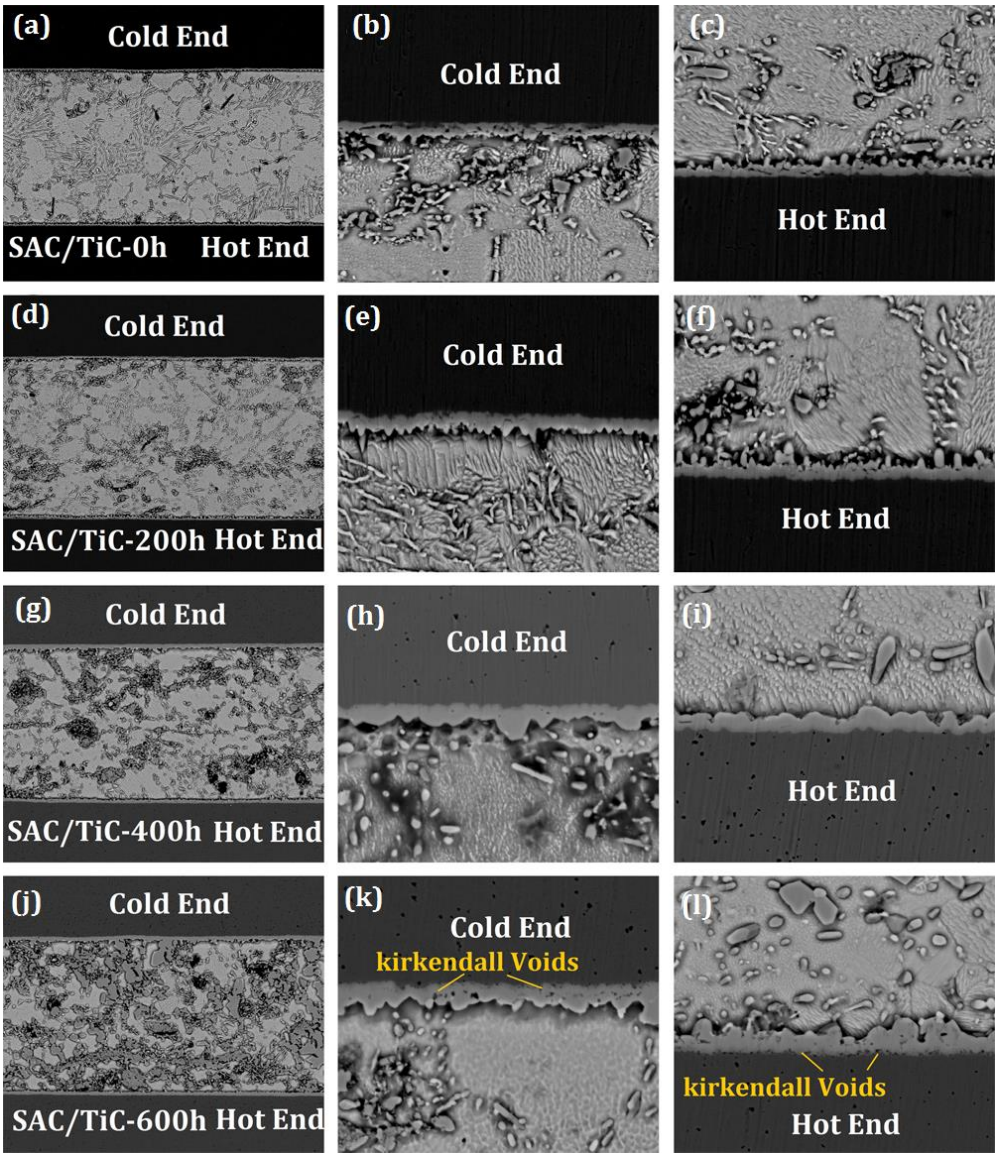

Figure 6.14 Microstructural evolution of SAC/TiC solder joint: (a)-(c) 0 h; (d)-(f) 200 h; (g)-(i) 400 h; (j)-(l) 600 h

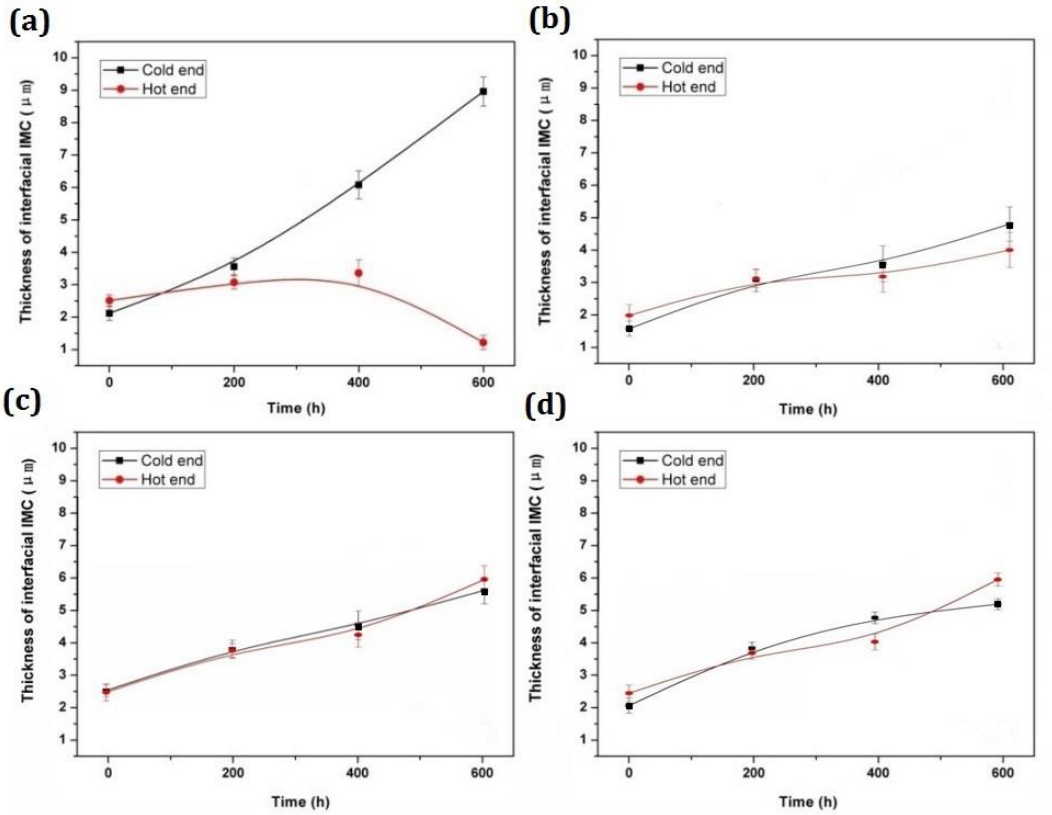

Figure 6.15 Thickness of interfacial Cu-Sn IMCs in different solder joints: (a) Cu/SAC/Cu, (b) Cu/SAC-FNS/Cu, (c) Cu/SAC-TiC/Cu (d) Cu/SAC-NG/Cu

Table 6.2 Thickness data of interfacial Cu-Sn IMCs in different solder joints

		SAC (μm)	SAC/FNS (μm)	SAC/TiC (μm)	SAC/NG (μm)
	0 h	2.12±0.16	1.86±0.25	2.74±0.24	2.23±0.28
Cold	200 h	3.56±0.18	2.88±0.23	3.85±0.18	3.78±0.23
end	400 h	6.08±0.24	3.23±0.34	4.49±0.26	4.67±0.19
	600 h	8.96±0.15	4.07±0.32	5.42±0.16	5.16±0.33
	0 h	2.51±0.28	2.14±0.26	2.69±0.22	2.48±0.25
Hot	200 h	3.07±0.32	2.92±0.21	3.81±0.19	3.65±0.18
end	400 h	3.36±0.19	2.98±0.27	4.23±0.33	4.14±0.24
	600 h	1.22±0.31	3.52±0.35	5.71±0.36	5.78±0.31

To compare with the microstructural evolution of solder matrix shown in Chapter 4, the ageing condition of high temperature (about 180℃) and large thermal gradient (1240K/cm) would not only lead to growth and coarsening of IMC grains, it also caused the formation and regularly migration of IMCs in the solder joints (especially for SAC305 solder joint). For interfacial microstructures, the thickness of interfacial IMC for all solder samples showed a continuous growth under isothermal ageing. However, under TM stressing, apparent difference was found in interfacial IMC for SAC305 solder; namely, the cold end showed a continuous increase while the hot end showed a serious damage, which is mainly caused by atomic migration. By contrast, although the thickness of interfacial IMCs in all composite solders also showed a continuous increase under TM condition, the growth rates for both ends are relatively close; this indicates that the addition of foreign reinforcement significantly lowered the effect of thermal gradient on migration of metal atoms, making the TM test more like a isothermal ageing

6.3.2.3 Inner structure of solder joint after TM stressing

In order to understand the distribution of IMCs in the solder joint after 600 hours of stressing, the grooves prepared with FIB (the depth of grooves was about 10 μm) were analysed. The observation results of SAC and three composite solders are shown in Figures 6.16, 6.17 and 6.18. It can be seen from Figure. 6.16 that massive Cu_6Sn_5 IMCs are distributed mostly in the central and cold-end regions of the SAC solder joints after 600 hours stressing, and some voids formed at the hot interface of the solder joints; these observation results agree well with the results in Figure 6.11. Similarly, the results for the SAC / FNS solder joint also confirm the results in Figure 6.12, namely, the quantity and size of Cu_6Sn_5 IMCs formed in this joint were relatively small and distributed mostly on the hot end of the solder joint after 600 hours of stressing. The obvious difference in the distribution of Cu_6Sn_5 IMC between SAC and SAC/FNS solder joints also confirmed inhibition of FNS reinforcement of formation and migration of IMCs during thermal stressing.

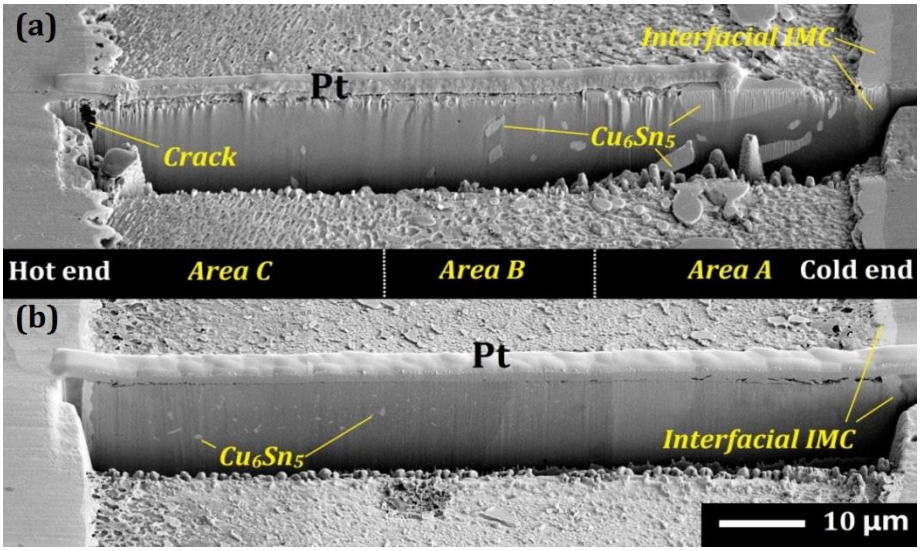

Figure 6.16 Images of subsurface layer: (a) SAC; (b) SAC/FNS

Based on the observation results shown in Figure 6.17, Cu-Ni-Sn IMCs formed in the SAC/NG solder joints often had the form of flocs; a large number of large clusters of flocculent IMCs are found in the central and hot-end of the solder joints. This is mainly due to the aggregations of NG formed during the reflow process. On the other hand, a number of irregular voids were found distributed in various locations in the solder joint, which might be due to the fact that reinforcement was easier to adsorb gas molecules and impurities. These adsorbents were introduced into the solder alloy during the preparation process; the residual gas molecules formed voids and inclusions in the solder joint during the subsequent reflow process. According to the results for the SAC/TiC solder joints in Figure. 6.18, their internal structure was relatively intact after 600 hours of stressing; the newly formed bulky Cu_6Sn_5 IMCs were dispersedly distributed throughout the solder joint area and they were larger in size than those in the SAC sample. This observation is basically consistent with Figure 6.14.

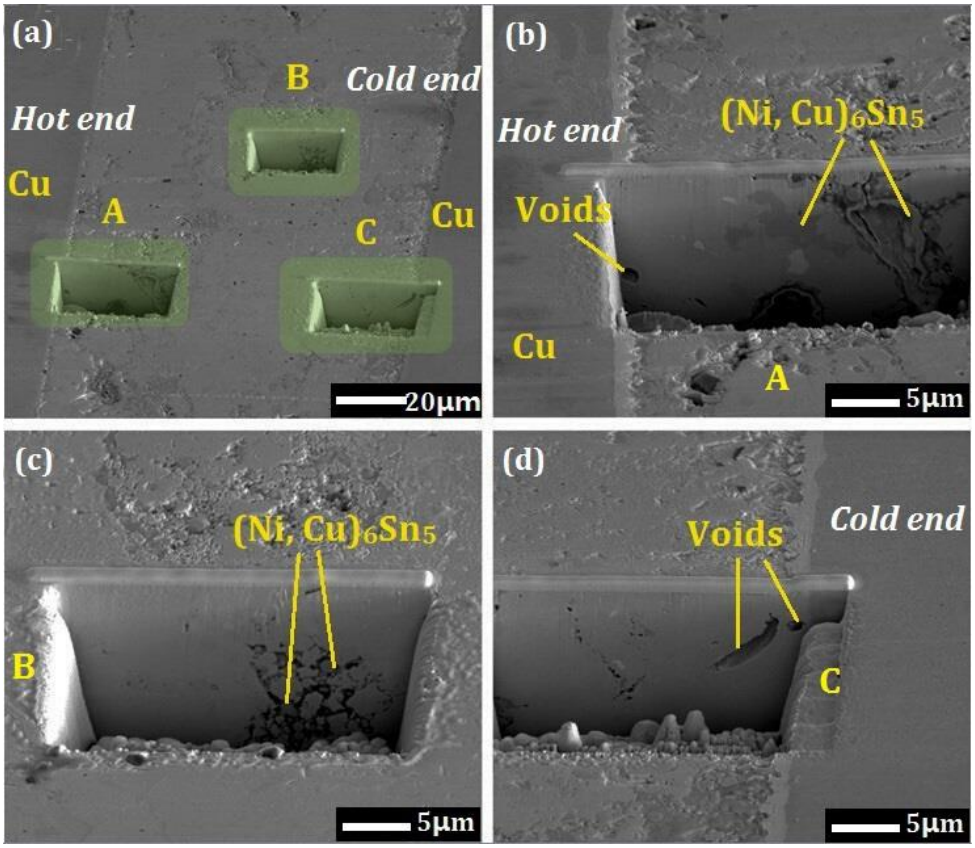

Figure 6.17 Images of subsurface layer of SAC/NG

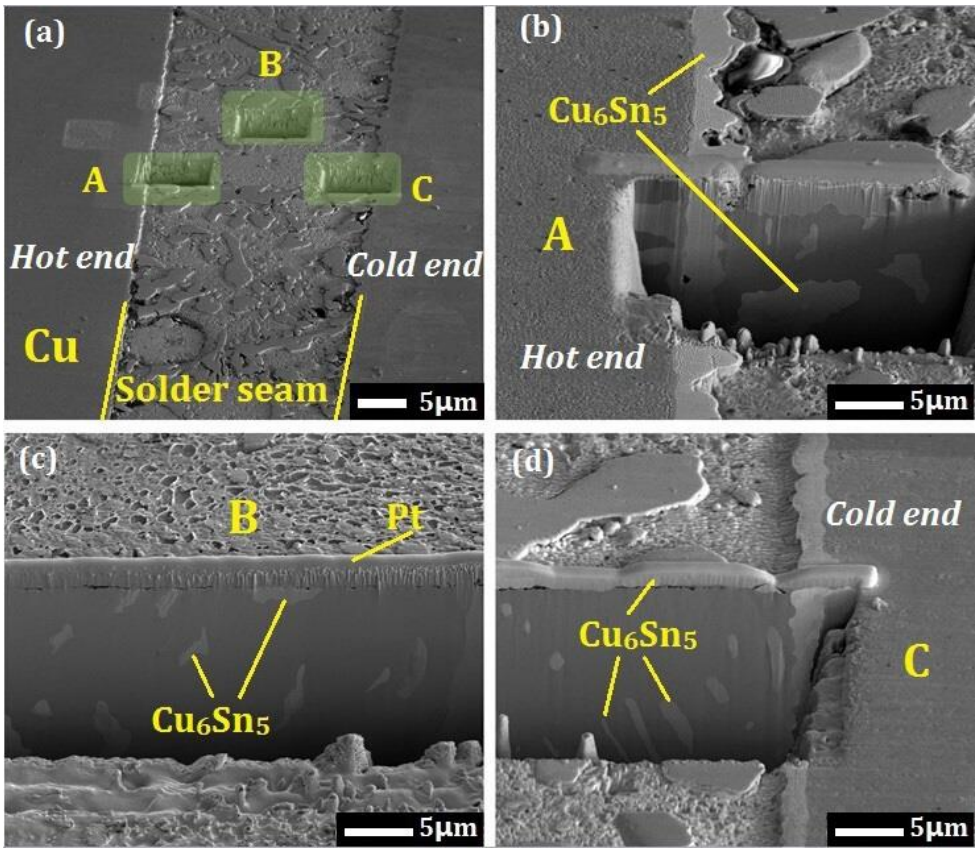

Figure 6.18 FIB images of subsurface layer of SAC/TiC

6.3.2.4 X-CT results

In order to evaluate the effect of the TM process on integrity of the inner structure of the solder joint, X-CT was used to scan the solder joint area of each sample before and after thermal stressing. The scanning results are shown in Figure 6.19.

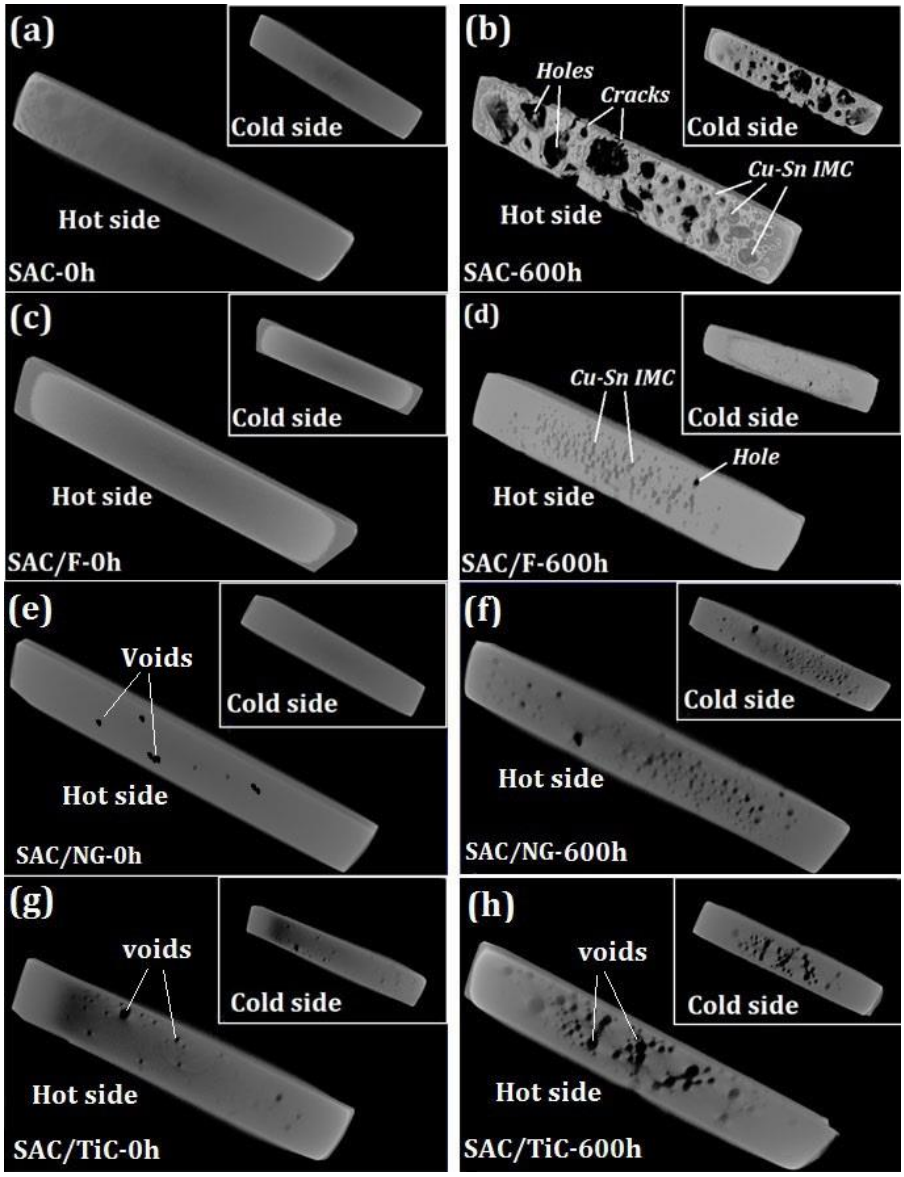

Figure 6.19 X-CT scanning results: (a-b) SAC; (c-d) SAC/FNS; (e-f) SAC/NG; (g-h) SAC/TiC

It was found that the internal structure of both SAC and SAC/FNS samples before TM stressing was relatively intact, without obvious defects such as voids or cracks, while a small number of voids were found in the initial state of SAC/NG

and SAC/TiC samples. This can be attributed to the effect of reinforcement added that can easily absorb gas molecules, not discharged during reflowing and causing defects such as porosity in the initial solder joint.

CT scanning results for each sample after 600 hours of stressing showed a large number of voids, cracks and Cu-Sn IMCs (dark-gray lumps) in the SAC solder joint (Figure 6.19b). This was due to migration of copper atoms from the Cu substrate to the solder joints under a large temperature gradient; these results are consistent with the observation in Sections 6.3.2.2 and 6.3.2.3. In contrast, after 600 hours of stressing, the internal structure of three composite solder joints was relatively intact. In particular, some small Cu-Sn IMCs were found inside the SAC / FNS solder joints after heat stressing, but their number and volume were much lower than those in the of SAC samples. Only some individual small voids formed in the solder joint, the whole structure did not show significant damage. IMCs in SAC / FNS composite solder joints were mainly distributed of the hot end; this result agrees well Figures 6.12 and 6.16b. Formation of bulk IMCs and voids was also found in the SAC/NG and SAC/TiC joints; in particular, this process was more serious in the latter solder joint. Formation of voids was mainly due to two reasons: 1) initial voids formed by air entrapment caused by exclusion of reinforcement during the reflow process; 2) atomic diffusion in the solder joint was different in different positions, and it was easy to form voids at the locations with a high diffusion rate.

Thus, the X-CT scanning results also indicated that appropriate addition of foreign reinforcement can effectively improve stability of the internal structure of the solder joint exposed to a large temperature gradient, improving the service life of the solders interconnect structure to a certain extent.

6.3.3 Elemental analysis of solder joints before and after TM stressing

The obtained results for microstructural evolution of solder joints under TM stressing confirmed that formation and migration of Cu-Sn IMCs could be very

serious. In order to understand dissolution behaviour of copper atoms under the stressing conditions of this experiment, ICP-OES was used to quantitatively analyse the copper content in different types of solder joints after various thermal stressing time. The ICP results are shown in Figures 6.20 and Table 6.3.

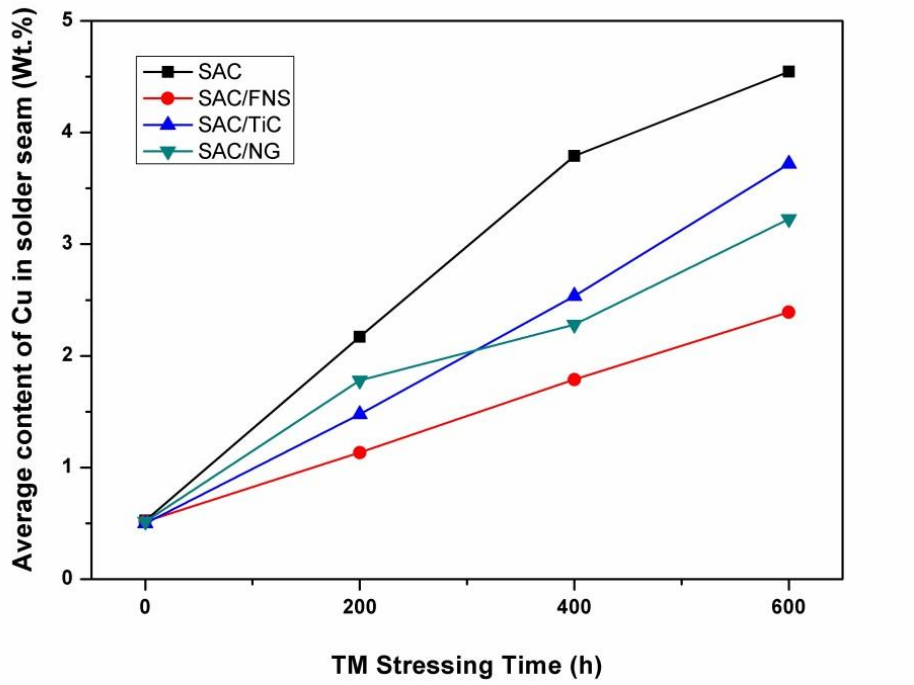

Figure 6.20 Evolution of Cu content in solder joints with stressing time

According to these data, the copper content in all samples increases with the increase of the thermal stressing time. It should be noted that the copper content is consistently higher in SAC solder joints compared to that in the other three welds during the entire thermal stressing period (200 hours to 600 hours). For three composite solders, the SAC/FNS solder joint had the lowest average copper content. Specifically, the average initial copper content in all solder joints was about 0.5% before thermal stressing, which is basically consistent with the copper content in the initial SAC alloy. After 600 hours of stressing, this content in the SAC solder joint reached 4.55%, 775% higher than the initial content. In contrast, the increments in SAC/FNS, SAC/NG and SAC / TiC solder joints were lower than the SAC sample: 309%, 525% and 647%, respectively. In addition, increase rate of copper decreased during the stressing period of 400-600 hours. This phenomenon can be explained by the results of related microstructural evolution.

According to Figures 6.12 and 6.16, the hot-end interface of the SAC sample was damaged seriously after 400 hours of stressing. The damage at the interface could block the way for copper atoms to diffuse from the substrate to the solder joints, resulting in a decrease in the diffusion.

Table 6.3 Weight percentage of Cu in solder joints after different stressing times

	SAC	SAC/FNS	SAC/TiC	SAC/NG
0 h	0.524	0.513	0.498	0.516
200 h	2.179	1.134	1.478	1.779
400 h	3.793	1.767	2.537	2.281
600 h	4.547	2.093	3.721	3.226

On the other hand, to further quantitatively analyse migration behaviour of copper atoms, the average migration rate of copper atoms in the sample during the thermal stressing period was also calculated. In order to avoid the error related to the damage at the interface in the SAC solder joint after a long-term stressing, the calculation were limited only stressing time of 0-400 hours. The migration rate of copper atoms was calculated with the following formula:

$$v = \frac{M(w_2 - w_1)}{T} \quad (6\text{-}1)$$

Here, v is the dissolution rate of copper atoms, M is the average mass of the solder joints, T is the stressing time, w_1 and w_2 are the copper contents of the solder joints after 0 and 400 hours of stressing, respectively. According to the ICP test results, after 400 hours of stressing, the copper content in the SAC solder joint was 3.27 wt. %; the average mass of the solder joint was 38 mg. Hence, about 1.24 mg copper dissolved in solder joints after 400 hours of stressing. Since the temperature difference generated by the TM set-up remained stable (about 1240 K/cm), the diffusion rate of copper atoms from the substrate to the SAC solder joint can be thus calculated as 3.1×10^{-6} g / h under this experimental condition. In contrast, after 400 hours of stressing, the increases in copper content in the SAC/FNS, SAC/NG and SAC/TiC joints were about 0.633 mg, 0.502 mg and 1.059 mg, respectively. The calculated respective dissolution rates for these

composite solders are 1.22×10^{-6} g/h, 1.09×10^{-6} g/h and 1.67×10^{-6} g/h, respectively. It is clear that the dissolution rates of copper in three composite solder joints are much lower than that for the SAC solder joint; the solder joints reinforced with FNS and NG were superior in reducing the copper dissolution rate. Based on the results of ICP and the calculations of dissolution rate of copper in this section, it is believed that addition of foreign reinforcement can effectively reduce the dissolution and migration rate of copper atoms in solder joints under a larger temperature gradient and, thus, inhibit TM behaviours in the solder joint.

6.3.4 Mechanical properties of solder joints before and after TM stressing

Nano-indentation was used to measure the hardness values of different solder joints after different stressing times; specific test methods and test areas are discussed in Section 6.2.2. The indentation loading and unloading curves of all samples are shown in Figure 6.21, while the average indentation depths of each sample are given in Table 6.4. The hardness values of each area calculated are shown in Figure 6.22 and Table 6.4.

From the nano-indentation test results and the calculated hardness data, it can be seen that the curves of all solder joints after 600 hours stressing show a greater dispersion compared with those for their initial state. For the SAC sample, hardness of the solder joint is obviously distributed in a gradient direction after 360 hours of stressing; the cold end was harder (the average indentation depth was 1186nm and the average hardness was 0.2434 GPa), while the hot end is relatively softer (the average indentation depth was 1527 nm and the average hardness was 0.1732 GPa). Average hardness of the central area of the joint was about 0.212 GPa, and it gradually decreased from the cold end to the hot one. This can be explained by considering microstructural evolution in the solder joint during stressing. From the microstructural observation of the SAC solder joints after 600 hours stressing in Section 6.3.2.2, a large amount of Cu_6Sn_5 IMC was enriched at the anode end; hardness of the solder joint near the hot end inevitably increased,

while the decrease in hardness at the hot side was mainly attributed to the relative increase in the number of Sn atoms.

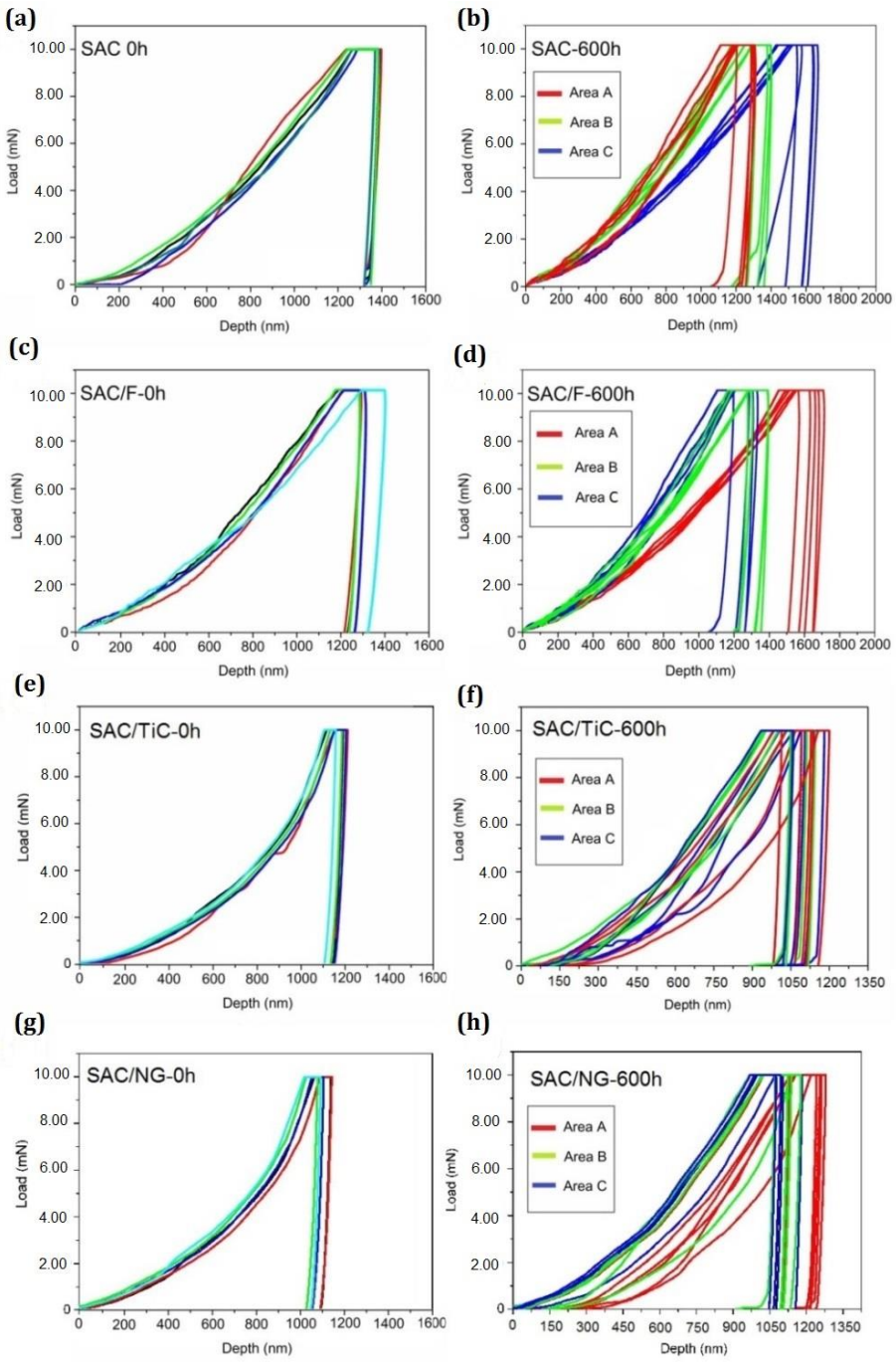

Figure 6.21 Test results of indentation before and after TM for 600 h: (a-b) SAC; (c-d) SAC/FNS; (e-f) SAC/TiC; (g-h) SAC/NG

Table 6.4 Average depth of indentation of different samples

Solder	Time	Average depth of indentation (nm)		
SAC	0 h		1327	
	600 h	A (cold)	B (central)	C (hot)
		1186	1318	1527
SAC/FNS	0 h		1271	
	600 h	A (cold)	B (central)	C (hot)
		1604	1274	1256
SAC/TiC	0 h		1138	
	600 h	A (cold)	B (central)	C (hot)
		1097	1074	1089
SAC/NG	0 h		1056	
	600 h	A (cold)	B (central)	C (hot)
		1226	1085	1063

According to the nano-indentation curves in Figure 6.21 and the average indentation depth data in Table 6.4, hardness of the SAC solder samples was the lowest (the indentation depth was about 1327 nm), while hardness of three composite solders increased to different extents: the average indentation depth for SAC/FNS, SAC/TiC and SAC/NG were 1271 nm, 1138 nm and 1056 nm, respectively. The corresponding hardness data also show that initial hardness of the SAC sample was about 0.2102 GPa, while that of the three composite solders reached 0.2237 GPa, 0.2517 GPa and 0.2703 GPa, respectively. The initial hardness levels of the solder joints obtained here were close to the corresponding data obtained in Chapter 5. Hardness of the composite solder joints improved obviously because of the dispersion and fine-crystal strengthening. In addition, similar to the observations analysed in Section 5.4, the nano-indentation curves of the composite solders are more discrete. Although the average indentation depths of composite solders were relatively small, their numerical dispersion was slightly larger than that of the SAC solder. This phenomenon means that distribution of

reinforcements in the solder joint was not uniform, and the reasons are explained in Section 5.3.3.

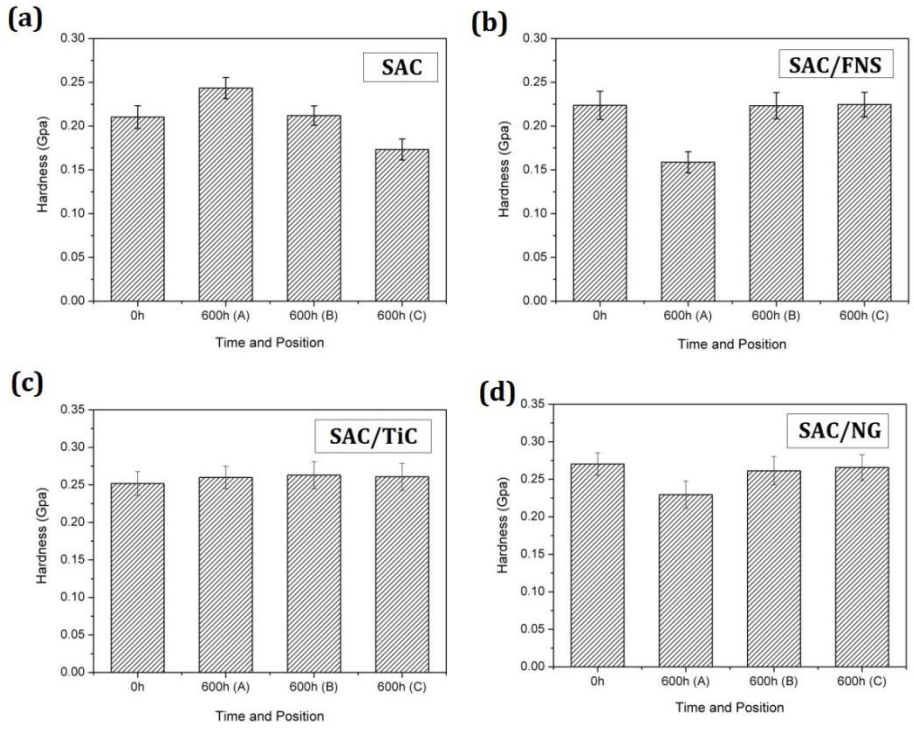

Figure 6.22 Average hardness distribution in different solder joints before and after thermal stressing

Compared with the SAC sample, the hardness data for the SAC/FNS samples after stressing were more spread. Specifically, the indentation depth and average hardness of the solder joint also showed an obvious gradient distribution, but the direction of this gradient was opposite to that of the SAC sample. After 600 hours of stressing, the hardness values of the SAC/FNS samples in the hot and central regions were maintained at their initial level (from 0.2237 GPa to 0.2233 GPa and 0.2245 GPa, respectively; so, the hardness change was almost negligible). However, the average hardness of the cold region decreased significantly-to 0.1587 GPa, with a reduction of 29%. The hardness results for SAC/FNS also correspond to those observed for the microstructure: the newly formed IMC were distributes mostly in the central and hot-end areas of the stressed solder joint. The decrease in hardness caused by grain coarsening during stressing and its increase caused by the dispersion of Cu_6Sn_5 IMCs might cancel each other, resulting in a little change in hardness of these regions. The decrease in hardness at the cold end

was mainly due to the lower content of Cu_6Sn_5 IMCs and coarsening of β-Sn.

For the SAC/NG samples, the distribution of hardness data also showed a decreasing tendency from the hot side to the cold side after 600 hours of stressing. Specifically, the hardness values at the hot, central and cold ends of the joint decreased from 0.2703 GPa to 0.2608 GPa, 0.2613 GPa and 0.2294 GPa, respectively. Although the hardness data for the hot end and central regions were lower than their initial values, the average decrease was only 3.4%. However, the hardness values for the cold end decreased more significantly, with a decline of 15%. The results of the hardness test were also closely related to the microstructural evolution of the solder joint. It can be seen from Figure 6.13 that the majority of Cu-Sn-Ni IMCs in the sample were distributed mostly in the hot-end and central regions, which could cause differences in the hardness distribution in the solder joint.

Table 6.5 Average hardness of solder joints before and after thermal stressing

	0 h	600 h (cold)	600 h (central)	600 h (hot)
SAC	0.2102	0.2434	0.212	0.1732
SAC/FNS	0.2237	0.1587	0.2233	0.2245
SAC/TiC	0.2517	0.2598	0.2629	0.2608
SAC/NG	0.2703	0.2294	0.2613	0.2657

The nano-indentation results for the SAC/TiC sample were also quite different from those for the SAC samples. Although the test curves for the stressed SAC /TiC sample showed a certain degree of dispersion compared with the initial results, the depth of indentation and average hardness values did not show a significant gradient distribution. Specifically, hardness of the whole SAC/ TiC solder joint increased slightly after 600 hours of stressing. The average levels of hardness of the cold-end, central and hot-end areas increased from 0.2517 GPa to 0.2598 GPa, 0.2608 GPa and 0.2629 GPa, respectively; the hardness values of the stressed solder joint in all regions were very close, without their obvious gradient

distribution. This phenomenon also corresponded to the microstructural characteristics of the solder joints, namely, newly formed IMCs, evenly distributed in the whole solder joint after stressing. The decrease in hardness caused by grain coarsening and the increase of hardness due to the newly formed Cu_6Sn_5 IMC jointly resulted in the slight increase in hardness of the solder joint.

6.4 Summary

A TM set-up based on the use of heating plates and thermoelectric coolers as designed and implemented together with the corresponding TM samples were prepared. The suitability of the set-up and samples was evaluated by means of finite element simulation and experimental observations. The surface morphology, microstructures, the IMC distribution, the dissolution rate of copper and the internal structural integrity and evolution of mechanical perties of different solder joints were characterized and analysed.

According to the experimental results, the appropriate addition of foreign reinforcement (FNS, NG and TiC) could also effectively suppress the formation, migration and growth of Cu_6Sn_5 and $(Cu, Ni)_6Sn_5$ and Cu_3Sn IMCs in composite solder joints during TM stressing. The addition of foreign reinforcement is positive to maintain the structural integrity of solder joints. The distribution of hardness data in TM stressed SAC, SAC/FNS and SAC/NG samples are all in a gradient direction. The difference is that the hardness in SAC sample increases gradually from the hot end to the cold end; the hardness distributions are in the opposite direction for SAC/FNS and SAC/NG. For the stressed SAC/TiC sample, the distribution of hardness data is relatively uniform and does not show a gradient distribution. The addition of three reinforcements can all retard the diffusion rate of Cu atoms from substrate to solder joints; the dissolution rate of the copper atoms from the substrate to the SAC solder joint was found to be 3.1×10^{-6} g/h. The values for SAC/FNS, SAC/NG and SAC/TiC were 1.22×10^{-6} g/h, 1.09×10^{-6} g/h and 1.67×10^{-6} g/h, respectively.

Chapter 7 Conclusions & Future work

7.1 Main conclusions

Based on the presented experimental results in previous chapters, the main findings in this thesis are therefore summarized in this chapter. As each chapter is focused on individual research topics, the main conclusions for entire thesis can be drawn in the following sections.

7.1.1 Basic characteristics of composite solders

1) With the addition of FNSs and TiC nanoparticles in the solder matrix, the microstructures become finer and more uniform than that of SAC plain solder; specifically, the Cu6Sn5 IMC particles were refined and evenly distributed in the eutectic area, while the rod-like Ag3Sn IMCs were changed into granular shapes after FNSs and TiC incorporation. With addition of NGs in the solder matrix, morphology of IMCs at the solder/Cu interface was changed from scallop-like to cauliflower-like; thickness of this interfacial IMCs was proportional to the amount of NGs added, which could be explained by diffusion of Ni. In addition, uniformly dispersed blocky $(Ni, Cu)_6Sn_5$ as well as the coarse Ag_3Sn IMCs were observed in the solder matrix after addition of NGs.
2) Negligible changes were found in the melting point and electrical resistivity of FNSs doped composite solders due to the relatively small amount addition of FNSs. The contact angle curve indicated that the appropriate amount of FNSs nanoparticles can enhance the wettability, while the excessive addition have an adverse influence on the wetting property of SAC composite solder. Only insignificant decline in electrical resistivity of NG doped composite solders was found related to lower resistivity of Ni and GNS. There was also a negligible change in the melting point in NG-reinforced solders, since nano-sheets were

added in relatively small amounts. However, the change in contact angle indicated that addition of nanoparticles enhanced wettability of the solder. The TiC reinforced composite solders were found have lower CTE values compared with the non-reinforced SAC solders, indicating their higher dimensional stability than that of the non-reinforced solder. Negligible changes in the melting point of the composite solders were observed together with wider melting ranges. The wettability results showed its improvement with incorporation of TiC nanoparticles into the solder matrix.

3) The results of Raman spectrum identified the existence of FNSs in the solder matrix. The added Ni-decorated graphene nano-sheets were found on the fracture surfaces after mechanical testing. The results obtained with EDS and Raman spectroscopy confirmed the existence of NGs in the solder matrix. The presence of TiC nanoparticles added in the solder matrix was also verified using XRD, SEM and EDS. However, some relatively big aggregations of TiC were found in the solder matrix; thus, how to improve the dispersion of the foreign reinforcement in the solder matrix should be further investigated.

7.1.2 Isothermal ageing

1) The morphology and thickness of interfacial IMC between solder and Cu pad show an obvious difference after adding foreign reinforcement to SAC solder. When the reinforcement is FNS, there is no obvious change in the morphology of interfacial IMC, however, the thickness of interfacial IMC show a decrease as the addition amount increases. When adding TiC, a “porous”-like interface is formed at the interface between solder and Cu pads, while the thickness of interfacial IMC is also show an obvious increase. When reinforcement is NG, a cauliflower-like interfacial IMC is observed at interface, while the thickness of interfacial IMC is also thicker than that of SAC sample.
2) As ageing time increases, the thickness of interfacial IMCs (Cu_6Sn_5 and Cu_3Sn) are both evidently increased. Although this phenomenon is also observed in

composite solders, the growth rate of interfacial IMCs is inhibited after adding FNS and NG reinforcement. When reinforcement is TiC, the initial "porous" interfacial gradually compacted during ageing process. In addition, compared with plain SAC solder, the growth of Cu_3Sn IMC in SAC/TiC solder is also suppressed to a large extent.

3) FNS and TiC reinforcement could effectively decrease the coarsening of Ag_3Sn and Cu_6Sn_5 during thermal ageing. After ageing, there are a mass of Cu-Sn-Ni IMC formed in SAC/NG solder matrix.

4) An appropriate addition of foreign reinforcement could improve the mechanical properties of solder joints under thermal ageing. The addition of TiC is more effective on improving the hardness of solder alloy, while the addition of NG is more useful on improving the shear strength of solder alloy.

7.1.3 Electro-migration

1) After 360 hours of EM stressing, extrusions at anode side of SAC solder joints with height of about 0.42 μm were found; although some fluctuations and coarsening structures were observed on surfaces of the three composite solder joints, their surfaces were more smooth than those of SAC samples.

2) According to the microstructural analysis, the Cu_6Sn_5 was formed first at the cathode side of SAC samples during the EM stressing period; with increasing stressing time, IMCs ultimately enriched at the anode side of solder joints. Cu_6Sn_5 and $(Cu，Ni)_6Sn_5$ formed initially in SAC/FNS and SAC/NG on the cathode. With the increase in the stressing time, these IMCs did not migrate to anode side, but distributed all around the solder joints. As for SAC/TiC solder joints, newly formed Cu_6Sn_5 IMCs enriched at the central and the cathode regions of solder joints during the stressing period. These findings demonstrate that addition of reinforcements restrained formation and migration of IMCs in solder joints during the EM stressing period to different extents.

3) Based on analyses of growth modes of interfacial IMCs, thickness of interfacial

IMCs at the anode side of SAC samples increased continuously, while at the cathode side it increased firstly and then decreased. After a long-term stressing, discontinued voids and defects formed in the IMC layer at the cathode side. The growth mode of interfacial IMCs of other three composite solders was relatively similar; thickness of the IMC layer at both cathode and anode sides increased with the increasing stressing time, with the increase rate at the anode side being higher than that at the cathode side. Besides, after long-term stressing, a significant growth of Cu_3Sn was observed in SAC and SAC/FNS samples, while this phenomenon was not found in SAC/NG and SAC/TiC samples, indicating that the addition of TiC and NG reinforcements suppress the growth of Cu_3Sn IMC.

4) The result of nano-indentation test performed before and after EM stressing showed that the hardness value of solder joints of SAC samples after EM stressing gradually decreased from the anode side to the cathode side. The distribution of hardness values in SAC/FNS and SAC/NG samples after stressing was more homogeneous, without significant gradients. The hardness value of solder joints in SAC/TiC samples after stressing was distributed in a gradient way; however, opposite to that of SAC samples, hardness increased gradually from the anode side to the cathode side.
5) Analysis of average failure life of different solder samples showed that addition of FNS and NG reinforcements could effectively improve the failure life of SAC solder alloys to a certain extent, while addition of TiC might threaten their failure life.

7.1.4 Thermo-migration

1) The interfacial stress caused by different diffusion directions and velocities of different metal atoms in the solder joint led to extrusion of the Cu3Sn layer at the hot interface of the SAC 305 sample. However, this phenomenon did not appear in the SAC/FNS, SAC/NG and SAC/TiC samples, indicating that

addition of foreign reinforcement can effectively lower tensile and compressive stresses caused by migration of metal atoms.

2) During the thermal stressing, Cu-Sn IMCs were formed in the SAC sample due to the dissolution of copper atoms into the solder joints. These IMCs formed first on the hot side of the solder joint and migrated to its cold end as the stressing time increased and eventually concentrated of the cold end. In other three composite solder joints, although Cu-Sn or Cu-Sn-Ni IMCs also formed in the solder joints, their distribution and migration behaviour were rather different from those in the SAC solder joints. Interfacial IMCs at the cold end of the SAC solder joint increased sharply with the stressing time, while the hot end was severely damaged after 600 hours of stressing. In contrast, thickness of interfacial IMCs of other three composite solder joints showed an increasing trend at both hot and cold ends.

3) According to the FIB results, flocculent reinforcement aggregations were found inside the SAC/NG solder joint, indicating that the reflow process might lead to an uneven distribution of reinforcement in the solder joint. In addition, X-CT scanning results showed that after 600 hours of stressing, the inner structure of the SAC solder joint was seriously damaged, and a large number of voids, cracks and large Cu-Sn IMCs formed. In contrast, although few voids and bulky IMCs formed in the composite solder joints, their overall structural integrity was much better than that of the SAC solder joints.

4) ICP-OES results demonstrated that copper contents of all solder joints increased with the stressing time. The maximum increase was found in SAC sample; after 600 hours, it was 4.55%, an increase of 775%. The contents of copper in other three composite solders were relatively lower: its increase in SAC/FNS sample was the lowest, about 309%. In addition, the dissolution rate of copper atoms from the substrate to the SAC solder joint was 3.1×10^{-6} g/h. The respective value for SAC/FNS, SAC/NG and SAC/TiC was 1.22×10^{-6} g/h, 1.09×10^{-6} g/h and 1.67×10^{-6} g/h, greatly reduced when compared with the SAC samples.

5) The distribution of hardness obtained with nano-indentation in the stressed SAC, SAC/FNS and SAC/NG samples was in a gradient direction. The difference was that hardness of SAC sample increased gradually from the hot end to the cold one, while distributions in SAC/FNS and SAC/NG were in the opposite direction. For the stressed SAC/TiC sample, the distribution of hardness data was relatively uniform and did not show a gradient distribution.

7.2 Future work

Due to the limit time and available resource during this PhD study, it is not possible to cover all the areas in certain depth and details, therefore several areas of potential future research that are worth of further investigation can be summarised as follows:

1) Based on the positive effect of NG reinforcement on improving the retained ratio of GNS in solder joint, more attempts should be made on preparing composite reinforcement with core-shell structure; the bonding strength between decorative layer and reinforcement also should be further discussed. In addition, to choose the most suitable decorative layer, more materials (such as Au, Ag and In, which are easy to react with molten solder alloy), more parameters (such as thickness of decorative layer and weight fraction of decorative elements) and reinforcement types also should be further studied.
2) The distribution of reinforcement added in the solder joint is the most important factor that directly affects the reliability of composite solder joint. However, it is hard to guarantee a homogenous distribution of foreign reinforcement in a solder joint using the existing processing routes (such as reflow). Therefore, solid-state welding methods, such as ultrasonic welding, can be adopted for preparing a composite solder joint so as to improve the retained ration and homogeneity of reinforcement in composite solder joint.
3) The electrical and heat conductivity of most ceramic reinforcement is relatively worse than that of metal reinforcement, the current and heat crowding will

thus be occurred around the reinforcement, leading to a mass of IMCs and cracks formed at the interface between reinforcement and solder matrix; these defects can significantly influence the stress distribution and the reliability of a solder joints. Therefore, it is necessary to further study the interfacial stability between reinforcement and solder matrix under different service conditions.

4) In consideration of the important effect of crystal orientation on diffusion of metal atoms, it is necessary to know deeply the influencing mechanism of "crystal orientation-metal diffusion-reinforcement", so as to seek a systematic package to suppress EM and TM behaviours.

5) In the actual service environment, solder joints used in various electronic products might suffer from mechanical vibration and shock. Additionally, the application environment, such as temperature and humidity, can also exert an effect on the reliability of composite solder joints. Up to now, the interactive mechanism between environmental parameters and EM /TM behaviours is still lacking. Therefore, a new "thermo-electro-mechanical-environmental" evaluation route based on experimental and modelling should be further developed.

References

[1] Y. W. Chang, S. H. Chiu, C. Chen, D. J. Yao, Effect of Si-die dimensions on electro-migration failure time of flip-chip solder joints, Materials Chemistry and Physics, 2011,127,85-90.

[2] K.N. Tu, Reliability challenges in 3D IC packageing technology, Microelectronics Reliability, 2011, 51, 517-523.

[3] S. Li, C. Basaran, A computational damage mechanics model for thermo-migration, Mechanics of Materials, 2009, 41, 271-278.

[4] M. F. Abdulhamid, C. Basaran, Influence of thermo-migration on lead-free solder joint mechanical properties, Journal of Electronic Packageing, 2009, 131, 011002.

[5] H. Y. Hsiao, C. Chen, Thermo-migration in Pb-free Sn-Ag solder joint under alternating current stressing, Applied physics Letters, 2009, 94(9), 092107.

[6] Zhao Z, Liu L, Hyun S C, Cai J, Wang Q, et al. Effect of nano-Al_2O_3 reinforcement on the microstructure and reliability of Sn–3.0Ag–0.5Cu solder joints [J]. Microelectronics Reliability, 2016, 60:126–134.

[7] Salleh MAAM, McDonald SD, Gourlay CM, Yasuda H, Nogita K, Suppression of Cu_6Sn_5 in TiO_2 reinforced solder joints after multiple reflow cycles[J]. Materials & Design, 2016, 108: 418-428.

[8] Zhao X, Wen Y, Li Y, Liu Y, Wang Y, Effect of g-Fe_2O_3 nanoparticles size on the properties of Sn-1.0Ag-0.5Cu nano-composite solders and joints [J]. Journal of Alloys and Compounds, 2016, 662: 272-282.

[9] Eid E.A, Fouda A.N, El-Shazly M. Duraia, Effect of adding 0.5 wt% ZnO nanoparticles, temperature and strain rate on tensile properties of Sn–5.0 wt% Sb–0.5 wt% Cu (SSC505) lead free solder alloy[J]. Materials Science & Engineering A, 2016, 657:104–114.

[10] Chen G, Peng H, Silberschmidt V V, Chan Y C, Liu C, Wu F, Performance of Sne3.0Age0.5Cu composite solder with TiC reinforcement: Physical

properties, solderability and microstructural evolution under isothermal ageing[J]. Journal of Alloys and Compounds, 2016, 685:680-689.

[11] El-Daly A A, Desoky W M, Elmosalami T A, El-Shaarawy M G, Abdraboh A M, Microstructural modifications and properties of SiC nanoparticles-reinforced Sn–3.0Ag–0.5Cu solder alloy[J]. Materials and Design, 2015, 65: 1196–1204.

[12] Xu S, Chan Y, Zhang K, Yung K.C, Interfacial intermetallic growth and mechanical properties of carbon nanotubes reinforced Sn3.5Ag0.5Cu solder joint under current stressing[J]. Journal of Alloys and Compounds, 2014, 595:92–102.

[13] Sun H, Chan Y C, Wu F, Effect of CNTs and Ni coated CNTs on the mechanical performance of Sn57.6Bi0.4Ag BGA solder joints[J]. Materials Science & Engineering A, 2016, 656:249–255.

[14] Ma D, Wu P, Improved microstructure and mechanical properties for Sn58Bi0.7Zn solder joint by addition of graphene nanosheets[J]. Journal of Alloys and Compounds, 2016, 671:127-136.

[15] Chellvarajoo S, Abdullah M Z, Khor C Y, Effects of diamond nanoparticles reinforcement into lead-free Sn-3.0Ag-0.5Cu solder pastes on microstructure and mechanical properties after reflow soldering process[J]. Materials & Design, 2015, 82:206–215.

[16] Wang Q, Zhu L, Chen X, Yan J, et al. Si particulate-reinforced Zn-Al based composites joints of hypereutectic Al50Si alloys by ultrasonic-assisted soldering[J]. Materials and Design, 2016, 107:41-46.

[17] Yang M, Ji H, Wang S, Ko Y, et al. Effects of Ag content on the interfacial reactions between liquid Sn-Ag-Cu solders and Cu substrates during soldering[J]. Journal of Alloys and Compounds, 2016, 679:18-25.

[18] Das S.K, Sharif A, Chan Y C, Wong N B, Yung W, Influence of small amount of Al and Cu on the microstructure, microhardness and tensile properties of Sn–9Zn binary eutectic solder alloy[J]. Journal of Alloys and Compounds, 2009, 481: 167–172.

[19] Ali B, Sabri M, Jauhari I, Sukiman N, Impact toughness, hardness and shear strength of Fe and Bi added Sn-1Ag-0.5Cu lead-free solders [J]. Microelectronics Reliability, 2016, 63:224–230.

[20] Tao Q B, Benabou L, Vivet L, Lee V N, Ouezdou F B, Effect of Ni and Sb additions and testing conditions on the mechanical properties and microstructures of lead-free solder joints[J]. Materials Science & Engineering A, 2016, 669:403–416.

[21] Tao Q B, Benabou L, Lee V N, et al. Viscoplastic characterization and post-rupture microanalysis of a novel lead-free solder with small additions of Bi, Sb and Ni[J]. Journal of Alloys and Compounds, 2017: 694:892-904.

[22] Ma Z L, Belyakov S, Gourlay C, Effects of cobalt on the nucleation and grain refinement of Sn-3Ag- 0.5Cu solders[J]. Journal of Alloys and Compounds, 2016, 682:326-337.

[23] Zhang L, Han J, Guo Y, He C, Effect of rare earth Ce on the fatigue life of SnAgCu solder joints in WLCSP device using FEM and experiments[J]. Materials Science & Engineering A, 2014, 597:219–224.

[24] Gao L, Xue S, Zhang L, et al. Effect of alloying elements on properties and microstructures of SnAgCu solders[J]. Microelectronic Engineering, 2010, 87:2025–2034.

[25] Mu D, Huang H, Nogita K, Anisotropic mechanical properties of Cu_6Sn_5 and $(Cu,Ni)_6Sn_5$[J]. Materials Letters, 2012, 86:46–49.

[26] Ma L, Zuo Y, Liu S, Fu Guo, et al. Whisker growth behaviors in POSS-silanol modified Sn3.0Ag0.5Cu composite solders[J]. Journal of Alloys and Compounds, 2016, 657:400-407.

[27] Sun H, Chan Y C, Wu F, Effect of CNTs and Ni coated CNTs on the mechanical performance of Sn57.6Bi0.4Ag BGA solder joints[J]. Materials Science & Engineering A, 2016, 656:249–255.

[28] Yang Z, Zhou W, Wu P, Effects of Ni-coated carbon nanotubes addition on the microstructure and mechanical properties of Sn–Ag–Cu solder alloys[J]. Materials Science & Engineering A, 2014, 590:295–300.

[29] Xu L, Chen X, Jing H, Wang L, et al. Design and performance of Ag nanoparticle-modified graphene/ SnAgCu lead-free solders[J]. Materials Science & Engineering A, 2016, 667:87–96.

[30] Wang F, Jin C, Liang H, et al. Effects of fullerene C60nanoparticles on A549 cells[J]. Environmental toxicology and pharmacology, 2014, 37:656–661.

[31] Li H, et al. High-mobility field effect transistors from large-area solution-grown aligned C60 single crystals[J]. Journal of the American Chemical Society, 2012, 134:2760–2765.

[32] John P, Harris F, Carbon Nanotubes and Related Structures[B]. Cambridge University Press, Cambridge, 1999.

[33] Calvert P. Nanotube composites: a recipe for strength[J]. Nature, 1999, 399:210–211.

[34] Komatsu K, Murata M, Murata Y, Encapsulation of molecular hydrogen in fullerene C60 by organic synthesis[J]. Science, 2005, 307:238–40.

[35] Watanabe H, Fukusumi M, Ishikawa K, Shimizu T, Superplasticity in a fullerene-dispersed Mg–Al–Zn alloy composite[J]. Scripta Materialia, 2006, 54:1575–1580.

[36] Chernogorova O, Drozdova E, Ovchinnikova I, et al. Structure and properties of superelastic hard carbon phase created in fullerene-metal composites by high temperature-high pressure treatment[J]. Journal of Applied Physics, 2012, 111:112601-5.

[37] Stroms E K. The Refractory Carbides, Refractory Materials Series[B]. Academic Press, New York, 1967.

[38] Toth L E. Transition Metal Carbides and Nitrides[B]. Academic Press, New York, 1971.

[39] Pierson H O, Handbook of Refractory Carbides and Nitrides[B]. Noyes Publications, Westwood, 1996.

[40] Liu, J, Andersson C, Gao Y, et al. Recent development of nano-solder paste for electronic interconnect applications[C]// Proceedings of the 10th Electronics Packageing Technology Conference (ECTC), Singapore, 2008: 84–93.

[41] Mokhtari O, et al. Disabling of Nanoparticle Effects at lncreased Temperature in Nanocomposite Solders[J]. Journal of electronic materials, 2012, 41(7): 1907-1914.

[42] Yang Z, Zhou W, Wu P, Effects of Ni-coated carbon nanotubes addition on the electromigration of Sn-Ag-Cu solder joints[J]. Journal of Alloys and Compounds, 2013, 581:202–205.

[43] Yang Z, Zhou W, Wu P, Effects of Ni-Coated carbon nanotubes addition on the microstructure and mechanical properties of Sn-Ag-Cu solder alloys[J]. Materials Science & Engineering A, 2014, 590:295-300.

[44] Liu P, et al. Effect of SiC nano-particle additions on microstructure and micro-hardness of Sn–Ag–Cu solder alloy[J]. Journal of electronic materials, 2008, 37(6):874–879.

[45] Lin D, Wang G, et al. The influence of copper nano-powders on microstructure and hardness of lead–tin solder[J]. Materials Letters，2002, 53:333–341.

[46] Zhang S, Chen Q. Fabrication of MWCNT incorporated Sn–Bi composite[J]. Composites Part B Engineering, 2014, 58(3):275-278.

[47] Lin D C, et al. Influence of titanium dioxide nano-powder addition on micro-structural development and hardness of tin–lead solder [J]. Materials Letters, 2003, 57:3193–3201.

[48] Nai S, Wei J, Gupta M. Effect of carbon nano-tubes on the shear strength and electrical resistivity of a lead-free solder [J]. Journal of electronic materials, 2008, 37:515–522.

[49] Nai S, Wei J, Gupta M. Improving the performance of lead-free solder reinforced with multi-walled carbon nano-tubes [J]. Materials Science and Engineering A, 2006, 423:166–175.

[50] Nai S, Wei J, Gupta M. Lead-free solder reinforced with multi-walled carbon nano-tubes [J]. Journal of electronic materials, 2006, 35:1518–1522.

[51] Kumar K M, et al. Single-wall carbon nanotube (SWCNT) functionalized Sn–Ag–Cu lead-free composite solders[J]. Journal of Alloys and Compounds, 2008, 450:229–237.

[52] Kumar K M, Kripesh V, Shen L, Tay A O. Study on the microstructure and mechanical properties of a novel SWCNT-reinforced solder alloy for ultra-fine pitch applications[J]. Thin Solid Film, 2006, 504:371–378.

[53] Nai S, Wei J, Gupta M. Influence of ceramic reinforcements on the wettability and mechanical properties of novel lead-free solder composites[J]. Thin Solid Film, 2006, 504:401–408.

[54] Shi Y W, et al. Creep properties of composite solders reinforced with nano- and micro-sized particles[J]. Journal of electronic materials, 2008, 37:507–514.

[55] Mavoori H, Jin S, creep-resistant, low melting point solders with ultra-fine oxide dispersions[J]. Journal of electronic materials, 1998, 27:1216–1222.

[56] Mavoori H, Jin S. Significantly enhanced creep resistance in low-melting-point solders through nanoscale oxide dispersions[J]. Applied Physics Letters, 1998, 73:2290–2298.

[57] Kao S T, et al. Controlling intermetallic compound growth in SnAgCu/Ni–P solder joints by nano-sized Cu_6Sn_5 addition[J]. Journal of electronic materials, 2006, 35:486–493.

[58] Lee H Y, Duh J G. Influence of Ni concentration and Ni_3Sn_4 nanoparticles on morphology of Sn–Ag–Ni solders by mechanical alloying[J]. Journal of electronic materials, 2006, 35(3): 494–503.

[59] Lee J H, Park D. J, et al. Reflow characteristics of Sn–Ag matrix in-situ composite solders[J]. Scripta Materialia, 2000, 42:827–831.

[60] Hwang S Y, et al. Microstructure of a lead-free composite solder produced by an in-situ process[J]. Journal of electronic materials, 2002, 31:1304–1308.

[61] Shen J, Liu Y C, Gao H X. In situ nano-particulate-reinforced lead-free Sn–Ag composite prepared by rapid solidification[J]. Journal of Materials Science, 2007, 18:463–468.

[62] Callister W D. Fundamentals of materials science and engineering[B]. New York: Wiley & Sons, 2004, 252-259.

[63] Shen J, Liu Y C, Han Y J, Tian Y M, Gao H X. Strengthening effects of ZrO_2 nano-particles on the microstructure and microhardness of Sn–3.5Ag lead-free solder, Journal of electronic materials[J]. 2006, 35:1672–1679.

[64] Lindemann F A. Über die Berechnung molekularer Eigenfrequenzen, Physical Chemistry Periodical[J]. 1910, 11:609–612.

[65] Frank G S. Size dependent thermal vibrations and melting in nano-crystals[J]. Journal of materials research, 1994, 9:1307–1313.

[66] Couchman P R, Jesser W A. Thermodynamic theory of size dependence of melting temperature in metals[J]. Nature, 1977, 269:481–493.

[67] Berry R S. When the melting and freezing point are not the same[J]. Scientific American, 1990, 262(8):68–74.

[68] Lewis L J, Jensen P, Barrat J L. Melting, freezing, and coalescence of gold nano-clusters [J]. Physical Review B, 1997, 56:2248–2257.

[69] Tai F, Guo F, et al. Processing and creep properties of Sn–Cu composite solders with small amounts of nano-sized Ag reinforcement additions[J]. Journal of electronic materials, 2005, 34:1357–1362.

[70] Amagai M. A study of nano-particles in Sn-Ag based lead free solders[J]. Microelectronic Reliability, 2008, 48:1–16.

[71] Yu D Q, et al. The formation of nano-Ag_3Sn particles on the intermetallic compounds during wetting reaction [J]. Journal of Alloys and Compounds, 2005, 389:153–158.

[72] Zhai Q, Guan S, Shang Q. Alloy thermo-mechanism: theory and application[B]. Beijing: Metallurgy Industry Press, 1999, 156–160.

[73] Schaefer M, Fournelle R A, Liang J. Theory for inter-metallic phase growth between Cu and liquid Sn-Pb solder based on grain boundary diffusion control[J]. Journal of electronic materials, 1998, 27:1167–1176.

[74] Li Z, Gupta M., High strength lead-free composite solder materials using nano-Al_2O_3 as reinforcement[J]. Advanced engineering materials, 2005, 7:1049–1054.

[75] Martin J W. Precipitation hardening[B]. Oxford: Butterworth Heinemann; 1998.

[76] Mughrabi H. Plastic deformation and fracture of materials[J]. Springer; 1993, 315–322.

[77] Chen C, Lin K. The reactions between electroless Ni-Cu-P deposit and 63Sn–37Pb flip chip solder bumps during reflow[J]. Journal of electronic materials, 2000, 29:1007–1014.

[78] Lee J Y, Kim J H, Yoo C D. Thermo-sonic bonding of lead-free solder with metal bump for flip-chip bonding[J]. Journal of electronic materials, 2005, 34:96–102.

[79] Sundaresan S, Rao M et al, Journal of electronic materials, 2007, 36, 324–331.

[80] Huntigton H B, Grone A R, Current induced marker motion in gold wires[J]. Journal of Physics and Chemistry of solids, 1961, 20:76-83.

[81] Fiks V B, On the mechanism of the mobility of ions in metals[J]. Soviet Physics-Solid State, 1959, 1:14-21.

[82] Campbell D et al. Thermo-migration and Electro-migration in zirconium[J]. Physical Review, 1969, 179 (3):601-622.

[83] Campbell D, et al. Inter-diffusion in a bulk couple of Pb-PbIn alloy[J]. Acta Metallurgica, 1976, 24:609-617.

[84] Roush W, Jaspal J, Thermo-migration in Pb-In solder[C]//Proceedings of the 32nd IEEE Electronic Components and Technology Conference, San Diego, CA, USA,1982, 342-351.

[85] Rinne G A, Issues in accelerated electro-migration of solder bumps[J]. Microelectronics Reliability, 2003, 43:1975-1982.

[86] Frear D R, Burchett S N, et al. Micro-structurally based finite-element simulation of solder joint behavior[J]. Soldering & Surface Mount Technology, 1997, 9(1):39-46.

[87] Ye H, Basaran C, et al. Pb phase coarsening in eutectic Pb/Sn flip chip solder joints under electric current stressing[J]. International Journal of Solids and Structures, 2004, 41:2743-2749.

[88] Wu B Y, et al. Joule heating enhanced phase coarsening in Sn37Pb and SnAgCu solder joints during current stressing[J]. Journal of Electronic Materials, 2008, 37(4):469-477.

[89] Chen C M, et al. Electro-migration effect upon the Sn-0.7 wt% Cu/Ni and Sn–3.5 wt% Ag/Ni interfacial reactions[J]. Journal of Applied Physics, 2001, 90(3):1208-1215.

[90] Kumar, M. He, et al. Effect of electro-migration on interfacial reactions between electroless Ni-P and Sn–3.5% Ag solder[J]. Thin Solid Films, 2004, 413:462-463.

[91] Gan H, Tu K. Polarity effect of electro-migration on kinetics of intermetallic compound formation in Pb-free solder V-groove samples[J]. Journal of Applied Physics, 2005, 97:063514.

[92] Kuo S M, et al. Polarity effect of electro-migration on inter-metallic compound formation in a Cu/Sn–9Zn/Cu sandwich[J]. Journal of Materials Research, 2008, 23(4):1087-1094.

[93] Chen L T, et al. Electro-migration study in the eutectic Sn-Bi solder joint on the Ni/Au metallization[J]. Journal of Materials Research, 2006, 21(4):962-974.

[94] Blech A, Herring C, Stress generation by electro-migration[J]. Applied Physics Letters, 1976, 29:131-139.

[95] Ren F, Nah J, et al. Electro-migration induced ductile-to-brittle transition in lead-free solder joints[J]. Applied Physics Letters, 2006, 89:141914.

[96] Nah J W, et al. Effect of electro-migration on mechanical shear behavior of flip chip solder joints[J]. Journal of Materials Research, 2006, 21(3):698-706.

[97] Ye H, Basaran C. Mechanical degradation of microelectronics solder joints under current stressing[J]. International Journal of Solids and Structures, 2003, 40:7269-7278.

[98] Chiang K, Lee C, et al. Current crowding-induced electro-migration in SnAg3.0Cu0.5 micro-bumps[J]. Applied Physics Letters, 2006, 88:072102.

[99] Chiu S H, Chen C. Investigation of void nucleation and propagation during electro-migration of flip-chip solder joints using x-ray microscopy[J]. Applied Physics Letters, 2006, 89:262106.

[100] Zhang L, et al. Effect of current crowding on void propagation at the interface between intermetallic compound and solder in flip chip solder joints[J]. Applied Physics Letters, 2006, 88:012106.

[101] Chiu S H, et al. Infrared microscopy of hot spots induced by Joule heating in flip-chip Sn-Ag solder joints under accelerated electro-migration[J]. Applied Physics Letters, 2016, 88:022110.

[102] Hu Y C, Lin Y H, et al. Electro-migration failure in flip chip solder joints due to rapid dissolution of copper[J]. Journal of Materials Research, 2003, 18(11):2544-2552.

[103] Ye H, et al. Thermo-migration in Pb–Sn solder joints under joule heating during electric current stressing[J]. Applied Physics Letters, 2003, 82:1045-1053.

[104] Hsiao H Y, Chen C, Thermo-migration in flip-chip Sn-Pb solder joints under alternating current stressing[J]. Applied Physics Letters, 2007, 90:152105.

[105] Huang T, Gusak A M, et al. Thermo-migration in Sn-Pb composite flip chip solder joints[J]. Applied Physics Letters, 2006, 88:14191.

[106] Ouyang F Y, Tu K N. Effect of entropy production on microstructure change in eutectic Sn-Pb flip chip solder joints by thermo-migration[J]. Applied Physics Letters, 2006, 89:221906.

[107] Yang D, et al. Micro-structural evolution and atomic transport by thermo-migration in eutectic tin-lead flip chip solder joints[J]. Journal of Applied Physics, 2007, 102:043502.

[108] Lin K L and Kuo S M. The electro-migration and thermo-migration behaviors of Pb-free flip chip Sn-3Ag-0.5Cu solder bumps[C]//Proceedings of the 56th IEEE Electronic Components and Technology Conference, San Diego, Calif, USA, 2006, 668-675

[109] Hsiao H Y and Chen C. Thermo-migration in Pb-free Sn-Ag solder joint under alternating current stressing[J]. Applied Physics Letters, 2009, 94:092107.

[110] Chen H Y, Chen C, et al. Failure induced by thermo-migration of interstitial Cu in Pb-free flip chip solder joints[J]. Applied Physics Letters, 2008, 93:122103.

[111] Basaran C, et al. Thermo-migration induced degradation in solder alloys[J]. Journal of Applied Physics, 2008, 103:123520.

[112] Li S and Basaran C. A computational damage mechanics model for thermo-migration[J]. Mechanics of Materials, 2009, 41:271-278.

[113] Abdulhamid M and Basaran C. Influence of thermo-migration on lead-free solder joint mechanical properties[J]. Journal of Electronic Packageing, 2009, 131: 011002.

[114] Takashi Itoh, Shoji Nitta, Shuichi Nonomura, X-ray diffraction patterns of C60 films by the thin film method and the intercalation of O2, Applied Surface Science, 113/l 14 (1997) 282-285.

[115] Wang J, Li Z, et al. Reinforcement with graphene nanosheets in aluminum matrix composites[J]. Scripta Materialia, 2012, 66:594–597.

[116] J. Liu, C. Andersson, Y. Gao, Q. Zhai, Proceedings of the 10th Electronics Packageing Technology Conference, EPTC'08(2008), 84–93.

[117] F. Lindemann, Physikalische Zeitschrift[J]. 1910, 11: 609-615.

[118] Tu K N, Zeng K. Tin-lead (SnPb) solder reaction in flip ship technology[J]. Materials science and engineering R, 2001, 34:1–58.

[119] Chao Y, Shih J, Adsorption study of organic molecules on fullerene with piezoelectric crystal detection system[J]. Analytica Chimica Acta, 1998, 374:39-46.

[120] Giannozzi P, Car R, Scoles G. Oxygen adsorption on graphite and nanotubes[J]. Journal of chemical physics, 2003, 118:1003-1006.

[121] Weber L, Fischer C, Mortensen A. On the influence of the shape of randomly oriented, non-conducting inclusions in a conducting matrix on the effective electrical conductivity[J]. Acta Materialia, 2003, 51:495–505.

[122] Weber L. Non-conducting inclusions in a conducting matrix: Influence of inclusion size on electrical conductivity[J]. Acta Materialia, 2005, 53:1945–1953.

[123] Srivastava V, Schneider A, et al. Effect of porosity and reinforcement content on the electrical conductivity of spray formed 2014-Al alloy+ SiCp composites[J]. Journal of Materials Science, 2004, 39:6821–6825.

[124] M. Gupta, G. Karunasiri, M.O. Lai, Effect of presence and type of particulate reinforcement on the electrical conductivity of non-heat treatable aluminum, Materials Science and Engineering A219 (1996) 133-141.

[125] Callister W D. Materials Science and Engineering: An Introduction[B]. Wiley- Interscience, Singapore (1994).

[126] Nai S, Wei J, Gupta M. Effect of carbon nanotubes on the shear strength and electrical resistivity of a lead-free solder[J]. Journal of Electronic Materials, 2008, 37:515–522.

[127] Kumar K, Kripesh V, Tay A. Influence of single-wall carbon nanotube addition on the microstructural and tensile properties of Sn-Pb solder alloy[J]. Journal of Alloys and Compounds, 2008, 455:148–158.

[128] Li Z, Gupta M. High strength lead-free composite solder materials using nano Al_2O_3 as reinforcement[J]. Advance Engineering Materials, 2005, 11:1049-1054.

[129] Li X, et al. Mechanical and thermal expansion behavior of laser deposited metal matrix composites of Invar and TiC[J]. Materials science and engineering A, 2000, 282: 86-90.

[130] Liu X D, Han Y D, et al. Effect of graphene nanosheets reinforcement on the performance of Sn-Ag-Cu lead-free solder[J]. Materials science and engineering A, 2013, 562:25-32.

[131] Kumar A, Chan Y C, et al. Interfacial microstructure and shear strength of Ag nano particle doped Sn–9Zn solder in ball grid array packages[J]. Microelectronics Reliability, 2009, 49:746–753.

[132] Fouzder T, Kumar A, Chan Y, et al. Effect of nano Al_2O_3 additions on the microstructure, hardness and shear strength of eutectic Sn–9Zn solder on Au/Ni metallized Cu pads[J]. Microelectronics Reliability, 2010, 50:2051–2058.

[133] Ferrari A C, Robertson J. Raman Spectroscopy in Carbon: from Nanotubes to Diamond[B]. Royal Society Press, London, 2004.

[134] Tay S L, Haseeb A, et al. Effect of Ageing Time on Interfacial Microstructure of Sn-3.8Ag-0.7Cu Solder Reinforced with Co Nanoparticles[C]//2009 International Conference on Electronic Packageing Technology & High Density Packageing (ICEPT-HDP), 655-661

[135] Choi W, Lee H M. Effect of Soldering and Ageing Time on Interfacial Microstructure and Growth of Intermetallic Compounds between Sn-3.5Ag Solder Alloy and Cu Substrate[J]. Journal of Electronics Materials, 2000, 29(10):1207-1213.

[136] Guo F, Lee J, Choi S, et al. Processing and Ageing Characteristics of Eutectic Sn-3.5Ag Solder Reinforced with Mechanically Incorporated Ni Particles[J]. Journal of Electronics Materials, 2001, 30 (9):1073-1082.

[137] Yoon J W, et al. Wettability and interfacial reactions of Sn–Ag–Cu/Cu and Sn–Ag–Ni/Cu solder Joints[J]. Journal of Alloys and Compounds, 2009, 486:142–147.

[138] Yoon J W, Chang B L, Kim D U, et al. Reaction diffusions of Cu_6Sn_5 and Cu_3Sn intermetallic compound in the couple of Sn-3.5Ag eutectic solder and copper substrate[J]. Metals & Materials International, 2003, 9(2):193-199.

[139] Yoon J W, Lee C Y, Lee C B, et al. Investigation of Interfacial Reactions between Sn–Ag–Bi–In Solder and (Cu, Electroless Ni–P/Cu) Substrate[J]. Zeitschrift Für Metallkunde, 1980, 600(2):291-300.

[140] V. C. Nardone, K. M. Prewo. On the strength of discontinuous silicon carbide reinforced aluminum composite[J]. Scripta Metallurgica, 1986, 20(1): 43-48.

[141] D. Z. Yang, The strengthening mechanism of dislocation, Harbin Institute of Technology Press, 1991：11.

[142] R. M. Aikin. L. Christodoulou. The role of quizzed particles on the yield stress of composites [J]. Scripta Metallurgica Material, 1991, 25(1): 9-14.

[143] Zhao R, Ma L, Zuo Y, et al. Retarding Electromigration in Lead-Free Solder Joints by Alloying and Composite Approaches[J]. Journal of Electronic Materials, 2013, 42(2):280-287.

[144] Hu X, Chan Y C, Zhang K, et al. Effect of graphene doping on microstructural and mechanical properties of Sn–8Zn–3Bi solder joints together with electromigration analysis[J]. Journal of Alloys & Compounds, 2013, 580(32):162-171.

[145] Tang Y, Li G.Y, Pan Y.C. Effects of TiO_2 nanoparticles addition on microstructure, microhardness and tensile properties of Sn–3.0Ag–0.5Cu–xTiO_2 composite solder[J]. Materials & Design, 2014, 55: 574–582.

[146] Gain A K, Chan Y C, Yung W. Microstructure, thermal analysis and hardness of a Sn–Ag–Cu–1 wt.% nano-TiO_2 composite solder on flexible ball grid array substrates[J]. Microelectronics Reliability, 2011, 51: 975–984.

[147] Ping L, Pei Y, Jim L. Effect of SiC nanoparticle additions on microstructure and microhardness of Sn–Ag–Cu solder alloy[J]. Journal of Electronics Materials, 2011, 37: 874–879.

[148] Chuang T H, Tsao L C, et al. Evolution of Ag_3Sn compounds and microhardness of Sn3.5Ag0.5Cu nano-composite solders during different cooling rate and ageing[J]. Materials & Design, 2012, 39: 475–483.

[149] Chellvarajoo S, et al. Effects of diamond nanoparticles reinforcement into lead-free Sn–3.0Ag–0.5Cu solder pastes on microstructure and mechanical properties after reflow soldering process[J]. Materials & Design, 2015, 82: 206–215.

[150] Yang Z, Zhou W, Wu P. Effects of Ni-coated carbon nanotubes addition on the microstructure and mechanical properties of Sn–Ag–Cu solder alloys[J]. Materials science and engineering A, 2014, 590: 295–300.

[151] Ren F, et al. In-Situ Study of the Effect of electromigration on strain evolution and mechanical property change in lead-free solder joints[C]// 56th Electronic Components and Technology Conference (ECTC), San Diego, 2006.

[152] Sadiq M, Lecomte J S, Cherkaoui M. Nanoindentation for measuring individual phase mechanical properties of Sn-Ag-Cu lead-free solders incorporating pileup effects[J]. Chaotic Model and Simulation, 2013, 2: 335-348.

[153] Chromik R, Vinci R, et al. Nanoindentation measurements on Cu–Sn and Ag–Sn intermetallics formed in Pb-free solder joints[J]. Journal of Materials Research, 2003, 18: 2251-2261.

[154] Jang G, Lee J W, Duh J G. The nanoindentation characteristics of Cu_6Sn_5, Cu_3Sn, and Ni_3Sn_4 intermetallic compounds in the solder bump[J]. Journal of Electronics Materials, 2004, 33: 1103-1110.

[155] Huang A T, Gusak A M, et al. Thermo-migration in SnPb composite flip chip solder joints[J]. Applied Physics Letters, 2006, 88: 141911-141913.

[156] Chen C, Hsiao H Y. Thermo-migration in solder joints[J]. Materials science and engineering A, 2012, 73: 85–100.

[157] Ouyang F Y, Kao C L. In situ observation of thermo-migration of Sn atoms to the hot end of 96.5Sn-3Ag-0.5Cu flip chip solder joints[J]. Journal of Applied Physics, 2011, (110)110:123525-123529.

[158] Chen, H. Peng, V.V. Silberschmidt, Y.C. Chan, F.S. Wu, C. Liu, Performance of Sn–3.0Ag–0.5Cu composite solder with TiC reinforcement: physical properties, solderability and microstructural evolution under isothermal ageing[J]. J Alloy Compd, 2016 (685) 680-689.